ESL-TR-95-1002

# CARRYING CAPACITY OF UNSURFACED RUNWAYS FOR LOW VOLUME AIRCRAFT TRAFFIC

## PHASE II , PHASE V

# THE BEHAVIOR OF REMOLDABLE SOILS UNDER AIRCRAFT LOADING

## FINAL REPORT

by

ILAN ISHAI , MOSHE LIVNEH
& RAPHAEL YARON

TECHNION - ISRAEL INSTITUTE OF TECHNOLOGY
TRANSPORTATION RESEARCH INSTITUTE

Haifa December 1994

ENGINEERING & SERVICES LABORATORY
AIR FORCE ENGINEERING & SERVICES CENTER
TYNDALL AIR FORCE BASE, FLORIDA 32403

Approved for public release; distribution unlimited.

## DISCLAIMER

Reference herein to any specific commercial product, process, or service by trade name, trademark, manufacturer, or otherwise does not constitute or imply its endorsement, recommendation, or approval by the United States Air Force. The views and opinions of authors expressed herein do not necessarily state or reflect those of the United States Air Force.

This report was prepared as an account of work sponsored by the United States Air Force. Neither the United States Air Force, nor any of its employees, makes any warranty, expressed or implied, or assumes any legal liability or responsibility for the accuracy, completeness, or usefulness of any information, apparatus, product, or usefulness of any information, apparatus, product, or process disclosed, or represents that its use would not infringe privately owned rights

This document is submitted as an historical record of work performed. Limitations of the available media rendered editing impractical; therefore it is retained “as is.”

# REPORT DOCUMENTATION PAGE

*Form Approved*
*OMB No. 0704-0188*

The public reporting burden for this collection of information is estimated to average 1 hour per response, including the time for reviewing instructions, searching existing data sources, gathering and maintaining the data needed, and completing and reviewing the collection of information. Send comments regarding this burden estimate or any other aspect of this collection of information, including suggestions for reducing the burden, to Department of Defense, Washington Headquarters Services, Directorate for Information Operations and Reports (0704-0188), 1215 Jefferson Davis Highway, Suite 1204, Arlington, VA 22202-4302. Respondents should be aware that notwithstanding any other provision of law, no person shall be subject to any penalty for failing to comply with a collection of information if it does not display a currently valid OMB control number.

**PLEASE DO NOT RETURN YOUR FORM TO THE ABOVE ADDRESS.**

| 1. REPORT DATE *(DD-MM-YYYY)* | 2. REPORT TYPE | 3. DATES COVERED *(From - To)* |
|---|---|---|
| 31-DEC-1994 | Final Technical Report | 17-JAN-1989 -- 30-DEC-1994 |

**4. TITLE AND SUBTITLE**

Carrying Capacity of Unsurfaced Runways for Low Volume Aircraft Traffic (Phases II and IV); The Behavior of Remoldable Soils Under Aircraft Loading

**5a. CONTRACT NUMBER**

F08635-89-C-0135

**5b. GRANT NUMBER**

**5c. PROGRAM ELEMENT NUMBER**

**6. AUTHOR(S)**

Ishai, Ilan; Livneh, Moshe, Yaron, Raphael

**5d. PROJECT NUMBER**

**5e. TASK NUMBER**

**5f. WORK UNIT NUMBER**

20541029

**7. PERFORMING ORGANIZATION NAME(S) AND ADDRESS(ES)**

Technion R&D Foundation
Israel Institute of Technology
Transportation Research Institute
Haifa, Israel

**8. PERFORMING ORGANIZATION REPORT NUMBER**

**9. SPONSORING/MONITORING AGENCY NAME(S) AND ADDRESS(ES)**

Engineering & Services Laboratory
139 Barnes Drive, Suite 2
Tyndall Air Force Base, FL 32403-5323

**10. SPONSOR/MONITOR'S ACRONYM(S)**

ESL

**11. SPONSOR/MONITOR'S REPORT NUMBER(S)**

ESL-TR-95-1002

**12. DISTRIBUTION/AVAILABILITY STATEMENT**

Distribution A: Approved for public release; distribution unlimited.

**13. SUPPLEMENTARY NOTES**

**14. ABSTRACT**

Unsurfaced runways and landing strips have been used extensively for aircraft operation in the past and present. The existing design methods for the performance prediction of these runways, frequently fail to yield a realistic estimation of the number of aircraft that can use the landing strip, up to its functional failure. One of the reasons for the large discrepancy between the predictions of the design methods and actual runway performance, is the phenomenon of soil remolding. Certain types of soil tend to remold and change their strength properties, as a result of imposed stress and strain. The soil strength changes, which happen during runway operation, alter the rate of deterioration of the runway condition and hence the number of cycles to runway failure. No description of the the behavior of this type of soils under repetitive aircraft loading was suggested in the past. The present research tackles the issue of soils remolding in the context of unsurfaced runways performance with the aim to better understand the phenomenon and to suggest ways to which consideration of soil remolding can be incorporated into the performance prediction process. ..... The different phases of the research provided verification (mainly qualitative verification) to the assumptions and presuppositions of the presented mechanistic model, for the description of remoldable soil behavior under repetitive wheel loading. Two different approaches have been sugeted for the implementation of the model results, for better prediction of the performance of unsurfaced runways.

**15. SUBJECT TERMS**

remoldable soils, carrying capacity of unsurfaced runways

| 16. SECURITY CLASSIFICATION OF: | | | 17. LIMITATION OF ABSTRACT | 18. NUMBER OF PAGES | 19a. NAME OF RESPONSIBLE PERSON |
|---|---|---|---|---|---|
| a. REPORT | b. ABSTRACT | c. THIS PAGE | | | Michael Coates |
| U | U | U | UU | 266 | 19b. TELEPHONE NUMBER *(Include area code)* |

Reset

# THE BEHAVIOR OF REMOLDABLE SOILS UNDER AIRCRAFT LOADING

TABLE OF CONTENTS

# ABSTRACT

Unsurfaced runways and landing strips have been used extensively for aircraft operation in the past and present. The existing design methods for the performance prediction of these runways, frequently fail to yield a realistic estimation of the number of aircraft that can use the landing strip, up to its functional failure. One of the reasons for the large discrepancy between the predictions of the design methods and actual runway performance, is the phenomenon of soil remolding. Certain types of soil tend to remold and change their strength properties, as a result of imposed stress and strain. The soil strength changes, which happen during runway operation, alter the rate of deterioration of the runway condition and hence the number of cycles to runway failure. No description of the behavior of this type of soils under repetitive aircraft loading was suggested in the past. The present research tackles the issue of soil remolding in the context of unsurfaced runways performance with the aim to better understand the phenomenon and to suggest ways by which consideration of soil remolding can be incorporated into the performance prediction process.

Within the framework of the research, a new mechanistic model for the behavior of dry remoldable soils under repetitive wheel loading, is developed and presented. The model describes the gradual creation of a two-layered soil system in which the upper layer of the soil is remolded. The presentation of the new model involved some assumptions regarding soil constitutive behavior, rate of change in the remolded layer depth, and the behavior of the two-layered soil under accumulating wheel passes.

Series of laboratory testing were conducted on two types of granular soils which tend to develop some degree of cementation during the process of drying. Soil samples were prepared and cured in the laboratory with the intention to simulate, as closely as possible, natural processes pertaining in the field. Laboratory tests which included shear tests and cyclic shear tests confirmed some of the mechanistic model presuppositions concerning soil pre-failure constitutive behavior, and the ability to use fatigue parameters to describe soil remolding caused by cyclic loading.

Based on the mechanistic model, an analytical system was built, using different software tools including FLAC, a finite difference software system. The analytical system comprised three main parts:

- Sub-system A - Describes the development of a two-layer structure in the remoldable soil, caused by repetitive loading of the soil surface. The numerical simulation of the process performs hundreds of wheel loads, positioned according to a pre-determined lateral wander, and assesses the depth of the remolded layer at each stage. Remolding in soil elements can be caused either by shear failure or by fatigue, caused by repetitive loading. A large number of cases were studied, to investigate the influence of soil properties and loading conditions on the remolding process. Some numerical validation of the model was done by checking the model response to cases with known analytical solutions. The results of the numerical model show the gradual development of the upper remolded soil with the progression of load cycles. In most cases studied, the depth of the remolded layer stabilizes with accumulated load applications on a value that depends on soil and loading conditions.

- Sub-system B - Finds the behavior of the two-layer soil structure as a function of the depth of the upper layer. The behavior is defined in terms of the penetration resistance of the soil structure, or in terms of rutting values caused by loading the two-layered soil. This sub-system, also based on numerical modeling, describes the growing sensitivity of the soil structure to loading, as the remolded layer depth grows.

- Sub-system C - Combines the results of the two preceding sub-systems, in an attempt to account for the incremental deteriorative effect of wheel loading on the runway condition, and use it to predict the number of loadings up to runway functional failure. Two different approaches to perform the above, were introduced. The accumulated damage approach which is more simplistic and makes some use of existing design nomograms, and the accumulated rutting approach which attempts to simulate ruts accumulation in the runway, and "declare" runway failure when some rutting criterion is violated. Though the first mentioned approach is simpler to implement, the accumulated rutting approach is preferable on the long run, since it attacks the fundamental cause for runway failure. Use of this approach requires further refinement of the numerical model as well as an extensive validation and tuning program. Flow charts and computer programs for the implementation of both approaches were introduced and their use was exemplified.

In order to provide feedback and validation to the mechanistic and numerical models, some series of laboratory moving wheel tests were conducted. A new loading wheel device was especially designed and built for the purposes of the research. The most important feature of this pneumatically operated device, is the ability to change the wheel lateral location from one loading cycle to the next. This feature enables simulation of the lateral wander of aircraft wheels on the runway. Soil samples for the loading wheel tests (of about 200 kg. each), were prepared and cured using complex and lengthy procedures, trying to simulate

natural drying processes in the soil. The tests conducted in two types of soil, gave some qualitative verification of the model regarding the creation of the remolded layer, stabilization of the remolded layer depth, and the general shape of the rut profile across the runway. Comparisons of the remolded layer depth, as observed during those tests, to that obtained by operating the numerical model using the same soil properties, yielded reasonable results. Rut depth values however, were much higher than those predicted by the numerical model, probably due to the cross sectional shape of the wheel that was used.

The different phases of the research provided verification (mainly qualitative verification) to the assumptions and presuppositions of the presented mechanistic model, for the description of remoldable soil behavior under repetitive wheel loading. Two different approaches have been suggested for the implementation of the model results, for better prediction of the performance of unsurfaced runways.

Recommendations for future research consist of an extensive validation program both in the laboratory and in the field. Additional subjects for further research include refinement of the numerical model, addition of dynamic problems consideration and widening the model to account for other types of remoldable soils.

## LIST OF SYMBOLS

| | |
|---|---|
| $\sigma_V$ | - normal vertical stres (kg/cm$^2$) |
| $\sigma_H$ | - normal horizontal stress (kg/cm$^2$) |
| $\sigma_{VH}$ | - shear stress on the horizontal plane (kg/cm$^2$) |
| $S_R$ | - relative stress level at a point |
| R | - radius of the Mohr circle of the momentary soil stress condition. |
| $R_{MAX}$ | - radius of the maximum Mohr circle capable of developing in the soil under identical average stresses. |
| $S_m$ | - maximum relative stress level developed in a soil element during one wheel loading |
| N | - number of loadings to failure |
| $C_1, C_2$ | - fatigue parameters of the unremolded soil |
| $E_A$ | - accumulated damage in a soil element. |
| D | - depth of the remolded layer (cm.). |
| B | - width of the loading wheel (cm.). |
| CBR | - California Bearing Ratio of the soil (%) |
| $CBR_0, CBR_R$ | - strength of the unremolded and remolded soil, respectively. |
| $\sigma_1, \sigma_3$ | - major and minor principal stresses, respectively (kg/cm$^2$). |

$C, \phi$ - soil cohesion ($kg/cm^2$) and internal angle of friction (deg.), respectively.

$R_A^i$ - accumulated rutting at the center of the wheel traffic lane after i wheel passes (cm.).

$R_P^i$ - primary rutting after i wheel passes (cm.).

$R_{CT}$ - maximum allowed value of the total rutting (cm.).

$R_{CP}$ - maximum allowed value of the primary rutting (cm.).

$R_\sigma, R_\varepsilon$ - indicators of similitude to linear elastic constitutive behavior.

$COH_0$, $COH_1$ - the cohesion of the unremolded and remolded soil, respectively ($kg/cm^2$).

P - average contact pressure of the wheel ($kg/cm^2$).

Den - soil density ($kg/m^3$).

$E_0$, $E_1$ - elastic moduli of the unremolded and the remolded soil, respectively ($kg/cm2$).

$\nu$ - the soil Poisson ratio.

LW - standard deviation of the normally distributed lateral wander of the wheel (cm.).

$CBR_D$ - the equivalent CBR value for a soil system having an upper layer of depth D.

# CHAPTER 1: INTRODUCTION

## 1.1 General

Unsurfaced runways and landing strips have been used extensively for aircraft operation in the past and present. During military operations and other emergencies (such as those induced by natural disasters), a need frequently arises to locate and prepare temporary landing strips for the use of various types of aircraft. Unsurfaced runways are not only prepared in emergency conditions. In many cases, these facilities are constructed in preparation for emergencies, as temporary landing strips, and in circumstances where the anticipated traffic volume does not justify the cost of conventional surfacing. Frequently, especially during situations of emergency, there is no possible means to perform any construction activities in the chosen land strip. In these instances, the main task of the field engineer is to predict the ability of the landing strip to carry the required number of given aircraft landings.

The issue of predicting the performance of unsurfaced runways has been studied since the 195Os, and even earlier. Several prediction nomograms, based mainly on empirical data (laboratory experiments, as well as field observations), have been suggested. The prediction nomograms estimate the capability of a given land strip to sustain a given number of landings and takeoffs of a given aircraft before the formation of ruts that are too deep for further safe runway operation.

A realistic estimation of the number of aircraft cycles that can be handled over a given land strip might have crucial operational importance, especially in emergency conditions. A too pessimistic estimation may, on the one hand, cause cancellation of planned activities, while on the other hand, a too optimistic one may cause discontinuation of operations during performance. However, comparing actual results of runway performance with values predicted by existing nomograms, frequently yields a very large scatter, up to two orders of magnitude in the number of aircraft operations to failure. Several factors contribute to the low reliability of the performance prediction nomograms, including the variability of soil properties along the runway; the problematic use of only one parameter for representing the soil strength; changing dynamic conditions, aircraft characteristics, etc.

One additional factor that contributes to the low reliability of the prediction methods, especially in certain kinds of soils, stems from changes occurring in soil strength during accumulated wheel repetitions. These variations in the soil strength, termed soil remolding, alter the runway ability to withstand further aircraft landings. In most cases, existing prediction methods do not take soil remolding into consideration, and if they do, the approach is very simplistic and lacks substantial justification. Accordingly, there is a need to develop a mechanistic model that will be capable of simulating the behavior of remoldable soils subjected to repetitive wheel loading. The implementation of such a model can assist in the modification of the existing prediction methods and improve their reliability.

This report which focuses on the issue of soil remolding is the final report within the research on the "Carrying capacity of unsurfaced runways for low volume aircraft traffic". The research plan consisted of five different phases, the major part of which were already accomplished.

Phase I (see Fig. 1.1) of the research (Ref. 32) was dedicated to review of the existing local Israeli technology in the field of unsurfaced runway's performance evaluation. Various laboratory tests and observations of actual landing exercises (Phase IV) executed at different occasions throughout the research period (Ref. 16), are utilized for validation and feedback in the course of the different phases of the research.

Phase III (Ref. 31-54) dealt with the DCP instrument which is offered as a central tool for field evaluation of unsurfaced runway's soil strength. The research surveyed current knowledge on the DCP, brought technical details of a new automated instrument developed in Israel, and established correlation between the DCP values and other accepted strength values, such as the CBR of the soil, internal angle of friction, and soil cohesion. The Israeli air force has already adopted the DCP, and uses it regularly for field evaluation of the bearing capacity of unsurfaced runways.

The main objective of this part of the research (Phases II and V, see Fig. 1.1), was to build a model which would physically describe the process of the soil's changing ability to carry aircraft landings.

The first report within Phase II (Ref. 55), was mainly dedicated to a literature review of the remolding phenomena subject. The present and final report elaborated on the suggested model, and tested it via numerical models and laboratory moving wheel testing.

As part of Phase V of the research some guidelines were established in order to utilise the model results for the improvement of the prediction methods of unsurfaced runways performance.

## 1.2 Research objectives and methodologies

As stated above, the existing methods for the prediction of unsurfaced runway performance fail to take into account the strength changes ensuing in soils which tend to be remolded under wheel loading. The principal aim of the present research was to develop and present a mechanistic model that depicts the behavior of remoldable soils under repetitive wheel loading.

Since the model is closely related to the constitutive behavior of the soil, it was decided to confine the study to dry granular soils which exhibit some degree of natural cementation in their initial state. The main reason for this choice is the relatively small measure of research conducted on this type of soil that is prevalent in the Middle East, as well as in other arid and semi-arid areas of the world. The main goal of the research was divided to the following specific objectives:

a. To investigate the behavior of dry granular soils which exhibit natural cementation;

b. To develop a mechanistic model and make use of different numerical means in order to describe the process of soil remolding under repetitive wheel loading;

c. To achieve qualitative verification of the processes transpiring in the soil according to the mechanistic model;

d. To suggest means by which the model can be implemented to improve the reliability of the performance prediction methods for unsurfaced runways.

In order to achieve objective (a), several series of laboratory experiments were conducted on two types of soil brought from different actual landing sites in the southern part of Israel. Reconstituted samples were prepared and cured in a fashion that enabled cementation to grow during the drying process. Apart from the tests required for soil type definition, the laboratory investigation concentrated on studying the elastic parameters of the soil, its constitutive behavior, strength parameters, and soil reaction to repetitive loading. The laboratory study was necessary in order to strengthen some of the presuppositions of the mechanistic model, and provide data required for the application of the numerical model.

The analytical system (objectives (b) and (d)) that simulated the process of repetitive wheel loading, was assembled with the aid of a numerical finite difference software (FLAC). Part of the modules were written in Turbo Pascal 6.0. The numerical system was operated under a variety of loading and soil conditions in order to study their influence on the remolding processes taking place in the soil exposed to repeated wheel loading.

A special loading device was designed and built in order to provide some means for verifying the results (objective (c)). This contraption enabled the application of moving wheel loading with the ability of changing the lateral positioning of the wheel at every loading cycle. The soil samples preparation and curing processes for the moving wheel tests were very complex and time-consuming. As a result, the verification of the mechanistic model within the context of the present research was mainly qualitative.

## 1.3 The structure of the work

Chapters 2 and 3 of the work describe the results of the literature survey conducted as the basis for the research. Chapter 2 concentrates on the research of remolding and loosening phenomena in various types of soils. Attempts to describe mathematically the constitutive behavior of remoldable soils and research dealing with the influence of direct wheel loading on the strength of soils, are reported. Chapter 3 outlines additional subjects relating to the issue of soil behavior under wheel loading; soil reaction to cyclic stress, stress patterns under a moving wheel, fatigue and bearing capacity of layered soil systems. The state of the art in the areas of "Off-the-Road Mobility" and unsurfaced runway research is also briefly discussed in order to provide the background for the present research.

After a summary of the main findings of the literature survey, Chapter 4 contains a description of the proposed mechanistic model for the behavior of remoldable soils under repetitive aircraft loading. The issue of creation of plastic zones in the soil under a surface load is discussed. The general analytical approaches and the research plan built in order to establish the validity of the mechanical model are also presented in Chapter 4.

Chapter 5 depicts the laboratory testing program which was conducted on two types of dry granular soils which exhibit cementation in their natural condition. Chapter 5 includes the description of the preparation and curing processes used in order to allow the soil samples to regain properties close to those observed in nature. The properties of the investigated soils are analyzed and discussed. These attributes were later used as input in the numerical system for the estimation of their behavior under cyclic wheel loading.

Chapter 6 gives the details of the analytical system which was built in order to quantify the mechanistic model. Some limited verification of the numerical system is made by comparing results to known analytical solutions. A detailed analysis of results of some series of computer runs of the numerical system is given. Chapter 6 includes detailed numerical directions as to the options that may be taken in order to use the main model results to obtain a modified forecast of unsurfaced runway performance.

Chapter 7 describes the new pneumatic moving wheel device which was designed and built especially for the present research. Among its other features, this device has the capability of changing the lateral position of the wheel from one loading to another, thus simulating the lateral wander of aircraft traffic. The procedure adopted for the preparation of soil samples for the moving wheel testing is also outlined. The results of tests conducted in the above device are given along with an analysis and comparison with results obtained in the numerical system for similar soil properties and loading characteristics.

Chapter 8 includes the summary and conclusions of the research. Recommendations for future research are given pertaining to analytical features of the model, widening the model to other types of soil, quantitative verification, and implementation of the model to practical use for unsurfaced runway performance prediction.

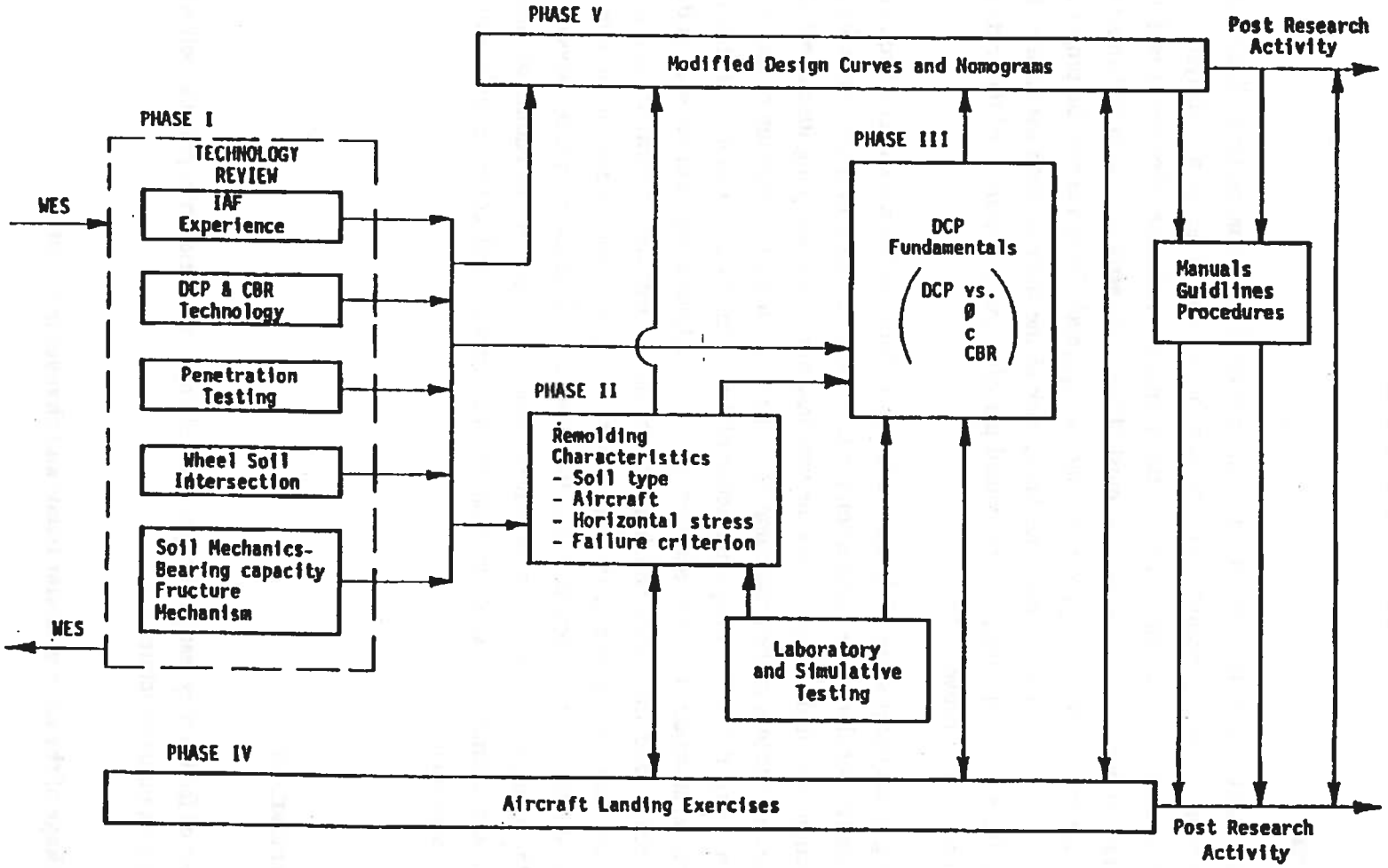


Figure 1.1 Summary of research methodology.

# CHAPTER 2: DISTURBANCE AND LOOSENING PHENOMENA IN VARIOUS SOILS

## 2.1 General

Despite the fact that soils are made up of a combination of individual particles, liquids and gasses, they are essentially treated as a continuum for purposes of design and analysis. This approach is convenient because most of the available mechanical theories regard the material as a continuum, and because in most of the cases associated with soil-structure problems the scale is big enough to allow such an approach. Nevertheless, the properties which represent the soil as a continuous body, such as the soil's strength parameters, are directly influenced by the nature of individual particles, the arrangement of the particles and the forces acting between them.

Remolding in the wider sense of the term refers to a change in the soil's internal structure and the relative position of the various soil particles. Soil remolding may take place during the collection of a field sample, where the very insertion of the sampling instrument into the soil causes changes in the positioning of the particles, during the digging of soil to be used for refilling, during kneading compaction of the ground by means of a roller, etc. The initial internal structure of the soil particles, the basic qualities of the particles such as their size and shape, and the forces which apply among the particles, determine to a great measure the extent of change in the soil's strength following the change in the internal structure. While the forces active among the larger soil particles are mainly physical in nature, the smaller particles, such as clayey particles, are subject to additional forces: chemical and chemical-physical. In light of this, granular and cohesive soils will be discussed separately.

## 2.2 Granular soils

A number of factors may lead to changes in the strength parameters of a granular soil while disturbing its initial structure:

### a. Breakage of the inter-granular bonds and changes in density

When a granular soil undergoes shear under drained conditions, the shear process is often accompanied by a change in density. For a certain type of soil it is possible to observe a

direct correlation between the confinement pressure exerted on the sample and the density (termed the critical density) which the sample will attain after a certain shear deformation. Fig. 2.1 (Ref. 1) displays shear stress vs. deformation and shear strain vs. void ratio curves, for two samples of the same type of sand, wherein at the beginning of the test, one sample was in a dense state while the other was in a loose state. The dense sample displayed the dilatation phenomenon while the loose sample densified and its void ratio decreased during shear. After a certain shear deformation both samples attained the same void ratio which is defined as the critical void ratio. Fig. 2.2 presents an example of the correlation between the confinement pressure and the volumetric changes obtained for a given type of sand. Each confinement pressure yields a specific critical density value, and this is the density which the soil will attain regardless of its initial density. As there is a direct relation between the density of the granular soil and its strength parameters, the conclusion is that when a soil element is sheared under low confinement pressure, its residual strength will be lower than the residual strength attained when the shear process is conducted under high confinement pressure.

In addition to the changes in density and strength which are expected during shear of granular soil, there is the added element of the breaking of the inter-granular bond. Fig. 2.3 illustrates this issue where, in order to create a shear plane in the granular soil (based on the assumption that the strength of the particles themselves is very high), the bond between the particles must be overcome. This situation leads to an increase in the soil's resistance to shear and to a peak phenomenon in the shear-stress deformation curve. Following a certain deformation, the strength decreases until it stabilizes at the residual strength appropriate for the confinement pressure under which the shear was conducted. When the initial soil density is significantly lower than the critical soil density, the peak phenomena is not observed, and the shear takes place in a strain-hardening mode (See Fig. 2.1, for loose soil). The effect of the density changes and the inter-granular bonds on the behavior of the soil during shear can be summarized in the following way: The parameters which affect the strength of a given type of soil are the initial soil density, the confinement pressure to which the soil is subjected during shear, and the extent of shear deformation to which the soil is subjected.

In the context of structural strength and density changes, it is important to mention the issue of the behavior of granular soils which are saturated or close to saturation during a fast shear. This is the situation which holds during the loading of an aircraft wheel. The fast loading makes it difficult for the water to drain from the soil during the passage of the wheel, and this may lead to a state of undrained shear in most types of granular soils, except perhaps for gravels and coarse sands which have high permeability values. In the

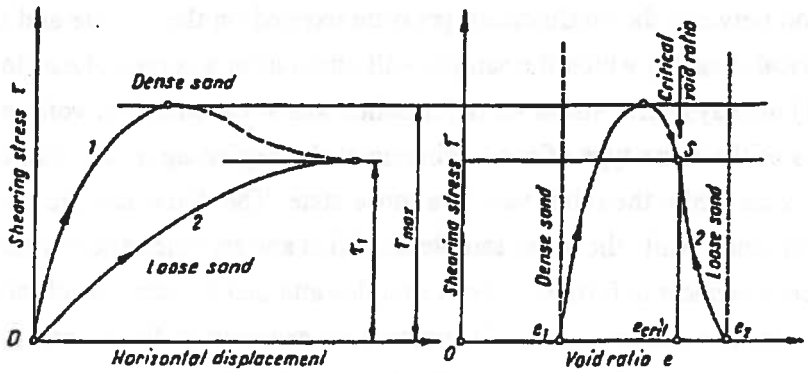


Fig. 2.1 Shear tests with loose and dense sand (Ref. 1)

ציור מס. 2.1 נסויים במדגמי קרקע חולית תחוחה ודחוסה (מ"מ ו)

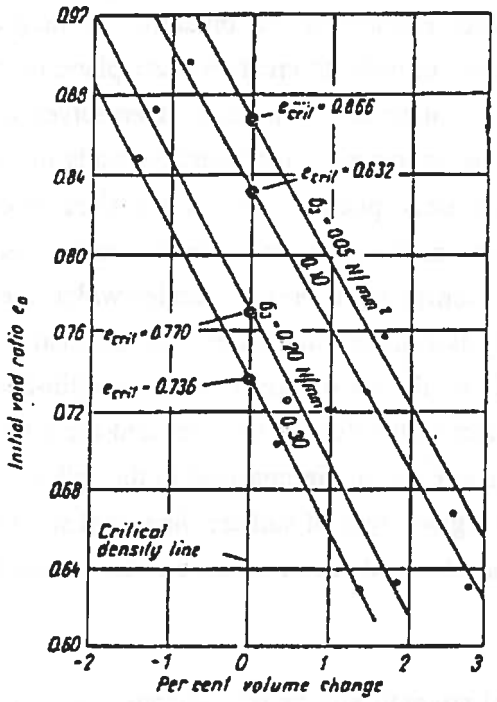


Fig. 2.2 Example on the relationship between the shear confinement pressure and the obtained critical void ratio (Ref. 1)

ציור מס. 2.2 דוגמא לקשר בין לחץ הכליאה ליחס החלל הקריטי המתקבל (מ"מ ו)

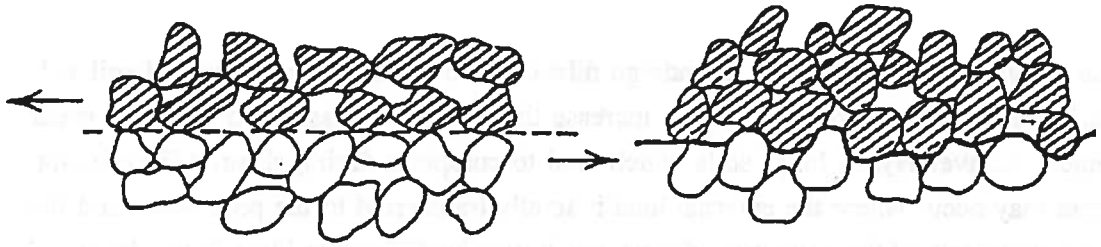

Fig. 2.3 Breakage process of the intergranular bonds in granular soil (Ref. 1)

ציור מס. 2.3 תהליך שבירת הקשר הבין גרגרי בקרקע גרנולרית (מ"מ 1)

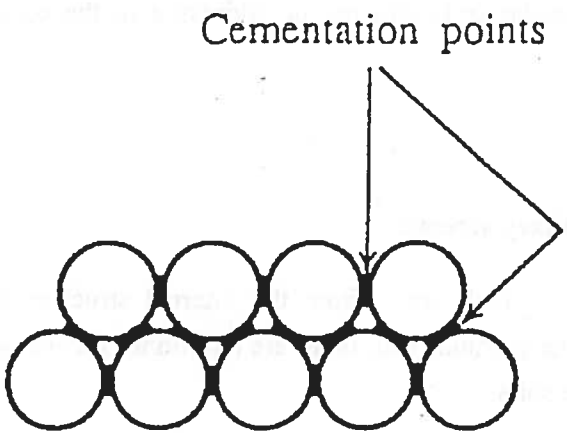


Fig. 2.4 Location of the cementation points in granular soils

ציור מס. 2.4 מיקום נקודות הצמנטציה בקרקעות גרנולריות

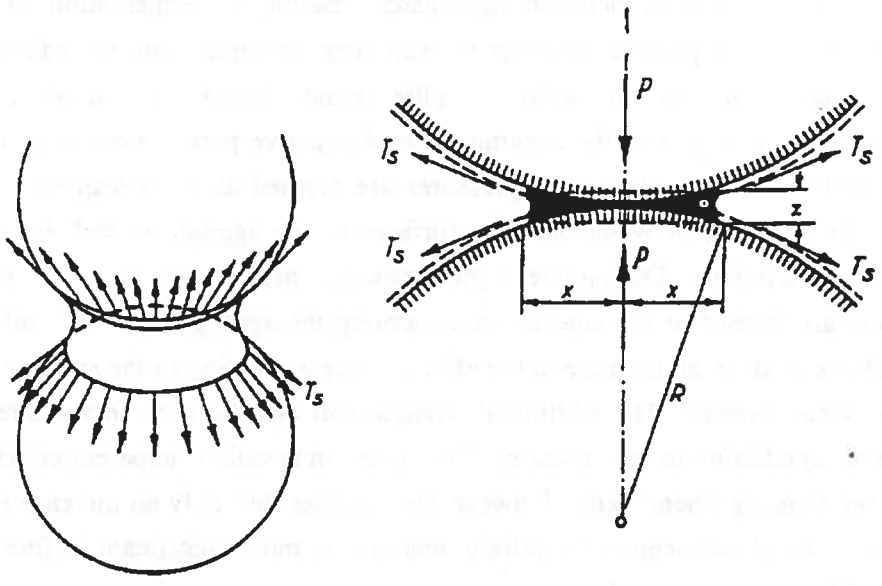


Fig. 2.5 Creation of apparent cohesion in granular soils as a result of capillary water pressure (Ref. 1)

ציור מס. 2.5 יצירת קוהזיה מדומה בקרקעות גרנולריות כתוצאה מלחצים קפילריים (מ"מ 1)

dense granular soils which tend to undergo dilatation during shear, the saturated soil will develop negative pore pressures which increase the effective stresses and the soil's shear strength. Conversely, in loose soils which tend to compress during shear, a liquefaction process may occur where the external load is totally transferred to the pore water and the structural strength of the aggregates disappears. It may be difficult to identify the danger of liquefaction in sandy soils as the risk of liquefaction occurs only under very high loading rates (wheel loadings). These loadings are hard to simulate during field testing, especially when the strengthening of the soil, once the load is removed, is very rapid in these soils.

The issue of saturated granular soils will not be addressed in the context of the present research.

**b. Cementation and capillary stresses**

In addition to the strength which arises from the internal structure and friction forces among the aggregates in the granular soil, there are additional factors which may increase the initial strength of these soils.

Fig. 2.4 presents a magnified sketch of the particles in a granular soil, among which cementation forces are at work. Tiny amounts of cement materials, which are sometimes almost indistinguishable in the gradation tests, concentrate, usually during drying processes, at the contact points between aggregates, leading to cementation of the aggregates. The cementation process increases the soil shear strength, and the additional strength is essentially cohesive in nature. A phenomenon which is similar to the cementation phenomenon is that of the accumulation of negative pore pressures between the aggregates in the soil. Negative pore pressures are formed as a consequence of a combination of the adhesion of water onto the surfaces of the aggregates and the water surface tension characteristic. During the drying process, membranes of water under negative pressure are formed at the contact points among the aggregates in the soil (see Fig. 2.5). The above leads to an increase in the effective stresses acting in the soil and thus also in the soil shear strength. The additional strength can also be seen in the strength envelope curve as an addition to the cohesion. This cohesion is called "apparent cohesion" as there is no true bonding phenomenon between the particles, but only an increase in the effective stresses. The phenomenon of capillary pressures is more significant in fine soils than in coarse. While in gravel and in coarse sands this phenomenon has no significant effect on the soil strength. in fine sands and silts, a meaningful increase in strength can sometimes be discerned as a consequence of capillary pressure. There is a direct

relationship between the additional strength resulting from capillary pressure and the specific surface of the aggregates. Both the capillary pressure and the cementation phenomena (in most actual cases) are very sensitive to the soil water content and they are mainly evident when the water content is relatively low.

The cementation and the capillary pressure phenomena are usually distinguished one from the other. However, in many cases the strength of the cementing material concentrated between the coarse aggregates is the result of capillary pressures among the aggregate's fines. In these cases, there is an especially high sensitivity of the cementing element to changes in moisture as the addition of even an extremely small amount of water (relative to the weight of the entire soil sample), may have considerable influence on the fine material concentrated in the contact points. The addition of water cancels out the suction in the fine material and diminishes the cementing forces between the aggregates.

Fig. 2.6 (Ref. 8) presents a typical shear stress-deformation curve for a soil with a significant cementing element. The initial strength is relatively high while later on, after a small shear deformation, a kind of "breakage" occurs in the cemented aggregate structure and the strength decreases quickly down to the residual strength value.

The cementation and capillary pressure phenomena, under low moisture content both disappear after shear and do not reappear unless the process of wetting and drying is repeated. This phenomenon stems from the fact that the tiny amounts of cementation agents have been detached from the contact points between the aggregates.

The occurrence of high initial strength in granular soils when water content is low, is rather frequent in arid and semi-arid climates in sandy areas, deserts, etc. Reference to the initial soil strength alone without an inspection of the soil's remolding potential, may lead to a false evaluation of the soil's ability to carry aircraft and other traffic.

## 2.3 Cohesive soils

The behavior of clay soils is far more complex than that of granular soils. In contrast to granular soils, where the inter-granular forces are mostly mechanical, clay soils combine mechanical forces with the forces of various chemical ties. The multiplicity of factors and forces which operate among the particles, leads different types of clays to behave in totally different ways, in accordance with their structure and the relative dominancy of the various forces. Similar to clay behavioral phenomena, soil remolding and behavior during shear are

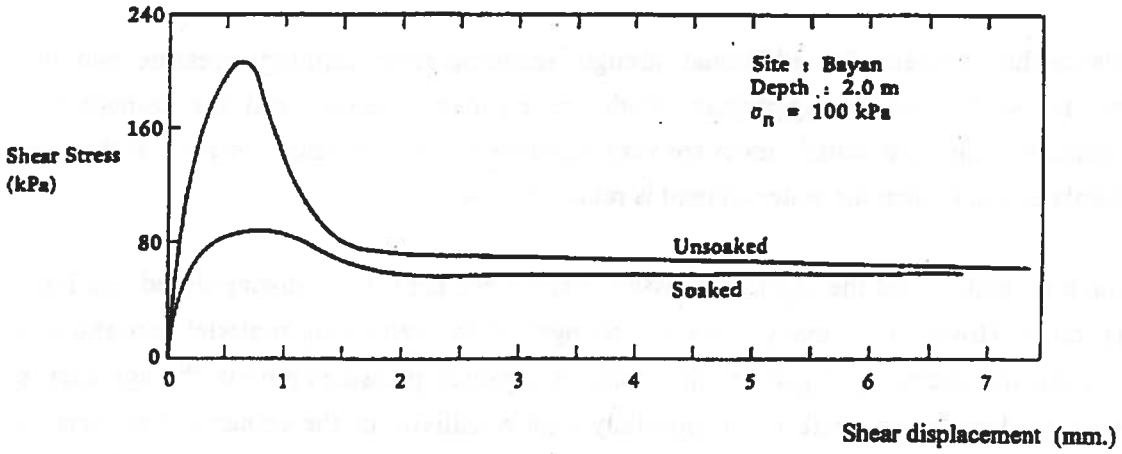


Fig. 2.6 A shear stress-deformation curve for granular soil with natural cementation (Ref. 8)

ציור מס. 2.6 עקום מאמץ גזירה - דפורמציה בקרקע גרנולרית עם צמנטציה טבעית (מ"מ 8)

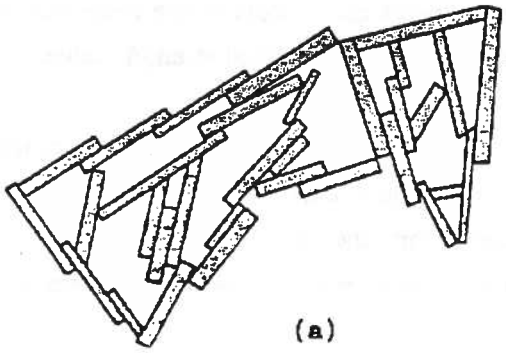


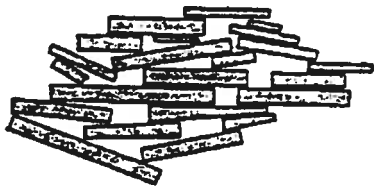


Fig. 2.7 Flocculation and dispersion in clay soils(Ref. 63):
(a) flocculated structure;
(b) dispersed structure

ציור מס. 2.7 יתוד וביזור בקרקעות חרסיתיות:
(a) מבנה מיותד (b) מבנה מבוזר (מ"מ 63)

also complex phenomena which change from one type of clay to the next. A number of basic factors may contribute to strength change in cohesive soils during shear.

**a. Inter-granular strength**

This phenomenon is very similar to that which occurs in granular soils, but on a much finer scale. Inter-granular bonding appears in over-consolidated cohesive soils in which the clay particles are locked in a dense structure. The shear process which breaks the interlocking between the clay particles causes local dilatation at the failure area and the formation of shear planes. The behavior of the shear stress-deformation curve for the over-consolidated soil will resemble that of dense granular soil (see Fig. 2.1) while the normally consolidated soil will behave more like loose granular soil. The more over-consolidated is the soil, the more pronounced is the tendency to attain a high peak strength followed by a decrease resulting from "breakage" of the particles' dense structure. When the soil is in a saturated state, negative pore pressures are generated during the shear process of the over-consolidated soil. These pressures increase the effective stresses in the soil, and the resulting peak strength of the soil.

**b. Clay bonding strength**

A phenomenon which is expressed by a shearing behavior similar to that obtained in over-consolidated soil. The source of this phenomenon is in strong chemical ties between clay particles formed by the presence of various materials such as Carbonate, Silica, Aluminum, Iron Oxides and various organic compounds. These bonds may cause the material to have a very high peak shear strength. Such a soil usually functions in a rigid way, wherein there is a kind of "breaking" of the structure once the peak strength point is passed.

A bonded clay, is a clay in which the internal structure among the clay particles, (or among groups of particles) is usually a flocculated structure. The flocculated structure (unlike the dispersed structure, see Fig. 2.7), is a more "open" structure in which particles are bound to each other mostly by edge to edge or edge to surface bonds (see Ref. 63). In the dispersed structure, the bonds between the particles are mostly surface-to-surface. The forces of attraction between the particles, which are created as a consequence of the nature of the clay particles and the presence of other materials, create a rigid structure whose strength is usually much higher than that of the dispersed structure. The shear behavior of a bonded clay will be expressed by a high initial strength resulting from the rigid structure, which later breaks so that the strength of the clay decreases significantly.

A phenomenon which is typical of structural cohesive soils is that of liquefaction. This phenomenon is characteristic of structured clay soils whose internal composition is very "open". The high void ratio permits high water content, while the bonds between the clay

particles preserve the soil's strength. In extreme cases, (depending on the type and character of the clay, and on other factors as well) the shear process may lead to a collapse of the soil structure, to the transfer of stresses from the particles to pore pressure, and sometimes even to the transformation of clay particles into a suspended state within the pore water. In this respect the ratio between the soil's peak strength and its residual strength is termed the soil's sensitivity, as described in following equation:

$$S_t = \frac{t_f}{t_r} \qquad [2.1]$$

where:

$t_f$ - is the peak shear strength.

$t_r$ - is the residual shear strength in large deformations.

Table 2.1 (Ref. 2). classifies clays according to their level of sensitivity. This table emphasizes the pronounced decrease of soil strength that may occur in certain types of soils.

**Table 2.1: Classification of Clays According to their Sensitivity Values**

**טבלה 2.1: סיווג חרסיתות על פי רמת רגישותן.**

| Level of Sensitivity | St |
|---|---|
| Insensitive | ~1.0 |
| Slightly sensitive clays | 1-2 |
| Medium sensitive clays | 2-4 |
| Very sensitive clays | 4-8 |
| Slightly quick clays | 8-16 |
| Medium quick clays | 16-32 |
| Very quick clays | 32-64 |
| Extra quick clays | >64 |

**c. The directionality of the clay particles**

The shape of the basic clay particle is long and flat. In the natural soil, the clay particles are arranged in different directions and in different structures in accordance with the forces acting among them. When shear deformations develop in the soil, those particles which are arranged in a direction opposing the direction of shear, produce forces which increase the shear resistance. During the shear, and as an outcome, the particles in the vicinity of the shear plane tend to gradually arrange themselves in a direction parallel to the direction of shear.

Fig. 2.8a presents a shear stress-deformation curve for a clayey soil. After attaining the peak shear strength, strength gradually decreases under greater deformations until it reaches its residual value. This phenomenon which appears in both over-consolidated and normally consolidated clays, adds to the shear strength of most clay soils. It is important to note the anisotropic nature of this phenomenon as compared with other phenomena related to changes in soil strength during shear. Halting the shear of the soil once it has attained the residual strength value, and proceeding with the shear in a direction perpendicular to the previous direction, will yield a high shear strength value. An additional shear deformation will be required in order to cause further turning of the clay particles in a direction parallel to the direction of the shear. It is important to note that the orientation of clay particles is relevant in soils where the clay component is dominant (over 40%). In soils with a low clay content (lower than 20%), this factor has no effect on the behavior of the soil. (See Fig. 2.8b)

## 2.4 The rate of change in the strength of potentially remoldable soils.

In order to evaluate the behavior of the runway, it is necessary to know the soil strength that the aircraft wheel encounters at every stage of the runway's life cycle. Assuming that soil structural remolding phenomenon indeed causes a change in strength, it is necessary to find a way to evaluate the rate of soil strength decrease during aircraft movement over the soil. Chapter 3 will address the issue of the effect of the wheel's movement on the remolding. This section will present some of the experimental relations found which appear in the literature between the amount of the soil's shear deformation and its strength.

Fig. 2.8, taken from Ref. 3, clearly illustrates the behavior of the strength change phenomenon in clayey soils, divided according to its elements. The peak strength is attained at small deformations (tests were conducted by means of a reversal shear box and a ring shear instrument) in the range of 0.5-3 mm in over-consolidated soil, and 3-6 mm. in

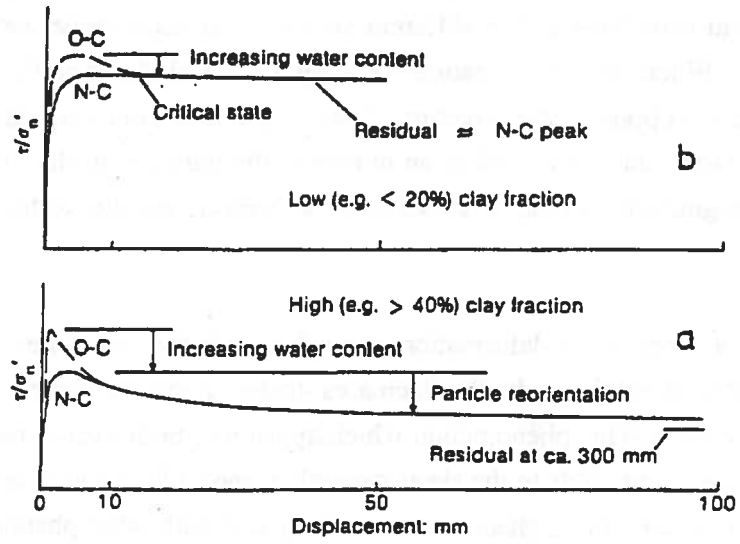


Fig. 2.8 Diagrammatic stress displacement curves (Ref. 3)

ציור מס. 2.8 עקומי מאמץ תזוזה סכימטיים (מ"מ 3)

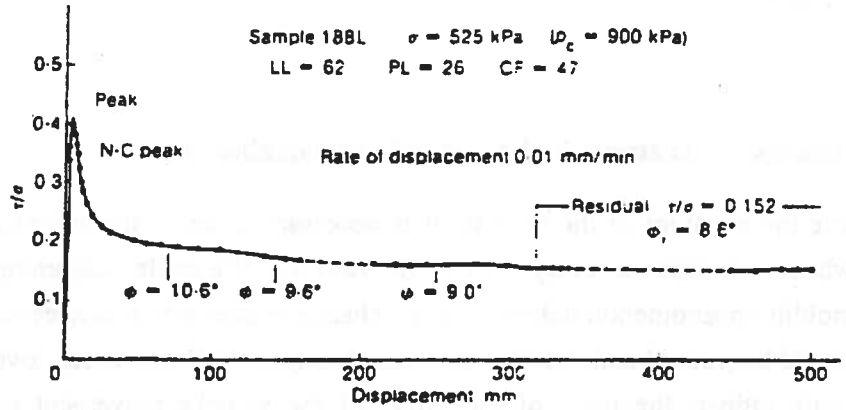


Fig. 2.9 Ring shear test results of bonded clay (Ref. 3)

ציור מס. 2.9 תוצאות ניסויים בקרקע חרסיתית קשורה בטבעת גזירה (מ"מ 3)

normally consolidated soil. The decrease in strength which stems from the breaking of the inter-granular bond, is fast and sharp and is expressed in low deformation values of 4-10 mm. Once the effect of the inter-granular bonding has been canceled, the effect of the particles' orientation (in soils with high clay fraction) is felt, and a slow and gradual decrease in strength can be observed down to the residual strength which is attained at a deformation range of 100-500 mm. The distinction between the strength segment arising from the inter-granular bonding and that arising from particle orientation, is based on the comparison of the behavior of over-consolidated samples and the normally consolidated samples of the same clay, wherein the normally consolidated clay does not display the inter-granular bonding phenomenon.

Similar to the inter-granular bonding phenomenon, the phenomenon of bonding strength stemming from a special structure and the existence of cementing ties, is also "rigid.," and the breaking of the structure takes place at very low deformations. Similar results were obtained with other natural clays as reported by Ref. 3 (see Fig. 2.9) and Ref. 4. Fig. 2.10 presents an example of the results of experiments which were conducted in a clayey soil, as reported by Ref. 3. For the undisturbed clay sample, one can clearly observe the "breaking" effect of the bonding phenomenon, wherein the peak is reached at deformations of less than 1 mm. The post-peak decrease in strength is very rapid and ends at a deformation range of 6-8 mm. Under the given test conditions, the soil strength in this clay decreased by about 50% within this deformation range.

Additional structural strength (stemming from cementation, chemical bonds and negative pore pressures) may be sensitive to confinement pressure conditions created during loading, probably because of the special structure and the fragile ties. Conditions of high confinement pressure (see Ref. 5) even lacking shear stress, may cause a substantial decrease in strength due to the breaking of bonds and the collapse of the stable structure.

A number of researches examined the behavior of the shear stress-strain function in various granular soils which include cementation, either natural or artificially contrived. Ref. 6 investigated the behavior of 4 soil types with natural cementation as well as sandy soil with the addition of 2% and 4% Portland cement, under static loading in a triaxial shear device. Figs. 2.11 a and b present the results of the tests for various confinement pressures in sands with high and intermediate natural cementation, respectively. The soil with the high cementation displays brittle behavior, while the soil with the intermediate cementation exhibits relatively ductile behavior, especially when the tests are carried out under high confinement pressure. Similar results have been obtained in other sand types. The less the cementation, the lower the confinement pressure under which the ductile behavior of the soil is displayed. The authors ascribe this behavior to the variable

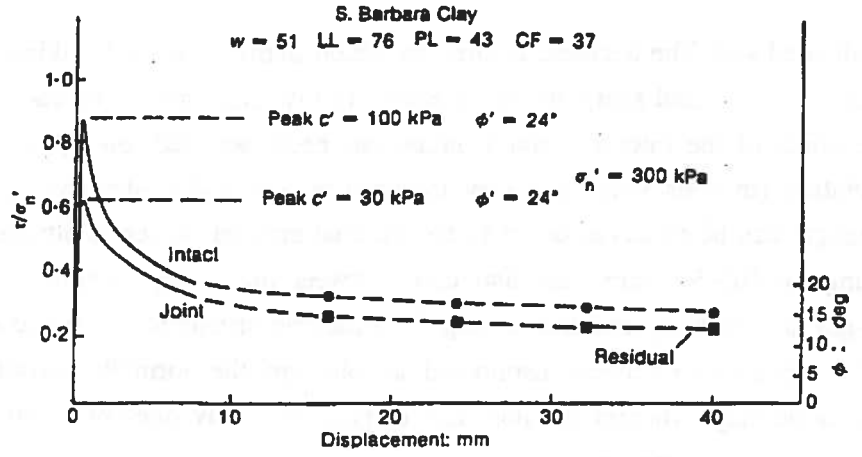


Fig. 2.10 Reversal shear box tests on intact clay (Ref. 3)

ציור מס. 2.10 נסויים ב- Reversal shear box בחרסית בלתי מופרת (מ"מ 3)

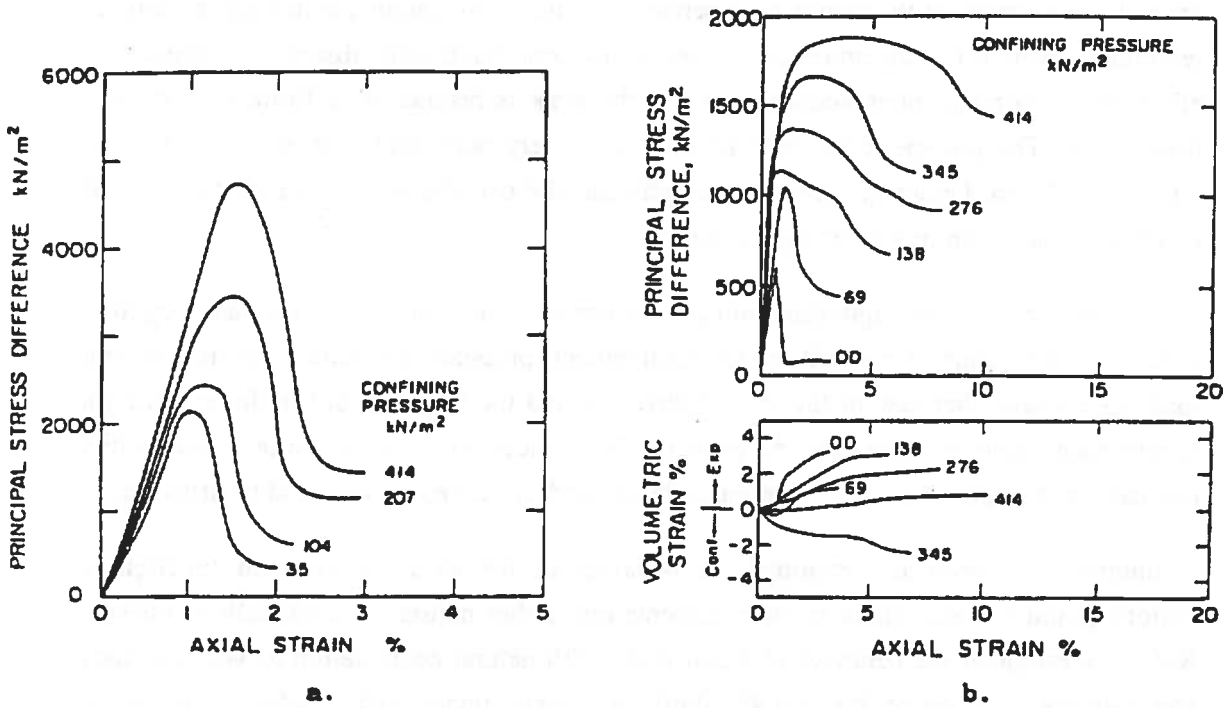


Fig. 2.11 Stress-strain curves in soil with natural cementation (Ref.6):
(a) High level of cementation;
(b) Medium level of cementation;

ציור מס. 2.11 עקומי מאמץ-עיבור בקרקע עם צמנטציה טבעית (מ"מ 6)
(a) רמת צמנטציה גבוהה
(b) רמת צמנטציה בינונית

contribution of the frictional strength, depending on the confinement pressure. Under higher confinement pressure, the frictional part in the strength of the material becomes dominant, and the effect of cementation becomes less salient, particularly in those cases where the cementation is not high. Another reason, not mentioned in the above reference, which may provide an explanation for the ductile behavior under high confinement pressures, is the "breaking" of the cementation as a consequence of the exertion of the confinement pressure itself. Similar results were obtained by Ref. 6 in an investigation of sandy soil with Portland cement added. When the failure envelopes derived from these experiments are constructed (see Fig. 2.12), an internal friction angle in the range of 37° 49° is obtained, and the cohesion resulting from the cementation is in the range of 0.1 kg/cm$^2$ in low-cementation soils and up to about 3.5 kg/cm$^2$ for high-cementation soils (natural soil).

Ref. 7 examined the strength and the bearing capacity of sandy soil with an addition of 1% Portland cement, with the aim of using the results to derive the behavior of soils with natural cementation. The added strength obtained as a consequence of the cementation was small (up to 0.25 kg/cm$^2$ to the soil cohesion).The behavior during shear was found to be "brittle" under low confinement pressures and relatively ductile under greater confinement pressures. The results of 5x30 cm plate loading experiments, showed an 8-fold increase in bearing capacity values caused by the addition of the relatively small amount of cementation. The explanation for this phenomenon can be found in the small dimensions of the plates; which served to convert the cohesion factor in the total bearing capacity of the plates to be the dominant factor. There is no doubt that this point is greatly significant in relation to the movement of the wheel over the soil. The experimental results indicate that there will be no change in the friction angle of the sand (about 34° in this case) as a consequence of the added cementation. An earlier research (Ref. 8) of naturally cemented soils of varying levels of cementation produced similar results.

Ref. 9 made use of sand stabilized with varying quantities of Portland cement, with the aim of emulating the behavior of naturally stabilized soils. Fig. 2.13 illustrates the change in the value of the brittleness coefficient Bc, as a function of the confinement pressure during shear, the amounts of the cementing materials, and the relative density of the stabilized soil. The brittleness coefficient Bc is defined as follows:

$$B_c = \frac{S_{peak}}{S_{resid}} \qquad [2.2]$$

where:

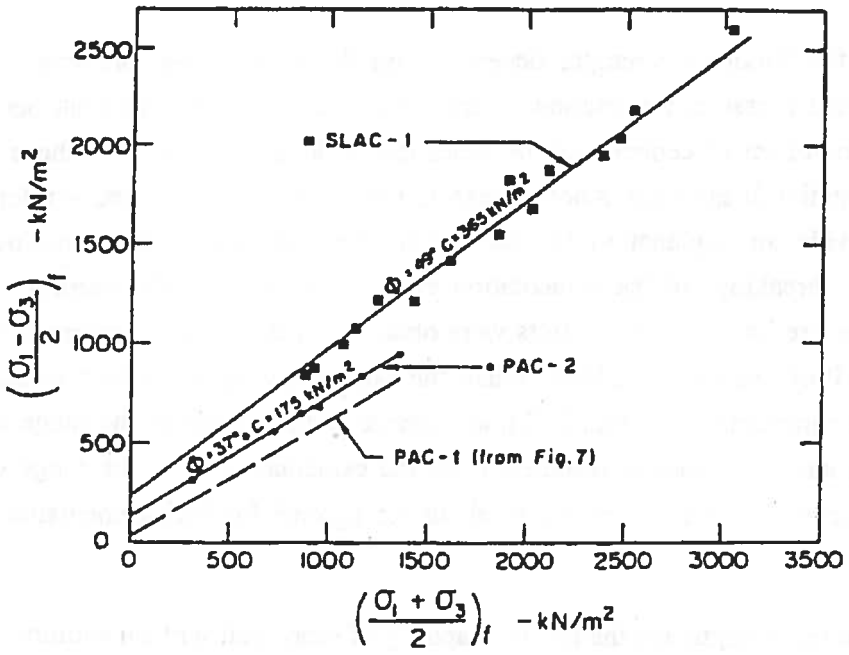


Fig. 2.12 Failure envelopes and peak strength parameters in soils with high and medium natural cementation (Ref. 6)

ציור מס. 2.12 מעטפת הרס ופרמטרי חוזק שיא בקרקעות בעלות צמנטציה טבעית ברמה גבוהה ובינונית (מ"מ 6)

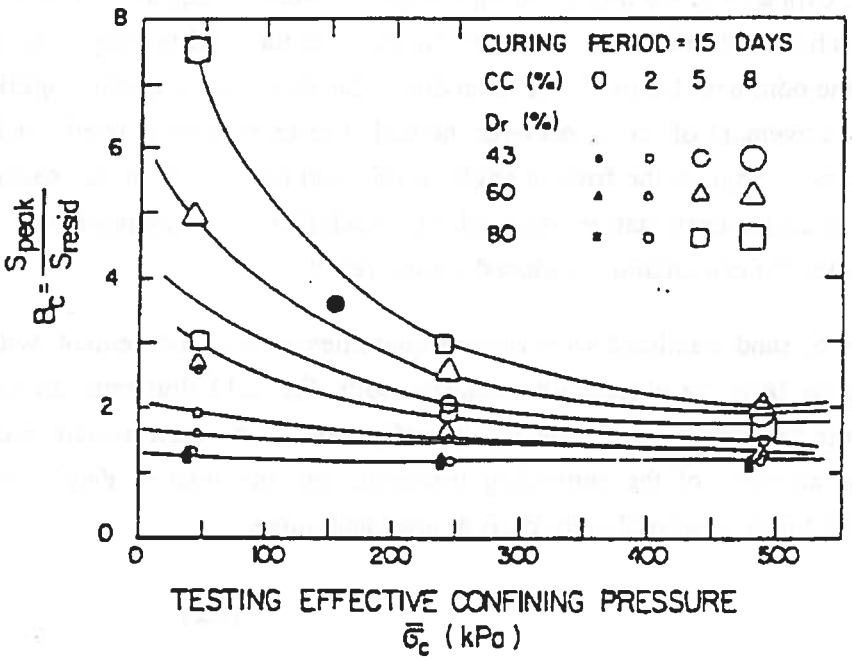


Fig. 2.13 The effects of confinement pressure on the value of the brittleness coefficient - $B_c$ at various levels of relative density and cementation (Ref. 9)

ציור מס. 2.13 השפעות לחץ הכליאה על ערך מקדם הפריכות - $B_c$ ברמות שונות של צמנטציה וצפיפות יחסית (מ"מ 9)

$S_{peak}$ - Peak material strength.

$S_{resid}$ - The material's residual strength.

From Fig. 2.13 it can be seen that the lower the confinement pressure during shear and the higher the cement content, the greater the value of Bc. Ref. 9 also analyzes the results of previous experiments in an attempt to evaluate the stress-strain behavior of soils with cementation. Figures 2.14 a and b illustrate the characteristic behavior under shear of strongly and weakly stabilized soils, respectively. Once again, the "brittle" behavior was more pronounced under low confinement pressures as compared with more ductile behavior under high confinement pressures. Linear-elastic behavior, almost up to peak strength, was mainly observed in soils with high cementation. Peak strength is usually achieved at deformations of 0.3-0.8%, followed by the characteristic decrease in strength.

Ref. 10 also addresses the problematic issue of conducting laboratory tests on unremolded samples of soil with cementation. An alternative method is presented, by which cementation is created in sand through the use of gypsum. The results of unconfined strength tests in samples stabilized with various quantities of gypsum, are presented in Fig. 2.15. The peak strength is achieved at axial deformations in the range of 0.5%, wherein a sharp decrease in strength is mainly observable in samples with high cementation. The higher the cementation, the more linear-elastic behavior observable along a greater part of the loading curve before peak strength is achieved. The material in which the cementation was carried out was obtained from a source which exhibits natural cementation, and the bonding agent was added to the remolded soil brought from the site. The authors consider that the addition of appropriate quantities of cement material can create a material which will constitute a good simulation of the natural material. with far lower preparation costs and avoiding the great variability which exists in natural soils.

Fig. 2.16 derived from Ref. 11 presents the development of the cohesive and frictional strength factors in granular soils with natural cementation along the Israeli coastal plain. It seems that the cohesive factor in the soil is maximally expressed in deformations lower than 1%, while the expression of the frictional factor is more gradual. The total peak strength of the soil in these tests was obtained under shear deformations of 2-5%. Similar results were obtained by other sources, such as Ref. 9, in soils which received additional cementation. Hence, it is obvious that the lower the soil confinement pressure (as in the case of a wheel moving over the surface of the soil) the lower the deformations at which peak strength is obtained. In addition, the low confinement pressure causes a more rapid decrease in strength following the peak, due to the relatively small influence of the frictional factor.

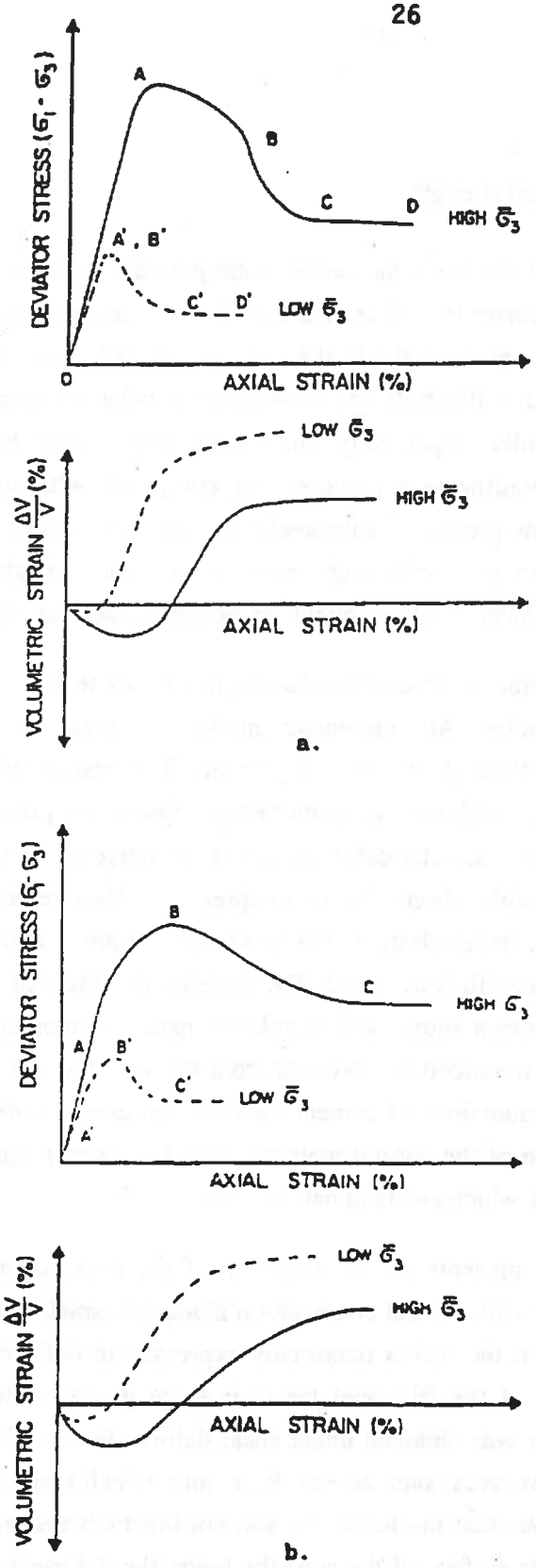


Fig. 2.14 Stress-strain behavior in cemented sand (Ref. 9):
(a) High level of cementation
(b) Low level of cementation

ציור מס. 2.14 עקומי מאמץ - עיבור בקרקע חולית עם צמנטציה (מ"מ 9)
(a) רמת צמנטציה גבוהה
(b) רמת צמנטציה נמוכה

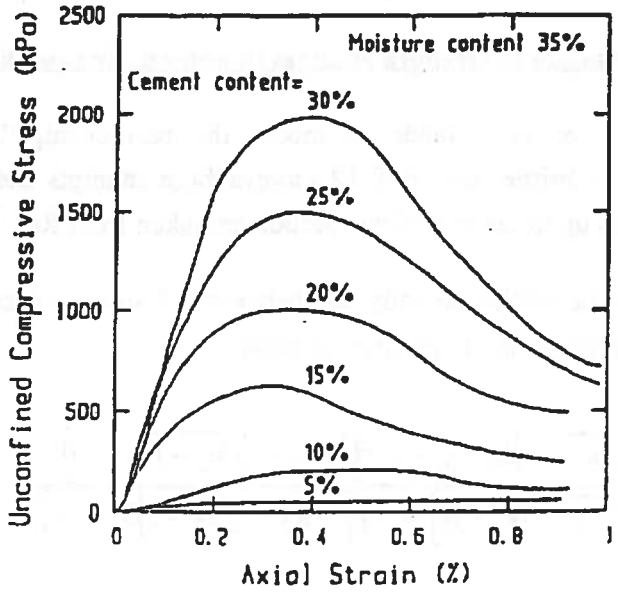


Fig. 2.15 Effect of cementation level on the stress-strain behavior of the soil (Ref. 10)

ציור מס. 2.15 השפעת רמת הצמנטציה בקרקע על עקומי מאמץ - עיבור (מ"מ 10)

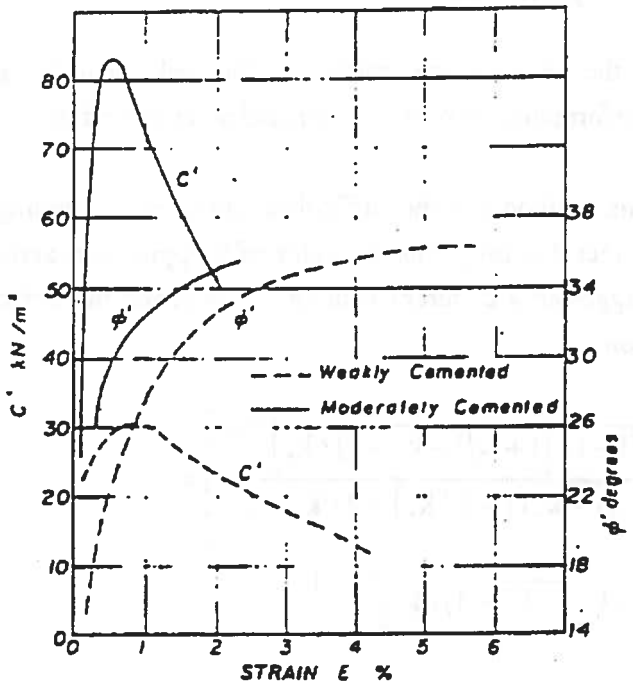


Fig. 2.16 Development of strength parameters with increasing strain in sandy soil with cementation (Ref. 11)

ציור מס. 2.16 התפתחות השפעת פרמטרי החוזק עם עלית העיבור בקרקע חולית עם צמנטציה (מ"מ 11)

## 2.5 Mathematical formulation of strength changes in potentially remoldable soils.

A number of attempts have been made to model the relationship between shear deformations and strength in brittle soils. Ref. 12 surveys these attempts and a summary is given herein. All references up to the end of this section are taken from Ref. 12.

The first attempt to describe mathematically the behavior of strain softening soils was made by M.G. Bekker who posed the following equation:

$$S/S_{max} = \frac{\exp\left[\left(-k_2+\sqrt{k_2-1}\right)k_1 \bullet j\right]-\exp\left[\left(-k_2-\sqrt{k_2-1}\right)k_1 \bullet j\right]}{\exp\left[\left(-k_2+\sqrt{k_2-1}\right)k_1 \bullet j_0\right]-\exp\left[\left(-k_2-\sqrt{k_2-1}\right)k_1 \bullet j_0\right]} \qquad [2.3]$$

where:

- $S$ - is the shear stress at a specific point j.
- $S_{max}$ - is the maximum stress.
- $j$ - is the deformation.
- $j_0$ - is the deformation at Smax.
- $k_1, k_2$ - are empirical constants.

This equation defines the soil's strength, relative to the peak shear strength, as function of the deformation, the deformation at peak strength and some empirical constants.

The drawbacks of this method are the difficulties involved in finding the empirical K values, as well as the fact that for j>>j0, the value of S approaches zero, which is, in fact, false. Oida (1979) suggested a different equation to describe the behavior of the stress-deformation correlation.

$$S/S_{max} = k_r\left[1-\frac{\sqrt{1-k_r}\left[1+\left(\sqrt{1-k_r}-1\right)/k_r\right]^{j/k_w}}{\sqrt{1-k_r}\left(1-2/k_r\right)+2/k_r-2}\right]\times \left[1-\left[1+\left(\sqrt{1-k_r}-1\right)/k_r\right]^{j/k_w}\right] \qquad [2.4]$$

where:

- $k_r$ - is the value $S_r / S_{max}$, which is the ratio of the residual shear strength to the maximum shear strength.

$k_W$- is the shear deformation, where S=Smax. ($k_W$ equals to $j_0$ in the previous equation).

This function fulfills the following requirements:

1. $S = S_{max}$ for $j = k_W$.

2. $\partial S / \partial J = 0$ for $j = k_W$. (The peak point is an extremum point).

3. $S = S_r$ where $j >> k_W$.

The $k_W$ value in the equation is relatively easy to resolve as it is the deformation at which the maximum shear strength is obtained. In cases where the Sr, the residual strength, can be determined, it is also possible to calculate $K_r = S_r / S_{max}$ and hence the entire strength function. In cases where the Sr value cannot be determined, it is possible to derive iteratively the value of Kr on the basis of the values of a number of points on the stress-deformation curve obtained from the experimental data. This method is rather complicated. The behavior of this equation for various Kr values is seen in Fig. 2.17a.

Another equation was proposed by Wong (1983):

$$S/S_{MAX} = K_r[1 + [1/(K_r(1-1/e))-1] \cdot \exp(1-j/K_W)] \cdot [1-\exp(-j/K_W)] \quad [2.5]$$

Where the definitions are as in Oida's equation. This equation is easier to calculate, but does not precisely fit the requirements for the first derivation which equals zero at j=Kw. (See Fig. 2.17b). Experiments conducted with loam have shown a relatively good correlation between the last two models and soil behavior, see Fig. 2.18 (Ref. 12).

The most important problem in the behavior of the proposed equations is that for the given ratio between the residual shear strength and the maximum shear strength, there is only a single functional relation between the deformation and the strength, rendering it impossible to express variations in the rate of strength change. As can been seen in Fig. 2.18, the soil behaves in a more brittle way than anticipated by both models.

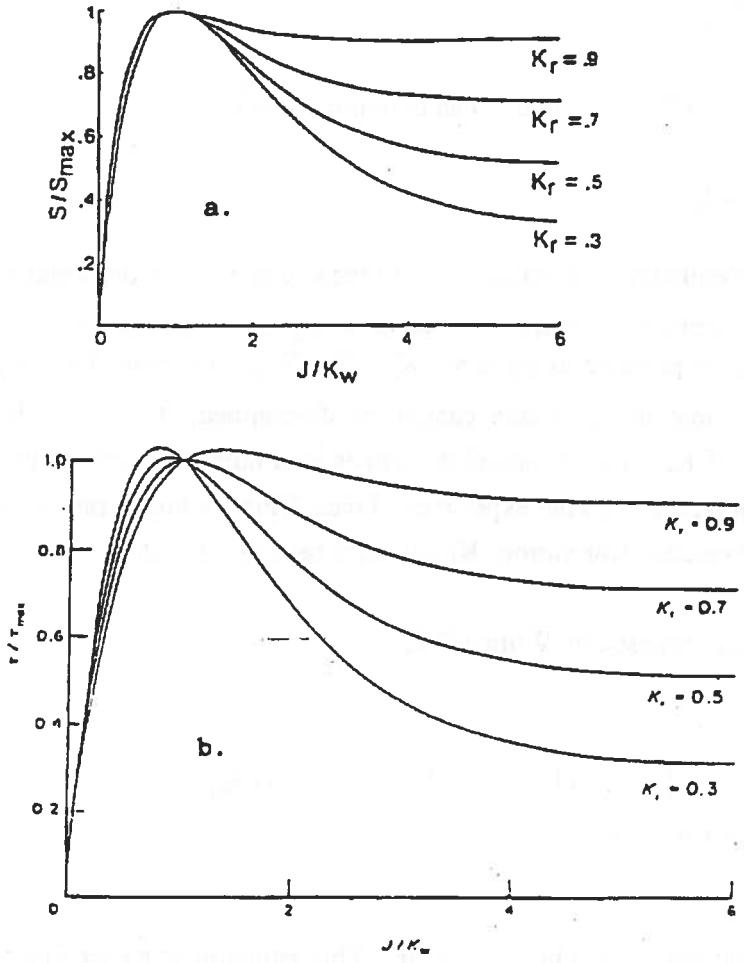


Fig. 2.17 Behavior of various equations describing stress-deformation relations in "brittle" soils (Ref. 12): (a) Oida's equation; (b) Wong's equation

ציור מס. 2.17 התנהגותן של משוואות מתמטיות שונות לתיאור עקומי מאמץ - דפורמציה בקרקעות "פריכות" (מ"מ 12)
(a) נוסחת Oida (b) נוסחת Wong

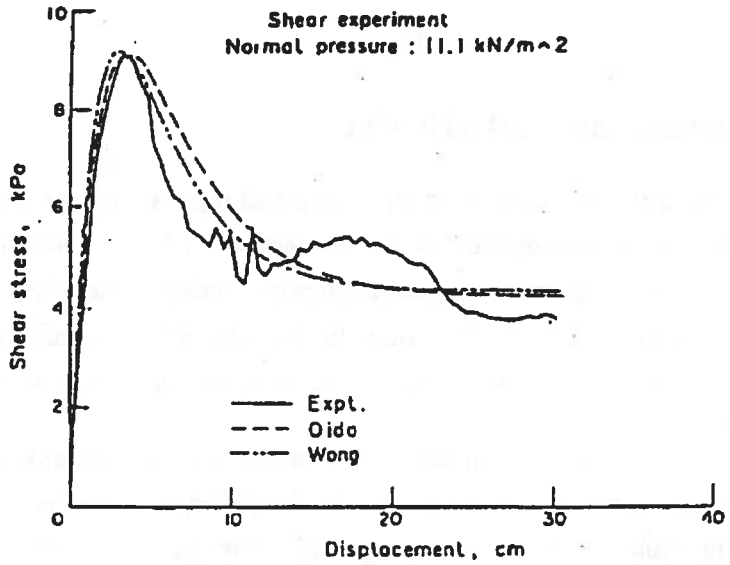


Fig. 2.18 Behavior of "brittle" soils during shear. Comparison between predicted and experimental data (Ref. 12)

ציור מס. 2.18 התנהגות קרקעות פריכות תחת גזירה. השוואה בין התנהגות חזויה לתוצאות מעבדתיות (מ"מ 12)

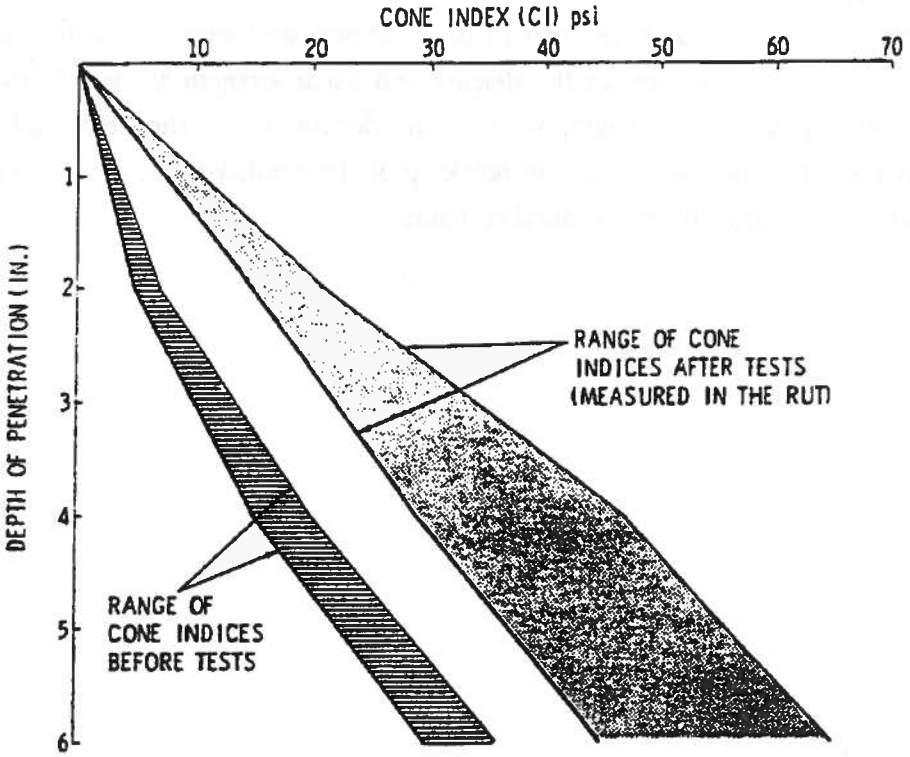


Fig. 2.19 Cone penetration resistance in loose sand before and after passage of wheel (Ref. 13).

ציור מס. 2.19 התנגדות לחדירת דקר קוני בקרקע חולית תחוחה לפני ולאחר מעבר גלגל (מ"מ 13)

## 2.6 Changes in soil strength under wheel loading

A number of references in the literature have addressed and reported on the phenomenon of soil strength change as a consequence of the passage of a loading wheel. Ref. 13 presents a discussion of the change in soil characteristics in relation to the wheel pass. The discussion centers on tandem-wheel systems, where the soil characteristics after the pass of the leading wheel must be known in order to analyze the behavior of the rear wheel.

Table 2.2 (After Ref. 13) presents estimates of the phenomena of strength changes in various soils in the rutting path as a consequence of the passage of the leading tandem wheel. The data in the table are no more than general estimates based on experiments conducted in various soils with the movement of a rigid wheel, in which the soil strength was measured by means of a cone penetrometer.

Figs. 2.19 and 2.20 show the distribution of soil strength before and after the passage of the wheel. Loose sandy soil showed a clear tendency to strengthen, probably due to its compression, as compared to loam, where a weakening of the soil was evident after the passage of the wheel. The big differences in soil strength before and after the passage of the wheel, demonstrate the importance of addressing this point. The behavior of the soil in the rutting lane is generally obtained by combining two factors with different effects on the soil strength. On the one hand, the soil in the confined area tends, in many cases, to compact, and hence an increase in the density and shear strength values. Conversely, phenomena of decreases in strength, such as the destruction of the cementation, the breaking of the inter-granular bonds, the breaking of the capillary ties, etc., appear as a consequence of remolding the soil's initial structure.

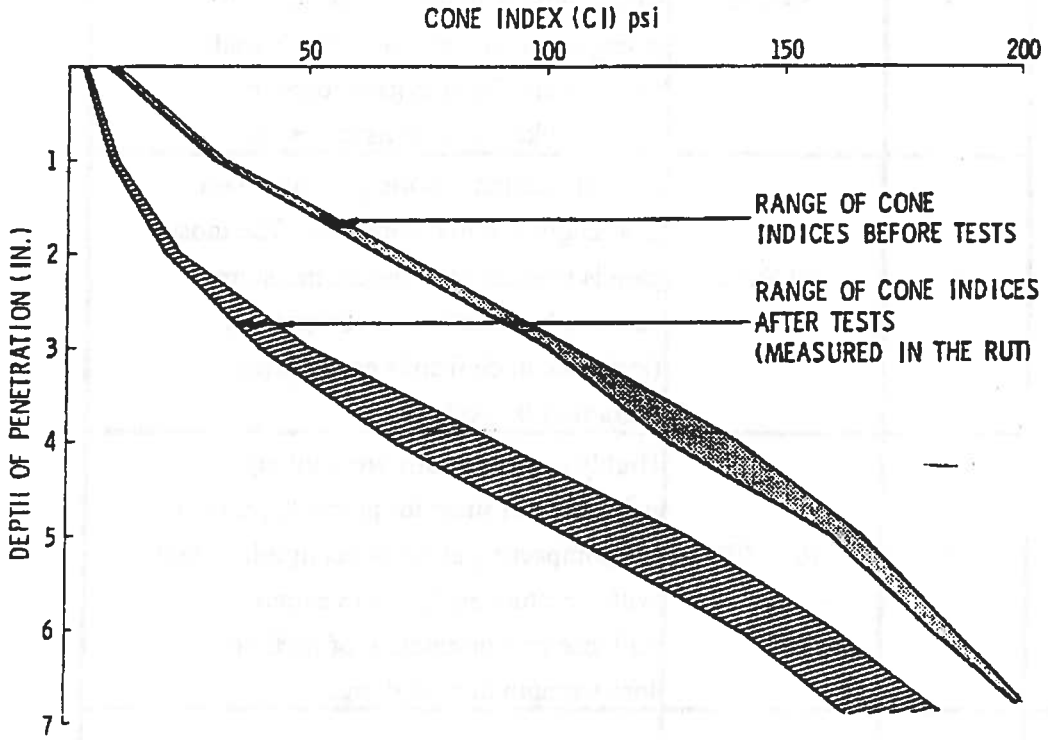


Fig. 2.20 Cone penetration resistance in loam soil before and after passage of wheel (Ref. 13).

ציור מס. 2.20 התנגדות לחדירת דקר קוני ב־ loam לפני ולאחר מעבר גלגל (מ"מ 13)

**Table 2.2: Changes in Soil Strength Under a Passing Wheel. (After Ref. 13).**

**טבלה 2.2: שנויים בחוזק קרקעות שונות כתוצאה ממעבר גלגל (מ"מ 13).**

| Soil Type | Category | Degree of Saturation | Effect on Soil Properties |
|---|---|---|---|
| SEDIMENTARY | a | 0-30% | Cohesionless loose soils gain in strength due to compaction. Very dense cohesionless soils (unlikely to occur in nature) lose strength due to reworking. Friable silt and clay are likely to gain strength. Loess is likely to lose its cohesion. |
| | b | 30-90% | Partially saturated soils generally gain in strength due to compaction. The most gain is attained at optimum moisture content. Information on compaction (available in civil soils engineering literature) is applicable. |
| | c | 90-100% | Highly saturated soils are unlikely to gain strength since for practical purposes the compacting effect is negligible. Clays with structure are likely to experience collapse or reorientation of particles and lose strength in reworking. |
| RESIDUAL | d | 0-100% | Residual soils usually exhibit some cohesion due to their structure. If wheel load breaks the structure (lead wheel sinks significantly), cohesive strength is likely to be lost in reworking. |

The soil strength after the passage of the wheel will be determined by the relative dominance of these two general factors of influence.

The high loading rate of the wheel dictates a situation of undrained loading which does not allow changes in volume in many soils, even those having a relatively coarse grading. In light of this, in soils close to saturation (category C in Table 2.2), loading is not accompanied with compaction. In this case one can therefore expect phenomena of strength decrease as a consequence of the disturbance of the original soil structure. When the soil's rate of saturation is lower, the compaction of the soil is usually possible and one can therefore obtain higher strength values after the passing of the wheel, especially in those cases where the original density was low and the structural strength (which was disrupted by shearing) was also low.

Ref. 14 presents the results of experiments conducted by repeated passes of a pneumatic wheel over sandy soils (only about 5% passing sieve #200) which contained cementation. The soil's strength as it changes with the number of wheel passes (see Fig. 2.21), demonstrates the above. The first pass of the wheel caused a 60% decrease in the soil's strength due to the breaking of the inter-granular cementation. Repeated passes of the wheel led to a gradual increase in the soil strength as a result of continued compaction of the sandy soil. Following the first pass, the cementation seemed to disappear, and the only factor which effected the change in strength was the compaction element.

In wet soil (no more details are given as to the moisture content of the soil), the decrease in soil strength was much less significant (only about 25%). Ref. 15 also reports actual aircraft landing exercises which were carried out in sandy areas in which cemented sand with relatively high strength was remolded and loosened by the very first aircraft landings.

## 2.7 Preliminary observations in granular remoldable soils under wheel loading.

Ref. 16., presents the results of landing exercises of C-130 aircraft at two sites in Israel. The local soils at the two sites lack plasticity and have been defined as A-1-b (site T) and A-2-4 (Site S) according to the AASHTO method. Despite the very high initial strength values obtained by means of DCP tests (CBR values in the range of 40%-100% at site T and in the range of 40%-80% at site S), extremely significant rutting was measured, far beyond that predicted by accepted design nomograms.

Fig. 2.22 presents an example of the rutting results obtained at site T along the runway following 6 and 10 cycles of C-130 landings. (The B value denotes the height difference

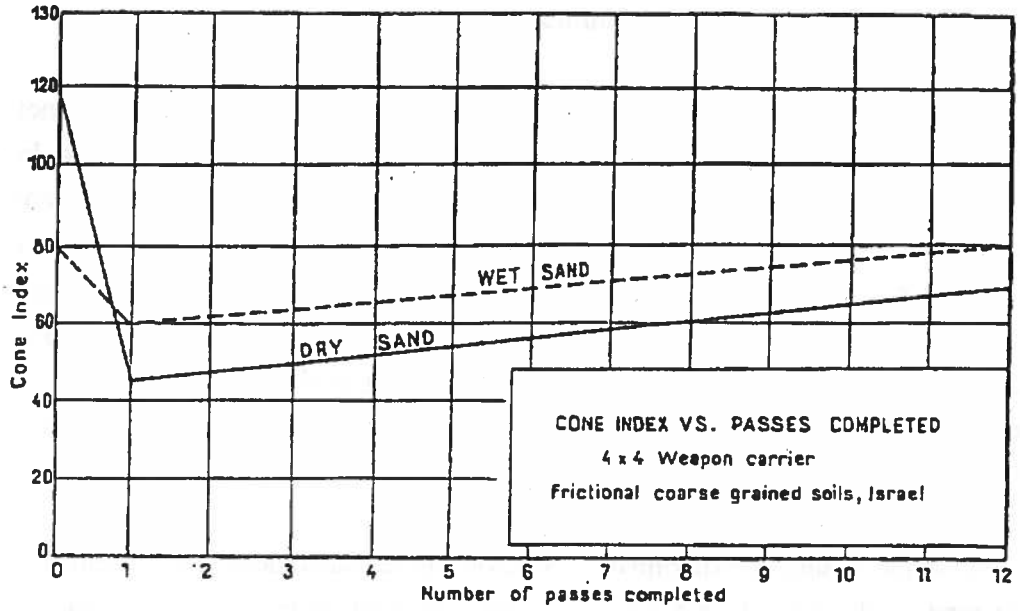


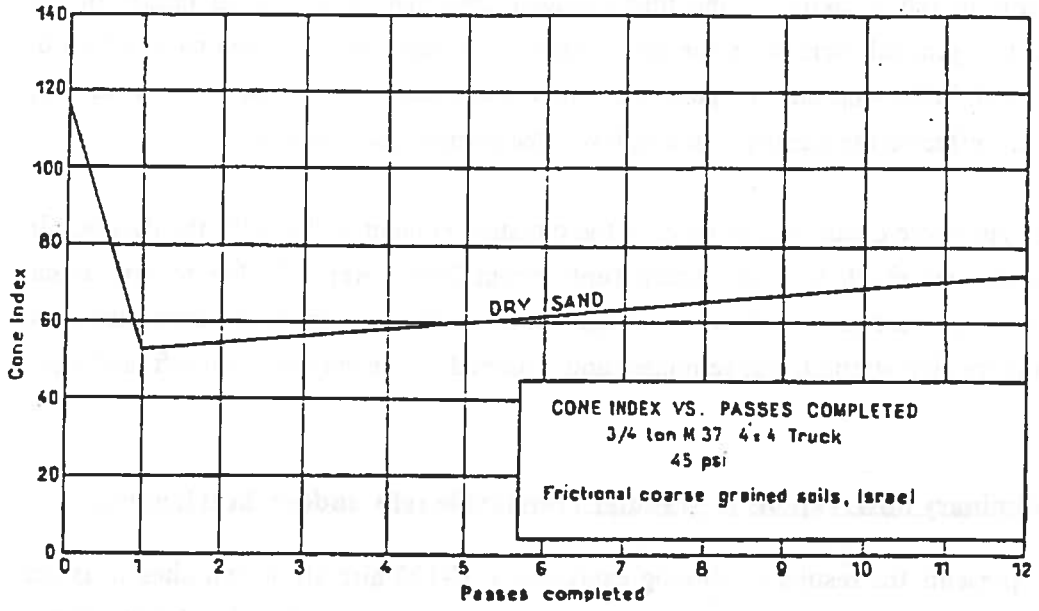


Fig. 2.21 Cone index Vs. vehicle passes in a sandy soil with natural cementation (Ref. 14)

ציור מס. 2.21 אינדכס קוני כנגד מספר מעברי רכב בקרקע חולית עם צמנטציה טבעית (מ"מ 14)

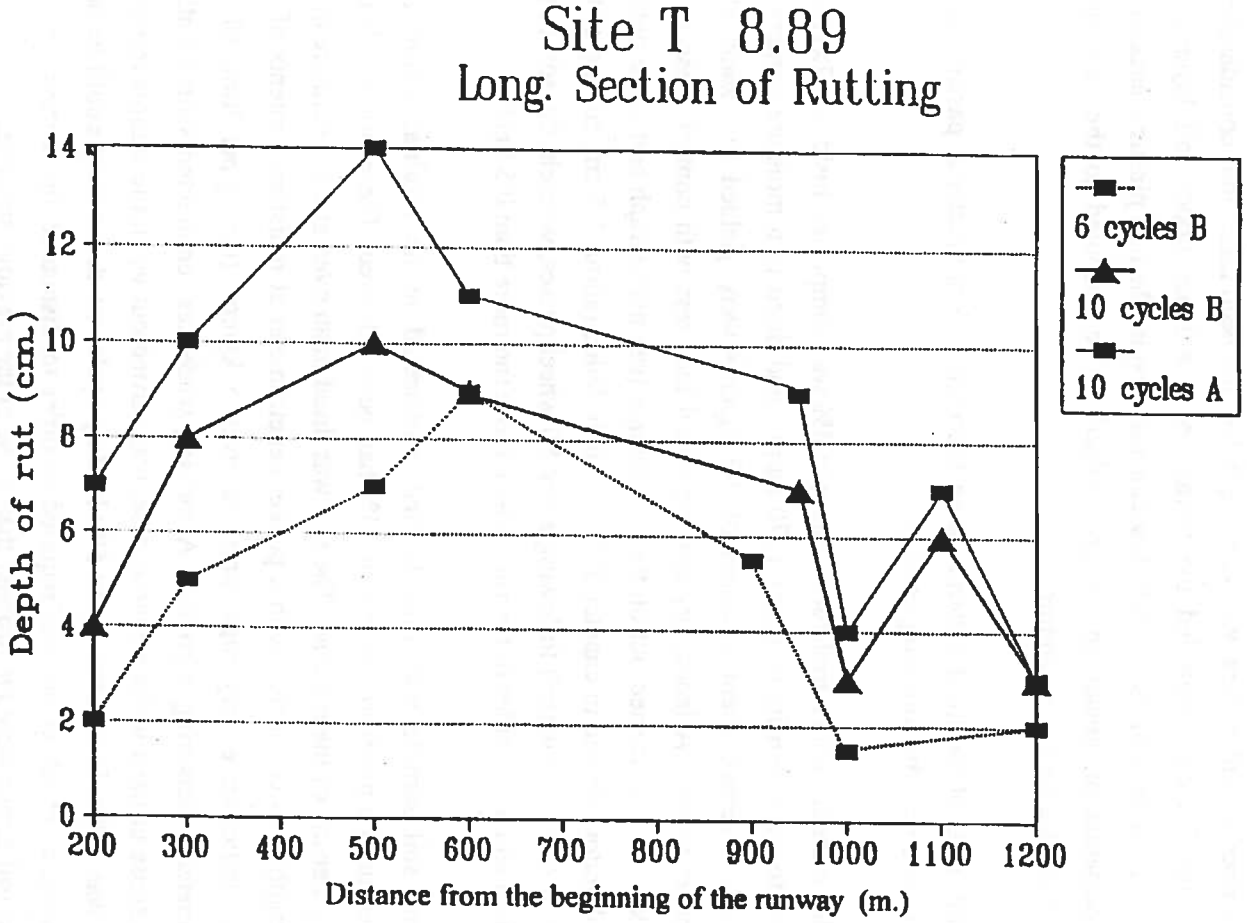


Fig. 2.22 Rutting results obtained at site T along the runway following 6 and 10 cycles of C-130 landings (Ref. 16).

ציור מס. 2.22 תוצאות חריצה שהתקבלו באתר T לאורך המסלול לאחר 6 ו- 10 מחזורים של מטוס C-130 (מ'מ 16)

from the original surface to the bottom of the rut, while the A value indicates height difference from the earth mounds at the sides of the rut to the bottom of the rut). Strength tests conducted at the center of the rut after the completion of each series of landings did not reveal any significant change in the soil's strength (Ref. 16). Strength tests conducted after the completion of the loading cycles revealed loose material at the bottom of the rut to a depth of a number of centimeters, whose strength had not been taken into consideration. Later tests at site T clearly revealed the formation of a loose upper soil layer as a consequence of the passage of the aircraft. It seems that despite the non plastic character of the soil, the cementation created in the unremolded soil contributed to the very high strength prior to the beginning of landings.

Initial laboratory tests of the local material taken from site T (only material passing sieve #10 was used), produced the following results:

a. Remolded material with a moisture content of 4% was compacted inside a 37x18x10 cm. mold, to a dry density of about 1770 kg/m$^3$, and dried to a moisture content of about 2.0%. Average strength values of 2-3 kg/cm$^2$ were yielded by means of a pocket penetrometer. A laboratory moving wheel load test with contact pressure of about 5 kg/cm$^2$ was carried out on the soil sample (see photograph and more details on the laboratory device in chapter 5) The sample failed (about 1.5 cm. rutting of the 15 cm. diameter rigid wheel) following about 80 wheel passes, wherein the soil in the rutting area and to the sides of the rut became loose (no more than 0.5 kg/cm$^2$).

b. The same soil sample was then leveled, compacted to its original height and moistened until a moisture content of 14% had been achieved. There was no change in the dry density of the material. The soil was dried in an oven at a temperature of 60 °C. Strength tests conducted with a pocket penetrometer at moisture contents of 3% and less, indicated a very high strength, over 5 kg/cm. (the upper limit of the penetrometer's measuring capacity). A moving wheel test conducted with identical loads to those utilized in the previous case, was carried out when the sample moisture content was 1.8%. Even after about 500 loading cycles no destruction could be seen in the sample. Much effort was required in order to dismantle the sample and the resultant soil lumps were far stronger than those of the previous specimen.

These preliminary data may explain the high initial strength of the soil at site T whose natural moisture content was in the range of 1%-2%. The in-soil drying process after rain produces inter-granular cohesion, probably through capillary pressures or minute quantities of cementing factors. A similar phenomenon seems to have been observed in site S as well,

and may have taken place at many other locations, mainly in arid and semi-arid areas where the natural humidity is low.

As mentioned previously, these strength factors are transient, and are annulled after the soil has been loaded to the point of failure. This phenomenon was clearly seen both at the site and in the laboratory in the form of loose and weak soil which was formed over the original soil.

Section 4.3 below presents details of initial experimental results obtained from induced remolding of the local soil at site T (table 4.1). The great difference in soil strength values before and after remolding, emphasizes the need to take this phenomenon into consideration in the design methods of unsurfaced runways.

# CHAPTER 3: SOIL REACTION AND SOIL REMOLDING UNDER CYCLIC AND WHEEL LOADING

## 3.1 Soil behavior under cyclic loading

The issue of accumulating plastic strains in the soil as a consequence of cyclic loading has been studied for a wide range of granular and cohesive soils. Ref. 17 presents a comprehensive survey of the literature and an investigation of the plastic strain characteristics in clayey and sandy soils subjected to cyclic loading at a low loading amplitude relative to the soil's strength. The residual strain accumulating during the loading cycles, called dynamic creep, is described by the equation:

$$\varepsilon_p = A \bullet N^{(1-m)} \qquad [3.1]$$

where:

$\varepsilon_p$ - is the plastic strain.

N - is the number of loading cycles.

A,m - are rutting constants.

This equation in different variations has been proposed by additional investigators quoted in Ref. 17 who have examined and showed its suitability for a wide range of materials. The parameter m has been found to be almost constant for the types of soils and aggregates examined, while the parameter A depends on the structure of the soil, the density, the moisture content, the stress exerted, the soil strength and the dynamic modulus of the soil. The A parameter is in fact the plastic strain resulting from the first load cycle.

Ref. 18 presents the results of cyclic loading experiments in sandy soil under various confinement pressures and changing deviatoric stresses. The correlation defined by equation [3.2] has been found to be a good descriptor of the phenomena of strain accumulation with repeated cycles.

$$\varepsilon_p = a + b \bullet Ln(N) \qquad [3.2]$$

where:

$\varepsilon$ - is the plastic strain;
N - is the number of loadings;
a, b - are empirical constants,

Fig. 3.1 (Ref. 18) graphically describes the results of one of a series of tests and presents the correlation between the plastic strain and the number of cycles for various deviatoric stresses.

The logarithmic relation given in equation [3.1] and the semi-logarithmic one in equation [3.2], present the two most accepted formulas relating plastic strain to the number of load applications. These relations were also adopted for the practical prediction of rutting in conventional pavements under traffic load (see, for example Ref. 19). In all the researches noted above, the stress level exerted on the samples was far lower than the stress required to achieve failure. When higher loads, closer to the load required to failure, were applied on the samples, a significant increase in the rate of plastic strain was noted, deviating from the expected according to the above mentioned equations (see Refs. 17 and 20).
The fact that high cyclic stress levels were hardly investigated can be ascribed to the situation where both in the areas of soil mechanics and conventional road design, the loading of the soil occurs in the low stress range in accordance with safety factors coefficients; the stress in the soil rarely exceeding 30%-40% of the soil's shear strength.

Where rigidly structured remoldable soils are concerned, plastic strains during cyclic loading (providing the maximum stress level is not too high) will be very low. Cyclic loading of the material may eventually lead to fatigue failure, breakage of the strengthened structure and the formation of large plastic strains. A research conducted on the behavior of cement stabilized soil under cyclic loading with stress values close to the soil's strength is reported in Ref. 21. Fig. 3.2 presents the results obtained for the predicted number of cycles to failure at various levels of stress. Testing was conducted for a number of types of soils with a rather high level of cementation. The results of this research correspond to the classic behavior of material fatigue under cyclic loading.

The behavior of roads comprising a thin surface seal constructed on lightly cemented bases and sub-bases was studied and reported in Ref. 22 . The failure in these roads is characterized by the formation of potholes in the pavement, causing much hindrance to drivers. Since these roads are surfaced, and the cohesion level in the base courses is relatively high (in the range of 2 kg/cm$^2$ and higher), the destruction of the road is mainly caused by fatigue failure of the upper part of the cemented layer. Contradictory to unsurfaced pavements and runways where

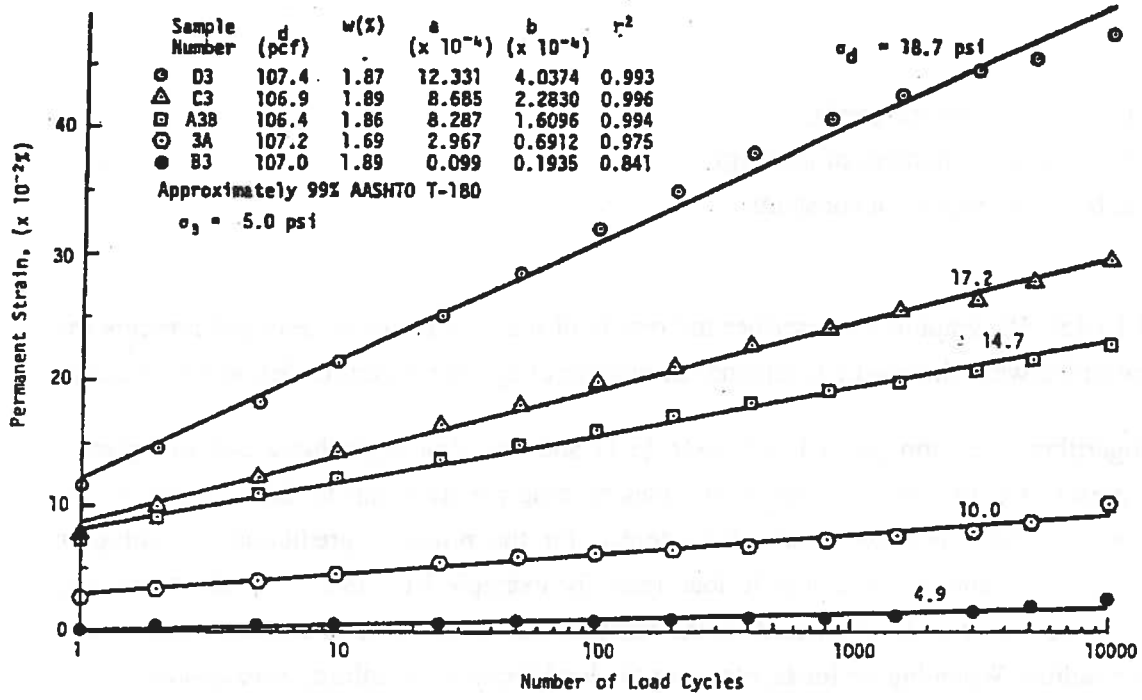


Fig. 3.1 Correlation between residual plastic strain and the number of cycles for different conditions of deviatoric stress. (Carried out under a confinement pressure of 5 psi). (Ref. 18)

ציור מס. 3.1 קורלציה בין העיבור הפלסטי למספר מחזורי עמיסה עבור תנאים שונים של מאמץ דביאטורי (מ"מ 18)

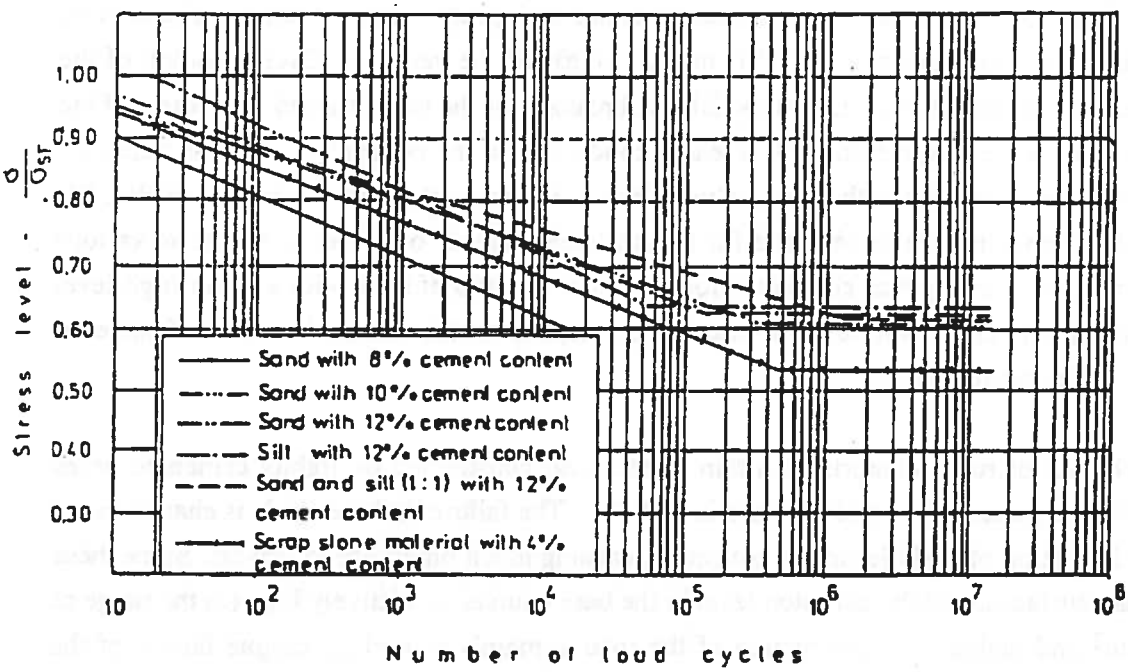


Fig. 3.2 Fatigue curves in soils stabilized with cement (Ref. 21)

ציור מס. 3.2 עקומי התעייפות בקרקעות מיוצבות בצמנט (מ"מ 21)

relatively light rutting levels can be tolerated, the remolding action in the cemented layers of conventional pavements causes a very rapid deterioration of the road functional condition.

### 3.2 Stress paths under a moving loading wheel.

Application under laboratory conditions of a stress path similar to that occurring in the field, is in many cases essential for a better understanding of soil shearing processes.

Ref. 23 presents an analysis of the state of stresses at a point under the pavement surface, resulting from the passage of a loading wheel. In order to facilitate the calculations, the soil was assumed to be an elastic homogeneous semi-infinite medium, and an equally spread load $P_0$, with a width of 2a, is applied to the soil. According to the Boussinesq equations for planar stresses, the following stress components are yielded (see Fig. 3.3):

$$\sigma_V = \frac{P_0}{\pi}\left[\theta_0 + \sin\theta_0 \cos(\theta_1 + \theta_2)\right] \qquad [3.3]$$

$$\sigma_H = \frac{P_0}{\pi}\left[\theta_0 - \sin\theta_0 \cos(\theta_1 + \theta_2)\right] \qquad [3.4]$$

$$\sigma_{VH} = \frac{P_0}{\pi}\left[\sin\theta_0 \sin(\theta_1 + \theta_2)\right] \qquad [3.5]$$

where:

$\sigma_V$ - is the normal vertical stress

$\sigma_H$ - is the normal horizontal stress

$\sigma_{VH}$ - is the shear stress on the horizontal plane

$\theta_0 = \theta_2 - \theta_1$

$\theta_2, \theta_1$ - is the angle in radians between the vertical and the line

connecting each of the ends of the loading surface to the point being tested in the soil. When the values of equations [3.3] - [3.5] are known, it is possible to calculate the principal stresses:

$$\left.\begin{matrix}\sigma_1 \\ \sigma_3\end{matrix}\right\} = \frac{\sigma_V + \sigma_H}{2} \pm \sqrt{\left(\frac{\sigma_V - \sigma_H}{2}\right)^2 + \sigma_{VH}^2} = \frac{P_0}{\pi}(\theta_0 + \sin\theta_0) \qquad [3.6]$$

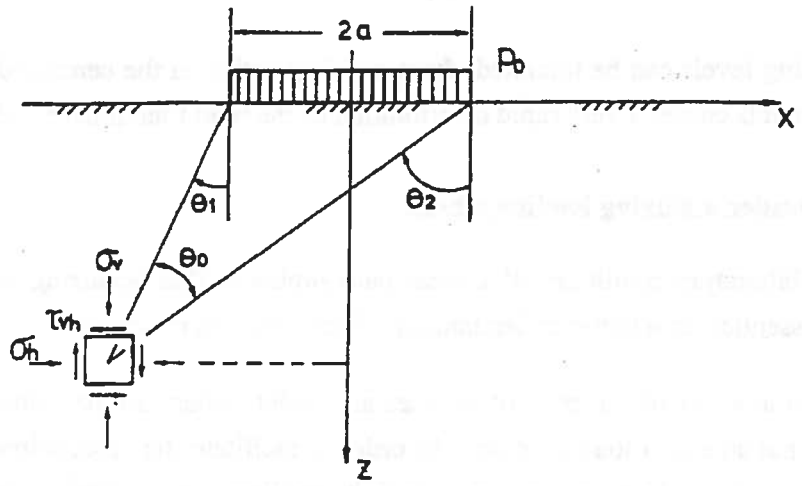


Fig. 3.3 Stress components of a point in homogeneous elastic soil under surface loading (Ref. 23)

ציור מס. 3.3 מרכיבי מאמץ בנקודה בתוך אלסטי הומוגני תחת עמיסה בפני השטח (מ"מ 23)

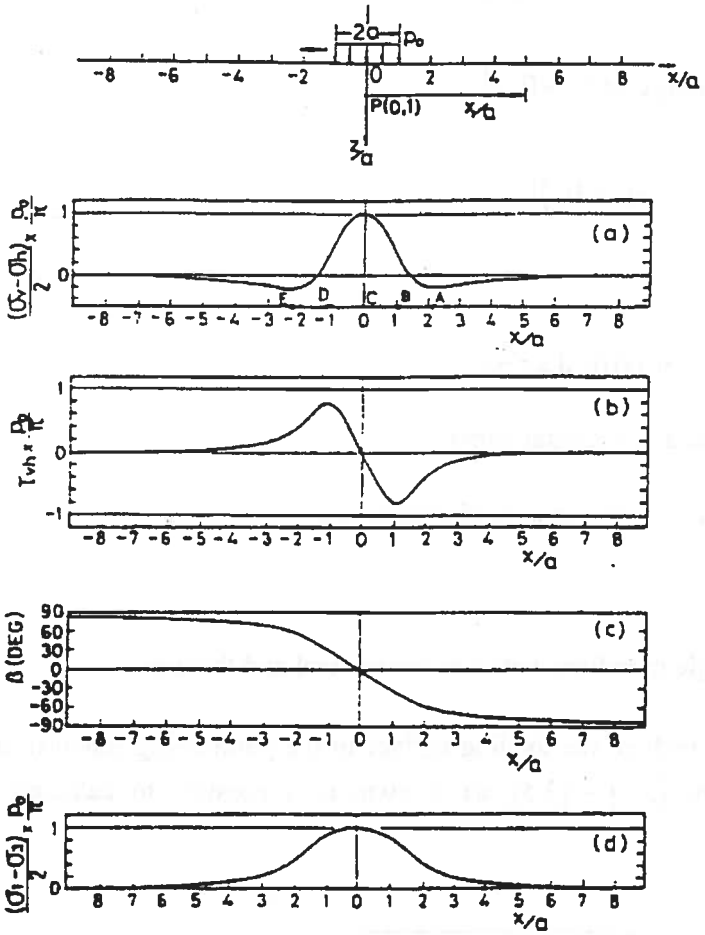


Fig. 3.4 Lateral distribution of a number of stress components at a point in homogeneous elastic soil under a surface loading of 2a diameter (Ref. 23)

ציור מס. 3.4 פרוס לרוחב של מספר רכיבי מאמץ בנקודה בקרקע אלסטית הומוגנית תחת עמיסה בפני השטח (מ"מ 23)

And the direction of the major principal stress relative to the vertical axis will be derived from:

$$tg2\beta = \frac{2 \cdot \sigma_{VH}}{\sigma_V - \sigma_H} = tg(\theta_1 + \theta_2) \qquad [3.7]$$

Thus, one can calculate the distribution of the various stress elements along the vertical plane at various distances from the loaded area (see Fig. 3.4 presented in Ref. 23). In the case of a moving wheel, every point at a certain depth will undergo the entire stress path as depicted in Fig. 3.4 during the passage of the wheel. Accordingly, when it is required to simulate the stresses acting on a point of soil under the load of a moving wheel, one must consider the simultaneous changes which take place in the size and the direction of the principal stresses at that point.

Cyclic shear tests on loose sand were conducted (see Ref. 23), using two different stress paths. The first was the conventional stress path of the triaxial compression test, and the second was a stress path which emulates the stress induced by a passing wheel (as depicted in Fig. 3.4). The results (see Fig. 3.5) show a great difference in soil reaction due to different stress paths (residual volumetric strain was up to 5 times greater in the latter stress path).

Actual wheel loading on unsurfaced soil is much more complex than assumed in the above analysis and the soil reaction is not purely elastic. However, the results given in Ref. 23 emphasized the importance of comparing as closely as possible the stress paths pertaining in the field, in order to understand better the soil behavior under the given condition.

The above issue is important when considering laboratory experiments intended to investigate soil behavior under wheel loads. Ref. 17 also addresses this issue, but on account of an absence of appropriate laboratory equipment, the experiments were carried out in a triaxial shear device, with alteration of the confinement pressure during loading. The desirable solution in this case is the simultaneous change of both the confinement pressure and the principal stress direction during the loading process.

## 3.3 Off-the-road mobility - general approaches to the prediction of wheel soil system.

The behavior of the wheel-soil system depends on a large number of parameters including:

1. Dimensions and structure of the loading wheel (width, diameter, tire profile shape and structure, inflation pressure, carcass characteristics, etc.);

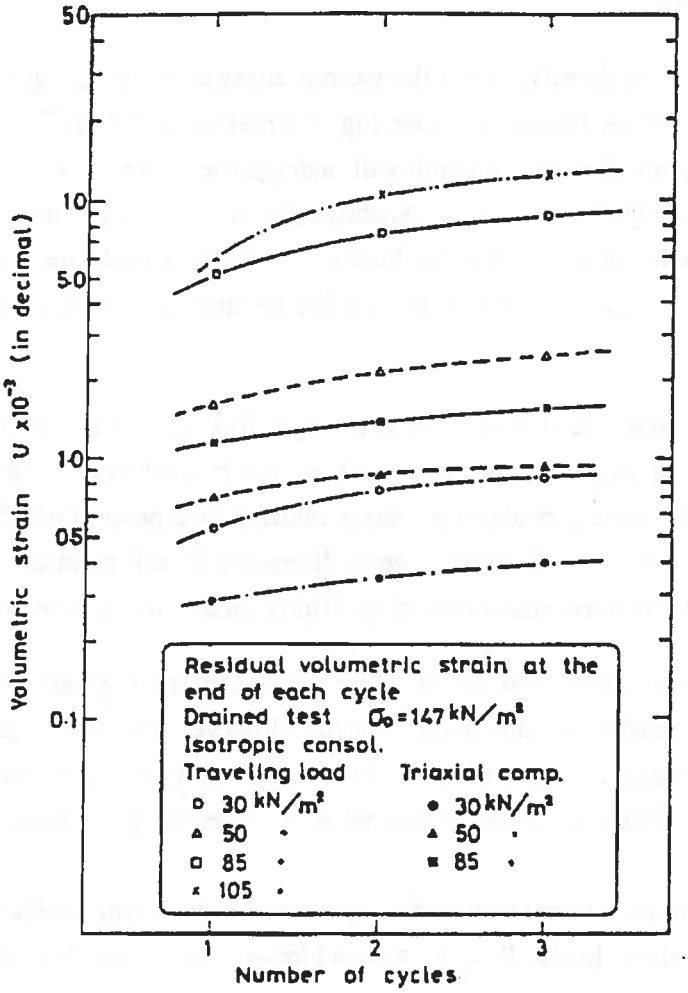


Fig. 3.5 Comparison of volumetric strains between samples tested under a moving wheel simulation and samples tested under regular triaxial shear (Ref. 23)

ציור מס. 3.5 השוואת עיבורים נפחיים בין מדגמים שנבדקו תחת סימולציה של גלגל נע לבין מדגמים שנבדקו בגזירה מרחבית רגילה (מ"מ 23)

2. Loading conditions (total wheel load, induced moment on wheel);
3. Soil parameters (soil constitutive laws, strength parameters, compaction, etc.);
4. Traffic conditions (lateral wander of wheel loadings, wheel velocity, slip and skid rates);
5. Wheel-soil interface.

A variety of methods were tested in order to predict the behavior of the wheel-soil system on unsurfaced roads and off-the-road. Due to the very complex nature of the system and the unavoidably high level of simplification, the selection of a particular method or approach was, to a great extent, influenced by its intended application. The different methods suggested for the solution of the problem can be divided into three main categories:

1. **Empirical Methods**

Several empirical methods, based on laboratory experiments and field observations, were developed in an attempt to build correlative relationships between the characteristics of the wheel-soil system and the predicted performance. The empirical prediction methods were built, in most cases, for direct practical purposes, a fact which dictated simplicity and ease of use. One of the earlier methods was the WES VCI model which was refined and developed by other groups (including the NATO mobility model). According to the WES (Waterways Experiment Station) model, a value of a VCI (Vehicle Cone Index) parameter, defining the minimum strength of the soil required for 1 or 50 vehicle passes, is calculated for given vehicle and loading characteristics. The soil strength is measured in the field by the use of a cone penetrometer, and its value is in CI (Cone Index) units. If CI value of the soil is less than the VCI, then a "no go" condition is established. If CI is larger than VCI, then CI-VCI (the "excess" strength) is used to predict the wheel-soil behavior in terms of sinkage, draw-bar pull, etc. Different relationships were established for granular and cohesive soils.

For single wheel performance, empirical models were developed by Freitag in WES (Ref. 24,25,26), in an attempt to consolidate data relating to the soil strength, loading conditions and wheel dimensions into one representative parameter (different number for sand-$N_S$ and for clay $N_C$). For example, for clayey soils, the parameter is:

$$N_c = \frac{CI * b * d}{W} * \left(\frac{\delta}{h}\right)^{1/2} \qquad [3.8]$$

where:

CI - cone index value of the soil;

b - width of the wheel;
d - wheel diameter
W - wheel total load
$\delta$ - tire deflection
h - tire height
$\left(\frac{\delta}{h}\right)$ - relative deflection of the air-inflated tire.

The above parameters are correlatively linked with different performance values of the wheel-soil system (see for example Fig. 3.6, from Ref. 26). A rather large number of modifications to the above method have been introduced during the last thirty years, but the basic separation into sandy and clayey soils remains.

The primary disadvantage of all the empirical methods is the lack of a theoretical basis linking the results to a logical model of the behavior of the wheel-soil system. Therefore, even small changes in the system's components (like different soil or dissimilar wheel diameter or tire structure), may lead to unpredictable results.

2. **Semi-Empirical Methods**

The semi-empirical methods are also based, to a large extent, on carrying out laboratory and field testing. However, an effort is made to incorporate some degree of physical logic into the solution, a fact which makes extrapolation of the results more acceptable. Some sources (Ref. 27), consider the Freitag method (ref. 24), as semi-empirical because it was originally developed through undimensional analysis of the problem.

The best known semi-empirical method is the one suggested originally by Bekker in 1956 (Ref. 12,27). The method assumes that the pressure exerted by the wheel on the soil is purely radial, and is equal to the normal pressure beneath a horizontal plate driven to the same depth. The wheel sinkage and forces acting on the wheel are calculated by use of different equations derived by integration of the reaction of the soil to the penetration and movement of the loading wheel. The suggested equations require the use of seven soil parameters, the values of which are measured and calculated by various laboratory and field tests, including plate penetration tests.

Special field testing devices (such as the Bevameter , Ref. 12), were built in order to enable practical use of the method. However, the need to find the value of seven soil parameters, compared to the one parameter required by other methods, is still the most problematic point in the suggested method.

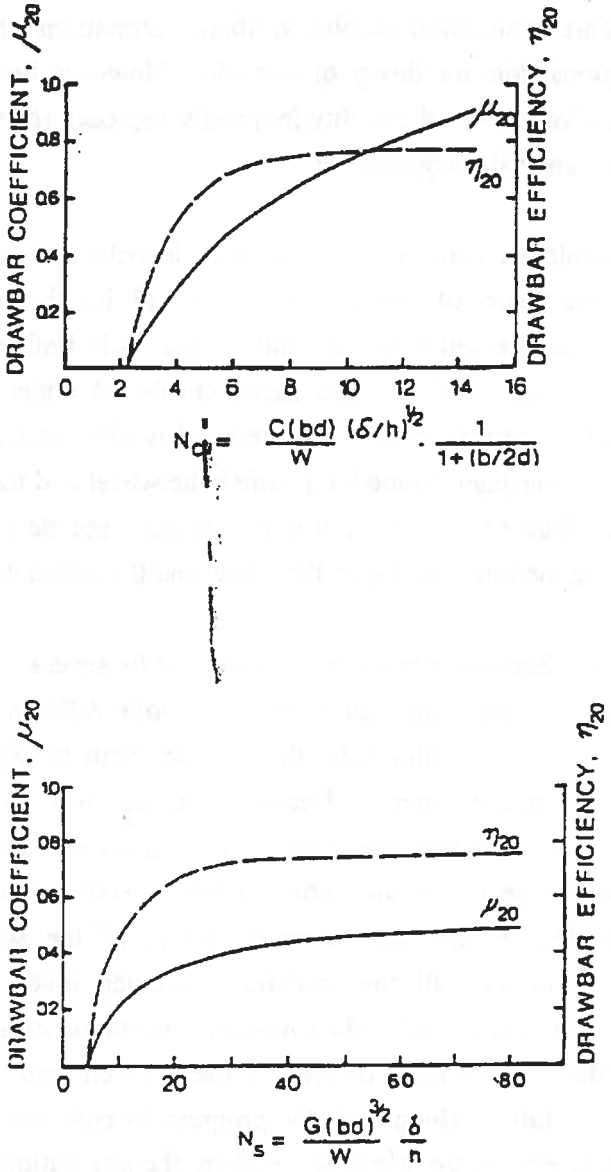


Fig. 3.6 Correlations between $N_C$ and $N_S$ to the drawbar performance of a wheel at 20% slip rate (Ref. 26)

ציור מס. 3.6 קורלציות בין מספר עבירות חרסית $N_C$ ומספר עבירות חול $N_S$ לערכי הסחב של גלגל ב- 20% החלקה (מ"מ 26)

3. **Analytical Methods**

A large number of analytical methods were developed for the prediction of the wheel-soil system (Ref. 12,28). Some earlier works attempted to analyze the system, assuming elastic behavior of the soil. This assumption enables to obtain estimations of stresses in the soil, based on accepted solutions from the theory of elasticity. However, the stress levels usually encountered in the area of off-the-road mobility frequently approach the strength of the soil; a fact which renders elastic analysis inappropriate.

Some methods were developed using limit analysis to describe soil behavior under wheel loading. According to the theory of plasticity, it is assumed that the soil behavior is rigid-perfectly plastic, and that all the soil within the failure zone is in limit equilibrium. Fig. 3.7 (Ref. 13), depicts an example of the failure zones developed under a moving wheel as calculated by the method of characteristics. Some researches (Ref. 62), attempted to describe the wheel-soil system by a mechanistic model in which the wheel and the soil are represented by systems of springs. Due to its nature, this model does not deal with soil stress but concentrates on predicting the forces acting in the wheel and the wheel-soil interface.

Numeric solutions to the wheel-soil system have been tried by several researchers during the last twenty years. The solutions were mainly based on finite difference and finite element methodologies. In the earlier investigations, the soil was usually assumed to be a linear elastic or piece-wise linear elastic material. Recent researches (Ref. 28), assume other types of soil constitutive laws such as viscoelastic, elastic-plastic and rigid-perfectly plastic models. Development during the last years presents certain headway in the wheel-soil analysis by the finite element method. Due to the very complex nature of the wheel-soil system and computing resources limitations, all the analytical methods involve a high degree of simplifying assumptions in their models. Most models concentrate on specific points, which seem to be indispensable from the point of view of the research goals, while omitting other less crucial points. In the future, along with the progress in both computing resources and knowledge of different aspects of the wheel-soil system, the integration of these features to a more general model will become feasible.

## 3.4 Existing methods for the prediction of the performance of unsurfaced runways.

The research in the area of unsurfaced runways was mainly concerned with trying to predict the capability of the runway to sustain a number of repeated aircraft loading. In comparison to the area of mobility and terramechanics research (see section 3.3), less effort was devoted to a close investigation of the details of wheel-soil interaction. Emphasis was placed on the other

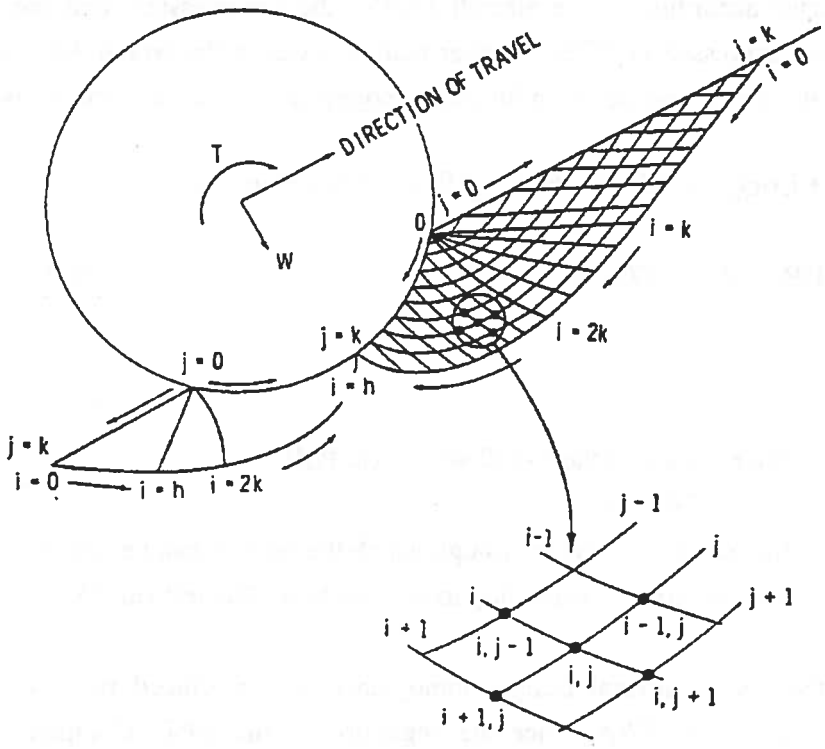


Fig. 3.7 Failure zones under a moving wheel (Ref. 13)

ציור מס. 3.7 גבולות איזורי ההרס תחת גלגל נע (מ"מ 13)

hand, on the influence of multiple number of loadings on the runway condition. All the accepted methods for unsurfaced runway performance prediction are highly empirical and based on laboratory experiments and field observations. Fig. 3.8 (Ref. 29) gives an example of a design nomogram used to predict the number of aircraft coverages up to the runway functional failure. A coverage means actual loading of the critical point in the runway. The cycle/coverage ratio can be calculated for each aircraft according to its wheel geometry and lateral wander (see for example Ref. 29). The above mentioned nomogram estimates the runway performance according to the aircraft ESWL, the tire pressure, and the equivalent strength of the soil expressed in CBR. Another relation used by the Israeli Air-Force for the operation of C-130 aircraft and based on former nomograms and local experience is (Ref. 30):

$$0.48966 \cdot \mathrm{Log}(p) + 0.580426 \cdot \mathrm{Log}(P) + 0.1716 \cdot \mathrm{Log}(N) -$$

$$-\mathrm{Log}(CBR) - 2.83227 = 0 \qquad [3.9]$$

where:

p - tire pressure of the C-130 wheels (in PSI)
P - is the ESWL (in lb.)
N - the number of cycles through which the runway can be operated
CBR - the soil strength according to the standard CBR test (in %)

In addition to the above, several design nomograms for unsurfaced runways have been published, especially in the USA, since the beginning of the 1950. Comparison of those nomograms (see Ref. 31), reveals differences of up to two orders of magnitude in the predicted number cycles for the same level of soil strength. Similar results are often obtained when comparing estimates made by the prediction nomograms to observations of actual unsurfaced runway operations (Ref. 16).

The above scatter of results stems from a variety of reasons, among them (Ref. 32):

1) The actual variation of soil strength from point to point along the chosen landing strip.
2) The inability of only one strength parameter (derived through the use of one of the penetration tests) to describe soil behavior successfully.
3) Changes in the dynamic nature of aircraft operations on the runway, such as "hard" landing, braking operations during landing, accelerated take-off, landing gear mechanical characteristics, etc.

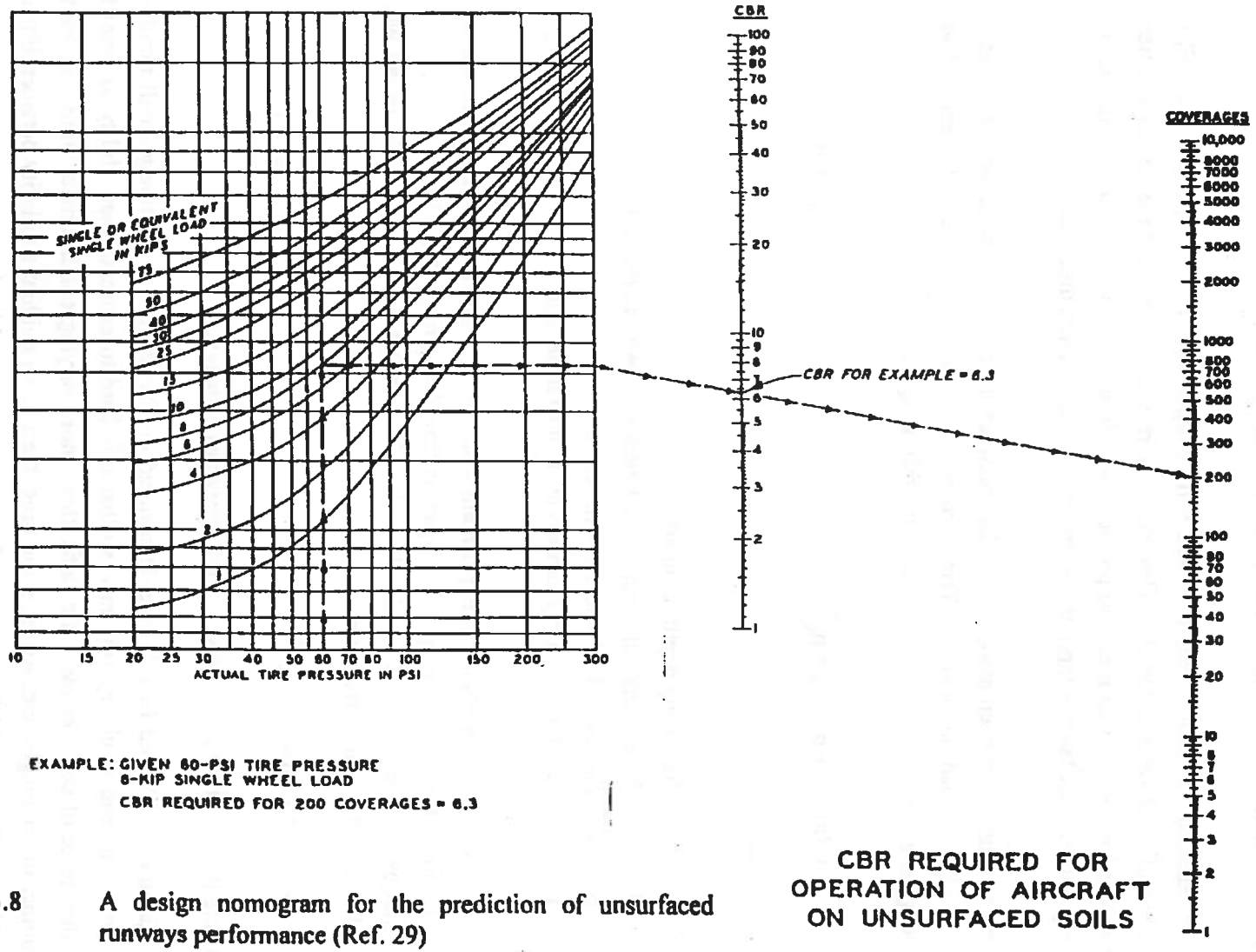


Fig. 3.8 A design nomogram for the prediction of unsurfaced runways performance (Ref. 29)

ציור מס. 3.8 נומוגרמה לחזוי מספר המחזורים להרס של מטוס על מסלול עפר (מ"מ 29)

4) Changes occurring in soil strength during, and as a result of, runway operation, a phenomenon which was the subject of the present research.

Some research has endeavored to assess soil strength from rutting values of the soil under wheel loading of various vehicles. This empirical research, conducted mainly for practical and operational purposes, was meant to provide the field engineer with a tool to estimate the soil strength to be used later as input in the performance prediction methods.

Some attempts have been made to correlate between the rutting of unsurfaced pavements and the number of load applications. Trials wherein clay soil was loaded with repeated vehicle coverages, as reported in Ref. 33, yielded the following correlation:

$$r = 0.00107 \cdot n^{0.5} \cdot d \cdot n_C^{-2.6} \qquad [3.10]$$

where:

r - is the rutting depth (in inches).
d - is the external diameter of the unloaded wheel (in inches).
n - is the number of wheel loading cycles.
$n_C$ - is the Clay Mobility Number, as defined in section 3.3.

The fit between the results of the experiment with a vehicle and the above equation, is seen in Fig. 3.9 for 2, 6 and 10 coverages (the figure is reproduced from Ref. 33).
Similar experiments reported in Ref. 33 with C-130 aircraft wheels and C-5A aircraft wheels, yielded the following correlation.

$$r = 0.001 \cdot d \cdot N_c^{-2.27n^{0.22}} \qquad [3.11]$$

Where the variables are defined as in the previous equation.

Equations [3.10] and [3.11] were determined on the basis of a relatively small number of experiments and in clayey soil only, so that it is hard to estimate their ability to describe a wider range of soils, or even the same clay, under varying conditions of moisture, loading, number of coverages, etc. At the same time, there is an evident similarity between Equation [3.10] and Equation [3.1]. Equation [3.1] (relating to the plastic strains accumulation in the soil) seems preferable from the point of view of the quantity of experiments and reports presented in the literature.

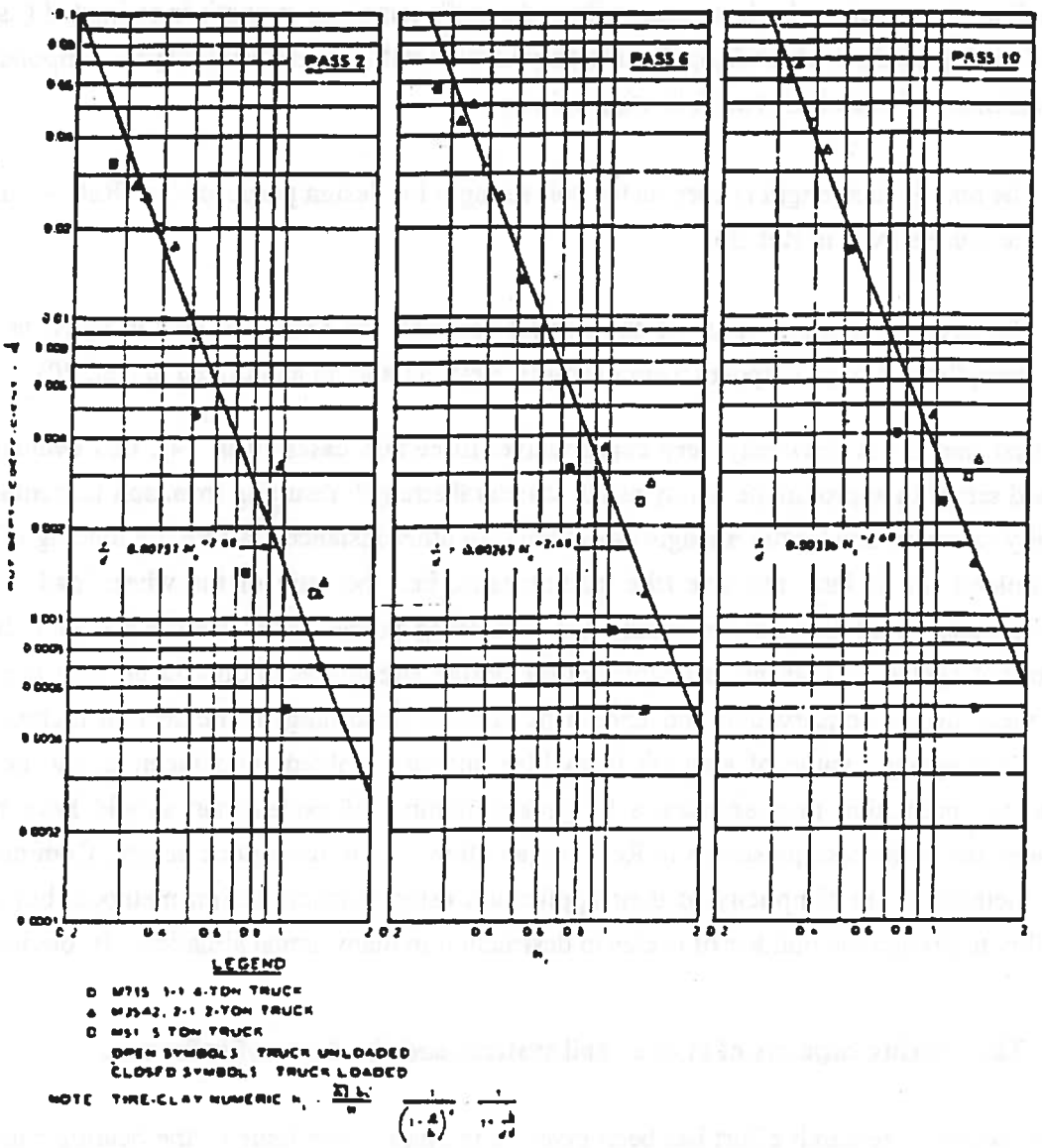


Fig. 3.9 Relation between $N_C$ and repetitive wheel rutting (Reported by Ref. 33)

ציור מס. 3.9 קשר בין ערך $N_C$ לבין חריצה הנגרמת על ידי מעבר חוזר של גלגל (מ'מ 33)

## 3.5 Approach of present design methods to the remolding phenomenon.

All existing design and prediction methods require, as part of the design process, that the value representing the soil strength be obtained in order to allow the prediction of the number of cycles to failure. The usual design process rarely includes any direct discussion of the soil remolding phenomenon. In those cases where the soil's remolded strength is estimated (using a field testing method which is applicable only in soils with a significant clayey component), use was made of one of the two following values:

a. The remolded strength is used as the soil strength for design purposes (see Ref. 34 and a literature survey in Ref. 35).

b. The average strength value of the natural soil and the remolded soil is taken as the strength for design purposes. (For example, Refs. 33 and 36 mentioned in Ref. 20).

The first method is obviously very conservative. In certain cases (Ref. 14), this evaluation method seems to approximate reality as the structural strength resulting from soil cementation actually seems to break after a single wheel pass. In other instances, where the loading of the unremolded soil is less intensive (the loading ratio, i.e., the ratio of the wheel load to the bearing capacity of the soil, is small), the remolding process may continue over a large number of cycles, so that the estimation of the design strength according to the first method may yield overly conservative and unrealistic results. According to the second method, in which the average value of strength (remolded and unremolded) was taken as the design value, the prediction may estimate a far greater number of cycles than should have been foreseen (as in the case presented in Ref. 14). and thus lead to dangerous design. Common to both methods is the simplicity of their application using existing design methods, but their inability to predict the number of cycles to destruction in many actual situations is obvious.

## 3.6 The bearing capacity of layered soil systems and the depth of influence.

Quite extensive research effort has been given in the past to the issue of the bearing capacity of layered systems (Ref. 37,38,39,40). In the two-layer case where the upper layer is weaker than the lower. the bearing capacity of the whole system depends on the thickness of the upper layer, and drops from the bearing capacity of the lower layer (for a zero thickness of the upper layer) to the bearing capacity of the upper layer (for a very deep upper layer).

An estimation is given (Ref. 39), of the bearing capacity of a footing on such a two-layer soil system:

$$q = q_{tv} + (q_{bv} - q_{tv})(1 - H/H_f)^2 \qquad [3.12]$$

where:

$q_{tv}$ - bearing capacity of the foundation on a homogeneous soil possessing the properties of the upper layer soil;

$q_{bv}$ - bearing capacity of the foundation on a homogeneous soil possessing the properties of the lower layer soil;

$H$ - thickness of upper layer soil;

$H_f$ - depth of failure surface beneath footing in a homogeneous soil possessing the properties of the upper layer soil.

The above relationship is valid where the bearing capacity values of the two layers do not differ significantly.

The present research focuses on the behavior of remoldable granular soils, which contain some degree of cementation before being remolded. In such a case, it may be shown that the bearing capacity of the soil after remolding (without the cohesive part of the soil's strength), is much lower than before the remolding action. For example, for a granular cemented soil subjected to a circular plate loading, we obtain (Ref. 41) a bearing capacity value of:

$$q = (1 + \frac{N_q}{N_c}) \bullet C \bullet N_c + 0.6 \bullet \gamma \bullet R \bullet N_\gamma \qquad [3.13]$$

for the following soil properties:

$\gamma$ = 1.9 $10^{-3}$ kg/cm$^3$ - density of soil

R = 0.4

$\phi$ = 40°

C = 0.1 kg/cm$^2$

one obtains $N_C$ = 75.31, $N_q$ = 64.2, $N_\gamma$ = 109.41

and q = 13.95 + 0.05 = 14.0 kg/cm$^2$

As can be easily perceived, if the cohesive part of the soil strength vanishes due to the breakage of the cementing bonds, the bearing capacity of the soil drops to less than 1% of the original bearing capacity.

In cases such as the above, a simplifying assumption can be made (Ref. 40), that the upper layer rests on a rigid (and unyielding) base. The general pattern of soil failure no longer resembles that shown in Fig. 3.10a. Instead, the upper soil is pushed aside between the loading element and the underlying layer in a squeezing action (Fig. 3.10b).
The bearing capacity of a foundation lying on such a soil system may be high, and approach the bearing capacity of the lower layer (for small relative values of the upper layer depth). Fig. 3.11 presents a table (Ref. 37) which contains modified $N\gamma$ values for a thin granular soil layer resting on a rigid foundation. According to this table, obtained through numerical analysis, the bearing capacity of a strip footing on a layer of $\phi = 40^\circ$ granular soil with 0.5 B depth (B is the width of the foundation), is 3.27 times the bearing capacity of the same foundation on homogeneous soil. An experimental research was conducted (Ref. 38), with sandy soil over a rigid base, yielding bearing capacity values ranging from 2 - 10 times higher than those obtained in (Ref. 37).

The accepted methods of performance prediction for unsurfaced runways require that a representative CBR value of the soil (or some other value representing the soil shear strength, such as DCP, AI, CI, etc.), be input into the calculation of the number of cycles to failure. Several suggestions are given in the literature as to the way of determining the above representing strength in cases where the soil strength changes with depth. Most of the suggested methods are practical, and lack sound physical basis.

Ref. 42 addresses CBR values down to a depth of 12", (termed as the influence zone or the critical layer). The representative CBR value is established as the mean of the values taken at depths of 6, 8, 10 and 12 inches. An influence zone of up to a depth of 12" is used by a number of other references dealing with aircraft landings on unsurfaced runways, and is also the depth usually used in mobility forecasting of ordinary or military vehicles on soil (see Ref. 43). The depth of the critical layer according to Ref. 44 depends on the type and weight of the vehicle, and on the strength profile of the soil. For wheeled vehicles weighing more than 50,000 lbs., the critical layer lies 9-15" from the surface. The strength value of the soil is determined in this case by averaging the cone index readings in the critical layer. In soils where the cone index readings do not increase consistently (or at least remain constant) with depth, the soil strength is determined for the critical layer, as well as for the 6" layer just under the critical layer, and the lower value is used as a measure of the soil strength. Ref. 45 refers to a depth of about 2 ft. as the recommended aircrafts' depth of influence, particularly aircraft with high air pressure such as fighter planes.

In a different manner, Ref. 46 establishes the depth of the layer which determines the soil's resistance to the wheel load according to the following two equations:

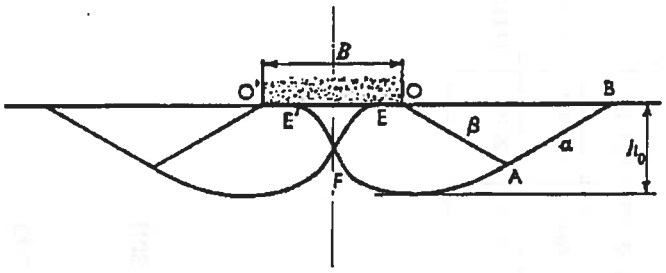


(a)

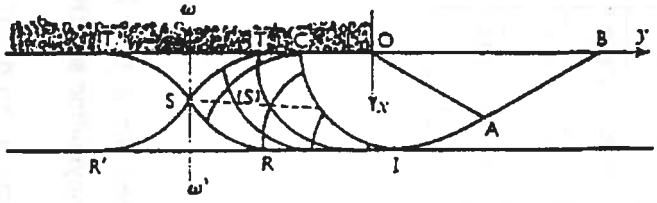


(b)

Fig. 3.10 Description of the general pattern of soil failure under surface loading
(a) homogeneous soil
(b) a layer of soft soil over a rigid nonyielding soil.

ציור מס. 3.10 תאור התפתחות ההרס בקרקע תחת עמיסה בפני השטח
(a) קרקע הומוגנית
(b) שכבת קרקע רכה על בסיס משטח קשיח

| $N_\gamma$ | $B/h$ / $\phi$ | | 1 | 2 | 3 | 4 | 5 | 6 | 8 | 10 | 15 | 20 | 30 | 40 |
|---|---|---|---|---|---|---|---|---|---|---|---|---|---|---|
| 85·70 | 40° | $B/h \leq 0{\cdot}81$ $F_\gamma = 1$ | 1·05 | 3·27 | 16·60 | 106·00 | 804·00 | $6{\cdot}15.10^3$ | $4{\cdot}54.10^5$ | $3{\cdot}90.10^7$ | $3{\cdot}30.10^{12}$ | $3{\cdot}80.10^{17}$ | | |
| 41·20 | 36° | $B/h \leq 0{\cdot}98$ $F_\gamma = 1$ | 1·00 | 1·87 | 5·60 | 21·00 | 90·00 | 407·00 | $1{\cdot}02.10^4$ | $2{\cdot}80.10^5$ | $1{\cdot}50.10^9$ | $1{\cdot}10.10^{13}$ | | |
| 14·70 | 30° | $B/h \leq 1{\cdot}3$ $F_\gamma = 1$ | | 1·20 | 2·07 | 4·23 | 9·90 | 24·80 | 178·00 | 1450·00 | $3{\cdot}81.10^5$ | $1{\cdot}30.10^8$ | $1{\cdot}95.10^{13}$ | |
| 2·84 | 20° | $B/h \leq 2{\cdot}14$ $F_\gamma = 1$ | | | 1·07 | 1·28 | 1·63 | 2·20 | 4·41 | 9·82 | 97·00 | 340·00 | $2{\cdot}60.10^5$ | $7{\cdot}00.10^7$ |
| 0·43 | 10° | $B/h \leq 4{\cdot}07$ $F_\gamma = 1$ | | | | | 1·01 | 1·04 | 1·12 | 1·36 | 2·28 | 4·33 | 20·00 | 113·00 |

Values of $F_\gamma = \dfrac{N'_\gamma}{N_\gamma}$



Fig. 3.11 Modified $N_\gamma$ values for a thin layer of granular soil overlying a rigid nonyielding soil (Ref. 37)

ציור מס. 3.11 ערכים מתוקנים של $N_\gamma$ עבור שכבת קרקע רכה המונחת על בסיס קשיח (מ"מ 37)

$$H_c = 0.64B \qquad [3.14a]$$

for a soil whose strength increases with depth, or:

$$H_c = 1.28B \qquad [3.14b]$$

for cases where the strength decreases with depth,

where:

B - is the width of the wheel's contact area;

$H_c$ - is the critical depth.

Equations [3.14a] and [3.14b] are based on an analysis of the failure mechanism developing during a state of plastic flow in cohesive non-frictional soils. The representative soil strength is calculated (according to Ref. 46), on the basis of the average soil strength up to a depth $H_c$, except for the upper 2 inches, in order to avoid a bias of the results caused by the loose upper soil layer.

Ref.45 and Ref. 47 (both in the context of unsurfaced runways), present solution methods based on numerical analysis of layered soil systems. In Ref. 47, the equivalent strength (in terms of CBR) is found by simulating the standard CBR test activated on the layered soil. The simulation is done by an elastic-viscoplastic finite element model. In Ref. 45 a similar method is suggested (for two layered soil systems), but instead CBR values, the basis for equating the strength of different soil structures are the sinkage and rut depth caused by a given load. Fig. 3.12 presents a nomogram for the determination of the equivalent soil strength, based on the above numerical solution. The model comprises an upper layer 2-12 inches thick, whose strength (based on obtained CI values) is greater or smaller than that of a lower layer of great depth. In this model, it is assumed that the strength within each layer is uniform, and no specific method of conducting strength tests and averaging their results is provided for practical use. The representative strength of the soil is calculated according to the following expression:

$$CI_{equiv} = K \bullet CI_S \qquad [3.15]$$

where:

$CI_{equiv}$ - is the representative soil strength;

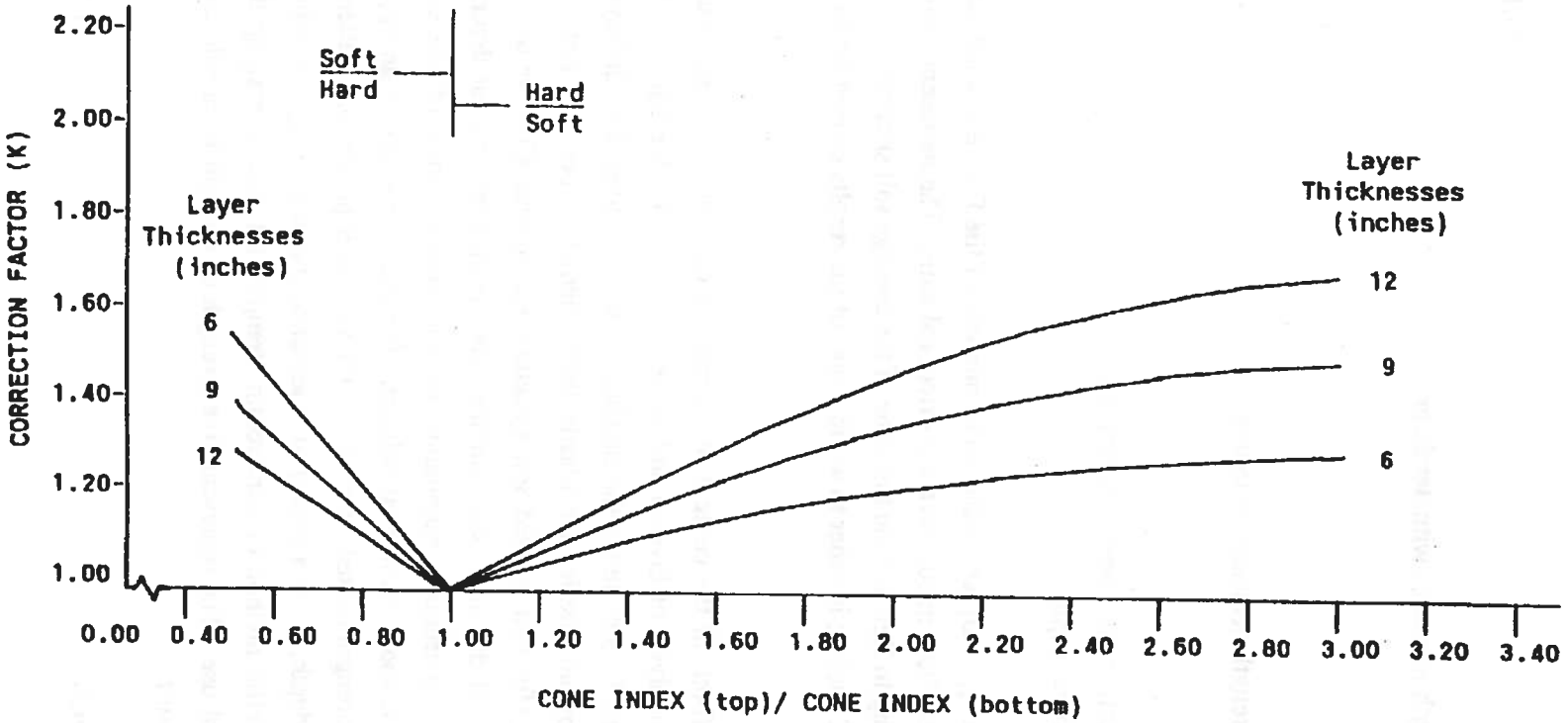


Fig. 3.12 Determination of an equivalent cone index value for layered soils (Ref. 45)

ציור מס. 3.12 קביעת ערך משוקלל של האינדכס הקוני עבור
מערכת קרקע דו־שכבתית (מ"מ 45)

$CI_S$ - is the strength of the weak soil layer in the two-layered structure;

K - is the multiplication factor given in Fig. 3.12.

The K values of Fig. 3.12 are a function of (a) the strength ratio between the upper and lower layer, and (b) the thickness of the upper layer.

# CHAPTER 4: THE PROPOSED MODEL FOR DESCRIBING THE BEHAVIOR OF REMOLDABLE SOILS UNDER AIRCRAFT TRAFFIC

## 4.1 Summary of the literature survey

Chapters 2 and 3 detail the findings of the conducted literature survey, regarding the behavior of remoldable soils under repeated loadings, as well as other issues relevant to the analysis of the wheel-soil interaction. The main points of the literature review, which are important for the presentation of the proposed model, are:

a. The behavior of remoldable soils under shear is usually predominantly elastic, quite rigid in the pre-peak zone (where the stress level is lower than the peak strength of the soil), and the plastic strains are very small. This behavior is very clear in dry granular soils which contain some degree of cementation, and in cohesive soils in which the additional strength is due to chemical bonding of the clay particles. After the soil reaches its peak strength (at low strain values) there is a fast decrease in the soil strength toward the remolded strength of the soil. The above phenomenon is especially salient when the shearing process occurs under low confining pressures as in the case of unsurfaced runways.

b. The stresses exerted on the soil by the moving wheel are high and frequently come close to the peak strength of the soil. Empirical relationships found, describing the development of plastic strains with the number of loadings, claim to be valid only for low stress levels (up to about 40% of the peak strength). Therefore, it is questionable whether those relations can be utilized for the solution of the problem that is the concern of the present research.

c. Because of the relatively rigid structure of the unremolded soil, it seems that for the problem at hand, deformations and hence rutting of the soil, are mainly due to post peak deformations in the already remolded soil. Plastic strains in the unremolded soil are relatively negligible.

d. Remolding of a soil element may be caused by cyclic loading of the soil at levels that are lower than the peak strength of the unremolded soil. In these cases, special fatigue

functions (S-N) may be built which relate the stress level in the soil to the number of load applications until failure, i.e., the remolding of the soil.

e. In saturated soils, the fast loading rate will dictate a condition of undrained shear in most cases and the soil density will remain stable during the shear. However, in the unsaturated soils, density changes will usually take place in the sheared soil. The soil density after shear is a function of the type of soil and the confinement pressure of the soil during the shear process.

f. In granular soils exhibiting cementation, it was found that the additional strength of the unremolded soil is mainly cohesive in nature. Destruction of the additional strength through the remolding of the soil, led to the disappearance of the cohesive part of strength (the C component in the Mohr-Coulomb equation), while the frictional part, the internal angle of friction, remained practically constant.

g. Additional strength factors in the soil, such as cementation, negative pore pressures and structural strength resulting from chemical bonds in clayey soils, are transient factors related to the shear processes in the soil. Strengthening processes (such as thixotropic processes) are not taken into consideration and the loss of strength is irreversible in the context of the pavement performance prediction.

h. Observations carried out at a landing site where the soil was a potentially remoldable granular soil, indicated that the rutting process was carried out through the remolding of the upper part of the soil, and the loss of the cementational element of the soil. Beneath the loose upper layer, the soil retained its original strength.

i. The passage of a moving wheel over the soil creates a stress path of special character that includes changes in the direction of the principal stresses. This phenomenon influences the reaction of the loaded soil. In order to obtain a reliable prediction of soil behavior through laboratory tests, it is recommended to simulate this stress path as closely as possible.

j. Most of the references dealing with the prediction of aircraft performance over unsurfaced runways do not consider the issue of soil strength change during operation. In those few cases that address this issue, the approach is both simplistic and very limited. The strength values taken in these cases were either the remolded strength of the soil or the mean value of the remolded and unremolded strength

values. No model was found to describe the development of soil strength change, under the cyclic loading of a moving wheel.

k. The numerical analyses of the wheel-soil system reported in the literature, are in most cases two-dimensional analyses. The two-dimensional analysis is mainly a consequence of calculational constraints. The wheel-soil system is extremely complex, and a 3-D description of the problem will require calculational resources that are usually unavailable.

## 4.2 The Proposed Mechanistic Model – General Description

Research of the trafficability and performance evaluation of unsurfaced runways, has given only a limited amount of attention to the issue of the change in soil strength with the accumulation of wheel coverages. In the very few cases where this has been done, the design calculations were based on the reduced soil strength which is the strength of the remolded soil, or, on the mean value of the original soil strength and the remolded soil strength. No attempt has been made to describe physically the phenomenon of the decrease in soil bearing capacity with the accumulation of aircraft coverages.

The initial step and an important part of the present research is the presentation of a new model to describe the behavior of soils subjected to remolding under repeated wheel loading. The model concentrates mainly on dry and brittle soil types which change their strength properties during shear. The essence of the model is the gradual formation of a layered soil structure, the upper layer being composed of remolded soil whose strength is often significantly lower than that of the underlying unremolded soil.

The proposed model deals with a soil system part of which being in plastic state. This situation, which is the result of the relatively high levels of stress exerted on the soil, can often be observed by the deep plastic ruts created in the runway (up to 10 centimeters and more per coverage). Due to the above, the usual models applied in the analysis of conventional pavements (in which the stress levels are low in comparison to the material strength) were found to be inappropriate for the analysis of the present model. The suggested model is based on the following principles:

1. The repeated wheel movement on the dry cohesive soil leads to remolding and a decrease in the strength of the original soil. The remolding process at any point of the soil is a consequence of one of the two following processes:

a. Loading the soil element to the point of shear strength (up to the soil failure envelope).

b. Soil remolding following fatigue processes which occur in the soil as an accumulating effect of the repeated loading, mainly at high levels of stress.

The brittle character of the soils treated in the research and the relatively low confinement pressures which develop during the shear process, make it possible to assume constitutive behavior similar to that shown in Fig. 4.1. The response of the material to the shear process is an elastic-plastic one, wherein at the point of shear failure there is a very rapid decrease in the soil's strength down to its residual strength.

The problem of remolding as a consequence of the fatigue process will be handled by monitoring the maximum stress level obtained at each wheel passage, and using the Miner criterion for accumulating the damage in each element.

The momentary relative stress level $S_R$ at each point in the soil, changes during the loading process and is determined by the equation:

$$S_R = \frac{R}{R_{max}} \qquad [4.1]$$

where (see Fig. 4.2):

$R$ - is the radius of the Mohr circle of the momentary soil stress condition.

$R_{max}$ - is the radius of the maximum Mohr circle capable of developing in the soil under identical average stresses.

and, $1 \geq S_R \geq 0$

The maximal relative stress level exerted on the soil element during **one** wheel loading is:

$$S_m = \max(S_R) \qquad [4.2]$$

**Assumed stress - strain relationship in dry remoldable soils.**

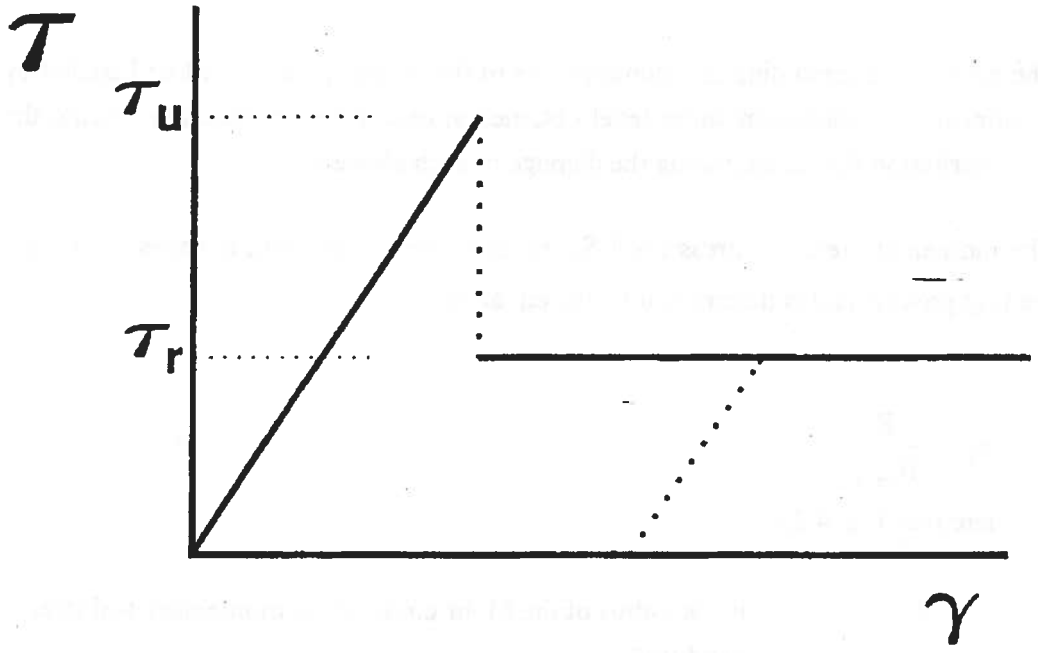


Fig. 4.1 Assumed constitutive behavior of dry remoldable soils.

ציור מס. 4.1 הנחת המודל המכניסטי לגבי ההתנהגות קונסטיטוטיבית של קרקעות יבשות הניתנות להפרה

# Determination of relative stress ratio.

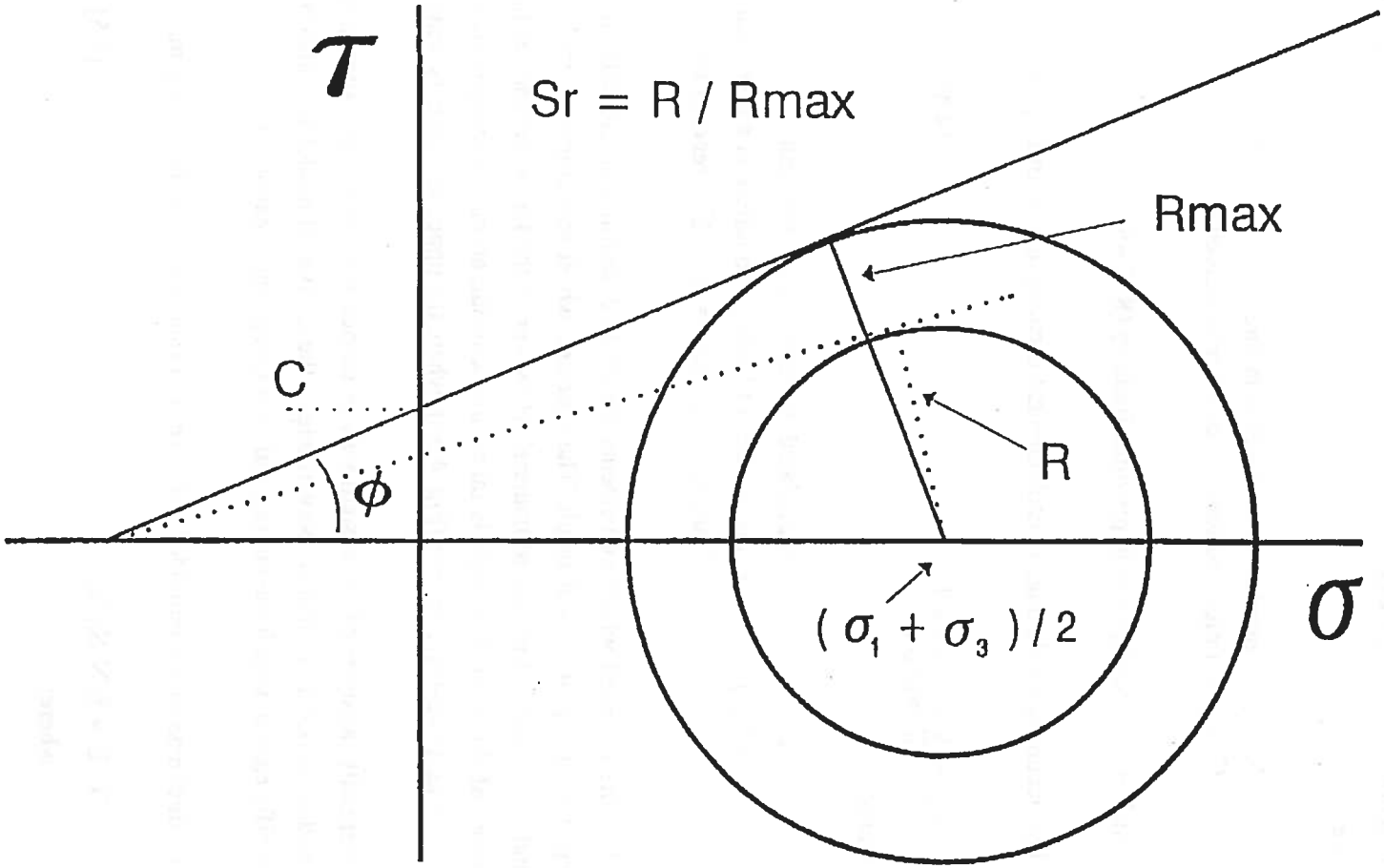


Fig. 4.2 Determination of the relative stress level at a soil element.

ציור מס. 4.2 קביעת רמת המאמץ היחסית בנקודה בקרקע

The fatigue parameters are determined by cyclic shear tests, and express a correlation between the maximal relative stress level and the number of cycles to failure. The general equation describing the soil fatigue phenomenon being formulated is:

$$\text{Log}(N) = C_1 - C_2 \cdot S_M \qquad [4.3]$$

where:

N - number of loadings to failure
$C_1, C_2$ - fatigue parameters of the unremolded soil

which is in accordance with previous findings (Ref. 48)

The accumulated damage in each element is calculated according to:

$$E_A = \sum_n \frac{1}{N(S_M)} \leq 1 \qquad [4.4]$$

where:

$E_A$ - accumulated damage in a soil element.
$N(S_M)$ - is the number of loadings to failure at a given value of $S_M$ and fatigue failure occurs once $E_A$ reaches the value of 1.

2. When the repeated wheel movements are applied within a single path, the structure depicted in Fig. 4.3a will result. The repeated wheel movement is applied within a kind of "trough" of remolded material. However, if the lateral wander of the repeated passes of the aircraft wheels is taken into consideration, the system created can be viewed as a two-layer system (Fig. 4.3b), where the upper soil layer is remolded.

Essentially, analysis of the system will be carried out under the assumption of lateral wander, as occurs in reality. Nevertheless, the analytical model will also relate to the specific case in which the aircraft traffic is completely channeled.

3. The thickness of the remolded soil layer is a function of the following main factors:

$$D / B = f(N, S_0, S_1, L) \qquad [4.5]$$

where:

D - is the depth of the remolded layer.

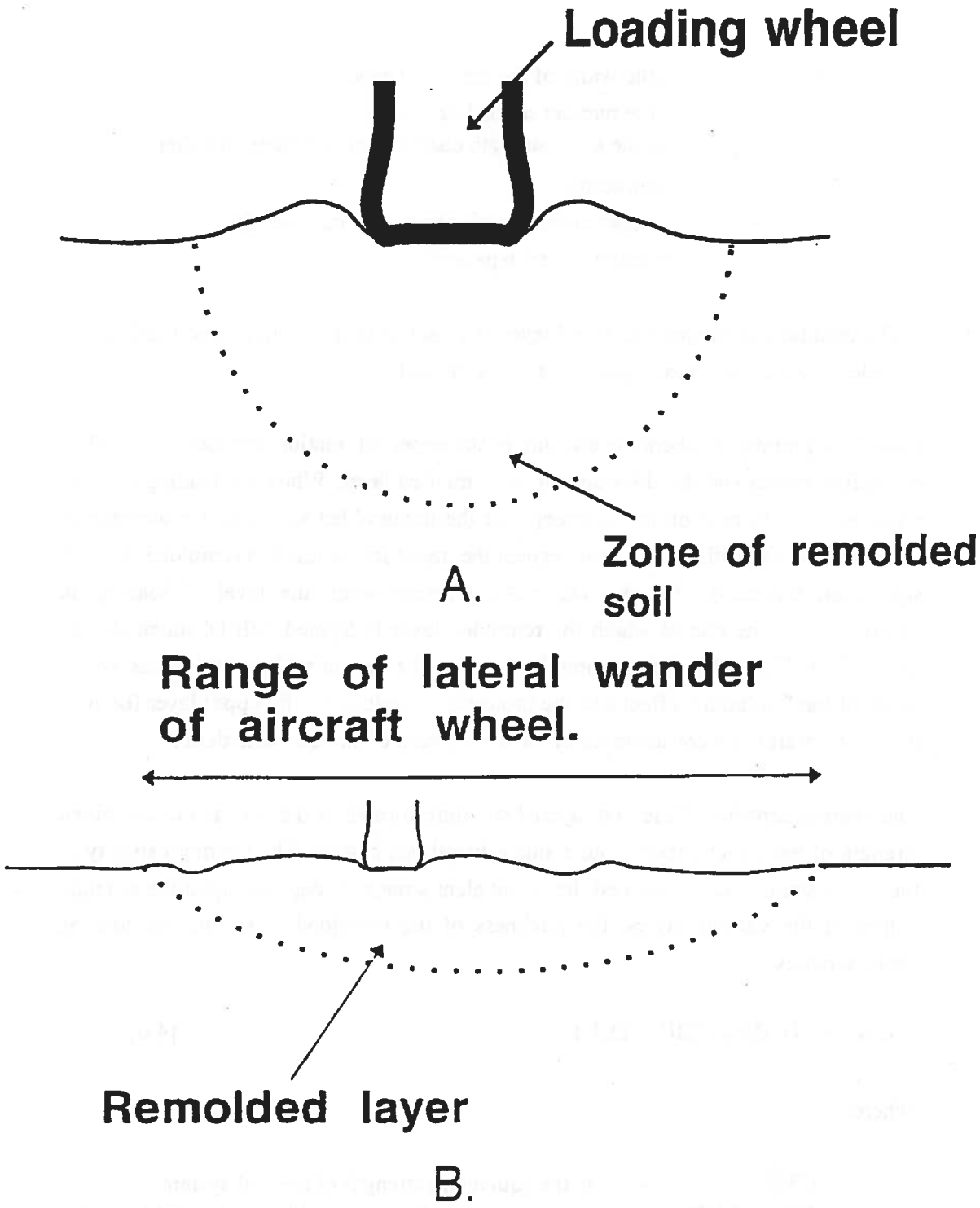


Fig. 4.3 Development of the remolded zone
(a) Channelized repetitive loading
(b) Repetitive loading with lateral wander.

ציור מס. 4.3 התפתחות האיזור המופר
(a) תנועה מתועלת
(b) מעבר חוזר של גלגל עם פיזור תנועה רוחבי

| | | |
|---|---|---|
| B | - | is the width of the loading wheel. |
| N | - | is the number of loading cycles. |
| $S_0$,$S_1$ | - | are the soil's strength characteristics before and after remolding. |
| L | - | are load characteristics such as total load, tire pressure, wheel type, etc. |

The thickness of the remolded soil layer increases with the accumulated loading cycles, until a certain asymptotic value is achieved.

Figure 4.4 presents a schematic drawing of the expected relation between the number of loading cycles and the thickness of the remolded layer. When the loading level is relatively high in relation to the strength of the unremolded soil, and the decrease in soil strength is significant, one may expect the rapid formation of a remolded layer of significant thickness (Fig. 4.4 curve A); whereas when the level of loading is relatively low, the rate at which the remolded layer is formed will be much slower (curve B in Fig. 4.4). The asymptotic value of the remolded layer thickness is the result of the "isolation" effect and the protection provided by the upper layer (be it in the plastic state) as a consequence of the distribution of stresses with depth.

4. The bearing capacity of the two-layered structure formed in the soil, is the combined strength of the various layers into a single functional system. The bearing capacity of the soil system, which is termed the "equivalent strength" depends upon the strength values of the various layers, the thickness of the remolded layer and the loading characteristics.

$$CBR = f(CBR_0, CBR_R, D, L) \qquad [4.6]$$

where:

| | | |
|---|---|---|
| CBR | - | is the equivalent strength of the soil system. |
| $CBR_0$,$CBR_R$ | - | is the strength of the unremolded and remolded soil, respectively. |
| D | - | is the thickness of the remolded layer. |
| L | - | are the loading characteristics. |

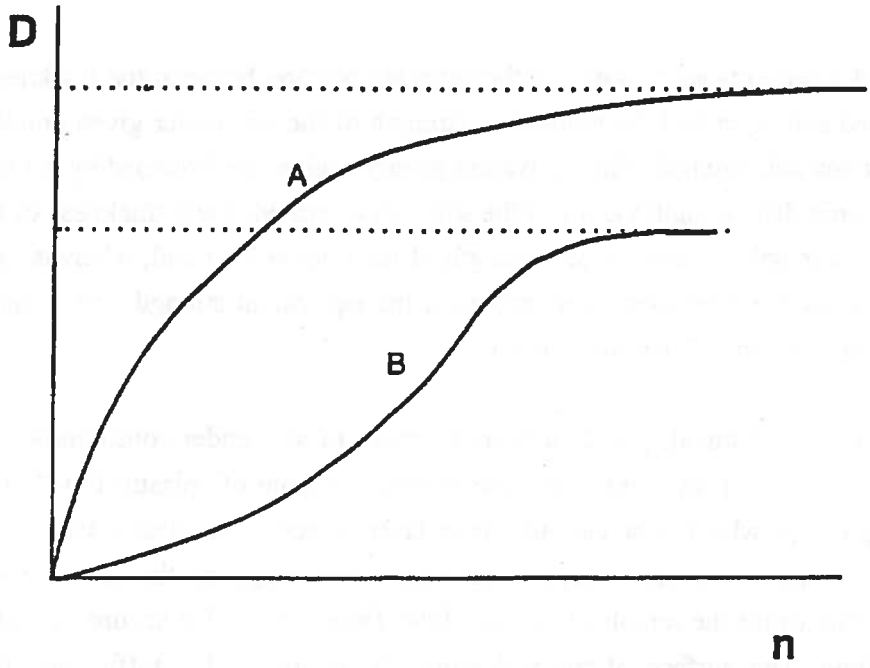


Fig. 4.4 Expected development of remolded layer depth.

ציור מס. 4.4 ההתפתחות הצפויה בעובי השכבה המופרת עם מספר מעברי גלגל

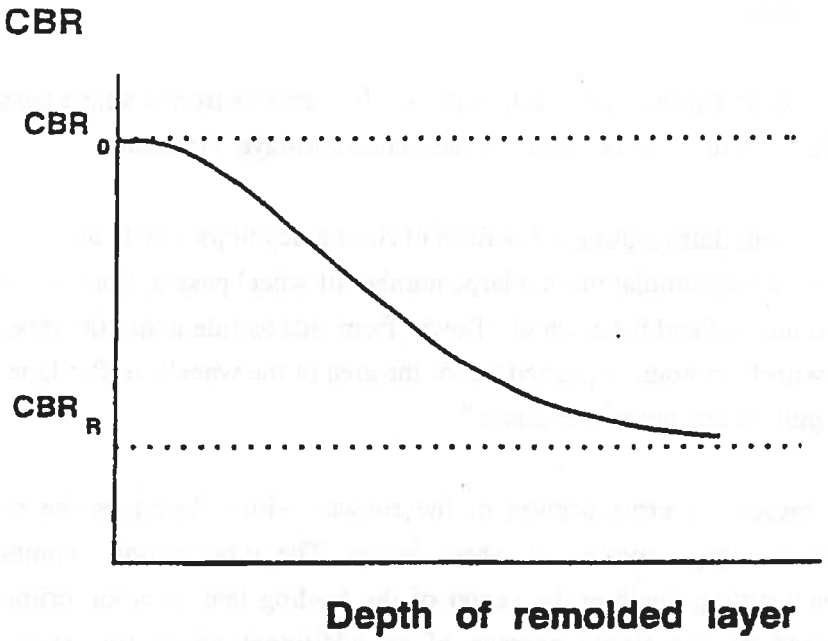


Fig. 4.5 Expected relation between the remolded layer depth and the equivalent strength of the soil.

ציור מס. 4.5 הקשר הצפוי בין עובי השכבה המופרת לבין החוזק השקול של הקרקע

Figure 4.5 presents an example of the expected relation between the thickness of the remolded soil layer and the equivalent strength of the soil under given conditions of loading and soil strength. The equivalent strength values are bounded by the remolded and unremolded strength values of the soil. For a remolded soil thickness of zero, the system's strength is equal to the strength of the unremolded soil, whereas, when the thickness of the remolded layer increases, the equivalent strength value approaches the strength value of the remolded soil.

5. The structure obtained, particularly in the types of soil under consideration, is such that the upper soil layer may be close or within a state of "plastic flow" during the loading of the wheel, whereas the lower layer is mainly in elastic state. Repeated passes of the wheel in various lanes within the range of the lateral wander of movement, cause the remolded soil to "flow" from side to side according to the point of loading. The surface of the soil along the width of the traffic lane is full of longitudinal ruts which change their location from one wheel loading to the next.

6. The functional failure of the runway has been defined as the point at which, under the given magnitude of rutting, it is no longer possible to operate safely aircraft of the given type above the landing strip. The total rutting is determined by means of two parallel processes:

   a. Primary rutting - the plastic rutting which results from a single passage of an additional wheel over the weakened two-layer structure.

   b. Accumulated rutting - this form of rutting develops slowly as a consequence of the accumulation of a large number of wheel passes. Some of the remolded soil mass which "flows" from side to side under the repeated wheel loadings, is pushed out of the area of the wheel's traffic lane, and is thus "taken out of the game."

Fig. 4.6a presents a cross section of the runway which describes the soil profile formed after a large number of wheel passes. The total rutting comprises the accumulated rutting depth at the center of the loading lane plus the primary rutting depth caused by the single passage of an additional wheel (or, at a far lower probability, the passage of 2 wheels or more in the same path).

The maximum rutting criteria are usually established according to the aircraft type, the landing gear and the aircraft operating conditions. The primary rutting criterion is

## Development of Rutting in Remoldable Soils Under Repetitive Aircraft Loading.

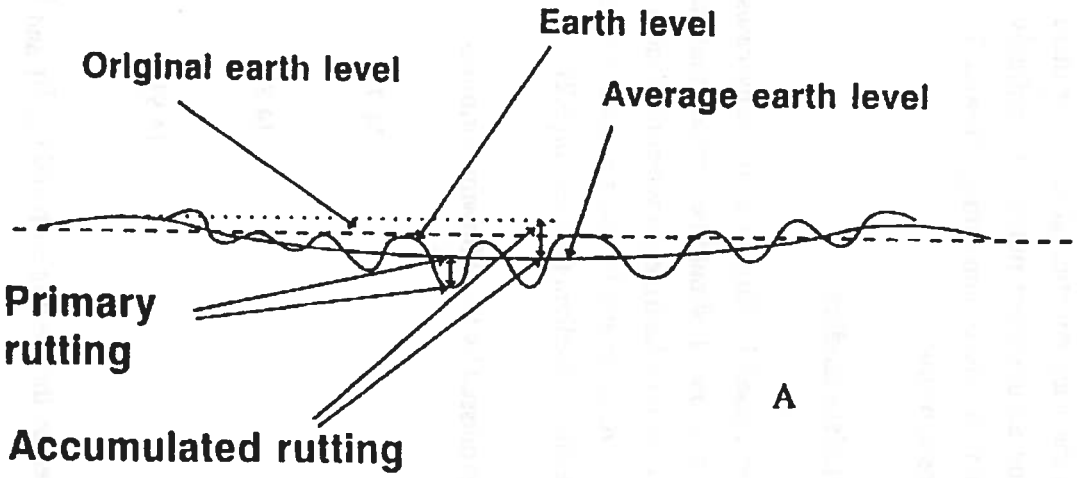


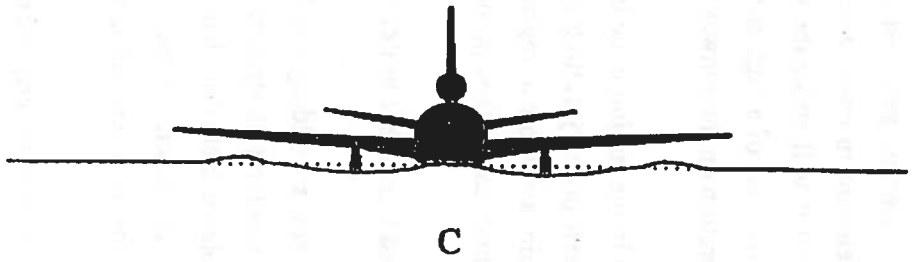


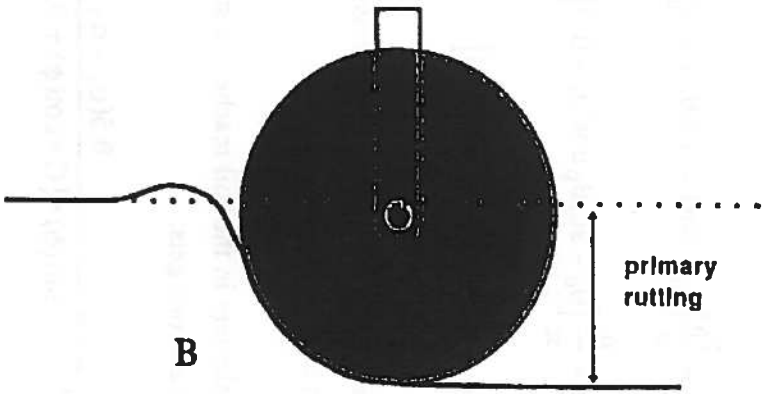


Fig. 4.6 (a) Cross-sectional view of aircraft traffic lane.
(b) Concept of primary rutting.
(c) Importance of total rutting in the performance of aircraft on unsurfaced runways.

ציור מס. 4.6 (a) התפתחות החריצה לרוחב נתיב התנועה
(b) עקרון החריצה הראשונית
(c) חשיבות ערך החריצה הכוללת בבצועי מסלולים ללא צפוי עליון

mainly determined in order to prevent excessive sinkage of the wheel in a single pass, as this may lead to excessively strong braking of the aircraft (see Fig. 4.6b) and even to the breaking of the landing gear and overturning of the aircraft. The total rutting criterion is mainly relevant in cases where the aircraft's body is low (see Fig. 4.6c) and there is a risk that it will strike the ground. Moreover, the steep cross sectional gradients created in the case of a high accumulated rutting, considerably diminish the safety of aircraft operation on the runway.

One of the problems in the rutting issue is the scant attention given in the literature to the difference between primary rutting and accumulated rutting. Accordingly, there are no separate criteria available in regard to the maximum rutting allowed. This fact will influence the numerical method proposed below.

## 4.3 Plastic zones created in the soil under surface loading

As stated in section 4.2, soil remolding can be caused by fatigue or in many cases as a result of the soil element reaching its strength envelope. It should be stressed that parts of the soil mass may reach plastic state (and hence be remolded), even when the load level is much lower than the bearing capacity of the soil. As an example it was chosen to study the case of a surface strip loading of a semi infinite elastic medium (see section 3.2).

The stresses at every point under the strip are expressed by the following formulas:

$$\sigma_V = \frac{P_0}{\pi}\left[\theta_0 + \sin\theta_0 \cos(\theta_1 + \theta_2)\right] \qquad [4.7]$$

$$\sigma_H = \frac{P_0}{\pi}\left[\theta_0 - \sin\theta_0 \cos(\theta_1 + \theta_2)\right] \qquad [4.8]$$

$$\sigma_{VH} = \frac{P_0}{\pi}\left[\sin\theta_0 \sin(\theta_1 + \theta_2)\right] \qquad [4.9]$$

Where p represents the vertical pressure exerted by the loading strip and $\theta_0$, $\theta_1$ and $\theta_2$ are angles as represented in Fig. 3.3.

If an element in the soil reaches its strength envelope the relative stress ratio has the value of 1.0 and one gets:

$$S_R = 1 = \frac{0.5(\sigma_1 - \sigma_3)}{\sin(\phi) \bullet [C \bullet \cot(\phi) + 0.5(\sigma_1 + \sigma_3)]} \qquad [4.10]$$

Where (see equation [4.1]):

$\sigma_1,\sigma_3$ - Major and minor principal stresses, respectively.

$C,\phi$ - Soil cohesion and internal angle of friction.

Combining equations [4.7]-[4.9] with equation [4.10] gives:

$$S_R = \frac{[(\sigma_H - \sigma_V)^2/4 + \sigma_{VH}^2]^{0.5}}{\sin(\phi) \cdot [C \cdot \cot(\phi) + (\sigma_H + \sigma_V)/2]} = \frac{p \cdot \sin(\theta_0)}{\pi \cdot C \cdot \cos(\phi) + p \cdot \theta_0 \cdot \sin(\phi)} \qquad [4.11]$$

Derivating $S_R$ with respect to $\theta_0$ :

$$\frac{\partial S_R}{\partial \theta_0} = \frac{[\pi \cdot C \cdot \cos(\phi) + p \cdot \theta_0 \cdot \sin(\phi)] \cdot p \cdot \cos(\theta_0) - p^2 \cdot \sin(\theta_0) \cdot \sin(\phi)}{[\pi \cdot C \cdot \cos(\phi) + p \cdot \theta_0 \cdot \sin(\phi)]^2} \qquad [4.12]$$

The first points to reach the plastic state fulfill both requirements :

1) $S_R = 1$ - The Mohr circle touches the strength envelope.

2) $\frac{\partial S_R}{\partial \theta_0} = 0$ - A maximum point as can be expected from stress distribution.

Making some mathematical manipulations. it can be shown that :

a) The first soil elements that reach plasticity are located at points satisfying :

$$\cos(\theta_0) = \sin(\phi) \qquad [4.13]$$

b) The minimum vertical pressure at which plastic state can be observed at the above points is :

$$p_{MIN} = \frac{\pi \cdot C \cdot \cos(\phi)}{\sin(\theta_0) - \theta_0 \cdot \sin(\phi)} \qquad [4.14]$$

where $\theta_0 = \cos^{-1}(\sin(\phi))$

The above can be used to find the minimal loading level at which it is expected to find some points in the soil (or pavement) that reached plasticity. As an example for a soil having the following properties:

$\phi$=35°

C=0.1 kg/cm$^2$

and a loading strip having a width of 5 cm , it is found that

$$p_{MIN} = 0.94 \quad kg/cm2 \qquad [4.15]$$

It is important to note that in the above example the bearing capacity value is almost 5 kg/cm$^2$, which means that even at a loading level 20% (and less) of the bearing capacity, points in the soil may reach plasticity. In remoldable soils (and also in some brittle paving materials), this point is very crucial since reaching plasticity may mean remolding of the soil element and a drastic change in its properties. In cases where remolding of the soil is not tolerable (such as in the case of cement stabilized bases and subbases in conventional pavements), the above analysis seems important in order to prevent early pavement deterioration.

The above analysis is later used in chapter 6 in order to authenticate the results of the numerical model.

## 4.4 General calculational approaches to the solution of the problem

Fig. 4.7 contains a general flowchart of the analytical system, based upon the proposed mechanistic model. The system's input includes the properties of the soil in its original and remolded states, including fatigue data, various loading factors such as the wheel load, the tire pressure, the geometry of the loading wheel and data concerning lateral wander of aircraft traffic. The analytical system comprises a number of sub-systems, as detailed below, of which the most important are:

- Sub-system A - which relates the number of aircraft wheel passes to the depth of the remolded soil layer. The aim of this system is to provide a function which will make it possible to evaluate the thickness of the remolded soil layer at every stage of the runway's life.

BEHAVIOUR OF REMOLDABLE SOILS UNDER REPETATIVE WHEEL LOADING.
FLOW CHART OF MAIN PROCESS PHASES.

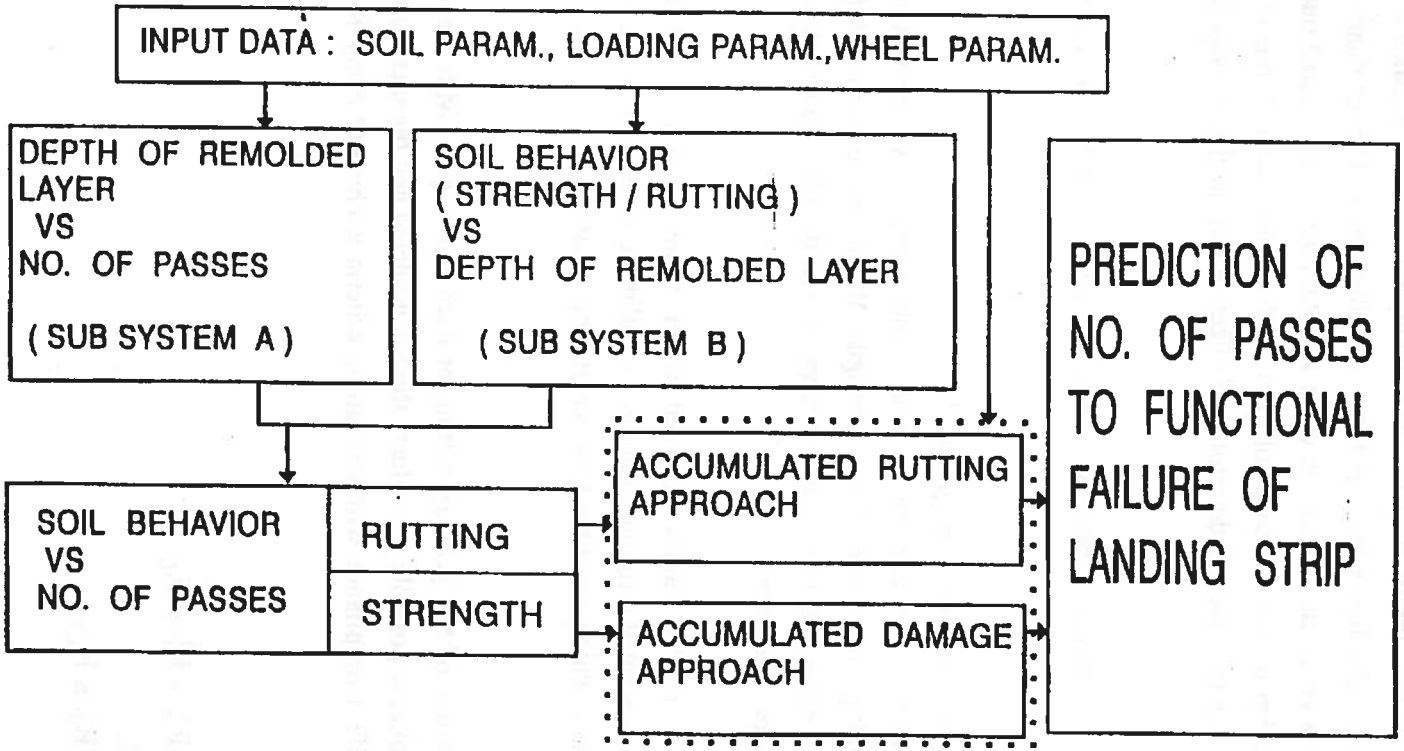


Fig. 4.7 General flow chart of the solution process.

ציור מס. 4.7 תרשים זרימה כללי של תהליך הפתרון

- Sub-system B - which relates the depth of remolded layer to the expected performance of the soil system as expressed through the soil bearing capacity or wheel rutting values.

- Sub-system C - which utilizes the output received from the two above sub-systems and integrates it to get a relationship between the layered soil performance and the accumulated number of aircraft wheel passes. A function is thus derived for evaluating the performance of the soil system at each stage. In order to obtain the final required output of the system, (i.e., the number of wheel passes until runway functional failure), one should find a way to account for the incremental deteriorative effect caused to the runway by repeated aircraft passes.

There are two different approaches (see Fig. 4.7) to the solution of the above mentioned issue:

**a. The accumulated rutting approach**

According to this approach, the expected runway rutting will be calculated at each stage under changing conditions of soil strength. When the total rutting (primary rutting + accumulated rutting) or the primary rutting, exceed the allowed criterion values, functional runway failure is declared.

The primary rutting values obtained under changing soil structure conditions, may preferably be derived through numerical calculation. Alternatively, use is made of existing empirical data which correlate between rutting values and soil strength (see for example Ref. 33).

The integration of the primary rutting at each wheel pass with the data on the lateral wander, makes it possible to evaluate the accumulated and the total rutting, throughout the runway's life. Compliance with the rutting criteria is checked every few passes according to:

$$R_A^i + R_P^i \leq R_{CT} \qquad [4.16]$$

and,

$$R_P^i \leq R_{CP}$$

where:

$R_A^i$ - is the accumulated rutting at the center of the wheel traffic lane (assuming normal distribution of the lateral wander)

$R_P^i$ - is the primary rutting corresponding to the soil's strength conditions after i wheel passes.

$R_{CT}$ - is the maximum allowed value of the total rutting.

$R_{CP}$ - is the maximum allowed value of the primary rutting.

The runway is considered to have functionally failed once one of the $R_{CT}$ or $R_{CP}$ criteria values are passed.

**b. The accumulated damage approach**

This approach is more simplistic than the accumulated rutting approach and is based on existing empirical data. This model estimates incremental runway damage caused by each additional passage of the wheel over the soil. The functional failure of the runway may be determined (see Ref. 32) by means of Miner's law (Ref. 49)

$$\sum_{i=1}^{N} \frac{1}{N_i} = 1 \qquad [4.17]$$

where:

$N_i$ - is the number of passes which would have been required in order to cause runway failure in the event that the soil strength had been constant at a level of $CBR_i$.

$CBR_i$ - is the equivalent strength of the soil system following i passes.

N - is the number of passes to runway functional failure.

In this case, use can be made of existing design nomograms, which assume a constant soil strength in order to determine the $N_i$ values appropriate for each given $CBR_i$.
Compared to the more fundamental character of the accumulated rutting approach, the accumulated damage approach is much more empirical and can give only rough estimates as to the performance of unsurfaced runways on remoldable soils.

A more detailed discussion of this issue is given in Chapter 6 which elaborates on the different calculational alternatives for the estimation of the number of wheel passes until functional runway failure.

The mechanistic physical model described above constitutes the general framework of the present study. The research's main goal was to present a new model for the development of

the functional failure of unsurfaced runways on remoldable soils. This model may have practical implications for the prediction of unsurfaced runway performance on soils of the type discussed herein. The research plan, built on the basis of the above described model, comprised three main stages :

1. The construction of a numerical system based on the mechanistic model, which will describe the behavior of the remoldable soil under repeated wheel movements within a specified range of lateral wander. This computational system is supposed to carry out the process shown in Fig. 4.7, while using different numerical means, and to provide the required output, i.e., a more accurate estimation of the number of aircraft passes up to runway functional failure. A detailed description of the analytical system is given in Chapter 6.

2. A series of laboratory tests aimed to investigate the properties and strength characteristics of the inspected soil before and after remolding. Cyclic shear tests were conducted in order to study soil behavior under cyclic loading at a relatively high level of stresses. Two types of dry granular soils that contain some degree of cementation in their natural state were studied during the research.

3. Conducting moving-wheel experiments for the purpose of qualitative validation and verification of the mechanistic model and providing a means for feedback and tuning of the analytical system. In order to carry out these experiments, a new laboratory moving-wheel apparatus was built, which makes it possible to carry out wheel loading while changing the lateral location of the wheel along the width of the sample, thus emulating actual loading conditions as they occur in the field.

The following chapters describe in detail the various research stages and elaborate on the results obtained.

# CHAPTER 5: LABORATORY TESTING OF REMOLDABLE DRY GRANULAR SOILS

## 5.1 General

One of the main elements in the proposed model input is soil properties on which the aircraft movements are being carried out. The laboratory tests are intended to provide as clear a picture as possible of the elastic and plastic characteristics of the soil, and to evaluate its response to repeated loadings at high levels of relative stress.

In many design and evaluation methods of conventional pavements, a single parameter (the CBR parameter) is often used to represent the strength of the subgrade and other structural layers. A similar approach was adopted in the area of unsurfaced runways. A single strength parameter, usually the result of one of the existing field penetration tests (DCP, air-field penetrometer, etc.) is employed for the evaluation process. The use of a penetration test in unsurfaced runway design is justified mainly by its simplicity and relative ease of use, especially when taking into account the emergency conditions wherein it is frequently applied.

However, contrary to the area of conventional roads, where the use of one strength parameter may give satisfactory results, the use of such a parameter in unsurfaced runways is very problematic due to the following:

1. The structural layers and the subgrade in conventional roads are in a confined state which prevents any significant deformation of the soil. However, in the case of unsurfaced runway, the soil surface at the sides of the wheel is practically unconfined.

2. In the upper structural layers in conventional surfaced pavements, the design methods present additional requirements to those of the CBR. These requirements ensure the presence of cohesive strength in the upper, less confined layers, such as the asphalt concrete layers and stabilized bases.

3. The commonly accepted stress levels in the subgrade of conventional surfaced roads and runways are relatively low, and may be as low as 40-50% of the strength of the material. On the other hand, unsurfaced runways frequently attain far higher levels of stress, which are close and even equal to the soil strength.

Where surface loading is concerned, particularly with a significant horizontal component, great importance may be ascribed to the cohesive component of the soil strength. In such an instance, cohesionless soils will yield at much lower loads than those observed in cohesive soils, even when their bearing capacity values as obtained in penetrometer and CBR testing are identical. In order to overcome the problem partially, it is a common practice in the area of unsurfaced roads and runways, to differentiate between two soil categories: granular and cohesive.. However, this differentiation is obviously simplistic and does not provide solutions for a wide range of soils.

In the context of the research and in the numeric analytical system which constitutes the heart of the proposed system, use has therefore been made of basic soil strength parameters which are accepted in the field of Geomechanics:

- $\phi$ The soil's internal angle of friction;
- C The soil's cohesion.

After obtaining results of the numeric model, the strength values may be converted back to penetration resistance terms in order to allow integration with accepted design nomograms and existing methodology.

There is no doubt, however, that in order to improve the prediction of unsurfaced runway performance, it is necessary to modify existing field-testing methods for obtaining the in-situ soil strength values. Thus, in future it will probably be necessary to add an additional test to the existing ones (the various penetrometer tests) in order to enable even a rough differentiation between the cohesive and the frictional components of the soil strength.

## 5.2 Types of tests and testing procedures

A number of soil parameters were examined in the course of the laboratory tests:

1. Elastic parameters - the value of the soil's Modulus of Elasticity, E, before and after remolding, was determined during the triaxial shear tests which were conducted as detailed below. The Poisson Ratio of the soil was assumed to be 0.3 - 0.4, and a sensitivity test of the numerical system indicated that its effect on the behavior of the system as a whole is relatively small.
2. Strength parameters - The internal angle of friction of the soil ($\phi$) and the soil cohesion (C) were measured through application of the Mohr-Coulomb law to the soil

under consideration. These values were used as the strength parameters in the analytical system. For purposes of comparison with existing design nomograms, CBR tests were also conducted. The CBR tests were carried out under dry soil conditions similar to those under which the other shear tests were performed. Shear tests were carried out both before and after the remolding of the soil, in order to obtain the soil's strength parameters in both conditions.

3. Fatigue parameters - As different points in the unremolded soil are loaded during different cycles at high levels of stress, certain points within the soil may fail as a result of fatigue. Accordingly, cyclic tests were conducted at high levels of stress (90% and more of the material failure strength) in order to quantify the parameters of equation [4.3]. This equation correlates between the relative level of stress at a given point in the soil and the number of cycles to failure at that point.

4. Gradation and indicative tests - These tests were conducted in order to characterize the types of soils used as fully as possible. These tests included mechanical gradation tests, specific gravity of aggregate, Atterberg Limits tests for material passing sieve #40, etc.

The main laboratory effort was given to the laboratory shear tests. which were carried out with three types of instruments:

1. A standard apparatus for triaxial shear testing;
2. A direct shear apparatus;
3. A laboratory shear apparatus for the performance of cyclic triaxial tests with simultaneous change of the principal stresses in order to derive fatigue parameters.

The two former instruments were used in order to test the soil samples by means of accepted standard tools, so that the results may be easily compared with the general literature on the subject. The main purpose of the direct shear apparatus was to find the residual behavior of the soil after its remolding.

The stress path undergone by any point in the soil under the wheel loading includes simultaneous changes both in the size and direction of the principal stresses. In the course of the present research, an attempt has been made to utilize the Hollow Cylinder Torsional device (HCT) which makes it possible to implement the shear process according to a pre-defined stress path which includes changes in both the direction and size of the principal

stresses (Ref. 50, 51). The soil samples used in this device were hollow cylindrical samples prepared in special molds. Although the technical preparations required in order to carry out these experiments were almost completed (including the construction of the molds in order to prepare the samples and the writing of an appropriate operating software for controlling the experimental process) it was decided to discontinue working in this direction. The main reason for this decision was the great difficulty involved in preparing the hollow soil samples which emanate from the brittle character of the hollow soil sample after it is dried and cured.

As an alternative solution, it was decided to carry out triaxial shear tests and include simultaneous changes in the size of the principal stresses during shear. A number of sources in the literature (see Ref. 52) adopted such a solution in the past as a good simulation of the stress path under a wheel's movement. In the course of the present study, a number of stress paths were constructed on the basis of an analysis of the stresses arising in an elastic medium under wheel loading (this analysis was similar to that conducted by Ishihara (Ref. 23), but with the addition of horizontal stresses (Ref. 53) induced by the loading wheel).

The platform chosen for the application of the above shear tests was that of the HCT device. The use of the instrument made it possible (after preparing an appropriate software application, based on the software presented in Ref. 50) to effect triaxial shear tests under a selected stress path, including simultaneous changes of the cell and axial pressures.

Fig. 5.1 presents a photograph of the HCT device and the computerized system connected to it. The system activation rate during the cyclic tests was one cycle every 2-3 minutes, which enabled the application of the selected stress path with a high degree of accuracy.

### 5.3 Preparation of soil samples

The construction of the soil samples for the laboratory shear tests required that a precise procedure of soil preparation, compaction and curing be established. As the tested materials are granular soils which develop cohesion while drying, and the intention of the laboratory tests was to simulate actual field conditions as closely as possible, the following main stages were established for the sample construction process:

A. Preparation of the soil - The soil samples were composed of material passing #10 only, in order to avoid the effect of coarser aggregates on the behavior of the relatively small soil samples. The sieved material was dried in an oven at a

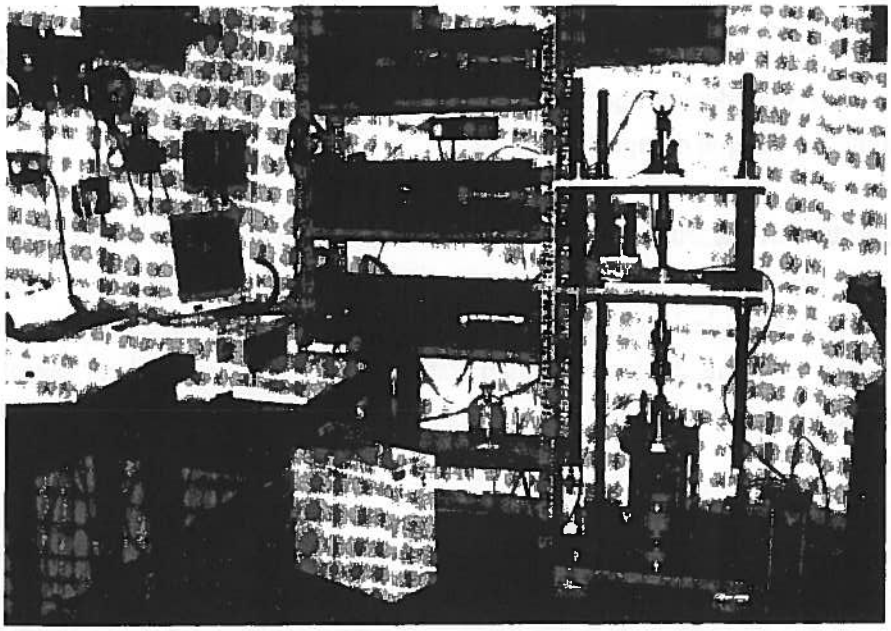

Fig. 5.1 The Hollow Cylinder Torsional Device used for cyclic triaxial testing.

ציור מס. 5.1 תצלום מתקן ה- HCT ששימש לצורך בצוע נסויי גזירה מרחבית מחזורית.

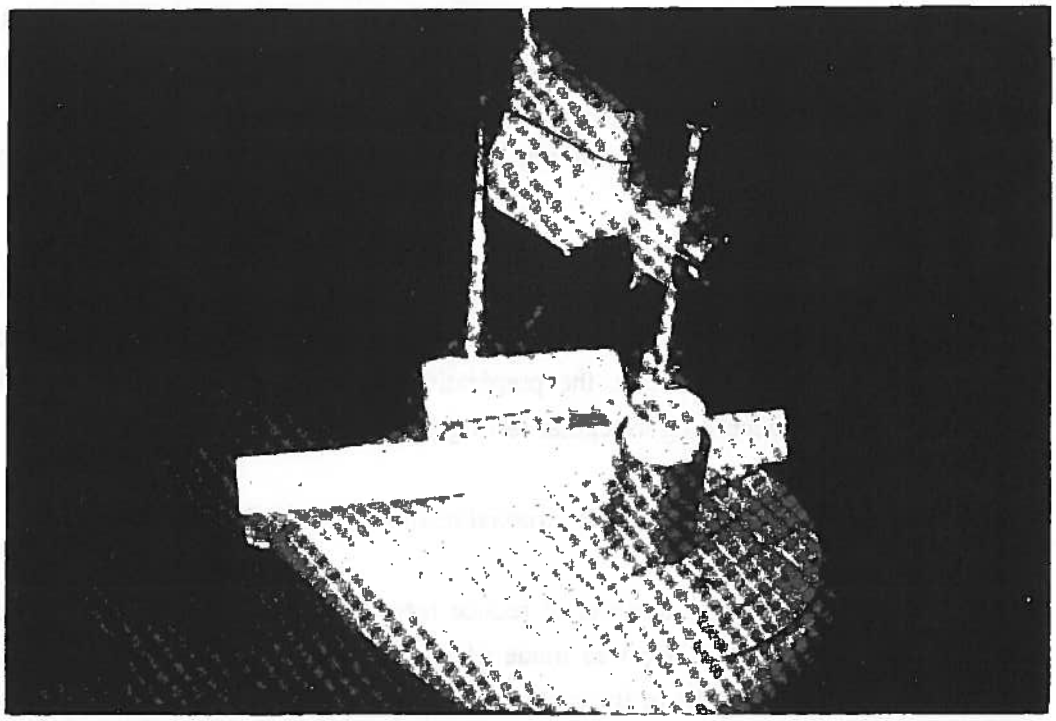

Fig. 5.2 Equipment used for epoxy "caps" positioning on soil samples.

ציור מס. 5.2 הציוד בו נעשה שימוש לצורך הצבת "כובעי" אפוקסי על גבי

temperature of 110°C for 24 hours. Water was then added to the dry material at a range of 8-10% (depending on the type of soil) of the dry material weight, in order to facilitate the sample compaction.

B. Compaction of the sample - After determining the required dry density, a quantity of wet soil was weighed before it was compacted into a mold. The compaction method applied was a single-layer static compaction, both for the direct shear samples, which were compacted inside the testing apparatus, and for the triaxial shear samples which were compacted in metal molds in order to create samples 80 mm high and 30 mm in diameter.

C. Soaking and drying the sample - After the compaction was completed, the sample was soaked on both sides, from above and below, so that it absorbed the maximum possible amount of water. After a day of soaking, the sample was transferred for drying in an oven at a temperature of 60°-65° for a period of at least one week. The entire compaction, soaking and drying process was accompanied by close weight control, and the drying in the oven was completed at a moisture level of about 0.5 - 1.0%. The process of soaking and then drying the sample was discovered to be crucial in order to allow the controlled and uniform development of cohesion within the sample. The soaking of the sample made it possible, during the drying process, for the remaining water and the fines (passing #200) to concentrate at the contact points between the coarse aggregates, thus creating capillary pressures and bonding expressed in the cohesive component of the dry soil's strength. Some trials in which drying the soil samples was done without first soaking them, lead to the creation of far weaker dry soil specimens.

D. Preparation of samples for testing - Due to the brittle nature of the soil investigated in the present research, special care had to be given in preparing the soil samples for testing. For the direct shear tests, the preparation of the samples after drying was simple and effected according to regular testing procedures.

The preparation of the soil samples for triaxial testing comprised two stages:

1) Taking the molds apart. In order to reduce forces exerted on the soil and avoid cracking of the sample, use was made of a thin layer of white paraffin (wax), applied on the inner walls of the mold. The paraffin layer (applied hot and liquid on pre-heated molds before sample preparation), liquefied at a temperature of about 53°. The dismantling of the molds from the soil sample was done

immediately after removing the sample from the drying oven, while the molds were still hot. This procedure ensured the existence of a thin and liquid separating layer between the mold and the susceptible soil sample.

2) Construction of special "caps" on both sides of the sample that comprise a metal disk plus a leveling layer of fast drying epoxy cement. These "caps" were meant to prevent the sample from failing at the edges during the tests as a consequence of an imperfect contact between the loading plates of the testing apparatus and the brittle and sensitive soil. Fig. 5.2 presents the equipment used to ensure the correct positioning of the "caps" on the soil sample. The samples were cured for an additional 24 hours before they were ready for use in the shear device. A picture of site T soil sample ready for triaxial testing is shown in Fig. 5.3.

## 5.4 Results of laboratory tests

All laboratory tests conducted during the research were carried out on natural soil samples procured from two sites (called sites T and S), used as actual aircraft landing sites in southern Israel.

### 5.4.1 Site T material

The soil is defined as silty material mixed with sand and flinty gravel. Fig. 5.4 describes the gradation curve of the soil at this landing site. About 20% of the material passes #200 sieve, but the material lacks plasticity (as can be seen in Fig. 5.5). Generally, the soil is well graded. According to the AASHTO method, the material may be classified as A-1-b (sand and gravel) and as GM, according to the Unified method.

Fig. 5.5 details the results of a CBR test system carried out on soil from site T. The maximum CBR value obtained for a moisture content of 7%, following 56 blows, was about 120%. The CBR value estimate for a dry density of 1950 kg/m$^3$ (about 91% of the max. density) was about 20%. It should be noted that these CBR tests were conducted in a saturated system, according to the regular procedure. In a dry state, the soil would yield higher CBR results, as a consequence of the formation of cementation forces which contribute to the cohesive strength of the soil.

Laboratory CBR tests were also conducted on dry soil samples from site T. These tests were meant to give some indication of the soil strength under conditions similar to the usual in-situ situation.. Only material passing #10 sieve was used, in order to decrease the

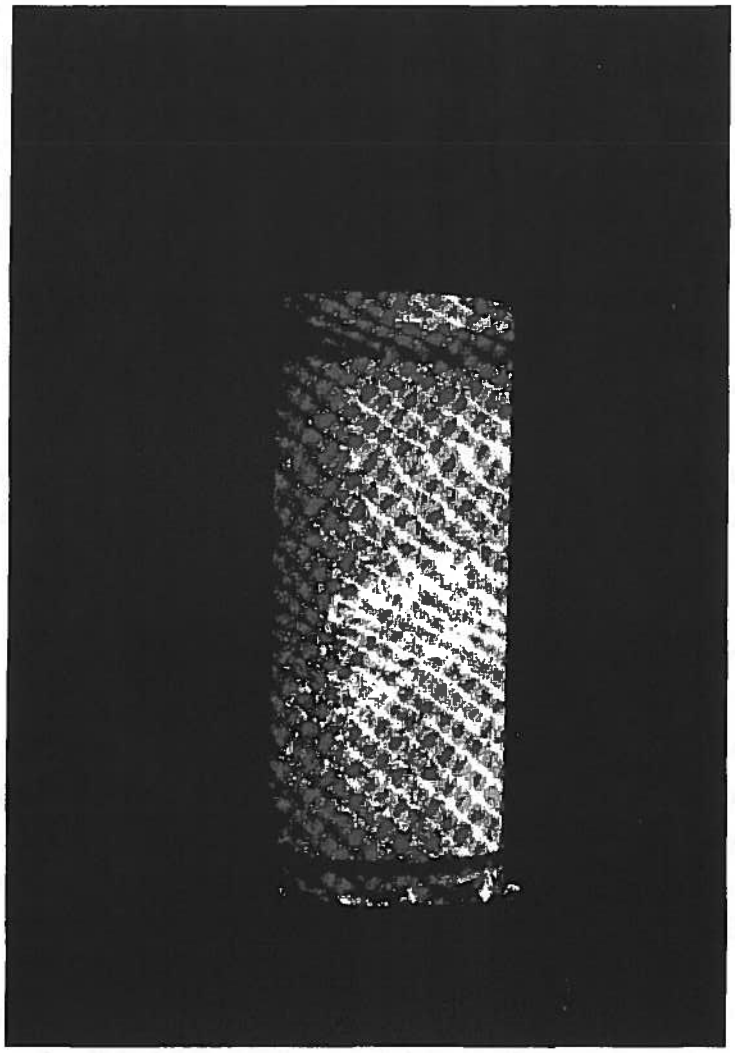

Fig. 5.3 Site T soil sample ready for triaxial testing.

ציור מס. 5.3 מדגם קרקע מאתר T לאחר אשפרה.

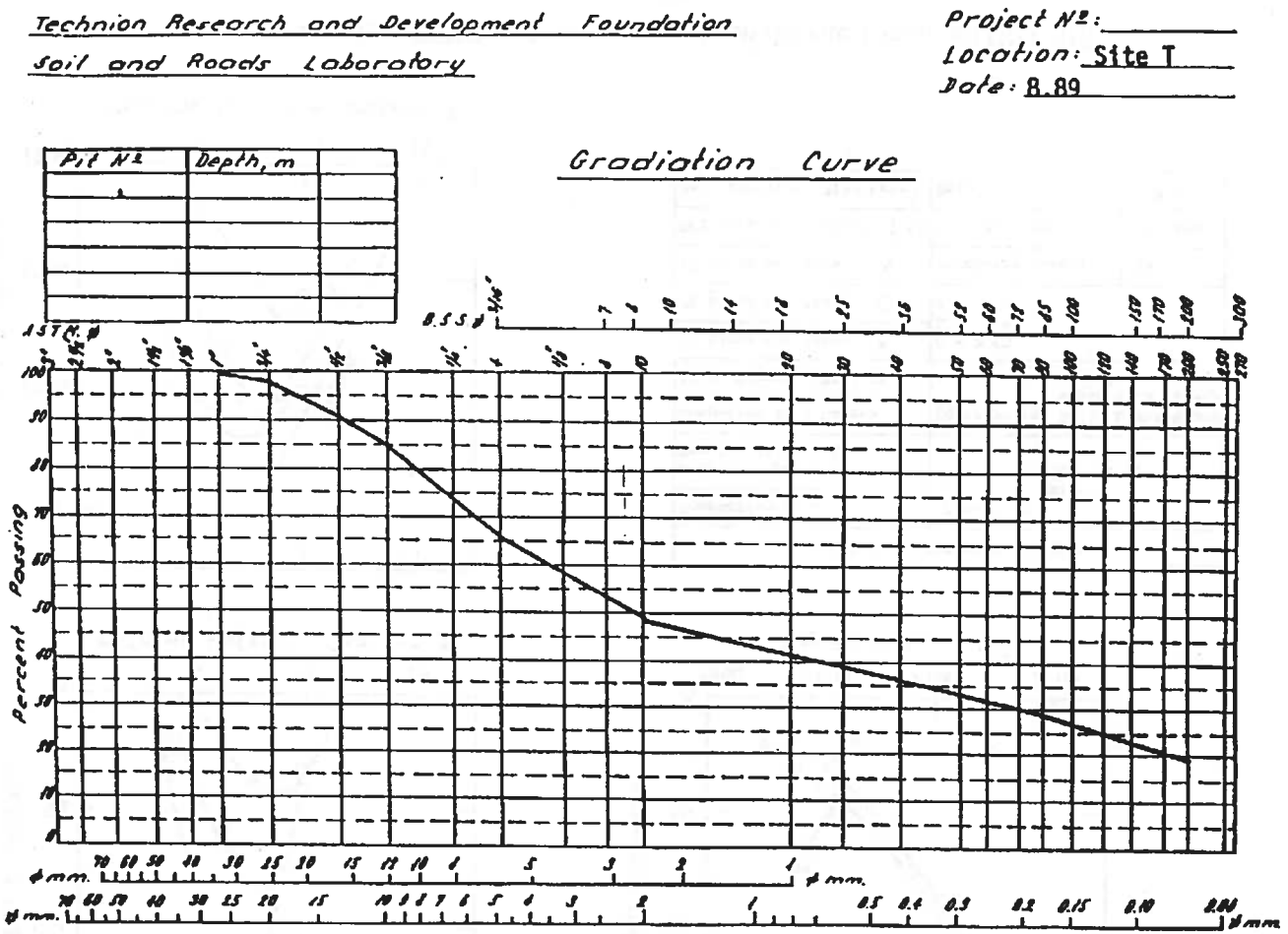


Fig. 5.4 Mechanical gradation test results on site T material (Ref. 16).

ציור מס. 5.4 תוצאות אנליזה מכנית של הקרקע באתר T.

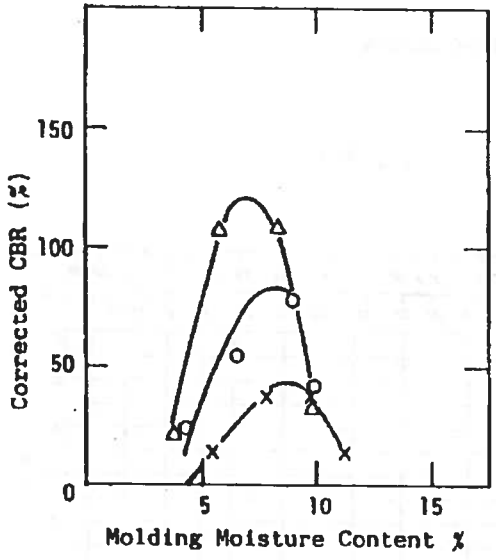


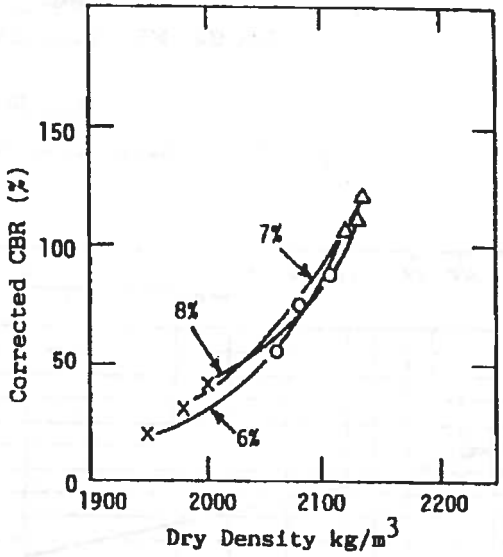


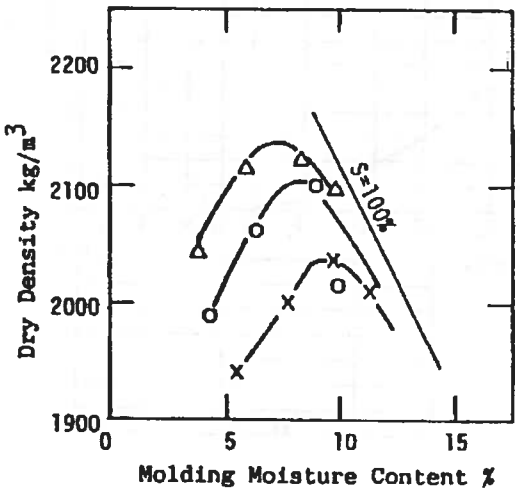


| CALIFORNIA BEARING RATIO TEST | | |
|---|---|---|
| Compaction Data | Plan for: Site T (Point No. 8) | |
| Sample diameter 6" Sample height 5" | | |
| Compacted in 5 Layers | Description: Silt, Light-brown mixed with flinty gravel | |
| 10lb. Hammer, 18" fall | | |
| 56 blows per layer △ | G = 2.69 L.L. = NP P.I. = NP | |
| 26 blows per layer ○ | | |
| 12 blows per layer × | Surcharge weight | 10 lb. |
| OPT.Moisture Content: 7.5% | Soaking time | 4 days |
| Max. Density: 2140 kg/m3 | Date | 8.89 |

Fig. 5.5 Results of CBR and indicative tests on the site T material (Ref. 16).

ציור מס. 5.5 תוצאות מערכת CBR וגבולות סומך על דגימות קרקע מאתר T.

influence of the coarse aggregates and enable subsequent relation with the results obtained in the laboratory shear tests. Some of the CBR tests were performed on samples which had undergone the curing processes described in section 5.3 and contained acquired cementation between the aggregates. Other tests were conducted on samples which were compacted in a dry condition and then sheared ( thus simulating the remolded state of the soil, having no cementation ). Table 5.1 summarizes the results of the above CBR tests on both "remolded" and "unremolded" reconstituted soil samples. All samples were compacted to a dry density of about 1650 kg/m$^3$ which is equivalent to a dry density of 1950 kg/m$^3$ of the original (unsieved) aggregate mix.

**Table 5.1 - CBR tests on dry samples from site T**

**טבלה 5.1 - בדיקות מת"ק במדגמי קרקע מאתר T, לאחר יבוש.**

| Sample No. | CBR Value "Unremolded" Strength | CBR Value "remolded" Strength |
|---|---|---|
| T17 | 37.6 % | |
| T38 | 30.5 % | |
| T78 | 44.8 % | |
| T81 | | 4.8 % |
| T81 | | 4.5 % |
| T60 | | 5.3 % |
| **Average Value** | **37.6 %** | **4.9 %** |

Although the number of tests was quite limited, the results clearly show the large difference between the strength of the "remolded" and the "unremolded" soil samples. The performance of a soil having CBR value of 5% is of course entirely different than that of a soil with a CBR value approaching 40% (see Fig. 3.8 ).

The results of the laboratory CBR tests (Table 5.1) can be compared with previous field tests conducted at site T. A DCP (Dynamic Cone Penetrometer) apparatus was used (see Ref. 54) to test soil strength under two conditions:

A) The original unremolded soil containing naturally acquired cementation;
B) The same soil but after a remolding and recompaction process (Ref. 55).

Table 5.2 describes the results of the field strength tests. Although density changes were not entirely avoided during the field testing, the general picture concurs with the laboratory CBR tests.

Fig. 5.6a shows an example of the results obtained in a direct shear test of soil sample from site T. The figure depicts the results of the shear process of a yet "unremolded" sample (a reconstituted sample that underwent a process of drying and curing) under vertical pressure of 2 kg/cm$^2$. Fig. 5.6b shows the results of a reversal shear test that was successively performed on the same sample in order to obtain values of the residual strength of the soil. Fig. 5.6C shows a summary of the results obtained from the four soil samples submitted to direct shear tests. According to these results, the internal angle of friction was 45$^o$-47$^o$, and no substantial change was noticed after the soil remolding. The level of cohesion was 0.95 kg/cm$^2$ before remolding and about 0.1 kg/cm$^2$ in the reversal tests.

**Table 5.2 - Results of field remolding tests at site T (Ref. 55)**

**טבלה 5.2 - תוצאות בדיקות הפרה בשדה באתר T (מ"מ 55).**

| Dry density (kg/m3) | | | CBR (%) | |
|---|---|---|---|---|
| Point No. | Before remolding | After Remolding | Before remolding | After Remolding |
| 1.1 | 2026 | 1839 | 47 | 5.8 |
| 2.1 | 1952 | Unmeasur. | 57 | 5.8 |
| 3 | 1844 | 1739 | 57 | 2.9 |
| 4 | 1803 | 1757 | 46 | 3.0 |

Part of the triaxial testing was conducted in a standard triaxial apparatus, and part in the HCT device. Fig. 5.7 presents a summary of the results obtained from the monotonous triaxial shear tests on the "unremolded" material. Linear regression applied on the results of the seven tests performed showed internal angle of friction values of 47$^o$ and initial cohesion of 0.85 kg/cm$^2$ ($R^2$ = 0.99). The results are fairly close to those obtained in the direct shear testing, and are later used as input for the analytical system. Fig. 5.8 summarizes the results of the triaxial tests conducted on "remolded " samples. Linear regression analysis on the results with the constraint of zero cohesion gave $\phi$ = 48.2° with $R^2$=0.988. Due to the small difference in the value of the internal angle of friction in the remolded and unremolded samples, it was assumed that remolding did not change the

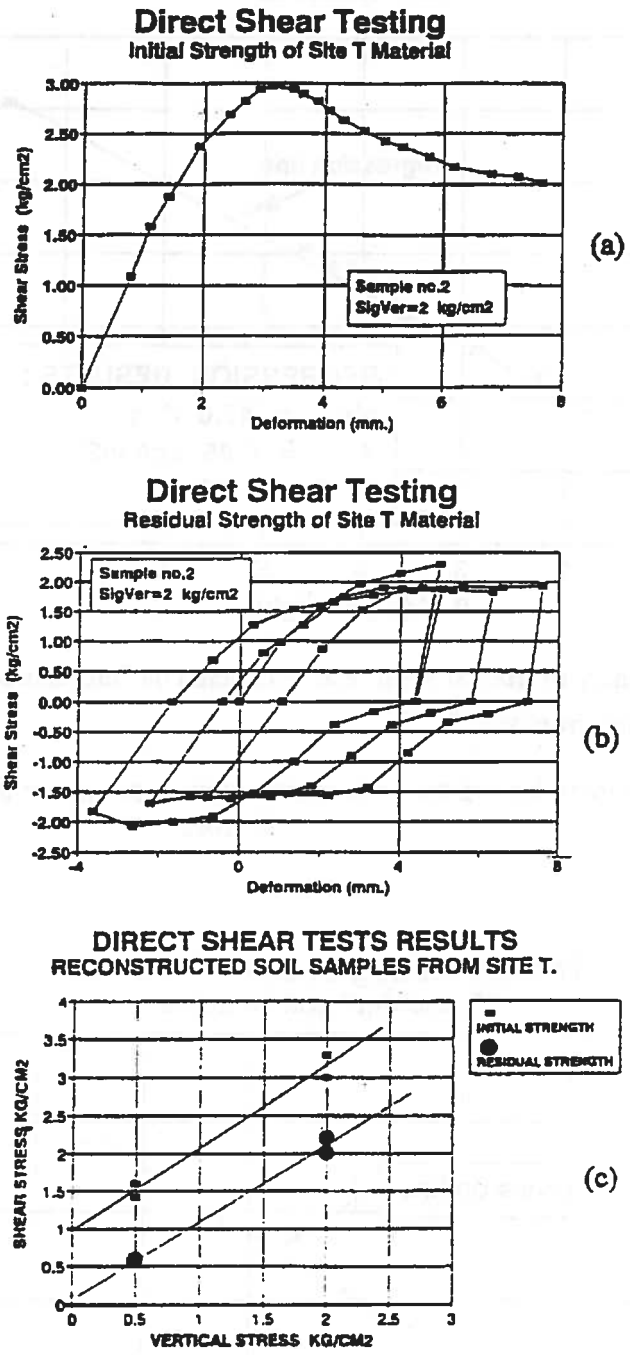


Fig. 5.6 Results of direct shear testing of site T material

(a) Direct shear of unremolded soil sample.

(b) Reversal direct shear of a remolded soil

(c) Summary of results from direct shear testing of site T material.

ציור מס. 5.6 תוצאות בדיקות גזירה ישירה - קרקע מאתר T

(a) גזירה ישירה של מדגם "בלתי־מופר"

(b) גזירה מחזורית של מדגם שהופר

(c) סיכום בדיקות גזירה ישירה על קרקע מאתר T

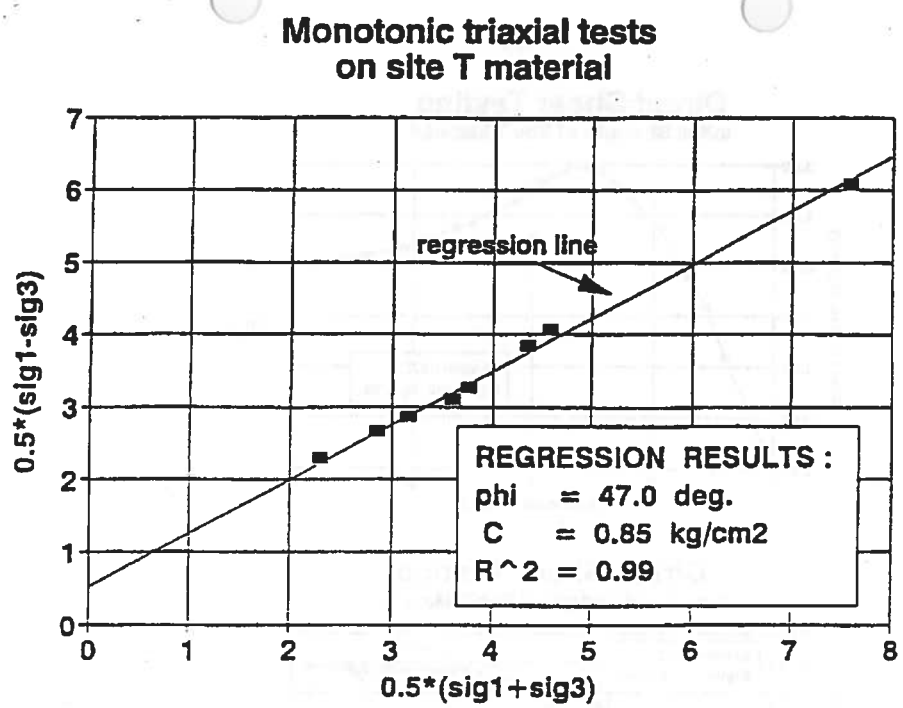


Fig. 5.7 Summary of triaxial shear tests conducted on "unremolded" soil samples from site T.

ציור מס. 5.7 סיכום בדיקות גזירה מרחבית של מדגמי קרקע "בלתי מופרים" מאתר T

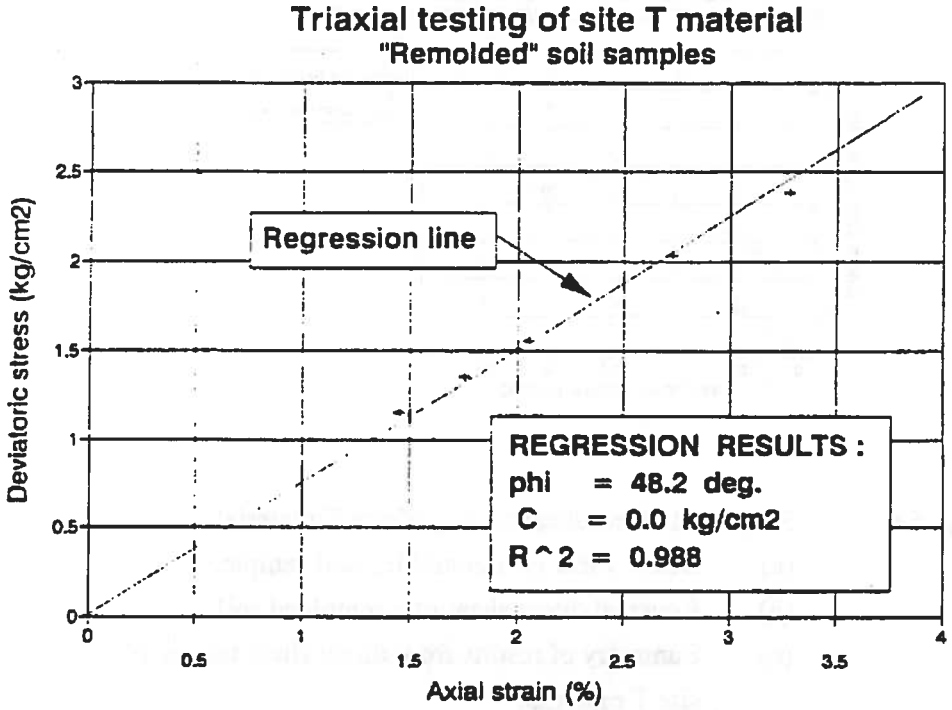


Fig. 5.8 Summary of triaxial shear tests conducted on "remolded" samples from site T.

ציור מס. 5.8 סיכום בדיקות גזירה מרחבית של מדגמי קרקע "מופרים" מאתר T

value of $\phi$. This assumption concurs with previous findings described in the literature survey (Chapter 2).

Some important conclusions can be drawn as to the constitutive behavior of the soil. Fig. 5.9 and 5.10 give some results of stress-strain curves obtained in the triaxial tests (for unremolded and remolded soil samples, respectively). For depiction purposes, a straight line was drawn for each sample that roughly parallels the stress-strain curve at the beginning of the test. Point A indicates the approximate location where the stress-strain curve diverts from the straight line with the initial modulus of elasticity. Point B denotes the location of sample failure (remolding of the soil). In the unremolded samples which were subjected to low confinement pressure, the axial strain at failure is less than 1% (Fig. 5.9). This value rose to about 1.3% in the samples subjected to higher confinement pressures. In the remolded soil samples (Fig 5.10), the point of failure extended to an axial strain of more than 3%.

In order to demonstrate the soil constitutive behavior relative to the assumed model behavior (see chapter 4), two parameters are introduced:

$$R_\sigma = \frac{\sigma_B}{\sigma_A} \qquad [5.1]$$

$$R_\varepsilon = \frac{\varepsilon_B}{\varepsilon_A} \qquad [5.2]$$

where:

$\varepsilon_B, \sigma_B$ - are the axial strain and deviatoric stress at the point of soil sample failure, respectively;

$\varepsilon_A, \sigma_A$ - are the axial strain and deviatoric stress at the point of divergence from perfectly elastic behavior, respectively.

$R_\sigma$ and $R_\varepsilon$ give a measure of the divergence of the soil behavior from that of the model assumption as illustrated in Fig. 4.1. In an "ideal" soil that has the assumed constitutive behavior, both parameters would have the value of 1.0. As can be seen in Fig. 5.9, $R_\sigma$ values in the unremolded samples are in the range of 1.1 - 1.35 (the lower values were obtained in samples tested under zero confinement pressure), and $R_\varepsilon$ values are 1.4 - 1.6. The $R_\sigma$ values obtained for the remolded soil samples (Fig. 5.10) were 1.5 and more, and the corresponding $R_\varepsilon$ values 5 - 10 (and more), much higher than those in the unremolded samples. As can be perceived from the results, the assumptions made as to the brittleness

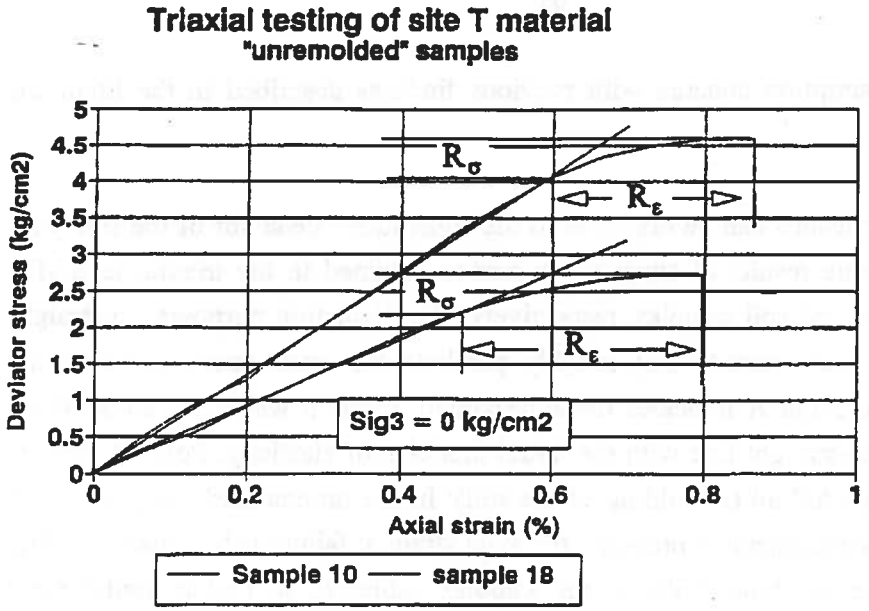


Fig. 5.9 An illustration of the stress strain behavior of "unremolded" soil samples from site T during a triaxial shear test .

ציור מס. 5.9 התנהגות עקומי מאמץ־עיבור בבדיקת גזירה מרחבית של מדגמי קרקע "בלתי מופרים" מאתר T

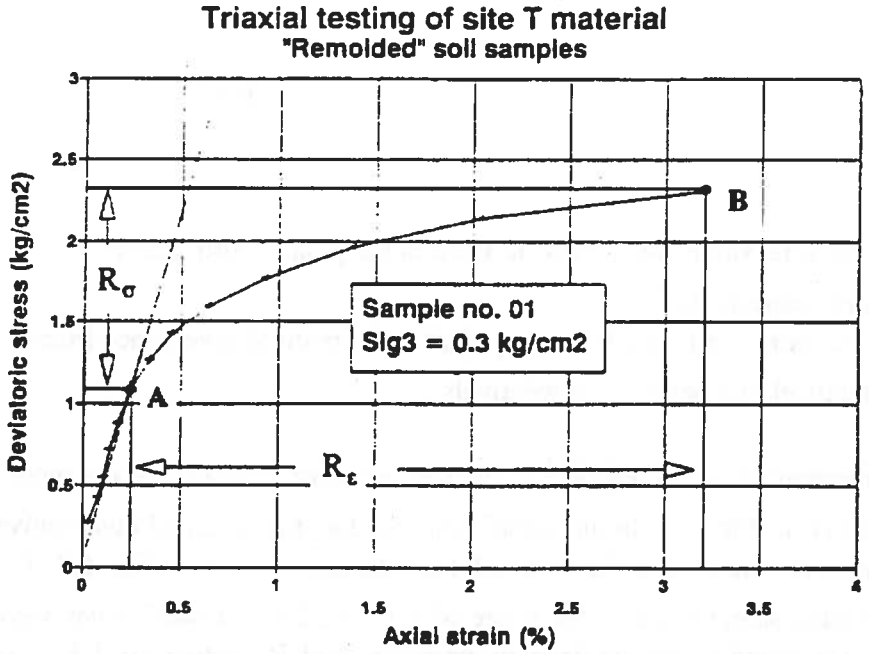


Fig. 5.10 An illustration of the stress strain behavior of "remolded" soil samples from site T during a triaxial shear test .

ציור מס. 5.10 התנהגות עקומי מאמץ־עיבור בבדיקת גזירה מרחבית של מדגמי קרקע "מופרים" מאתר T

and the closeness to elastic behavior of the unremolded dry soil, seem to conform with the laboratory findings.

Module of elasticity values obtained in the laboratory tests (calculated as the secant modulus of deformation at the pre-peak zone of the soil) move along a wide range of 600-1400 kg/cm$^2$ for the unremolded soil and 200-300 kg/cm$^2$ for the remolded site T soil samples.

As noted previously, cyclic triaxial shear tests were also performed, using the HCT device. According to the strength values of the unremolded soil, special stress paths were built with the intention of achieving stress levels in the range of 90-100% of the soil strength. Fig. 5.11 shows an example of the stress path and development of the relative stress level exerted on a sample of soil along a loading path. It is clearly seen that the maximum relative stress level is not achieved when the wheel is above the point of the soil but only at a certain distance from it, when the confining pressure decreases to a very low level. The maximal relative stress level reached in the case presented in Fig. 5.11 is 93.5% of the soil strength (according to the strength parameters of the unremolded soil).

Fig. 5.12 depicts the results of a cyclic shear test performed under the stress path described in Fig. 5.11 The figure shows the development of axial strains including plastic strains in the sample. After about 200 cycles the sample failed.

Fig. 5.13 summarizes the results of the cyclic shear tests conducted on soil samples from site T. Regression performed on the results gave the following fatigue formula:

$$\log(N) = 35 - 35 \cdot S_R \qquad [5.3]$$

with $R^2 = 0.983$

5.4.2 Site S material

Fig. 5.14 and 5.15 present the results of gradation, Atterberg limits and conventional CBR tests conducted on soil brought from site S. More than 95% of the soil passed #40 sieve and about 20% passed the #200 sieve. As in the site T material, the fine fraction of the soil showed no plasticity. According to the AASHTO method, the material may be classified as A-2-4 (silty sand) and as SM, according to the Unified method.

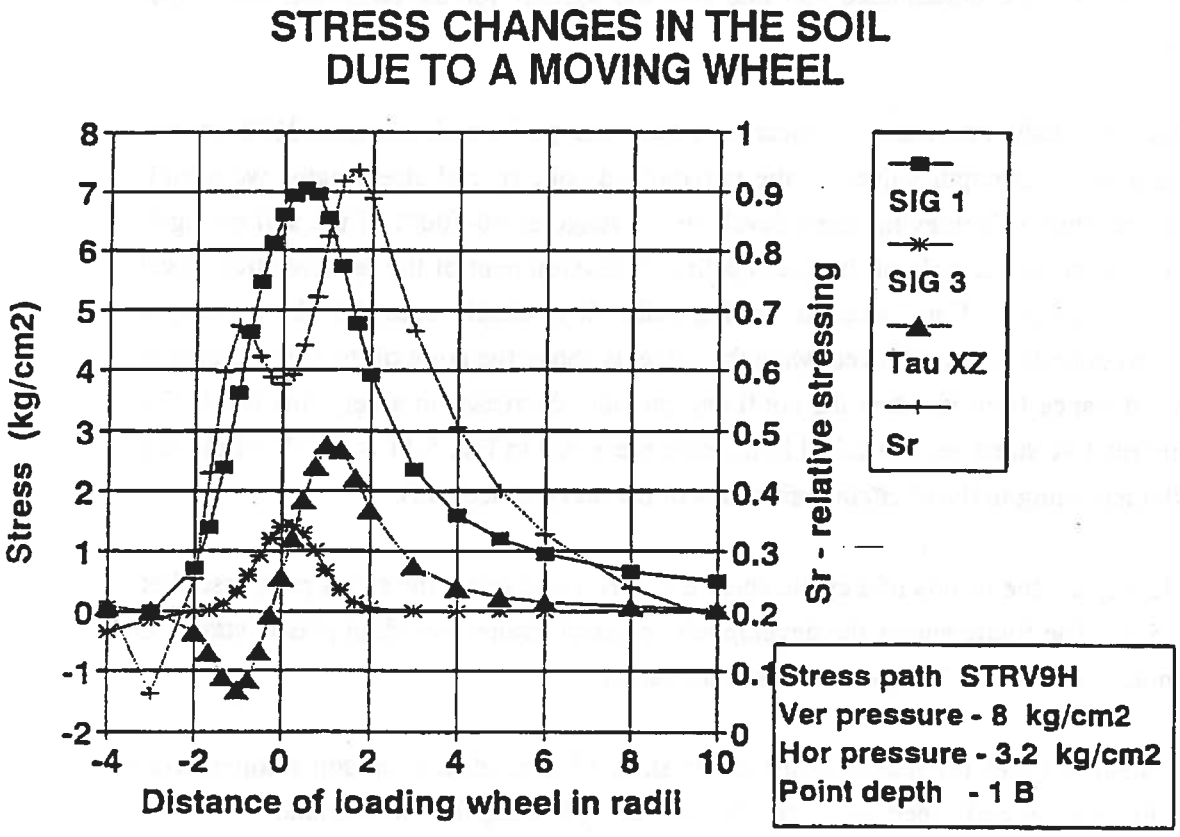


Fig. 5.11 Stress path and relative stress level in a soil element under a moving surface loading (semi-infinite, homogeneous, elastic, and isotropic medium).

ציור מס. 5.11 מסלול מאמצים ורמת המאמץ היחסי באלמנט בקרקע, תחת עומס נע על פני השטח (בהנחת מרחב חצי־אינסופי, הומוגני, אלסטי ואיזוטרופי).

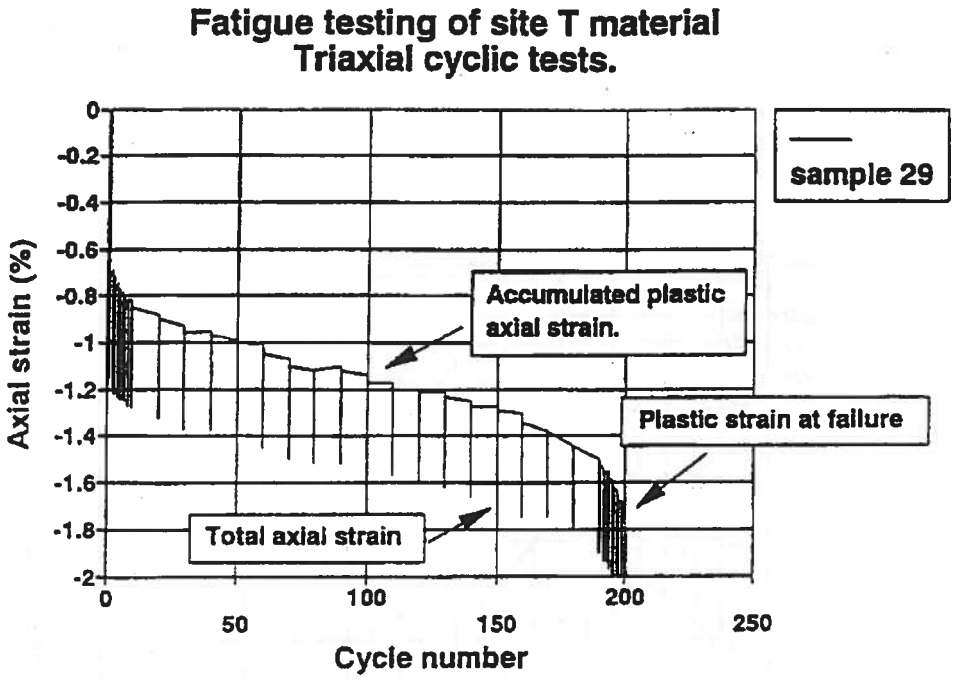


Fig. 5.12 Strain development in an "unremolded" soil sample under cyclic shear test.

ציור מס. 5.12 התפתחות עיבורים במדגמי קרקע "בלתי מופרת" מאתר T תחת עמיסה מחזורית.

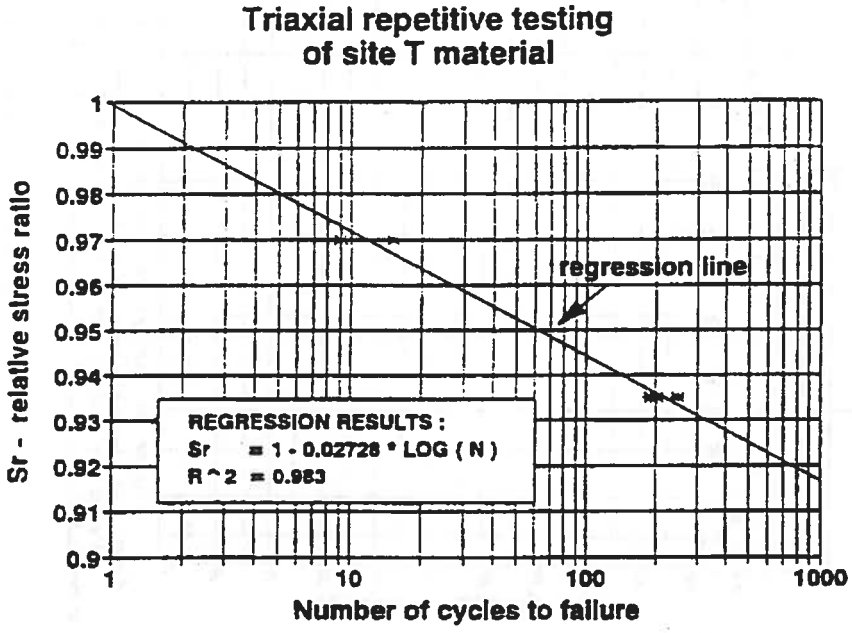


Fig. 5.13 Summary of cyclic shear tests results on the site T material.

ציור מס. 5.13 סיכום תוצאות גזירה מחזורית על מדגמים "בלתי מופרים" מאתר T.

Technion Research and Development Foundation
Soil and Roads Laboratory

Project Nº: _____
Location: Site S
Date: 1.90

Gradiation Curve

| Pit Nº | Depth, m | |
|---|---|---|
| | | |
| | | |
| | | |
| | | |
| | | |
| | | |

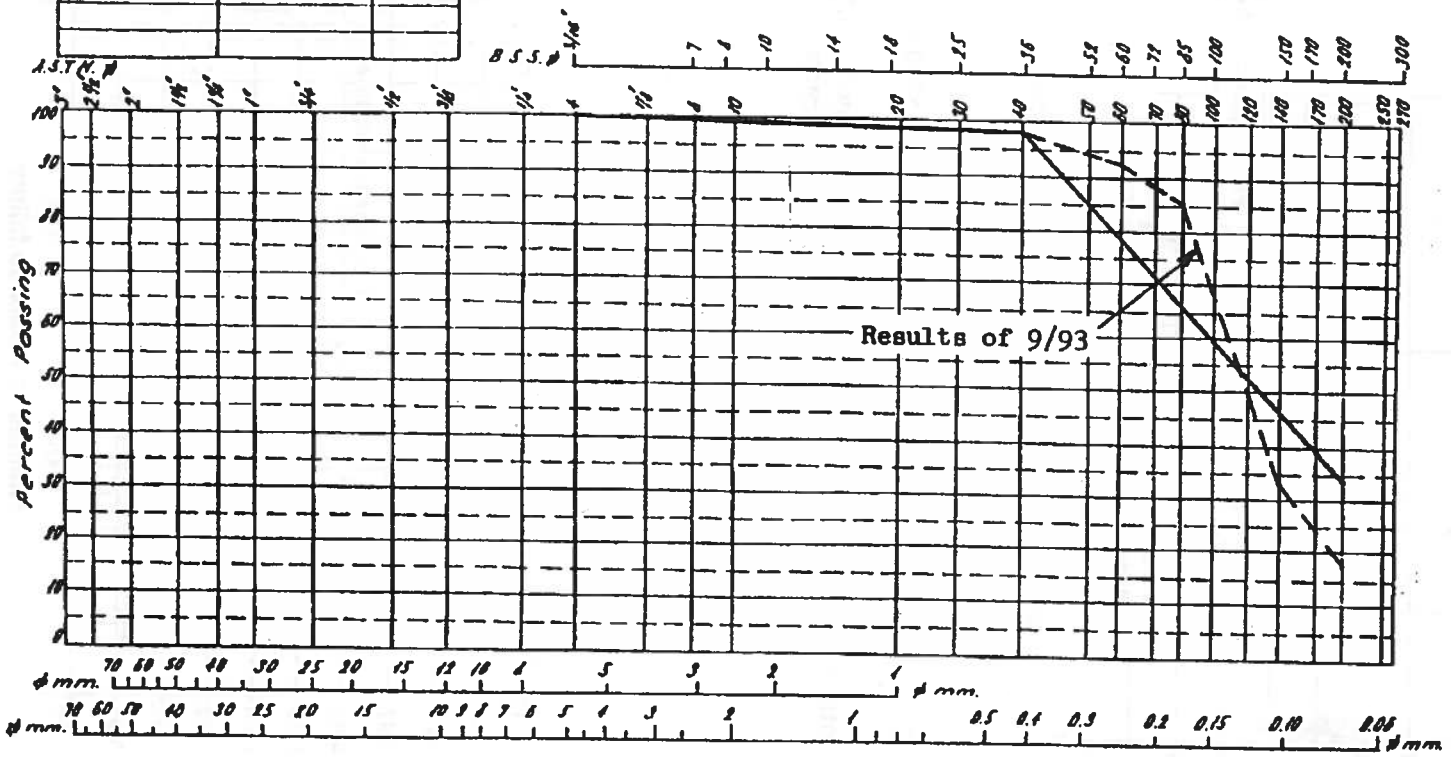


Fig. 5.14 Mechanical gradation test results on site S material.

ציור מס. 5.14 תוצאות אנליזה מכנית של הקרקע באתר S.

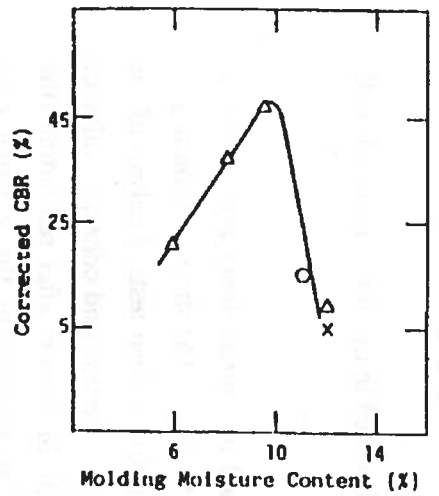


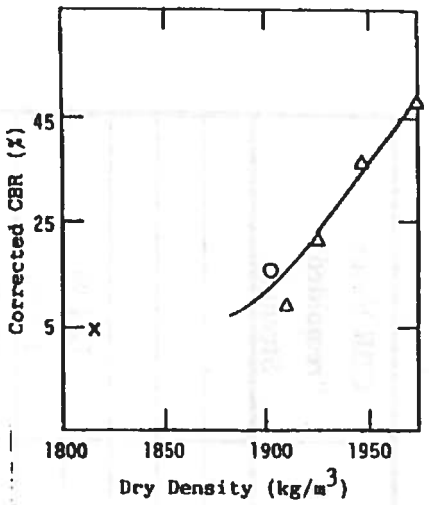


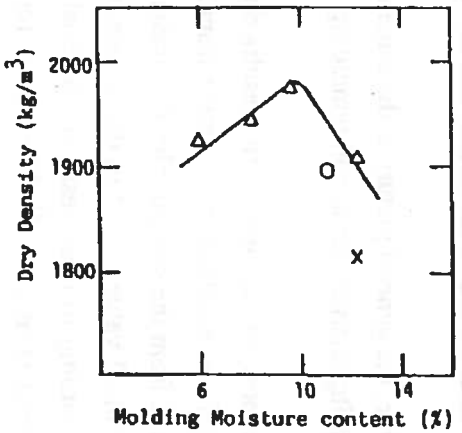


| CALIFORNIA BEARING RATIO TEST | | |
|---|---|---|
| Compaction Data | Plan for: Site S | |
| Sample diameter 6" Sample height 5" | | |
| Compacted in 5 Layers | Description: Light-brown silty sand | |
| 10lb. Hammer, 18" fall | | |
| 56 blows per layer △ | O - L.L. - NP P.I. - NP | |
| 26 blows per layer O | | |
| 12 blows per layer X | Surcharge weight | 10 lb. |
| OPT. Moisture Content: 10% | Soaking time | 4 days |
| Max. Density: 1980 kg/m3 | Date | 1.90 |

Fig. 5.15 Results of CBR and indicative tests on the site S material

ציור מס. 5.15 תוצאות מערכת CBR וגבולות סומך על דגימות קרקע מאתר S.

As with the site T soil, laboratory CBR tests were also conducted on dry soil samples from site S. Since the amount of coarse fraction is negligible in this soil, practically all the aggregate fractions were included in the tests. Table 5.3 summarizes the results of the CBR tests on both "remolded" and "unremolded" reconstituted soil samples. All samples were compacted to a dry density of about 1700 kg/m$^3$ which is close to the soil density found at the site.

**Table 5.3 - CBR tests on dry samples from site S**

**טבלה 5.3 - בדיקות מת"ק במדגמי קרקע מאתר S, לאחר יבוש.**

| Sample No. | CBR Value "Unremolded" Strength | CBR Value "remolded" Strength |
|---|---|---|
| S11 | 78 % | |
| S27 | 29 % | |
| S20 | 77 % | |
| S38 | | 12.1 % |
| S17 | | 8.2 % |
| S78 | | 7.8 % |
| **Average Value** | **61.3 %** | **9.3 %** |

As seen in the table, the general picture is the same as observed in the site T material, with soil strength dropping sharply due to soil remolding.

Fig. 5.16a and b show an example of the results obtained in a direct shear and a reversal direct shear tests of "unremolded" soil sample from site S. Fig. 5.16c shows a summary of the results obtained from the soil samples that underwent direct shear tests. Analysis of the results gives an initial value of 36$^o$ to the internal angle of friction and cohesion value of 0.54 kg/cm$^2$. According to these tests, the internal angle of friction after remolding (the reversal shear tests) is about 44$^o$. The above result (an increase of the $\phi$ value after remolding ) is not expected according to the results of the literature survey. Running linear regression under the assumption of an initial cohesion value of 0.3 kg/cm$^2$ (as was found in the triaxial tests, see below), the value of the internal angle of friction rose to the more probable value of 46°.

Fig. 5.17 presents a summary of the results obtained from the monotonous triaxial shear tests on the "unremolded" material. Linear regression applied on the results of the six tests

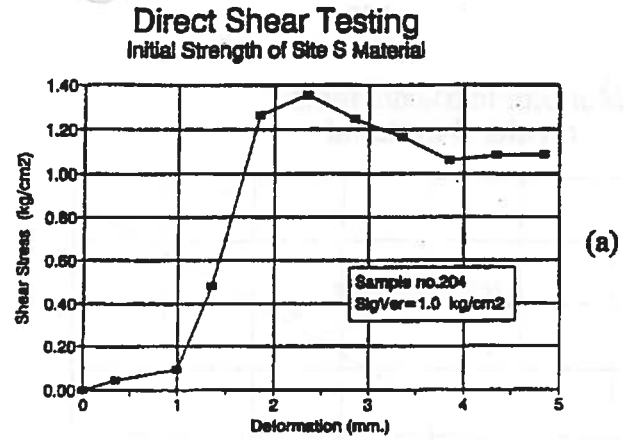


(a)

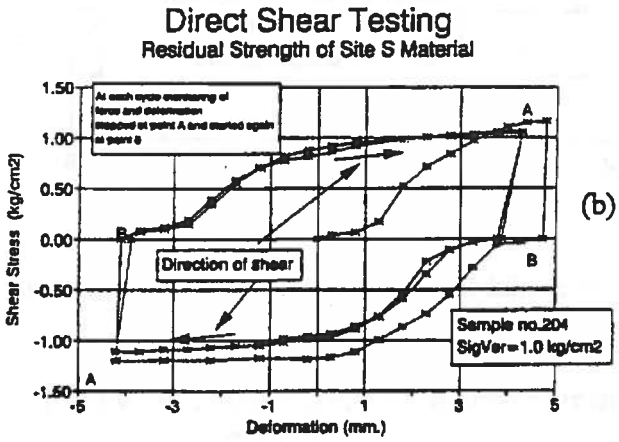


(b)

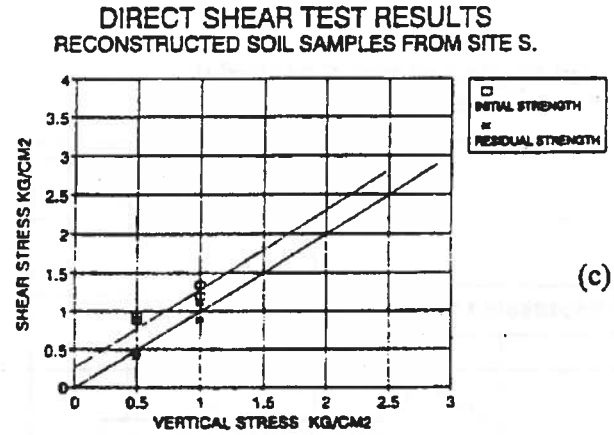


(c)

.Fig. 5.16 Results of direct shear testing of site S material

(a) Direct shear of "unremolded" soil sample.

(b) Reversal direct shear of a remolded soil

(c) Summary of results from direct shear testing of site S material.

ציור מס. 5.16 תוצאות בדיקות גזירה ישירה - קרקע מאתר S

(a) גזירה ישירה של מדגם "בלתי־מופר"

(b) גזירה מחזורית של מדגם שהופר

(c) סיכום בדיקות גזירה ישירה על קרקע מאתר S

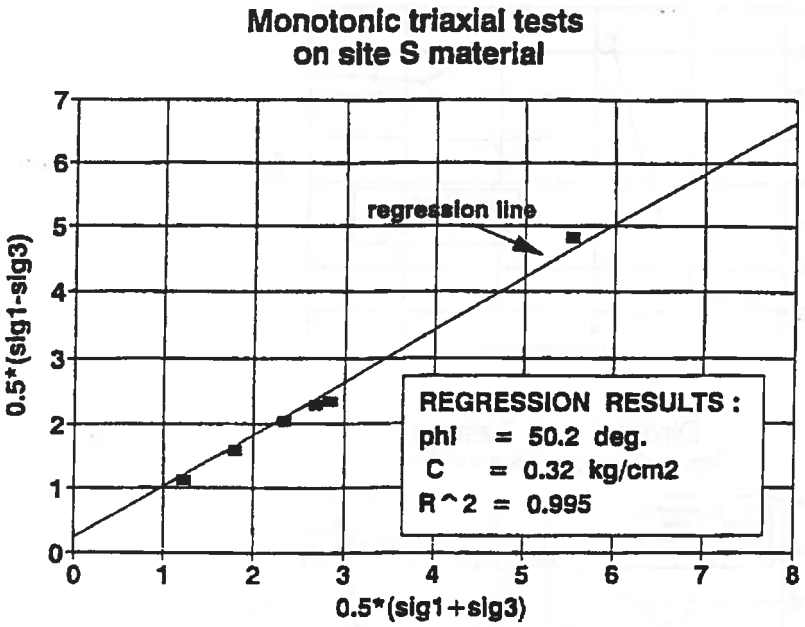


Fig. 5.17 Summary of triaxial shear tests conducted on "unremolded" soil samples from site S.

ציור מס. 5.17 סיכום בדיקות גזירה מרחבית של מדגמי קרקע "בלתי מופרים" מאתר S

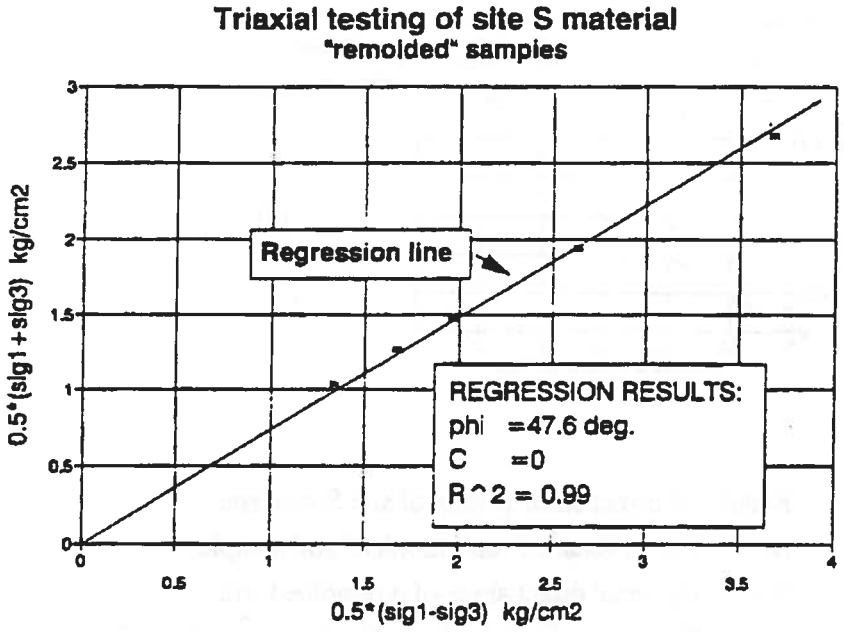


Fig. 5.18 Summary of triaxial shear tests conducted on "remolded" samples from site S.

ציור מס. 5.18 סיכום בדיקות גזירה מרחבית של מדגמי קרקע "מופרים" מאתר S

that were performed shows internal angle of friction values of 50.2° and initial cohesion of 0.32 kg/cm$^2$ ($R^2$ = 0.995).

Fig. 5.18 summarizes the results of the triaxial tests conducted on "remolded" samples. Linear regression analysis on the results with the constraint of zero cohesion yielded $\phi$ = 48.2° with $R^2$=0.988. As with the site T material, it was assumed that remolding did not change the value of $\phi$ which remained constant at a value of 50°.

Fig. 5.19 and 5.20 give some results of stress-strain curves obtained in the triaxial tests (for unremolded and remolded soil samples, respectively). As previously seen in the site T soil, the unremolded sample behavior (Fig. 5.19) was much more brittle than that of the remolded ones (Fig. 5.20). In the unremolded samples, the axial strain at failure is around 1% while in the remolded samples, the point of failure extends to an axial strain of more than 4%.

Using the parameters presented in equation [5.1] and [5.2], one obtains $R_\sigma$ values in the unremolded samples in the range of 1.1 - 1.25 (the lower values were obtained in samples tested under lower confinement pressure), and $R_\varepsilon$ values are 1.3 - 1.6. The $R_\sigma$ values obtained for the remolded soil samples (Fig. 5.20) were 1.5 and more, and the corresponding $R_\varepsilon$ values 2.8 - 7 (and more). The results obtained are similar to those for the site T material and indicate that in the tested dry remoldable soils, the pre-remolding behavior is close to linear-elastic. As could also be seen during the conduction of the shear tests, the response of the unremolded samples to shear was brittle, and sample failure was characterized (see Fig. 5.21) by breakage of the samples.

Modulus of elasticity values obtained in the site S soil tests were 400-700 kg/cm$^2$ for the unremolded soil and 100-300 kg/cm$^2$ for the remolded soil samples.

Triaxial cyclic tests were also conducted in the HCT device on soil samples from site S. As was done with the site T material, regression was performed on the results, assuming N=1 for $S_R$=1. The regression yielded $C_1$ and $C_2$ values of about 40 with $R^2$=0.9. Since only three samples were tested, due to technical problems that aroused in the shear device, the results should be dealt with caution.

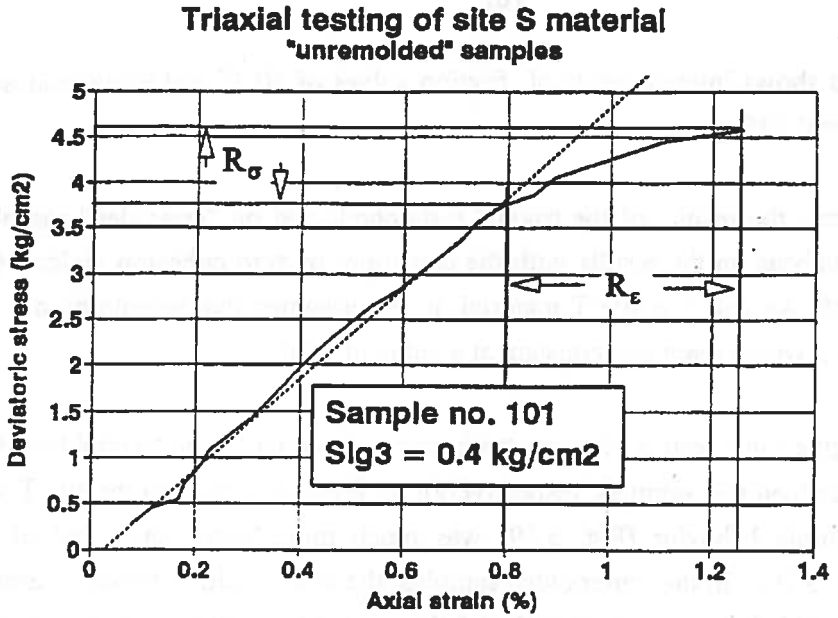


Fig. 5.19 An illustration of the stress strain behavior of "unremolded" soil samples from site S during a triaxial shear test .

ציור מס. 5.19 התנהגות עקומי מאמץ-עיבור בבדיקת גזירה מרחבית של מדגמי קרקע "בלתי מופרים" מאתר S

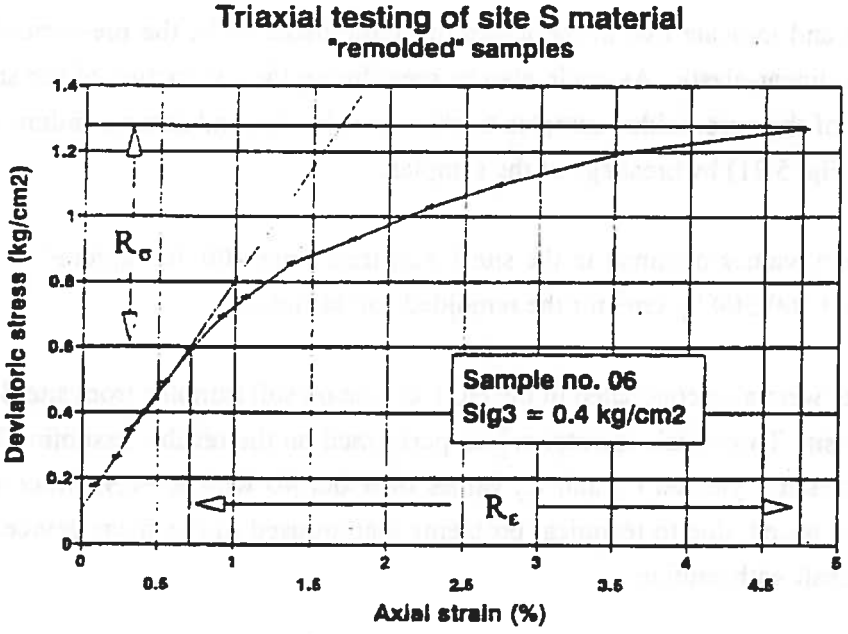


Fig. 5.20 An illustration of the stress strain behavior of "remolded" soil samples from site S during a triaxial shear test .

ציור מס. 5.20 התנהגות עקומי מאמץ-עיבור בבדיקת גזירה מרחבית של מדגמי קרקע "מופרים" מאתר S

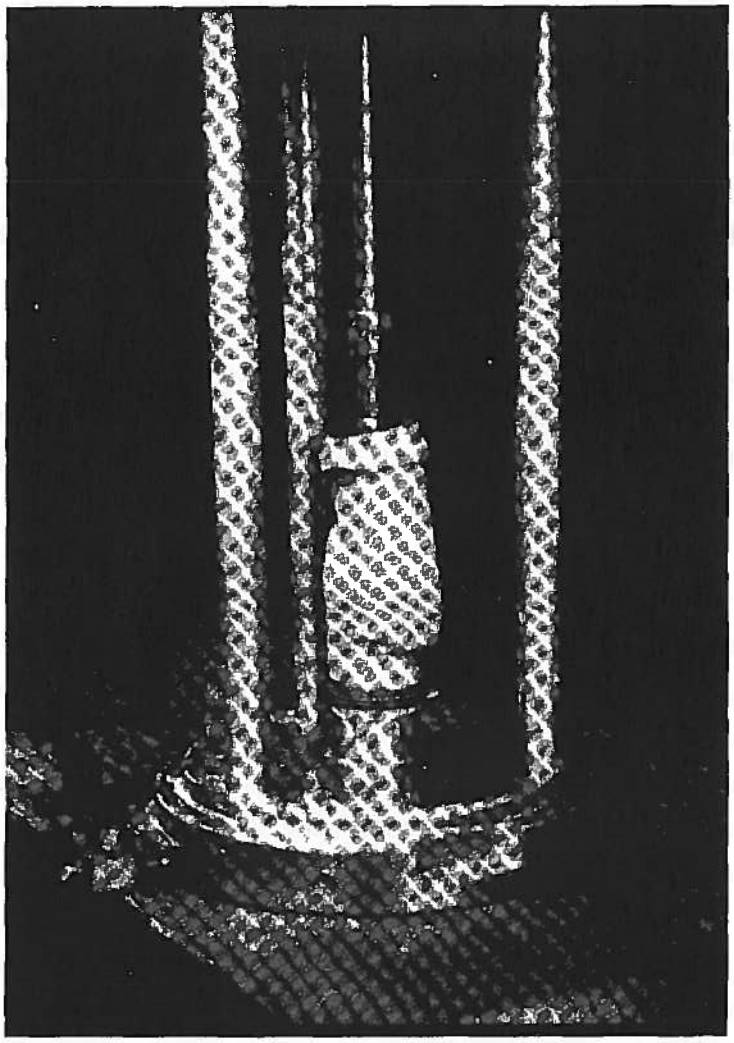

Fig. 5.21 A photograph illustrating the brittle nature of failure of an unremolded soil sample under triaxial shear testing.

ציור מס. 5.21 תצלום להדגמת האופי הפריך של מדגם קרקע "בלתי מופר" מאתר S.

## 5.5 Summary

Two types of soils were investigated during the laboratory testing phase of the research. The testing program included gradation and indicative tests, shear strength, CBR, and cyclic shear tests. The soils that were chosen to be studied, were both granular soils which attain some degree of natural cementation during the process of drying. Testing of such a kind of soils in the laboratory, required the adoption of complex procedures of sample preparation and curing, intended to simulate natural in-situ processes

The results of the laboratory testing program gave some verification to the mechanistic model assumptions in the following main points:

A. The remolding action of the naturally cemented soils is characterized by the nullification of the cohesive part of the soil strength. No significant change was noticed in the frictional part of strength (assuming no change takes place in the soil density).

B. The constitutive behavior of the naturally cemented soil before remolding is predominantly linear-elastic. Plastic strains in the pre-peak zone are negligible, and the soil elastic modulii are much higher than their value after remolding. Once a soil element reaches its strength envelope (according to Mohr-Coulomb failure criterion), there is a fast decrease in the soil strength toward the residual (remolded) strength. These points substantiate the mechanistic model assumed constitutive behavior of the unremolded soil.

C. Repetitive loading of a soil sample to levels that are lower than the soil strength may also lead to failure and remolding in the sample. The number of loading cycles needed to cause sample failure, depend upon the stress level exerted on the sample and may be described by a semi-logarithmic fatigue function.

Apart from backing up the presuppositions of the mechanistic model, the results obtained during the laboratory tests were applied as input for the operation of the numerical model. The numerical model results, as obtained using the properties of both tested soils, could thereby be later compared to the results of the moving wheel tests which were conducted with the same types of soils (see Chapter 7).

# CHAPTER 6: THE ANALYTICAL SYSTEM

## 6.1 Software Systems and Principal Assumptions

The highly complicated nature of the presented mechanistic physical model render it practically impossible to reach a closed analytical solution to the problem. All efforts were therefore directed towards a numerical solution which will describe the essential features of the model. After evaluating a number of software systems, the FLAC system was chosen (Ref. 56) to serve as the principal software package in the development and application of the analytical system.

The FLAC system is a two-dimensional explicit finite difference code which simulates the behavior of soil and other systems which may undergo plastic flow when they reach their yield limit. The system was originally built with a special focus on soil and rock problems, and can be utilized with a number of built-in constitutive models. FLAC is not friendly to occasional users but provides frequent ones with a powerful and flexible instrument, including the ability to build new constitutive laws or modify existing ones.

The main reasons for the choice of the FLAC system were:

1. Proficiency of the system to deal with cases of considerable plastic deformations in the soil. The explicit solution tackles these cases very efficiently relative to implicit finite element methods.

2. The explicit solution method, that enables tracking the processes (stresses, strains, deformations, etc.) in the wheel-soil system as they occur is extremely necessary in cases of considerable "plastic flow" during the loading process. The above feature also simplifies the detection of "bugs" in the numerical model since the whole process can be observed step by step.

3. The working method of the FLAC system does not require the construction and updating of large matrices. This fact enables the use of IBM compatible PC's (type 386 and above) to solve comparatively large problems in sizes of thousands of elements, with relatively modest memory requirements (for example: a 10,000-element model under Mohr-Coulomb requires only 4 MB internal memory).

4. The FLAC system was built with specific emphasis on geotechnical problem-solving, thus facilitating use of the system to solve problems examined in the present research.

5. The usage of the FLAC system by some researchers in the Technion's Road and Soil Department was useful in achieving a deep knowledge of the system, and enabled mutual discussions and consultations which contributed to the development of the numerical models.

The numerical models in the FLAC system were written with the use of an internal system language and the formulation of Batch files that serve as input for the software running. The same internal language was used during the research to modify part of FLAC built-in modules and to add consideration to other features such as soil fatigue. Integration of the numerical models' results, as well as additional parts of the analytical system, were written with the use of the TURBO-PASCAL 6.0 of Borland Co.

A few basic assumptions and presuppositions were acted upon when constructing the analytical system:

1. The basic soil behavior is according to the Mohr-Coulomb model and the constitutive law is elastic-plastic. This model was chosen as the most suitable for the dry granular soil that was the main soil type studied. The most significant change effected in the basic constitutive law is the existence of discontinuity at the failure point of the soil, when the soil strength decreases to its residual value. For soils, in which the remolding process is not sudden and depends on the plastic shear strain undergone by the soil, strain softening constitutive law may be utilized.

2. Use of a two-dimensional modeling. The solution of the numerical problem was achieved by using two dimensional modeling with the assumption of plane strain conditions. Although a 3-D modeling of the problem could have many advantages, the complexity of the model increases to such an extent that unavailable computing resources would be essential.. For that reason, most of the numerical researches in the field of wheel-soil interaction still use 2-D modeling.

3. Dealing with dynamic problems. The numerical models within the framework of the present research were built with the assumption of quasi-static conditions. Reference to the dynamic aspects of the problem will be possible in the future by the use of the FLAC system which includes (in its latest version) a special module for dynamic

modeling. The inclusion of the above issue will no doubt demand the use of dynamic parameters which are unknown at the present.

## 6.2 The principal analytical sub-systems.

The purpose of the analytical system was to perform numerical simulations of the repeated soil loading by aircraft wheels and to provide a better estimation of the runway expected performance. Fig. 4.7 gives a schematic drawing of the analytical system structure. This system comprises a few essential sub-systems:

### 6.2.1 Sub-system A - The development of a two-layer soil structure.

This sub-system was designated to perform estimation of the remolded soil layer depth as a function of the number of aircraft wheel passes. The models for wheel-soil simulation were built with the FLAC system. Due to the two-dimensional limitations of the model, two possible ways to analyze the system were examined:

1. Analysis of system behavior by numerically conducting a longitudinal cut of the wheel. Fig. 6.1 shows the resulting network of elements that represent the wheel-soil system. The system consists of a central cylinder representing the center of the wheel, surrounded by concentric multi-element rings that portray the elastic tire. Simulation was performed by exerting vertical force (which represents the wheel load) on the wheel center and after stabilization of the system, the wheel was forced at a horizontal, very low, steady speed, until one quarter of a turn was completed. During the wheel rotation the stresses were recorded, according to which the remolded soil depth, as caused by the wheel motion, was determined. Repeated reactivating the above process on the two layers soil enabled construction of a relation between number of wheel loading cycles and the depth of the remolded layer that develops in the soil. The longitudinal cut of the wheel is the most commonly used in research dealing with wheel-soil interaction by numerical means (Ref. 27). This kind of a cut enables keeping track of the forces and stresses that the wheel exerts on the soil in various operational conditions.

2. Simulation of a cross section of the wheel. Fig. 6.2 shows a schematic drawing of a section in the soil with a loading area of the same width as the loading wheel. In this case, an accurate model of the wheel cross section was not built in order to avoid the substantial increase in the number of elements in the model, and the significant expansion in the computer time needed to solve the problem. This model enables the

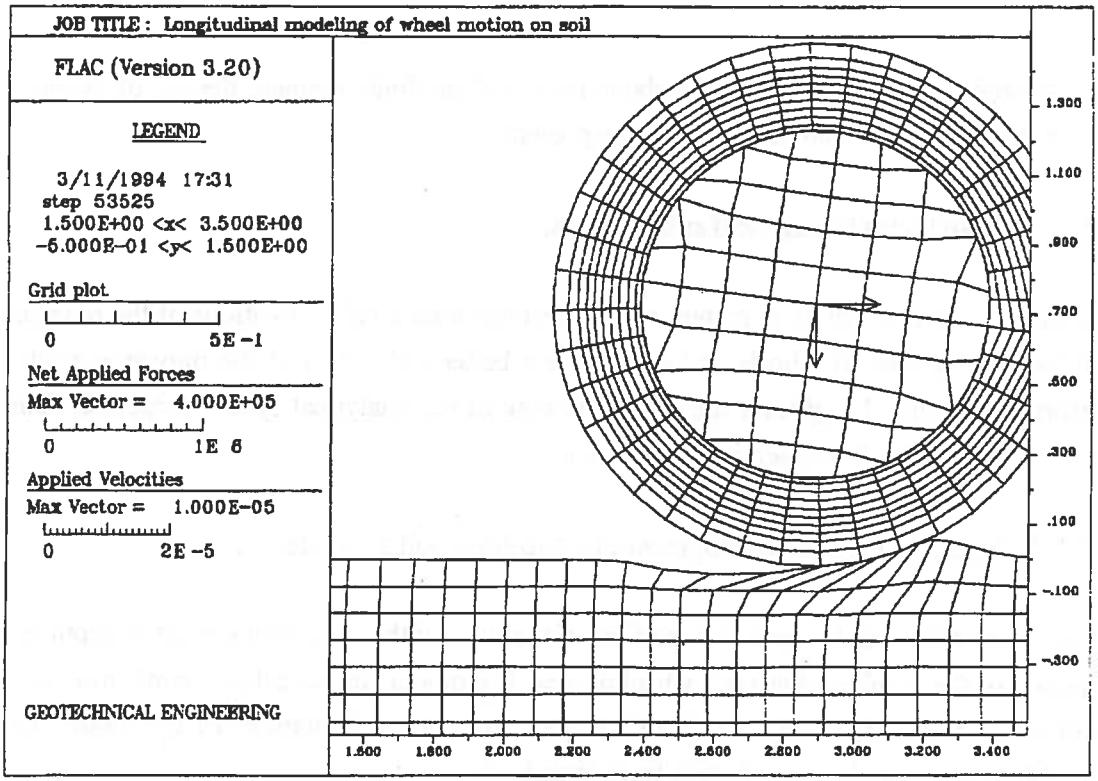


Fig. 6.1 FLAC model representing a longitudinal cut of a loading wheel.

ציור מס. 6.1 רשת אלמנטים במערכת FLAC ליצוג חתך אורכי של גלגל מעמיס על קרקע.

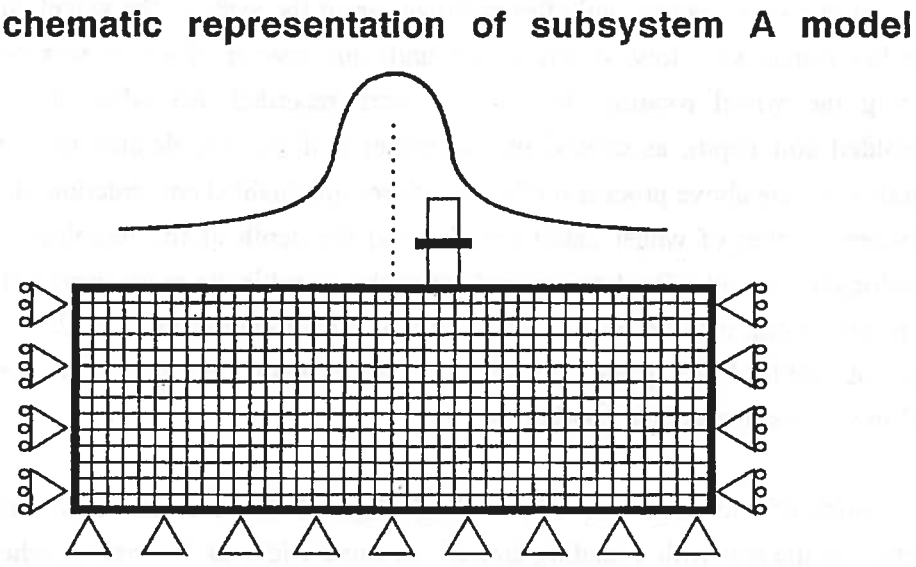


Fig. 6.2 A schematic representation of a cross-section of the wheel-soil system.

simulation of repeated wheel loading whereas the wheel location can be laterally changed from one loading to the next according to a predetermined distribution. Wheel loading simulation is achieved by exerting vertical pressure (using the same pressure as the contact pressure of the wheel) on a strip with a width similar to that of the loading wheel. After stabilization of the numerical system the pressure is withdrawn and a loading is performed in another location according to the given lateral wander. Throughout the whole process of loading and reloading the stress levels at every point in the soil are monitored. When an element in the soil has reached failure, it is marked as a remolded element and its properties undergo the required changes.

The dimensions of the constructed models were determined in order to minimize, as much as possible, the effects of the boundaries on the system. In accordance with Ref. 12 and others it is acceptable, when performing a numerical analysis, to take a soil section with dimensions of depth and width about 5 times that of the contact length of the wheel. Other points that effected the dimensions of the soil in the numerical models were the wheel movement (in the longitudinal cut) and the lateral wander (in the cross section). The number of elements in each of the models was 1500-2000.

After concluding series of runs of the system in both the aforesaid cuts, it was decided to concentrate on solving the problem by using a cross section model of the wheel. This decision was made for the following reasons:

a) The chosen approach enables simulating the loading process taking into account the lateral wander of aircraft traffic;

b) When making a longitudinal cut of the wheel, in soils with high plastic deformation, the wheel movement causes the formation of a soil mound in front of the wheel. As the wheel is (in the 2-D numeric model) a continuous cylinder, the above mentioned soil mound keeps growing, and may cause excessive distortion of the elements in the soil model (see Fig. 6.1). In some runs, instabilization of the numerical system was caused by the "crushing" of overly deformed elements;

c) Forming a cross section of the wheel enables accounting for the stresses and deformations which occur in the soil across the width of the wheel. The above is especially important when large plastic ruts are formed in the wheel path and soil mounds develop at both its sides.

The input parameters needed for operating the numerical model consisted of the width of the loading wheel, the contact pressure, soil properties before and after remolding (elastic characteristics, strength and fatigue parameters) and the expected distribution of lateral location of the loading wheel.

Each cycle of the computer run included the following steps (see Appendix A1 for a listing of the source code written in the FLAC language):

a) Determining the location of load application. Load lateral location was set to be distributed normally around the center of the soil model with a predetermined standard deviation. This normal distribution of the lateral location of the wheel is in accordance with observations reported in the literature (Ref. 16);

b) Applying the wheel load on the soil. The surface of the soil is subjected to a vertical pressure (which equals the wheel contact pressure), applied at the above lateral position with a width equal to the width of the wheel;

c) Allowing the stepping of the system until the system stabilizes. Stabilization of the model is determined according to the maximum value of unbalanced force encountered at the grid points of the model. When the value of the maximum unbalanced force plunges below a predetermined limit, stepping is stopped. During the loading cycle, continuous monitoring is performed to observe the maximum relative stress level ($S_R$) obtained in each element. In order to avoid transient fluctuations caused by the numerical process to influence the results, some filtering activities were performed on the value of $S_R$. Following system stabilization, unloading of the wheel is done, and again the model is allowed to stabilize.

d) Detecting newly remolded elements and accounting for fatigue damages. After completion of the load cycle (loading and unloading), all unremolded elements are scanned. For those elements in which the $S_R$ value is 1.0, remolding is declared and the soil properties are changed to the remolded soil properties. For those elements in which $S_R$ value is less than one, use is made of equation [4.3] and [4.4] (with the fatigue parameters determined by the laboratory cyclic shear tests) to calculate the incremental and the accumulated damage to the element. An element in which the accumulated damage reaches the value of 1.0 is remolded and its properties changed.

Each run of the computer program simulates hundreds of wheel load cycles. The program monitors the stresses and deformations in the soil mass during loading and unloading of

the wheel. The accumulated damage in each element is "remembered" throughout the whole process, while the value of the maximum relative stress level is reset to zero at the beginning of each load cycle. The main output obtained for given loading data and predetermined soil parameters is the depth of the remolded soil layer as a function of number of passes executed.

6.2.2 Sub-system B - The behavior of a two-layer soil structure.

This sub-system should provide an estimation of the behavior of the two-layered soil system as a function of the depth of remolded layer and the soil properties before and after remolding. Two alternative approaches were taken:

A) Sub-system B1 - This sub-system provides an estimation of the equivalent strength of the double-layered soil as expressed by its bearing capacity value. In order to evaluate the bearing capacity of the soil under changing strength conditions, an attempt was made to develop an appropriate analytical solution. Based on limit-analysis theories, some basic equations were developed for the behavior of soil that has variable strength properties with depth. By application of the method of characteristics, these equations were used to establish an analytical solution giving a lower limit value for the bearing capacity of the soil. A special software written in Turbo Pascal 6.0 enables the evaluation of bearing capacity values of soil whose strength vary with depth, under an inclined loading of a plate grouser. Appendix B includes some details about the development process, the finite difference equations, and the software. In addition, some trial runs of the system, under different loading and soil conditions are raised and discussed. Comparisons with known solutions yielded good results and some validation to the system. However, in cases where the first derivative of the strength properties ( $\partial\phi/\partial Z$, $\partial C/\partial Z$ ) was not continuous, instability of the numerical system was frequently observed.

Since the remolding phenomenon in dry granular soils is characterized by the creation of definite soil layers, some problems resulted in implementing the above system as part of sub-system B1. It should be noted however that for many types of soils where the remolding process is less abrupt, the soil profile created is much smoother, and the suggested system can be used for bearing capacity estimations, including cases of inclined loading, such as braking action.

In light of the above, the equivalent strength of the system was found by numerical analysis of the resistance to penetration of the double-layered system. The numeric

model constructed with the aid of the FLAC system simulates a soil section loaded by a long and rigid strip (plane strain conditions are assumed). For symmetry reasons, the soil section could be split vertically into two and thus save computational efforts. Soil properties in the double-layered system are set to be the same as those obtained in the laboratory tests for the soil, before and after remolding. The model simulates the penetration of the strip into the soil, at low vertical speed. The soil resistance to the penetration of the rigid strip is continuously measured during the process. For every 1000 steps of the FLAC system, a check is made of the maximal recorded resistance to the penetration. Soil bearing capacity condition is declared when either the rate of penetration resistance increase is very low (less than 0.5% from one check to another), or when penetration reaches a depth of 15% of the penetrating strip width.

The model (see appendix A2 for the program listing) is run in succession for increasing values of the top layer thickness, thus creating a function that relates the penetration resistance of the two-layered system to the thickness of the upper layer. It should be noted that the results obtained (both for zero depth and for large depth of the upper layer) using real soil values are lower than expected according to bearing capacity calculations. The above is due to the influence of the elastic modulii of the soil on the results. The simulated test resembles to the CBR test in which the obtained value is more attached to the modulus of deformation of the soil. For validation purposes, trial runs were also conducted with the same soil properties except that the soil was highly stiffened. The results of these runs gave penetration resistance values, at both extreme points, which were very close to those expected according to bearing capacity theories.

B) Sub-system B2 - This sub-system provides an estimation of the primary rut depth created by the wheel which loads the double-layered soil. A numerical model built in FLAC (see appendix A3) simulates a wheel having given contact area, imposing a vertical pressure on the two-layered soil. The program is operated until stabilization (the rate of wheel sinkage becoming very low) and then the load is released and stabilization is reached again. The process is repeated three times to simulate consecutive wheel loads on the same point, and the rutting values are recorded. By operating the program under different values of the remolded layer depth, a relation is built between the rut created during the first wheel loading (and the second and third loadings as well) and the depth of the remolded layer.

Rutting values caused by a loading wheel, are dependent upon many factors including contact pressure, carcass stiffness, tire diameter and cross sectional shape, and the wheel-soil interface properties. The model used in sub system B2 estimates rutting as obtained by the numerical modeling of an elastic circular flat plate. When the soil bearing capacity is higher than the wheel contact pressure, the tire is flattened by the soil and the wheel-soil interface is (in many cases) not far from being flat. Rutting estimates by the numerical system may change quite considerably with changing properties of the wheel-soil system. For example, when the loading element may not be considered flat (or close to flat), or when the wheel-soil interface is not perfectly rough (as was assumed in the above mentioned examples). The computer program (appendix A3) was built so as to enable changing part of these variables, but further refinement and investigation in this subject are needed.

It should be mentioned that the rutting values received by numerical modeling cannot be accurate due to the large simplifying assumptions made regarding the wheel-soil interface and the constitutive laws of the soil. Only with a three-dimensional system, an accurate wheel model and more precise constitutive law (especially of the remolded soil), is it possible to arrive at more precise evaluations of the deformations in the vicinity of wheel-soil interface. Although simple and easy to implement, the elastic-plastic constitutive law gives only a rough estimation as to deformations in the remolded soil, especially under the high stress levels exerted.

### 6.2.3 Sub-system C - Performance prediction of unsurfaced runways.

This sub-system integrates the results received in sub-systems A and B, with an ultimate aim to estimate better unsurfaced runway performance in remoldable soils. This sub-system was written in TURBO-PASCAL software.

The former sub-systems are:

Sub-system A - relates between the number of passes and the remolded layer thickness.

Sub-system B - relates between the remolded layer thickness and the soil equivalent strength (sub-system B1) or alternatively the soil expected rutting values (sub-system B2).

Integration of the above results (see Fig. 6.3) enables receiving a relationship that describes the soil condition (through its strength or through the predicted rutting values) as a

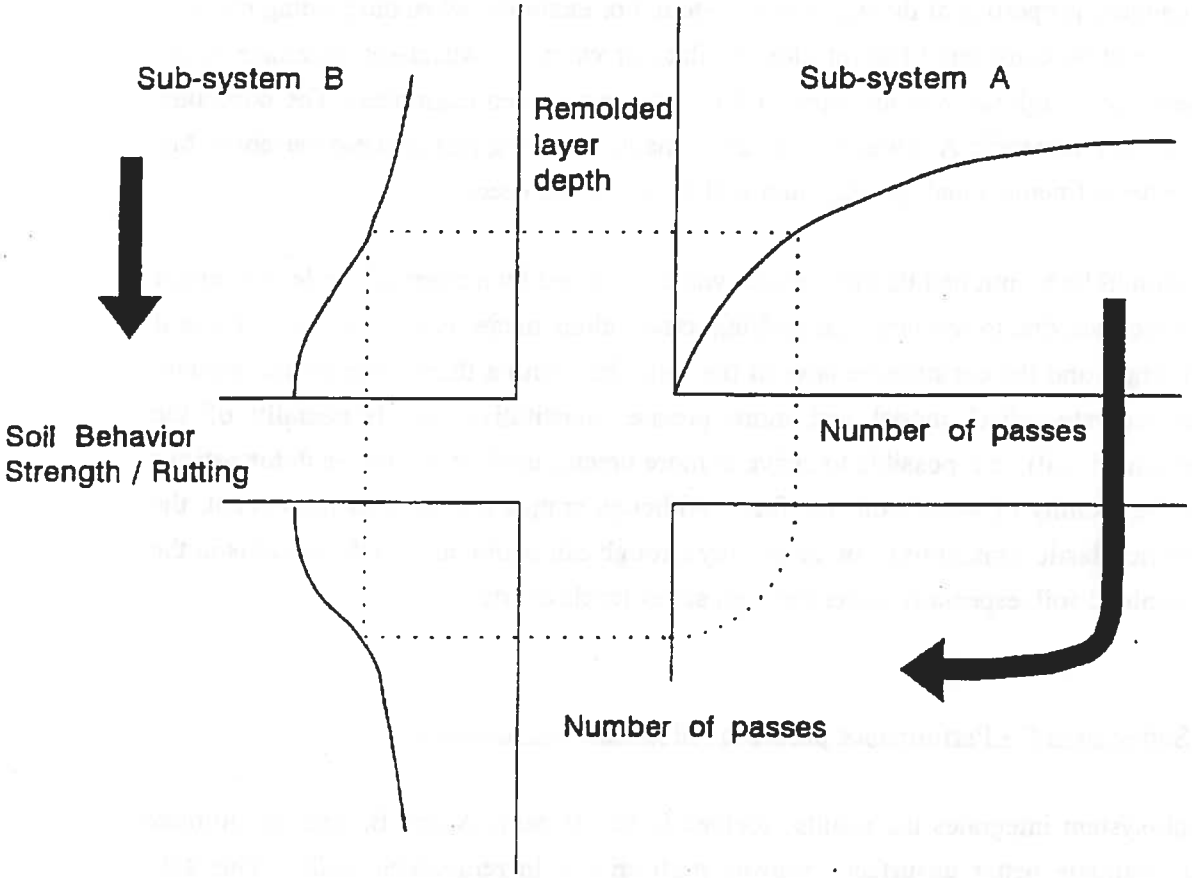


Fig. 6.3 Derivation of the relationship between soil condition (strength or rutting values) and accumulated wheel passes.

ציור מס. 6.3 מציאת הקשר שבין התנהגות הקרקע (על פי ערכי חוזק או חריצה) לבין המספר המצטבר של מעברי גלגל.

function of the accumulated wheel passes. As specified in Chapter 4, this relationship can be used to arrive at an estimation of the runway's performance by two separate approaches:

A. The accumulated rutting approach

According to this approach, the expected runway rutting will be calculated at each stage under changing conditions of soil structure. When the total rutting (primary rutting + accumulated rutting) or the primary rutting, exceed the allowed criterion values, functional runway failure is declared. Fig. 6.4 presents a flow chart of the solution process based on the accumulated rutting approach. The main input data required for the solution are:

1. Evaluation of the primary rut depth at each stage of the runway life. Two alternatives were thought of as possible in this case:
   - Use can be made of empirical correlations of this type which appear in the literature (section 3.4 in the literature survey) and can be employed for estimating the primary rut as a function of the soil strength (as predicted by sub-systems A and B1). This alternative can easily be implemented but suffers from relatively scarce sources which may be valid but only to the conditions and soils on which they were carried out.
   - Usage of direct numerical evaluations of primary rut depth at each point of the runway life as predicted by sub-systems A and B2. The main advantage of using this alternative is the ability to check the rutting in a two-layer system. When properly validated by laboratory and field tests, it can provide a solution which is better associated to actual wheel-soil conditions.

2. Accumulated rutting evaluation as a function of the number of wheel passes. This value expresses the average rutting developed at the center of the traffic lane of the aircraft wheel. An algorithm and a computer program written within the framework of the research perform an estimation of the accumulated rutting value, based on some data and assumptions including:

   - width of the traffic lane;
   - width of the loading wheel;
   - number of wheel loads;
   - standard deviation of the lateral wander of wheel loads;
   - width of the soil mounds created at both sides of the loading wheel (soil mounds are assumed to have rectangular shape);

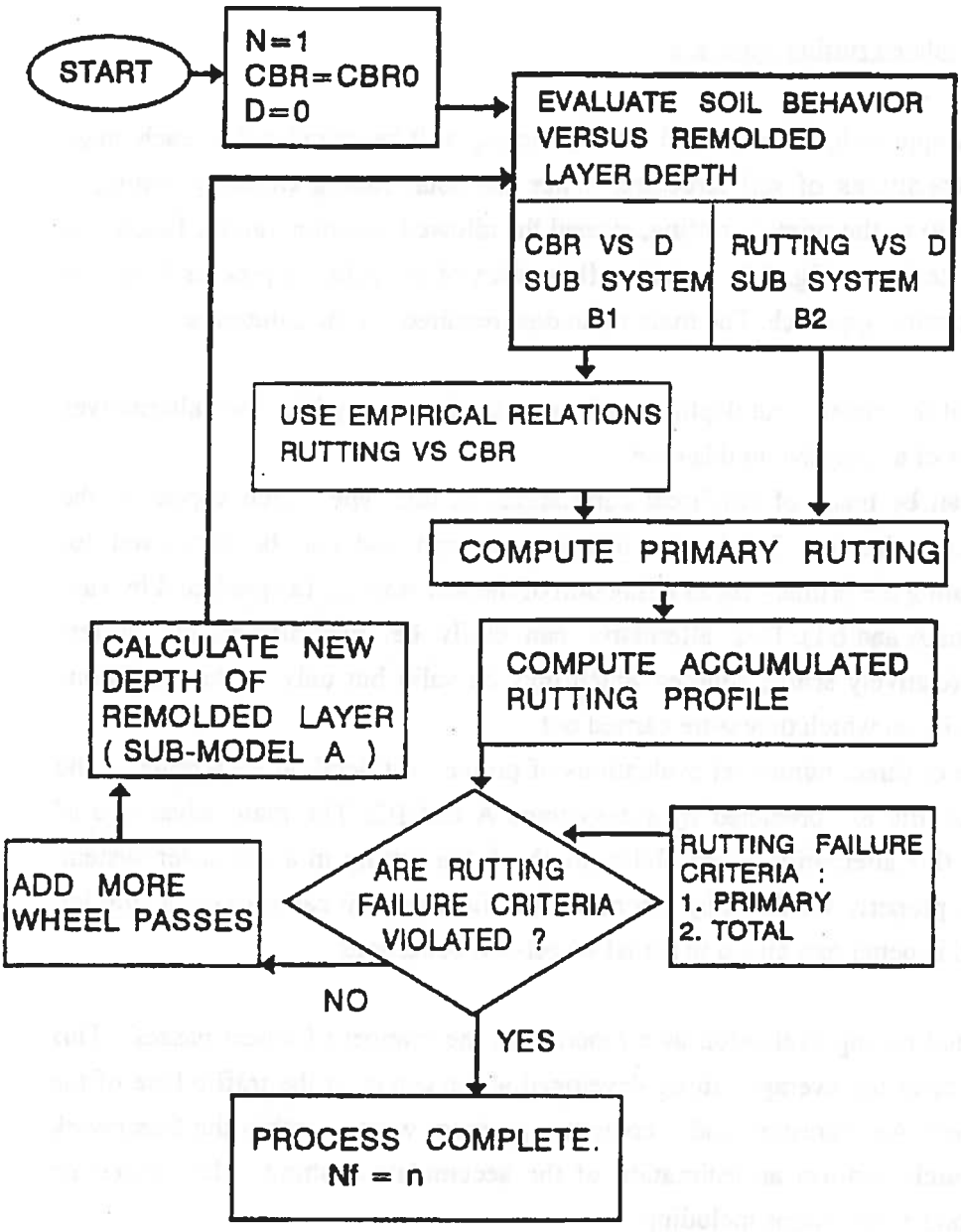


Fig. 6.4 Flow-chart of the accumulated rutting approach solution process.

ציור מס. 6.4 תרשים זרימה של תהליך הפתרון על פי גישת החריצה המצטברת.

- primary rutting values (for up to three consecutive loadings on the same point) as a function of the accumulated number of loads (resulting from the integration of sub-systems A and B2) conditions.

The listing of the computer program is given in appendix A4. Fig. 6.5 depicts an example describing the development of the accumulated rutting across the width of the wheel traffic lane for a set of assumed input data.

3. Primary rutting and accumulated rutting criteria. There are some sources that address the subject of permissible values of rutting for different aircraft. Only rarely is there a distinction between the issue of primary rutting, to the issue of overall rutting (accumulated rutting + primary rutting). In this context, two types of ruts may be distinguished. Rut type A (Fig. 6.5) is calculated as the difference between accumulated rut depth and the height of the developing soil mounds. Rut type B (Fig. 6.5) only measures the depth of ruts from the original surface level. Rut type A is usually the relevant type for determining runway performance. Theoretically, it is possible to determine, for each aircraft, the maximal permissible values for the various types of rutting (see Ref. 45). When considering C-130 aircraft, the value of overall rutting in non-braking areas of the runway may not exceed 10-15 cm. (Ref. 45, 32).

The solution process (Fig. 6.4) is performed according to the following steps:

(a) For the first cycle, the soil strength equals that of the unremolded soil. The depth of the remolded layer equals zero.
(b) Calculate the size of the primary rutting according to:
   - the soil strength, resulting from the combination of sub-systems A and B1, if empirical correlations (such as Ref. 33) are used.
   - an integration of sub-systems A and B2, if numerical rut estimations are used.
(c) Calculate the size of the accumulated rutting.
(d) Check if the primary rutting or the overall rutting are higher than rutting criteria values. If so, pass on to step h.
(e) Add another small number of passes.
(f) Find an updated value of the remolded layer depth (sub-system A).
(g) Return to stage b.

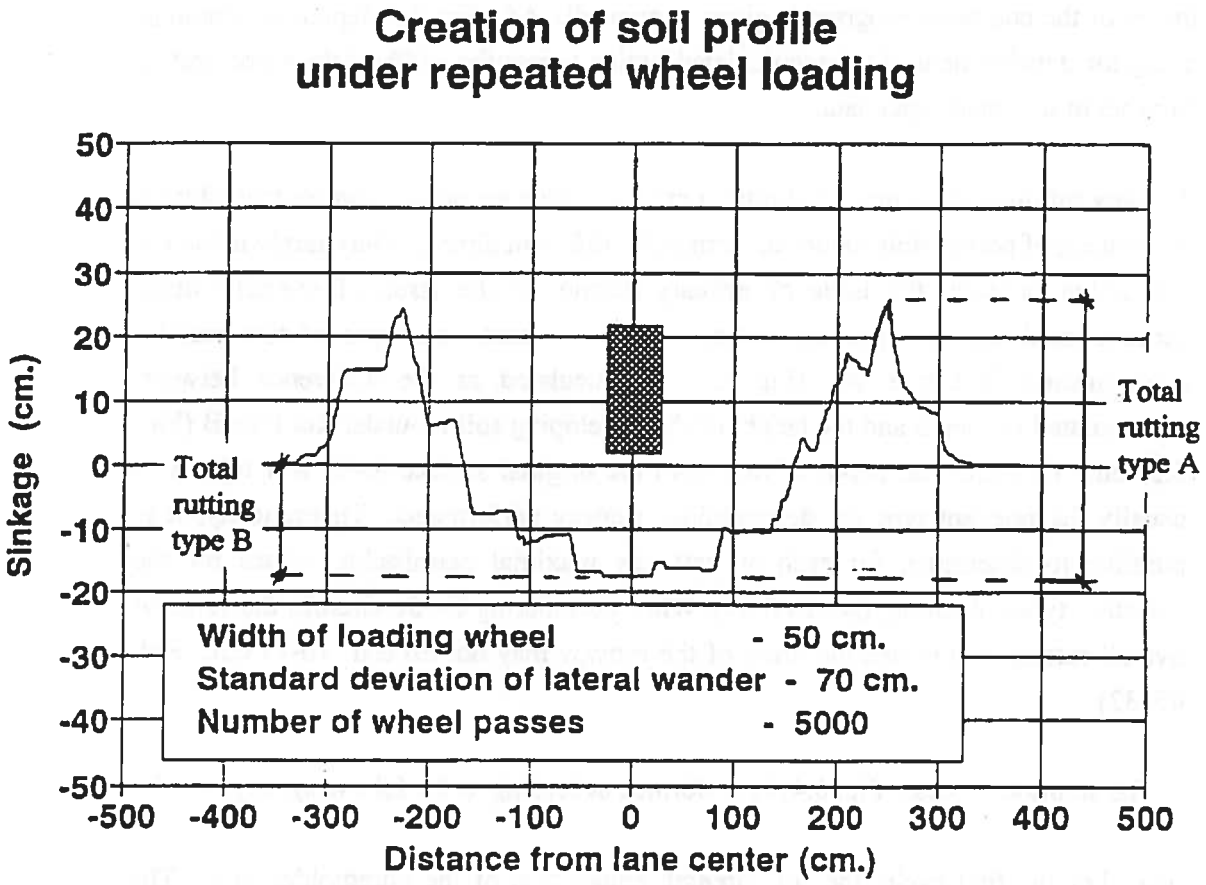


Fig. 6.5 Development of accumulated rutting across the width of the wheel traffic lane.

ציור מס. 6.5 התפתחות החריצה לרוחב נתיב התנועה.

(h) Number of passes N up to now is the number of predicted passes up to the functional failure of the runway.

Appendix A4 contains a listing of a Turbo Pascal program which gives runway performance prediction based on the accumulated rutting approach with rutting calculated numerically by sub-system B2.

B. The accumulated damage approach

As stated earlier in chapter 4, this model estimates and accumulates the incremental runway damage caused by each additional passage of the wheel over the two-layer soil structure. According to this approach direct use of a design nomogram for unsurfaced runways is made. It is assumed that the conventional prediction methods can be relied upon when no significant change occurs in the soil strength during the runway life. For example, Fig. 6.6 presents a design nomogram currently used by the IAF for C-130 aircraft (Ref. 32) and is based on equation [3.9] in section 3.4. For known loading conditions, a cut can be drawn from the above nomogram to create a relation between the soil strength and the number of aircraft passes to failure (Fig. 6.7 built for ESWL of 30,000 lb. and 5 $kg/cm^2$ inflation pressure).

As described by equation [4.17], the incremental damage caused to the runway by pass no. i is calculated (by a function similar to that in Fig. 6.7) to be $D_{mi}$= 1/Ni where Ni is the number of passes to failure in a runway having a current equivalent strength of CBRi. Consequently, drawn from Fig. 6.7 a new function can be built (Fig. 6.8) relating between the incremental damage caused to the runway by one pass and the present strength of the runway. At each stage of the runway life, the incremental damage of an additional pass is calculated according to its current strength and accumulated up to the functional failure of the runway.

Fig. 6.9 presents a flow chart of the process, which includes the following steps:

(a) For the first cycle, the equivalent strength of the soil equals that of the unremolded soil; the depth of the remolded layer is zero.
(b) Calculate the number of passes to failure for the current equivalent strength, and the incremental damage caused to the runway.
(c) Calculate the accumulated damage value.
(d) Is the accumulated damage value larger than 1 ? If so, go on to step i.
(e) Add another loading cycle.

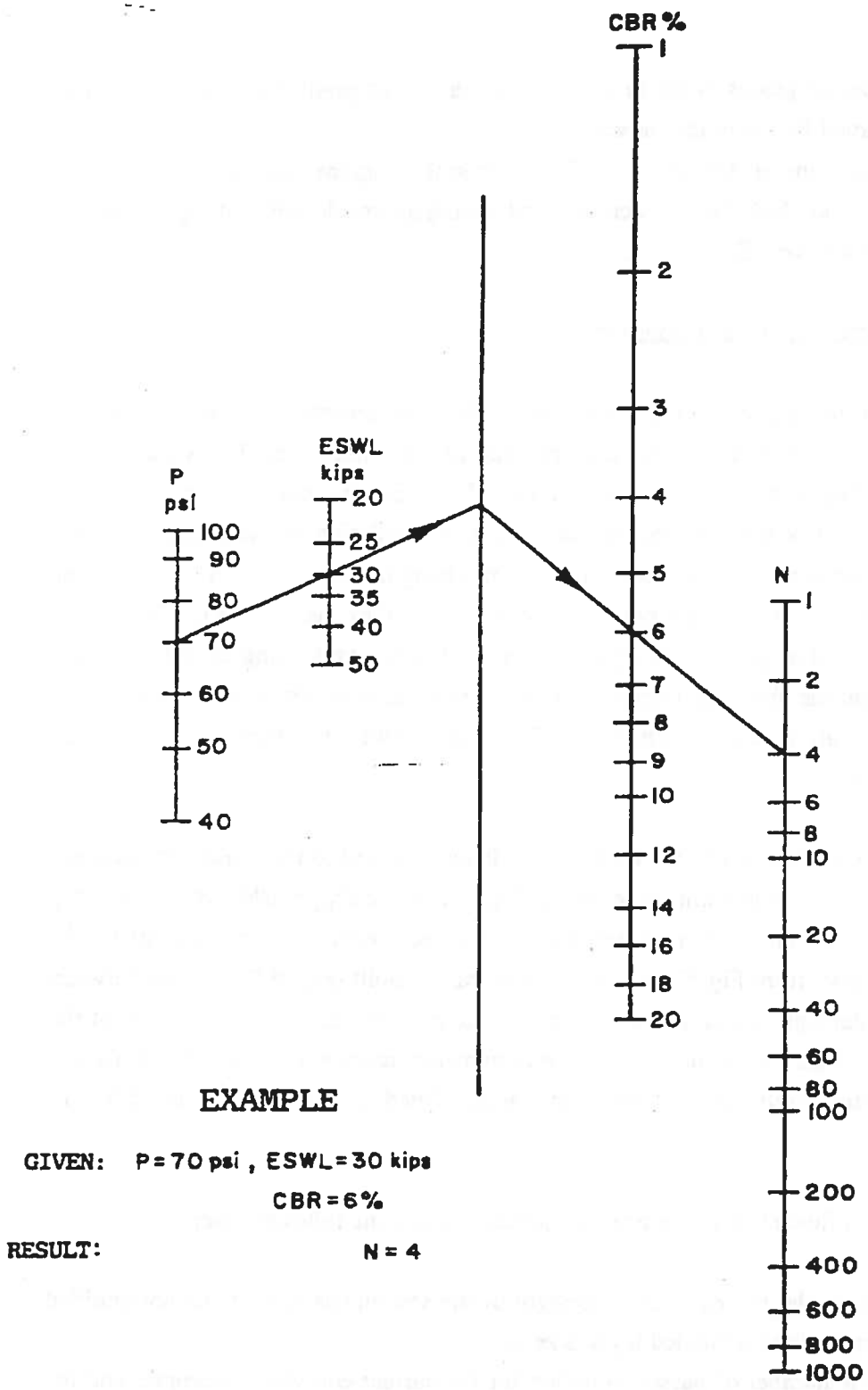


Fig. 6.6 An IAF design nomogram for C-130 aircraft

ציור מס. 6.6 נומוגרמת תיזוי של חיל האויר הישראלי עבור מטוסי C-130.

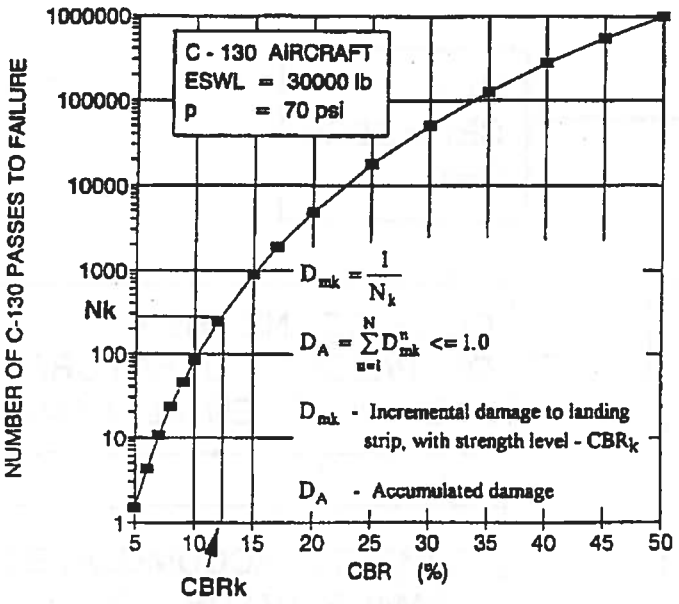


Fig. 6.7 A typical cut of the IAF design nomogram (Fig. 6.6) for given loading conditions.

ציור מס. 6.7 חתך בנומוגרמת החיזוי של ח"א ישראלי עבור ערכי עמיסה נתונים.

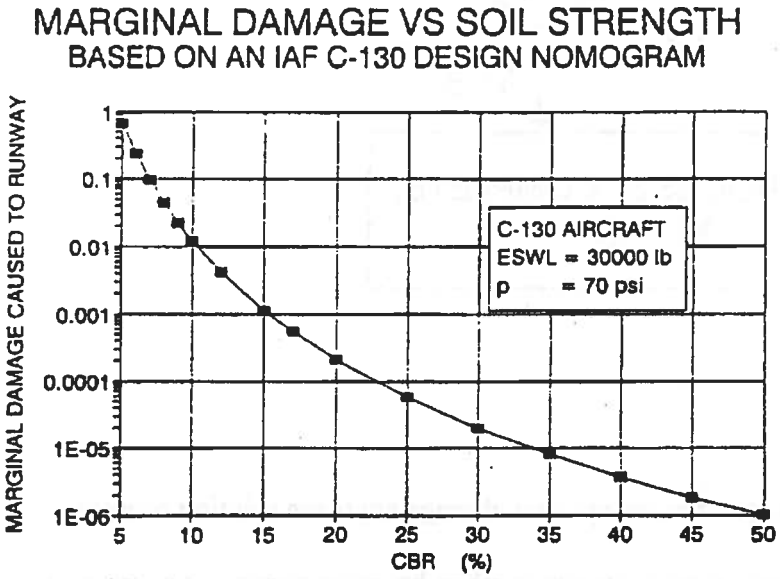


Fig. 6.8 Incremental runway damage Vs soil strength.

ציור מס. 6.8 הנזק השולי הנגרם למסלול כפונקציה של חוזק הקרקע (נגזר מציור מס. 6.7).

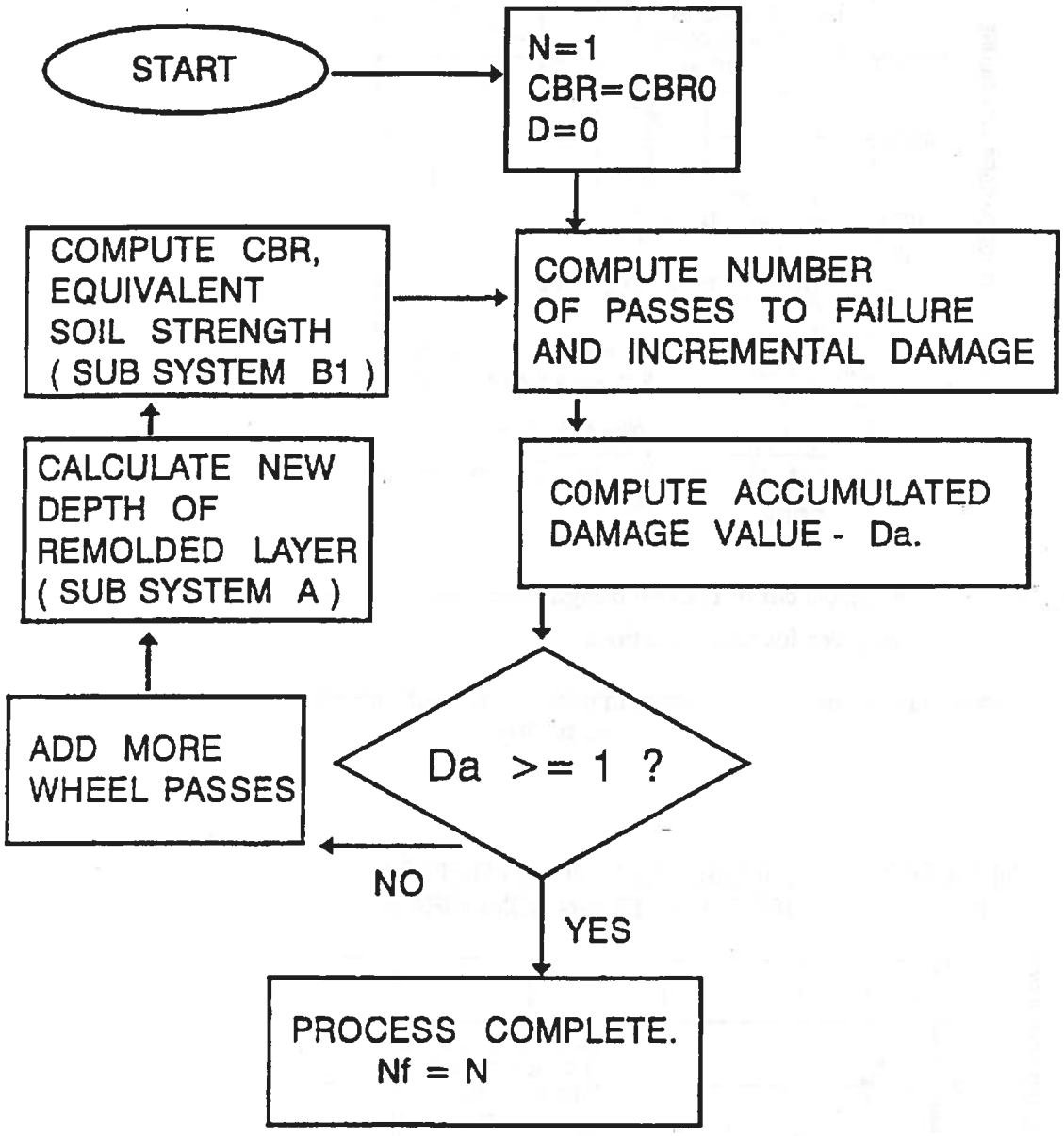


Fig. 6.9 Flow chart of the accumulated damage approach solution process.

ציור מס. 6.9 תרשים זרימה של תהליך הפתרון על פי גישת הנזק המצטבר.

(f) Calculate the updated depth of the remolded layer (sub-system A).
(g) Calculate the updated equivalent strength of the soil system for the newly calculated remolded layer depth (sub-system B1).
(h) Return to step b.
(i) Terminate; the number of passes up to now is the estimation of the passes to runway failure.

According to the accumulated damage approach, use is made of conventional design nomograms for unsurfaced runways in non-remolding soils. These nomograms are integrated as an independent module into the system. Therefore, periodic updates of these nomograms as well as specific ones built according to local experience can be smoothly consolidated into the system. Appendix A5 includes the listing of the program written in order to estimate runway performance according to the accumulated damage approach.

The accumulated damage approach is simpler and the integration with conventional design methods has its own practical advantages. This approach assumes that the prediction capability of the existing methods is good enough for non remoldable soils, and that the role of the suggested model is to present modifications for the case of remoldable soils, where the soil reaction to loading changes throughout the runway life. Conversely, the accumulated rutting approach solves the problem by treating directly the accumulation of ruts which are the principal cause for the runway functional failure. If rutting values can be found numerically with acceptable precision, then the presented analytical method can serve as a performance prediction tool independent of the existing methods. In such a situation the prediction of the performance of non remoldable soils would be a special case of the presented method. One of the main advantages of the accumulated rutting approach is that it does not inherit the problems of the existing design methods. However its implementation requires relatively high precision in the numerical estimations of rutting. This task can only be achieved by accurate modeling of the wheel-soil interface and the constitutive laws of the soil and requires an extensive validation and tuning process.

## 6.3 Analytical verification of the numerical model

This section reports various attempts to impart some validation to the main numerical model (sub-system A) through comparison with other accepted analytical solutions. As mentioned in section 6.2.1, the numerical model simulates repetitive wheel loading on the soil system. Some parts of the soil are in a state of plastic flow during the loading process while other parts remain in the elastic state. Moreover, parts of the soil are already

remolded and possess different properties. No closed analytical method was found to furnish solutions to such complex situations.

Due to the above, verification of the numerical model built in FLAC against other analytical solutions could be achieved only in these two extreme situations:

A) The elastic state, where the load is sufficiently low so that no plastic flow occurs;

B) The state of limit equilibrium where the load reaches the soil bearing capacity.

The numerical model which was built in FLAC for the solution of the main problem of the research was used for the purposes of validation . For the elastic case the "wheel" was only lightly loaded so that no element in the soil would reach plastic state. The distribution of stresses in the soil was compared to the known solution of a surface strip loading on an elastic semi-infinite medium (Ref. 57). Table 6.1 gives the results of the state of stresses in selected points under the "wheel". Point locations are expressed in terms of A=B/2 (where B is the width of the loading strip), and stresses are normalized with respect to the imposed surface pressure. Plane strain conditions are assumed. Comparing the analytical results with those obtained by the numerical model gives differences of up to 5%. This result seems very satisfactory taking into consideration the quite coarse geometrical discretization used in the numerical model.

**Table 6.1: Comparison of Methods for the Stress Conditions under a Strip Loading of an Elastic Medium.**

**טבלה 6.1: השוואת שיטות למציאת מצב מאמצים בקרקע אלסטית תחת עמיסה בפני השטח.**

| Distan from axis | Depth | $\sigma_Z$ | | | $\sigma_X$ | | | $\tau_{XZ}$ | | |
|---|---|---|---|---|---|---|---|---|---|---|
| in A | in A | FLAC | Analyt | Dif (%) | FLAC | Analyt | Dif (%) | FLAC | Analyt | Dif (%) |
| 0.25 | 0.87 | 0.816 | 0.84 | 2.9 | 0.22 | 0.226 | 2.7 | 0.082 | 0.078 | 4.9 |
| 0.25 | 1.97 | 0.528 | 0.544 | 3.0 | 0.045 | 0.044 | 2.3 | 0.048 | 0.05 | 4.1 |
| 1.25 | 0.87 | 0.32 | 0.316 | 1.2 | 0.258 | 0.27 | 4.6 | 0.242 | 0.252 | 4.1 |
| 1.25 | 1.97 | 0.35 | 0.348 | 0.6 | 0.112 | 0.112 | 0.0 | 0.17 | 0.175 | 2.9 |
| 2.25 | 0.87 | 0.041 | 0.04 | 2.5 | 0.172 | 0.18 | 4.6 | 0.086 | 0.082 | 4.7 |
| 2.25 | 1.97 | 0.148 | 0.144 | 2.7 | 0.15 | 0.148 | 1.4 | 0.14 | 0.141 | 0.1 |

In order to find the bearing capacity of the soil under the "wheel", a similar geometrical model was built, in which the loading strip (plane strain conditions) was forced vertically into the soil. Bearing capacity condition was "announced" when the pressure needed to force the loading strip stabilized (and the sinkage of the "wheel" was no more than 15% of its width). As an example, the model was run with the following properties (Mohr-Coulomb model):

$\phi = 35°$ - Internal angle of friction
$C = 0.1$ kg/cm$^2$ - Soil cohesion
$\gamma = 1600$ kg/m$^3$ - Soil density
$B = 10$ cm. - Loading strip width

The accepted equation for bearing capacity of soil subjected to a strip loading at surface gives:

$$q_A = C \bullet N_C + 0.5 \bullet \gamma \bullet B \bullet N_\gamma \qquad [6.1]$$

and for the above soil one gets (Ref. 41):

$N_C = 46.12$
$N_\gamma = 48.03$

and

$$q_A = 0.1 \bullet 46.12 + 0.5 \bullet (1.6 \bullet 1E-3) \bullet 10 \bullet 48.03 = 5.0 \text{ kg / cm2}$$

Fig. 6.10 presents the development of the pressure needed to force the "wheel" into the soil during the loading process. As can be seen, the pressure stabilized at a level of 4.8 kg/cm$^2$ with fluctuations of about ±10%. The above result can be considered very satisfactory, thus providing some level of validation to the model operation at a state of limit equilibrium.

Further verification of the numerical model was done by using the analysis described in section 4.3. For the same soil properties ($\phi$=35°,C=0.1 kg/cm$^2$), a numerical model built in

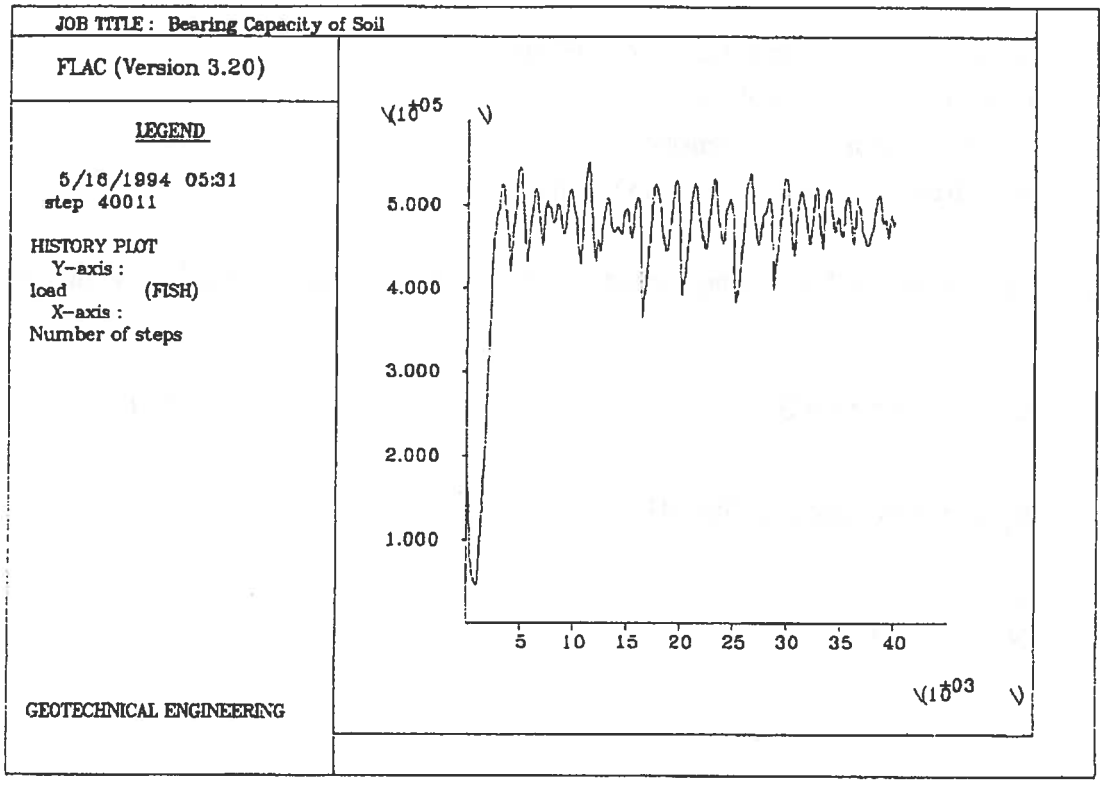


Fig. 6.10 Development of pressure needed to force the "wheel" into the soil (Flac simulation of soil penetration resistance) .

ציור מס. 6.10 התפתחות הלחץ הנדרש להחדרת "גלגל" לקרקע (תוצאות מודל שנבנה במערכת FLAC ).

FLAC was operated. The model was given the similar geometrical and behavioral properties as the one later used for the main numerical model. For purposes of comparison, the soil was assumed to have very low density. At a load level of about 0.95-1.0 kg/cm$^2$ some points in the soil reached plasticity, a result which is in good accordance with the analytical result ($p_{MIN} = 0.94$ kg / cm2). Fig. 6.11 presents the location of the plastic points as anticipated by the analytical and the numerical methods. The general shape is of two symmetric circular arcs beginning at the loading strip corners and almost meeting at the axis of symmetry. As before, the numerical results were in general agreement with the analytical ones.

## 6.4 Results of the analytical system

This section concentrates on a survey and analysis of the results obtained in different computer runs of the numerical sub-systems.

### 6.4.1 Sub-system A

Most of the work was devoted to sub-system A, since its function is the essence of the research. Table 6.2 contains the main input data items used in different computer runs of sub-system A. The data includes:

- FILE - filename of the FLAC program;
- $COH_0$ - the cohesion of the unremolded soil;
- $COH_1$ - the cohesion of the remolded soil;
- $\phi$ - the soil internal angle of friction before and after remolding respectively;
- P - average contact pressure of the wheel;
- B - width of wheel;
- Den - soil density (assumed constant during remolding);
- $E_0$ - elastic modulus of the unremolded soil;
- $E_1$ - elastic modulus of the remolded soil;
- $\nu$ - the soil Poisson ratio (assumed constant);
- LW - standard deviation of the normally distributed lateral wander of the wheel;
- C1,C2 - value of the fatigue parameters in equation [4.3].

Most of the sub-system A computer runs were carried out with the same model dimensions as those of the mold and the loading wheel of the laboratory moving wheel device (see Chapter 7). A smaller part of the computer runs were conducted with models having similar dimensions to the C-130 aircraft with a 48 cm width loading wheel and a soil section of 6 m. width and 2.5 m. depth.

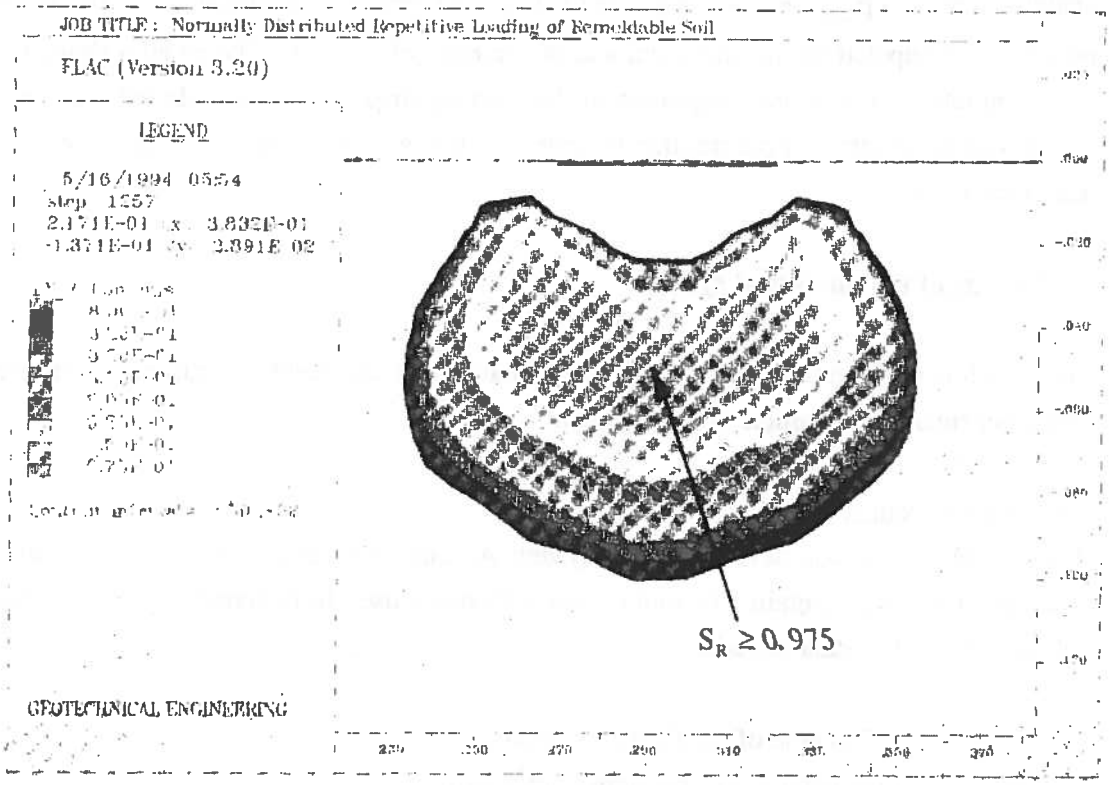


Fig. 6.11 Location of first points to be remolded under surface loading (results of Flac simulation).

ציור מס. 6.11 מיקום הנקודות הראשונות המופרות בקרקע תחת עמיסת שטח (תוצאות מודל שנבנה במערכת FLAC).

**Table 6.2: Input data for various subsystem A runs**

**טבלה 6.2: נתוני קלט לריצות שונות שבוצעו בתת־מערכת A**

| No. | file | $COH_0$ | $COH_1$ | $\phi$ | P | W | Den | $E_0$ | $E_1$ | $\nu$ | LW | C1,C2 |
|---|---|---|---|---|---|---|---|---|---|---|---|---|
| | | kg/cm2 | kg/cm2 | deg. | kg/cm2 | cm. | kg/m3 | kg/cm2 | kg/cm2 | | cm. | |
| 01 | t35_cc | 0.2 | 0.001 | 35 | 1.0 | 5.0 | 1700 | 1000 | 500 | 0.3 | 6.25* | 20.0 |
| 02 | t35_bb | 0.1 | 0.001 | 35 | 1.0 | 5.0 | 1700 | 1000 | 500 | 0.3 | 6.25* | 20.0 |
| 03 | t47_8_1 | 0.8 | 0.001 | 47 | 5.0 | 5.0 | 1950 | 1000 | 500 | 0.3 | 6.25 | 20.0 |
| 04 | f30_1 | 0.5 | 0.05 | 30 | 4.0 | 5.0 | 1950 | 1000 | 750 | 0.4 | 6.25 | 20.0 |
| 05 | f30_2 | 0.5 | 0.05 | 30 | 2.0 | 5.0 | 1950 | 1000 | 750 | 0.4 | 6.25 | 20.0 |
| 06 | f30_3 | 0.5 | 0.05 | 30 | 3.0 | 5.0 | 1950 | 1000 | 750 | 0.4 | 6.25 | 20.0 |
| 07 | f35_1 | 0.5 | 0.05 | 35 | 4.0 | 5.0 | 1950 | 1000 | 750 | 0.4 | 6.25 | 20.0 |
| 08 | f35_2 | 0.5 | 0.05 | 35 | 3.0 | 5.0 | 1950 | 1000 | 750 | 0.4 | 6.25 | 20.0 |
| 09 | f35_2_de | 0.5 | 0.05 | 35 | 3.0 | 5.0 | 1462 | 1000 | 750 | 0.4 | 6.25 | 20.0 |
| 10 | f35_2_el | 0.5 | 0.05 | 35 | 3.0 | 5.0 | 1950 | 1500 | 1125 | 0.4 | 6.25 | 20.0 |
| 11 | f35_3 | 0.5 | 0.05 | 35 | 2.0 | 5.0 | 1950 | 1000 | 750 | 0.4 | 6.25 | 20.0 |
| 12 | f35_4 | 0.5 | 0.05 | 35 | 2.5 | 5.0 | 1950 | 1000 | 750 | 0.4 | 6.25 | 20.0 |
| 13 | f35_5 | 0.5 | 0.05 | 35 | 3.5 | 5.0 | 1950 | 1000 | 750 | 0.4 | 6.25 | 20.0 |
| 14 | fat10 | 1.0 | 0.1 | 45 | 8.0 | 48 | 1950 | 1000 | 750 | 0.4 | 60.0 | 35.0 |
| 15 | fat11 | 1.0 | 0.1 | 45 | 5.0 | 5.0 | 1950 | 1000 | 750 | 0.4 | 6.25 | 35.0 |
| 16 | fat12 | 1.0 | 0.1 | 45 | 6.0 | 5.0 | 1950 | 1000 | 750 | 0.4 | 6.25 | 35.0 |
| 17 | fat13 | 1.0 | 0.1 | 45 | 7.0 | 5.0 | 1950 | 1000 | 750 | 0.4 | 6.25 | 35.0 |
| 18 | fat14 | 1.0 | 0.1 | 45 | 8.0 | 5.0 | 1950 | 1000 | 750 | 0.4 | 6.25 | 35.0 |
| 19 | fat20 | 1.0 | 0.1 | 45 | 4.0 | 5.0 | 1950 | 1000 | 750 | 0.4 | 6.25 | 35.0 |
| 20 | t_g5_1 | 0.85 | 0.01 | 47 | 5.0 | 48.0 | 1950 | 1000 | 250 | 0.4 | 60.0 | 35.0 |
| 21 | s50_3_d | 0.3 | 0.01 | 50 | 1.75 | 5 | 1700 | 500 | 200 | 0.4 | 6.25 | 35 |

The computer runs were usually operated for 500 wheel loads, where the lateral location of each load was determined according to a normal distribution with a standard deviation as noted in table 6.2. Part of the cases (for example nos. 1,2 in the above table )were operated in a channeled mode in order to simulate the creation of the remolded zone in this type of traffic.

Fig. 6.12 presents a picture of the remolded soil mass created after 500 wheel loads in case no. 15 in table 6.2. The creation of kind of bursts of remolded elements which knife cut the unremolded soil, can be explained by the brittle character of the dry granular soil. The

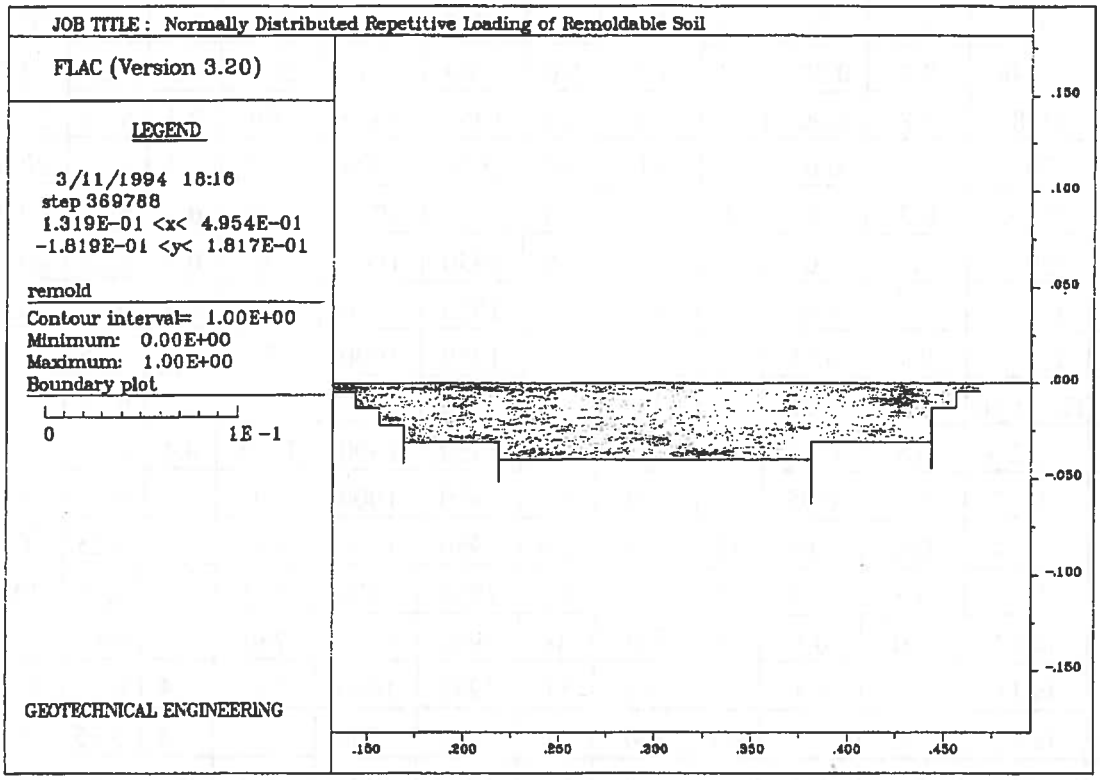


Fig. 6.12 Remolded soil mass, created after 500 load applications in model no. 15 in table 6.2.

ציור מס. 6.12 אזור הקרקע המופרת שהתפתח לאחר 500 מחזורי עמיסה במודל מס. 15 (טבלה 6.2).

assumed shape of the constitutive law, which was reasonably confirmed by the laboratory tests, causes immediate remolding once a soil element has reached its strength envelope.

Fig. 6.13 describes the depth of the remolded layer (measured at the center of the model) as a function of the number of wheel loads (results of case no. 15). For contact pressure of 5 $kg/cm^2$, it can be seen that after 28 loadings, remolding of the soil occurred up to a depth of 2.6 cm (about 50% of the width of the loading wheel). After 200 cycles the thickness of the remolded layer increased to 3.5 cm, and after 260 cycles the remolded layer reached a depth of about 4.5 cm (about 90% of the loading wheel width). No more remolding occurred up to the conclusion of 500 load cycles. Fig. 6.14a summarizes the results of cases no. 15-19 in which all input data are identical except for the loading pressure exerted by the wheel. For a low contact pressure (4 $kg/cm^2$) no soil remolding occurred during 500 cycles while, for higher contact pressures, the remolding occurred at a higher rate and stabilized at higher values of the remolded layer depth. For a wheel pressure of 8 $kg/cm^2$, a 2.3•B depth of remolded layer was obtained, B being the wheel width. Fig. 6.14b shows the influence of the loading pressure on remolding as obtained in cases 7,8,11,12,13. All the runs clearly show the tendency to a stabilization of the remolded layer thickness on a value dependent upon soil and loading conditions. Clearly, due to the nature of the numerical solution, involving discretization of the problem, the remolded layer thickness changes in "steps" and not in a continuous fashion as would be presumed in reality.

Fig. 6.15 presents the vertical displacement caused to a surface point at the middle of the runway as a function of the number of accumulating wheel loads (case no. 15). It can be seen that the general direction is, as expected, downward, but fluctuations do occur due to alternating upheaval and rutting of points (depending on the point of load application). The rut created after 500 loadings is in this case about 3.5 mm. The rutting increases as the pressure on the wheel grows, as for example case no. 18 (vertical pressure 8 $kg/cm^2$) in which the rutting reached 3.5 cm. after 500 loadings. Fig. 6.16 shows soil displacement caused by wheel loads which occurred in case no. 18. The pattern of soil elements being "squeezed" to the sides and heaving at both sides of the wheel was as expected in the two layer soil structure. It should be remembered however that rutting values obtained from sub-system A are very inaccurate due to coarse discretization of the wheel. Sub-system B2 was especially built for rutting estimation and its grid of elements is much finer.

Another point worth mentioning is that due to the high values of the fatigue parameters (equation [2.3]), the effect of the fatigue factor on the system is not high. For a relative stress level of 95%, about 60 loading cycles are needed, for the site T material (as given in cases no. 15-19), to be brought to the point of remolding. Therefore, during the numerical

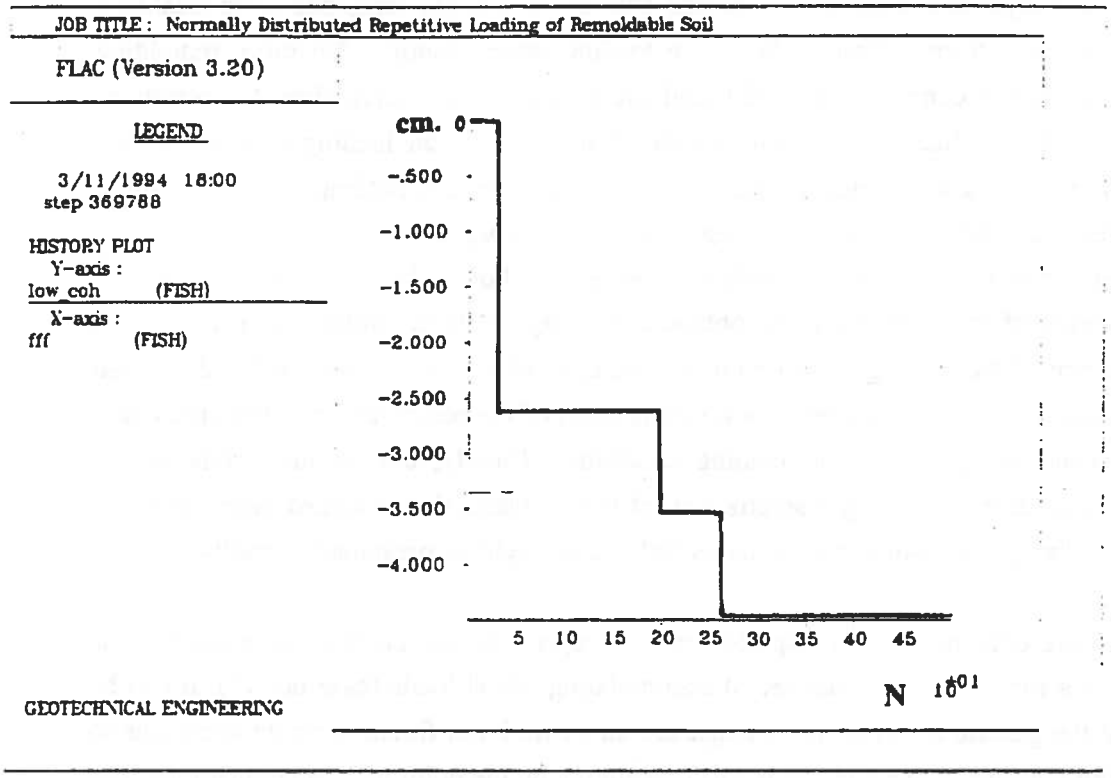


Fig. 6.13 The development of the remolded layer depth as a function of number of load applications (model no. 15 in table 6.2).

ציור מס. 6.13 התפתחות עומק השכבה המופרת כפונקציה של מספר מחזורי העמיסה (מודל מס. 15 טבלה 6.2).

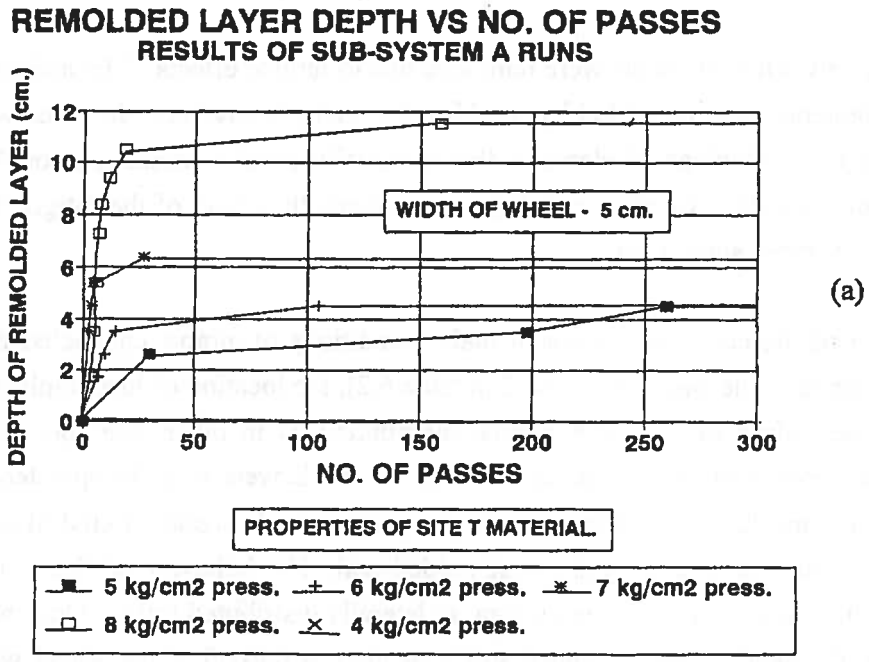


(a)

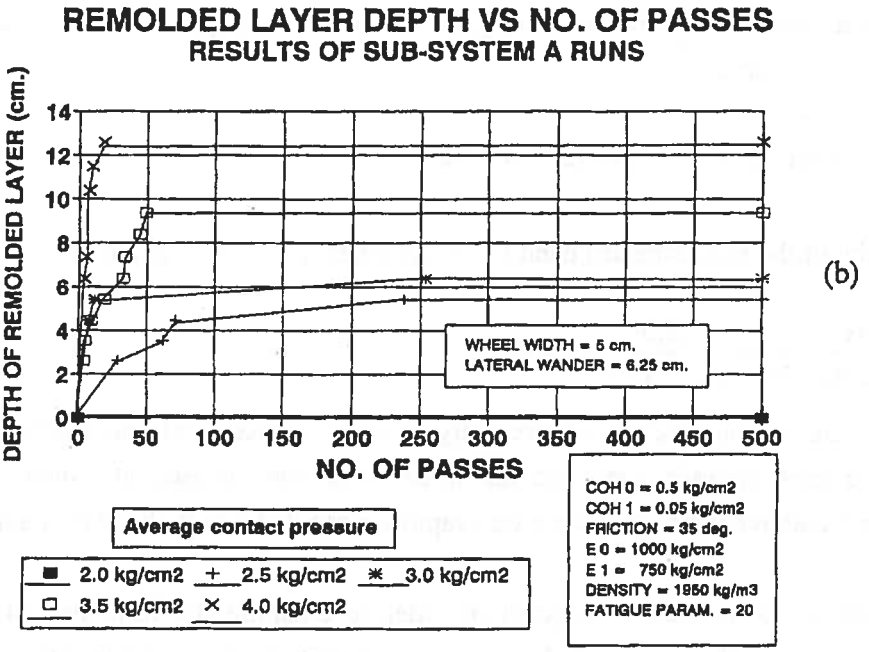


(b)

Fig. 6.14 The influence of loading pressure on the development of the remolded layer depth
(a) Models no. 15-19, table 6.2 (b) Models no. 7,8,11-13, table 6.2.

ציור מס. 6.14 השפעת לחץ העמיסה על התפתחות עומק השכבה המופרת
(a) מודלים מס. 15-19 (b) מודלים מס. 7,8,11-13, טבלה 6.2

system runs only a few elements were remolded due to fatigue effects. The majority of the remolded elements were remolded by reaching the strength envelope. In cases where the load is light the percentage of elements that eventually reach remolding through fatigue grows. In soils which possess lower fatigue parameters, the effect of the fatigue factor on soil behavior is more significant.

A small part of the cases was operated under conditions of almost channeled traffic. In these runs (for example cases no. 1 and 2 in table 6.2), the location of load application was determined according to the same normal distribution as in other runs, but only those wheel loads whose centerpoint was at the range of ±0.5B were actually operated. As was expected in the mechanistic model, the wheel repetitive loads created a kind of a "trough" of remolded soil surrounded by the unremolded soil. The behavior of the soil is quite different in the channeled traffic cases than in laterally distributed traffic. Once remolding is observed, the depth of the remolded soil is as high as 0.8-1.0 of the wheel width. The above is due to the fact that the elements which are most highly stressed and are located at a band under the wheel (as shown in section 4.3), keep on being stressed up to failure. For example the model run no. 1 in table 6.2 showed first remolding after 673 loadings (actual loadings) to a depth of 4.5 cm. Comparing the remolded soil depth with that predicted by equation [4.13] yields::

$$\theta_0 = \cos^{-1}(\sin(\phi)) = \cos^{-1}(\sin(35°)) = 55°$$

and the depth of the most stressed band under the wheel center is anticipated as:

$$D = \frac{B/2}{\tan(\theta_0/2)} = \frac{2.5}{\tan(55/2)} = 4.8 \text{ cm.}$$

As can be seen, the numerical result was very close to the analytical one. Elements located between the most stressed band and the wheel were less stressed, but once remolding occurred in the above band, they were very rapidly remolded due to the loss of support.

Some sensitivity tests were conducted in order to examine the influence of changing certain input data on the results. Reducing the soil density in the model by 25% (case no. 9 vs case no. 8 in table 6.2), caused an increase in the rate of remolding and 15% increase in the final depth of the remolded layer after 500 load cycles. Although the change is not significant, the direction of change is logical, since lower soil density provides less resistance to the surface load. Another test was carried out by increasing the elastic modulus of the soil by 50% (case no. 10 vs case no. 8 in table 6.2). The change caused a certain decrease in the rate of remolding but the remolded layer depth as recorded after 500

cycles was the same. It seems that the results are not sensitive to changes in the stiffness of the soil.

Due to the discrete nature of the numerical model network, the remolded layer depth changes its value in a stepwise mode. The long time needed for sub-system A operation (measured in days of uninterrupted operation for each model run), influenced the chosen size of model elements and the limited number of load cycles operated in each run (500 load cycles). For the operation of sub-system C, the actual remolded depth at each load cycle was used (a step function), and it was assumed that the remolded layer depth stabilizes its value after 500 cycles. Further refinement of the model network size, and operation of sub-system A for larger number of load cycles (to avoid extrapolation in sub-system C operation), would improve the accuracy of the whole model.

The results of sub-system A are written to an ASCII file in the form of Number of passes Vs. Depth of the remolded layer, to be later used in sub-system C.

### 6.4.2 Sub-system B1

An example of sub-system B1 results, on data of site T material, is presented in Fig. 6.17. It shows the decrease in the overall penetration resistance of the soil from the state of unremolded homogeneous soil to the state of a thick remolded layer, whose depth is twice the width of the loading strip. The rate of decrease, in the penetration resistance of the soil system is low for shallow depth values of the upper layer, then there is a sharp decrease in the penetration resistance towards stabilization for high values of the upper layer depth. For the site T soil, at an upper layer depth of 1•B, the penetration resistance of the soil system is about 25% of the soil penetration resistance in a homogeneous unremolded soil, and 2 times higher than that in a homogeneous remolded soil. Stabilization of the penetration resistance occurs at a remolded layer depth of about 1.25•B. The general behavior of the above relationship, was the same in a similar model operated with the properties of site S material.

Up to this point, all numeric analyses were performed using the soil strength parameters and elastic modulii. Since according to the accumulated damage approach, use is made of accepted prediction nomograms, the penetration resistance results should be converted to CBR values. The results of laboratory CBR tests which were conducted on "remolded" and "unremolded" samples of the two soils (given in tables 5.1 and 5.3) were used for this purpose according to the following formula:

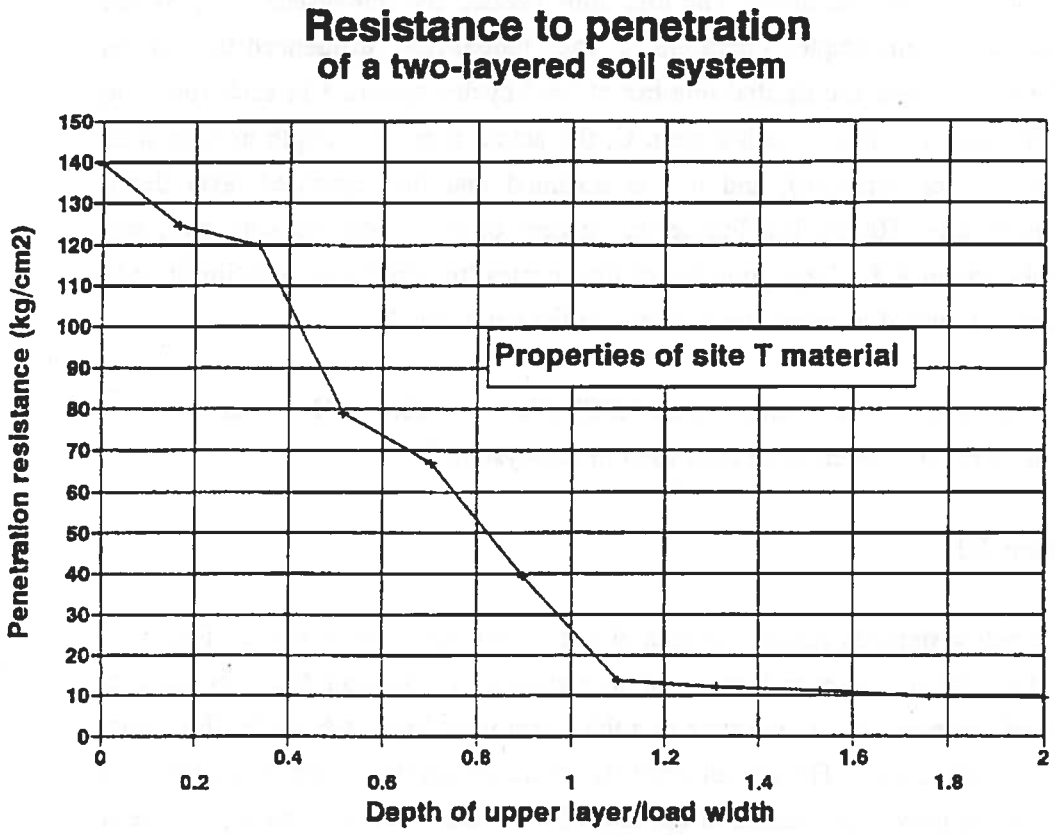


Fig. 6.17 Penetration resistance as a function of the remolded layer depth (sub-system B1, properties of site T material):

ציור מס. 6.17 התנגדות להחדרה כפונקציה של עובי השכבה המופרת (תת־מערכת B1, נתוני קרקע מאתר T ).

$$CBR_D = CBR_R + (CBR_U - CBR_R) \cdot \frac{(PR_D - PR_R)}{(PR_U - PR_R)} \qquad [6.2]$$

where:

$CBR_D$ - the equivalent CBR value for a soil system having an upper layer of depth D.
$CBR_R$ - the CBR value of the homogeneous remolded soil.
$CBR_U$ - the CBR value of the homogeneous unremolded soil.
$PR_D$ - the penetration resistance for a soil system having an upper layer of depth D.
$PR_R$ - the penetration resistance obtained for a large depth of the remolded upper layer.
$PR_U$ - the penetration resistance of the homogeneous unremolded soil.

Using equation [6.2], a relation is built between the depth of the remolded layer and the equivalent CBR value of the soil system. Fig. 6.18a and b show the results the CBR vs. Depth as obtained for the site T and site S soils respectively. It should be mentioned that although the results are normalized (depth of the remolded layer is given in terms of the loading element width), sub- system B1 should be run with loading element width as close as possible to that in reality in order to avoid biasing the results. The above relation, in the form of a list of specific CBR-depth points, is written into an ASCII file later to be used in sub-system C.

### 6.4.3 Sub-system B2

The displacements caused in a two-layer soil structure (having the properties of site S material), by the loading of an axisymetric plate (having 3.8 cm. radius), are qualitatively exemplified in Fig. 6.19. The numerical model built for rutting estimation was operated for different values of soil properties (unremolded and remolded) and loading data. In each run the sinkage and rutting values for different depths of the remolded layer were calculated. Fig. 6.20a presents an example of the results of sinkage and rutting evaluation for a soil which possesses the properties of site S material, under a 2 $kg/cm^2$ load pressure. The difference between sinkage (measured when the wheel still loads the soil) and rutting (measured after unloading is finished) gives some indication as to the elastic response of the soil system, and its value increases with increasing values of the upper (and less stiff) layer depth. Fig. 6.20b gives the accumulated rutting values predicted by the numerical model after 1, 2 and 3 consecutive load cycles of the same spot.

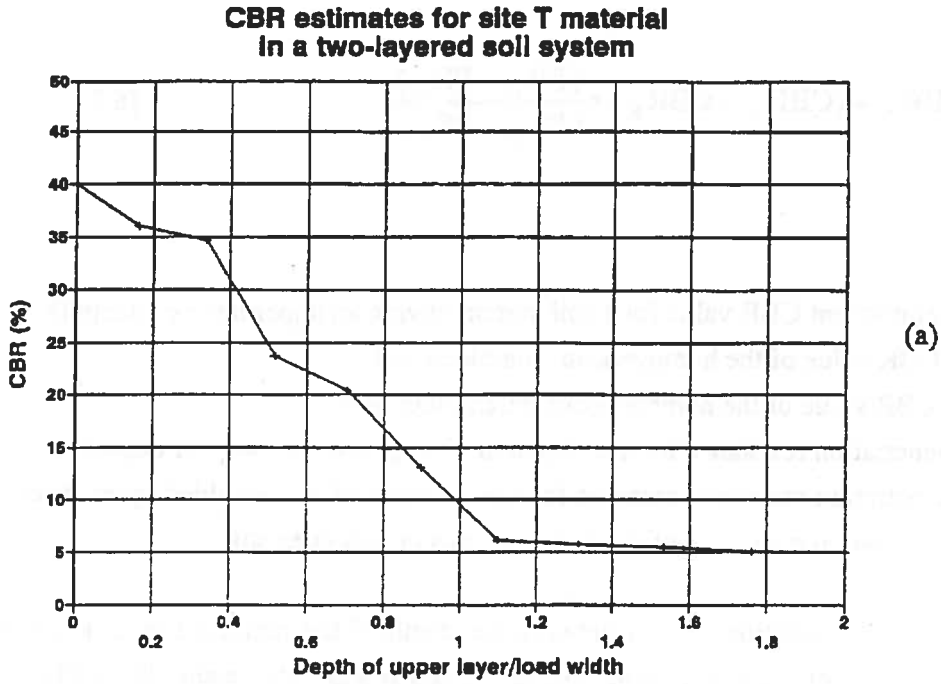


(a)

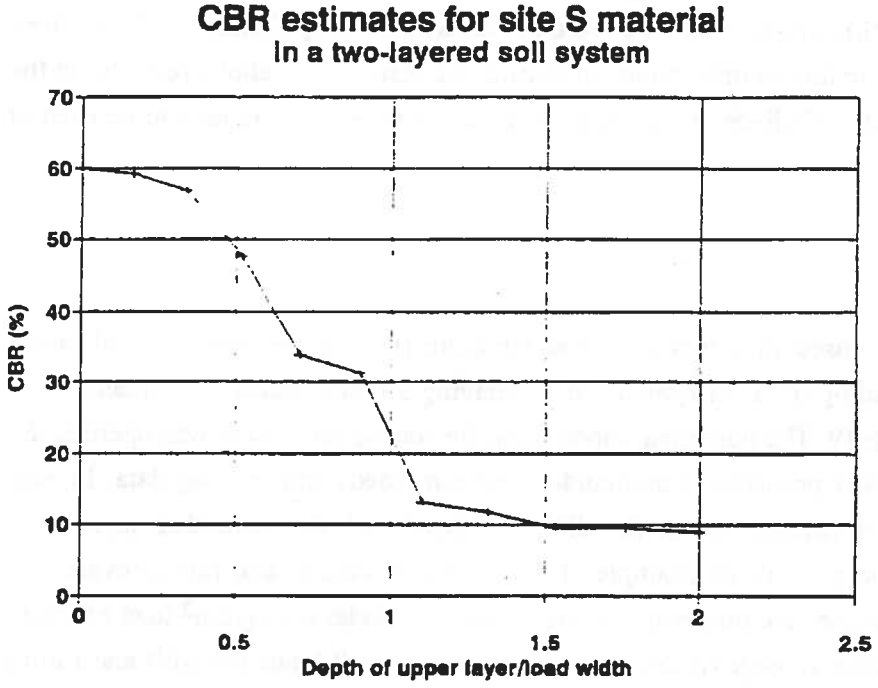


(b)

Fig. 6.18 Equivalent CBR values of a two-layered soil system, as a function of the remolded layer depth
(a) Soil parameters of site T material.
(b) Soil parameters of site S material.

ציור מס. 6.18 ערכי מת"ק מיצג של מערכת דרשכבתית כפונקציה של עומק השכבה המופרת
(a) נתוני קרקע אתר T (b) נתוני קרקע אתר S .

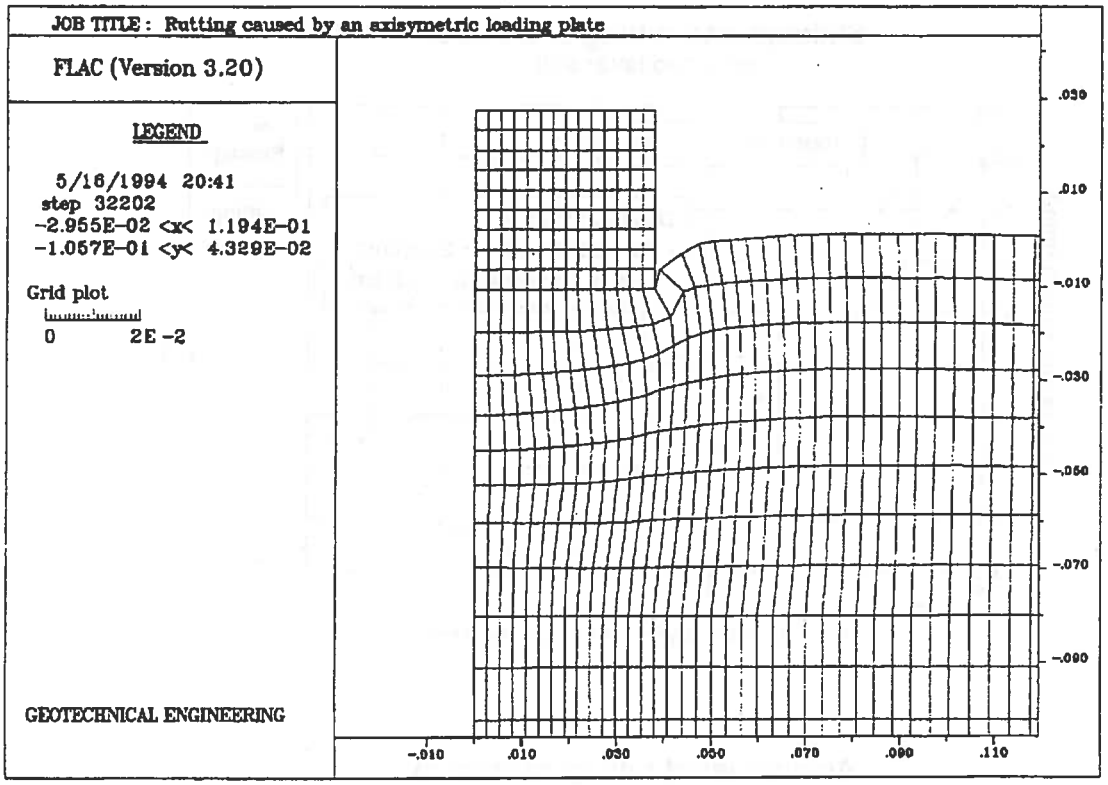


(a)

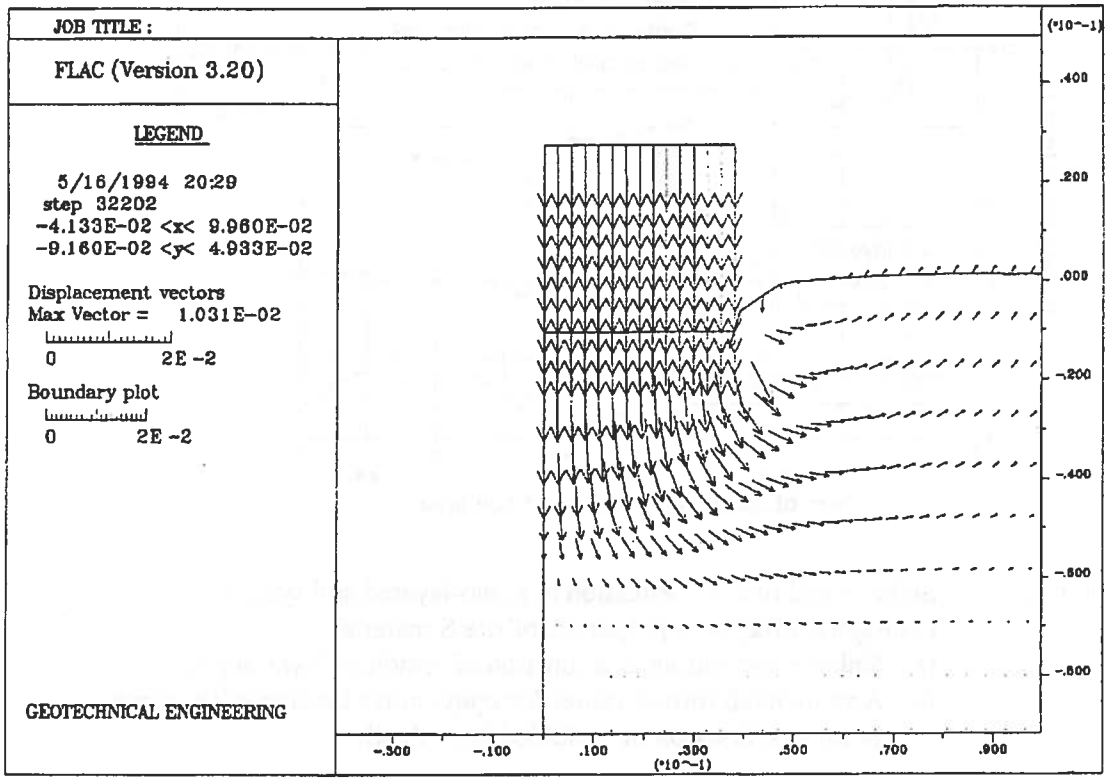


(b)

Fig. 6.19 Model grid distortion (a), and displacements (b) caused in a two-layered soil system, subjected to axisymetric plate loading (sub-system B2).

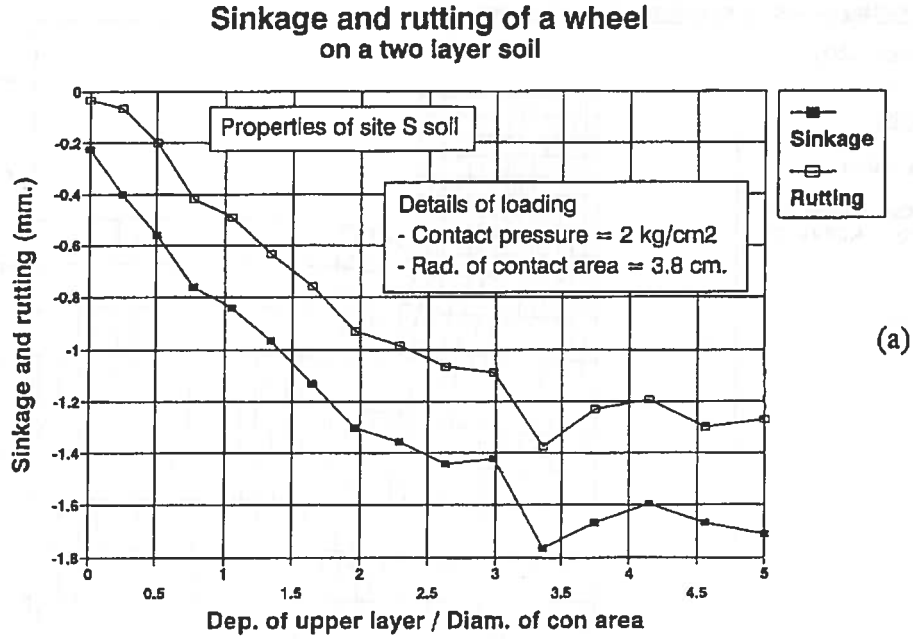


(a)

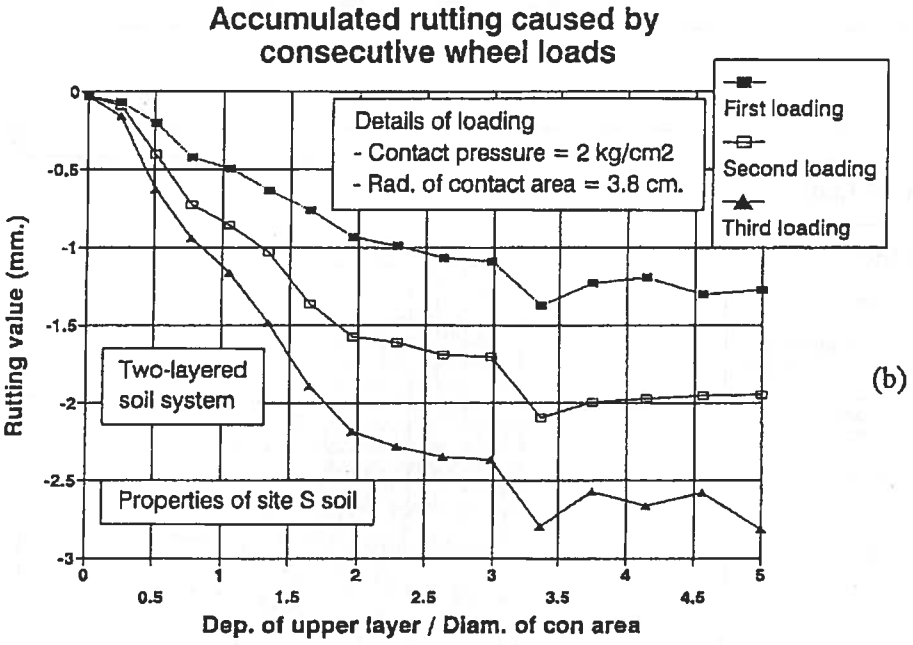


(b)

Fig. 6.20 Sinkage and rutting evaluation in a two-layered soil system (sub-system B2) with properties of site S material
(a) Sinkage and rutting as a function of remolded layer depth.
(b) Accumulated rutting values for consecutive loading of the same point as a function of remolded layer depth.

ציור מס. 6.20 הערכת שקיעה וחריצה במערכת קרקע דרשכבתית (תת־מערכת B2 ), עבור נתוני קרקע מאתר S
(a) שקיעה וחריצה כפונקציה של עומק השכבה המופרת.
(b) חריצה מצטברת המתקבלת מעמיסה חוזרת של אותה נקודה.

It can be noted that rutting values keep on increasing with depth, and stabilization is only observed at high values of the upper layer (3•B and more). This phenomenon, also seen in all other runs that were conducted in sub-system B2, is different from that observed in sub-system B1, where stabilization of soil behavior occurred at depth values of 1-1.25•B.

Fig. 6.21 presents the results obtained by operating the numerical model for different values of the upper layer internal angle of friction, under a larger loading plate with 5 kg/cm$^2$ load pressure. As could be foreseen, the rutting values increase with decreasing values of $\phi$. For $\phi$=30 deg. the rutting mounts to much higher values, up to 20% of the loading plate diameter, due to reaching the soil bearing capacity.

The above relationship, in the form of a list of the predicted rutting values as a function of the upper layer normalized depth, is written into an ASCII file later to be used in sub-system C.

6.4.4 Sub-system C

A. The accumulated rutting approach

The results of sub systems A and B2 are required for the operation of the computer program for performance prediction, based on the accumulated rutting approach. Fig. 6.22 presents the results of these two sub-systems, operated with the properties of site T soil, and with loading conditions that are close to those pertaining in C-130 aircraft operation (case no. 20 in table 6.2, with about 5 kg/cm2 contact pressure and 50 cm. contact width). Fig. 6.23 shows the structure of the files which were used as input for the operation of sub-system C, as well as the printout of the user-computer interaction preceding software activation. The total width of the runway was taken as 8 m., and the soil mounds forming at each side of the wheel were assumed to be twice the width of the wheel. The rutting failure criteria are taken to be 3 cm. for primary rutting, and 10 cm. for total accumulated rutting (criteria A and B). The output files produced by the software system provide an estimation of the runway surface profile (a cross section of the runway) at the end of simulation, as well as a logging of rutting development, which is made pass by pass during simulation operation. Fig. 6.24 includes a printout of the output files for the above example, while Fig. 6.25 graphically presents ruts accumulation and the final surface profile as predicted by the simulation software. Total rut criterion A is first violated after 454 load cycles and after 746 cycles its value attains 15 cm.

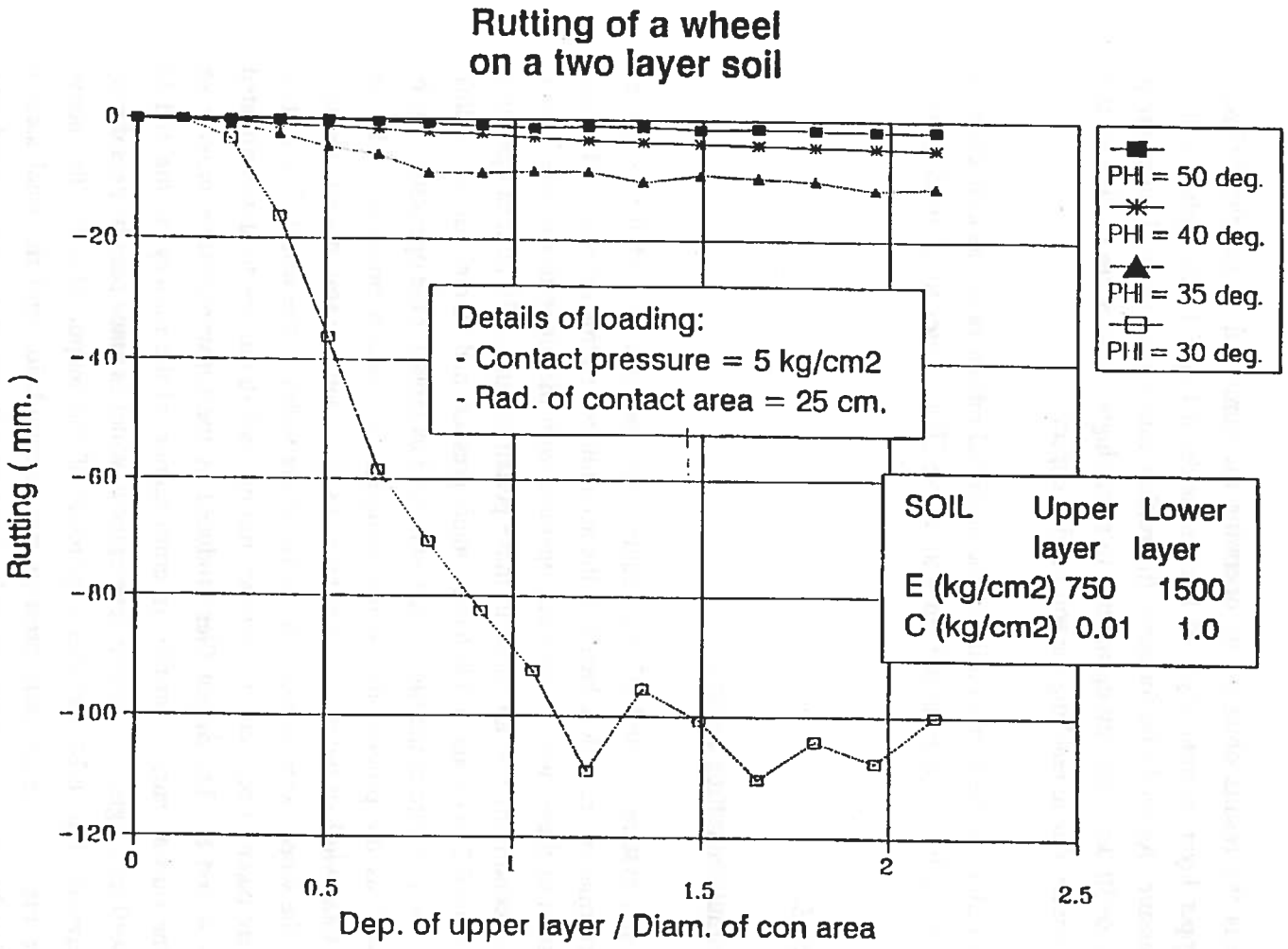


Fig. 6.21 Predicted rutting values in a two-layered soil system as a function of the internal angle of friction.

ציור מס. 6.21 הערכת חריצה במערכת קרקע דו־שכבתית כפונקציה של זוית החיכוך הפנימית.

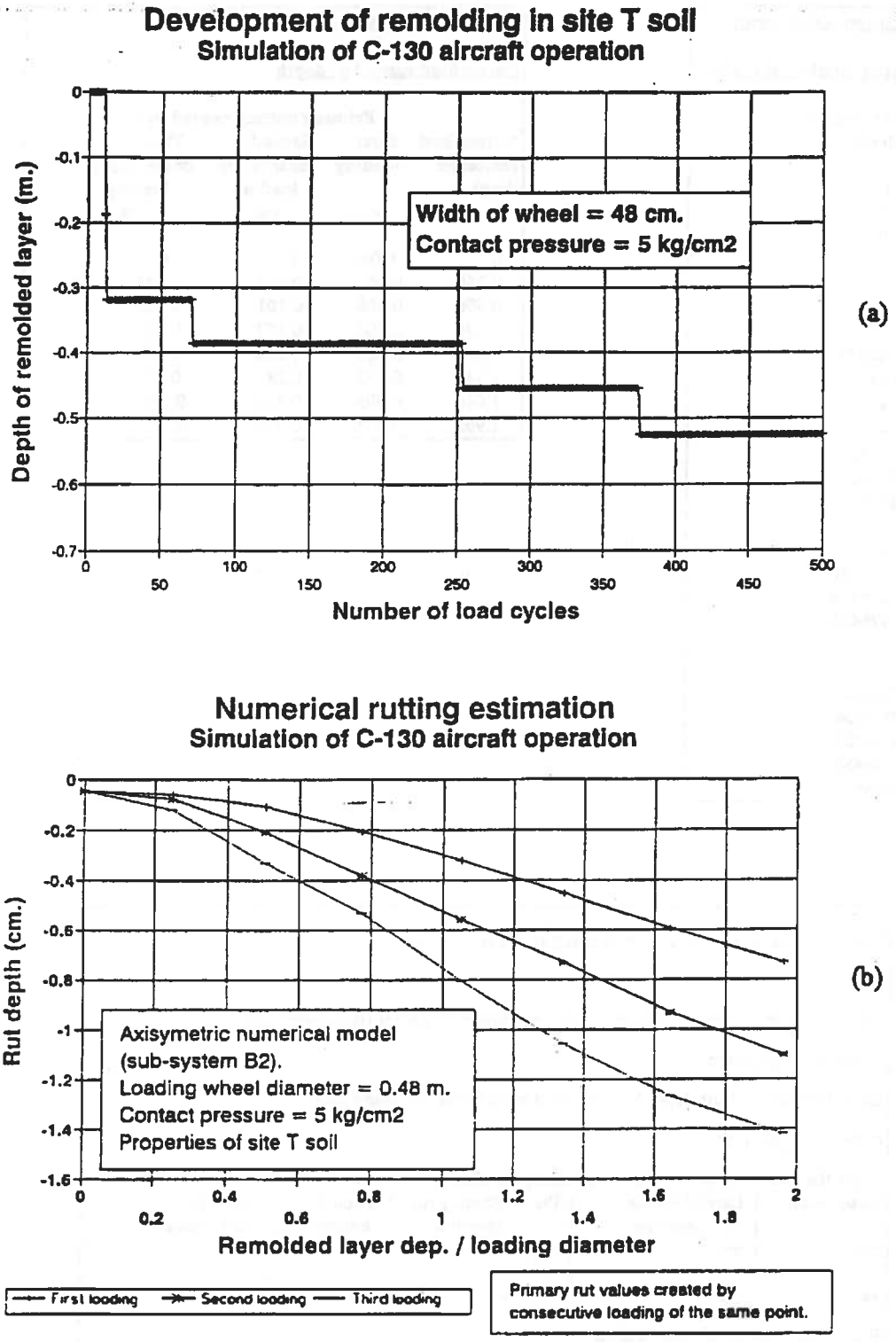


Fig. 6.22 Results of the analytical system, simulating C-130 aircraft operation on site T soil.
(a) Sub-system A results (model no. 20, table 6.2).
(b) Sub-system B2 results.

ציור מס. 6.22 סימולציית הפעלה של מטוסי C־130 , תוצאות המערכת האנליטית
(a) תוצאות תת־מערכת A (מודל מספר 20 , טבלה 6.2)
(b) תוצאות תת־מערכת B2

**Normalized remolded depth vs Accumulated number of cycles.**

| Cyc. no. | Remolded depth |
|---|---|
| 0 | 0 |
| 1 | 0 |
| 2 | 0 |
| 3 | 0 |
| • | • |
| • | • |
| 56 | 0.664375 |
| 57 | 0.664375 |
| 58 | 0.664375 |
| • | • |
| • | • |
| 96 | 0.805625 |
| 97 | 0.805625 |
| 98 | 0.805625 |
| • | • |
| • | • |
| 380 | 1.096458 |
| 381 | 1.096458 |
| 382 | 1.096458 |
| • | • |
| • | • |
| 496 | 1.096458 |
| 497 | 1.096458 |
| 498 | 1.096458 |
| 499 | 1.096458 |
| 500 | 1.096458 |

**Primary rutting values vs Normalized remolded depth**

| Normalized remolded depth | Primary rutting caused by - First loading cm. | Second consecutive loading cm. | Third consecutive loading cm. |
|---|---|---|---|
| 0 | 0.046 | 0 | 0 |
| 0.248 | 0.06 | 0.017 | 0.043 |
| 0.506 | 0.108 | 0.101 | 0.125 |
| 0.774 | 0.206 | 0.177 | 0.15 |
| 1.052 | 0.321 | 0.236 | 0.249 |
| 1.342 | 0.451 | 0.28 | 0.33 |
| 1.646 | 0.595 | 0.338 | 0.338 |
| 1.962 | 0.731 | 0.371 | 0.317 |

**User - computer interaction preceding program operation**

Enter filename of Remolded layer depth Vs. Number of passes (including path)

c:\tp6\rafi\t_g5_1.rem

Enter filemane of Ruts depth Vs. remolded layer depth (including path)

c:\tp6\rafi\t_g5_1.rut

Enter the following values regarding loading conditions:

| Load width cm. | Lateral wander std. deviation cm | Phi deg. | Primary rut criterion cm. | Total rut criterion A cm. | Total rut criterion B cm. |
|---|---|---|---|---|---|
| 48 | 60 | 47 | 3 | 10 | 10 |

Enter total number of wheel passes

1000

Fig. 6.23 Sub-system C - the accumulated rutting approach. Structure of input files and user-computer interaction.

ציור מס. 6.23 תת־מערכת C - גישת החריצה המצטברת. מבנה קבצי הקלט ואינטראקציה מחשב - משתמש.

CALCULATION OF SOIL SURFACE PROFILE
UNDER REPETITIVE LOADING

Program name - sub_c1.PAS

Remolded layer depth Vs. Number of passes, given
in file - c:\tp6\rafi\t_g5_1.rem

Rutting values Vs. Remolded layer depth, given
in file - c:\tp6\rafi\t_g5_1.rut

Wheel width in cm. - 48

Standard deviation of lateral wander - 60

| Point no. | Point level (cm.) | No. of loadings |
|---|---|---|
| 1 | 0.000 | 0 |
| • | • | • |
| • | • | • |
| 85 | 0.087 | 0 |
| 86 | 0.087 | 0 |
| • | • | • |
| • | • | • |
| 203 | 7.742 | 3 |
| 204 | 7.742 | 3 |
| 205 | 7.742 | 3 |
| 206 | 7.742 | 3 |
| 207 | 7.725 | 3 |
| 208 | 6.789 | 4 |
| • | • | • |
| • | • | • |
| 405 | -6.611 | 329 |
| 406 | -6.611 | 328 |
| 407 | -6.611 | 327 |
| 408 | -6.611 | 323 |
| 409 | -5.918 | 329 |
| 410 | -5.918 | 325 |
| • | • | • |
| • | • | • |
| 573 | 10.662 | 5 |
| 574 | 10.592 | 5 |
| 575 | 10.526 | 5 |
| • | • | • |
| • | • | • |
| 800 | 0.000 | 0 |

CALCULATION OF RUT DEVELOPMENT
UNDER REPETITIVE LOADING

Program name - sub_c1.PAS

Remolded layer depth Vs. Number of passes, given
in file - c:\tp6\rafi\t_g5_1.rem

Rutting values Vs. Remolded layer depth, given
in file - c:\tp6\rafi\t_g5_1.rut

Wheel width in cm. - 48

Standard deviation of lateral wander - 60

Allowed Primary rutting - 3.00cm.

Allowed Acc. rutting B - 10.00cm.

Allowed Acc. rutting A - 10.00cm.

Accumulated rutting A criterion first violated at cycle no. - 454

| Cy. no. | Rem. depth / Load wid. | Prim. rut. (cm.) | Acc. rut. B (cm.) | Acc. rut. A (cm.) |
|---|---|---|---|---|
| 1 | 0.0 | 0.05 | 0.01 | 0.02 |
| 2 | 0.0 | 0.05 | 0.02 | 0.05 |
| • | • | • | • | • |
| • | • | • | • | • |
| 318 | 0.9 | 0.28 | 3.01 | 6.46 |
| 319 | 0.9 | 0.28 | 3.00 | 5.75 |
| 320 | 0.9 | 0.28 | 3.05 | 5.80 |
| • | • | • | • | • |
| • | • | • | • | • |
| 453 | 1.1 | 0.34 | 3.71 | 9.83 |
| 454 | 1.1 | 0.34 | 3.87 | 10.08 |
| 455 | 1.1 | 0.34 | 3.91 | 10.18 |
| 456 | 1.1 | 0.34 | 3.70 | 10.06 |
| • | • | • | • | • |
| • | • | • | • | • |
| 745 | 1.1 | 0.34 | 5.94 | 14.98 |
| 746 | 1.1 | 0.34 | 5.99 | 15.03 |
| 747 | 1.1 | 0.34 | 6.03 | 15.06 |
| • | • | • | • | • |
| • | • | • | • | • |
| 999 | 1.1 | 0.34 | 6.15 | 17.21 |
| 1000 | 1.1 | 0.34 | 6.18 | 17.25 |

Fig. 6.24 Sub-system C - the accumulated rutting approach. Structure of output files.

ציור מס. 6.24 תת־מערכת C - גישת החריצה המצטברת. מבנה קבצי הפלט.

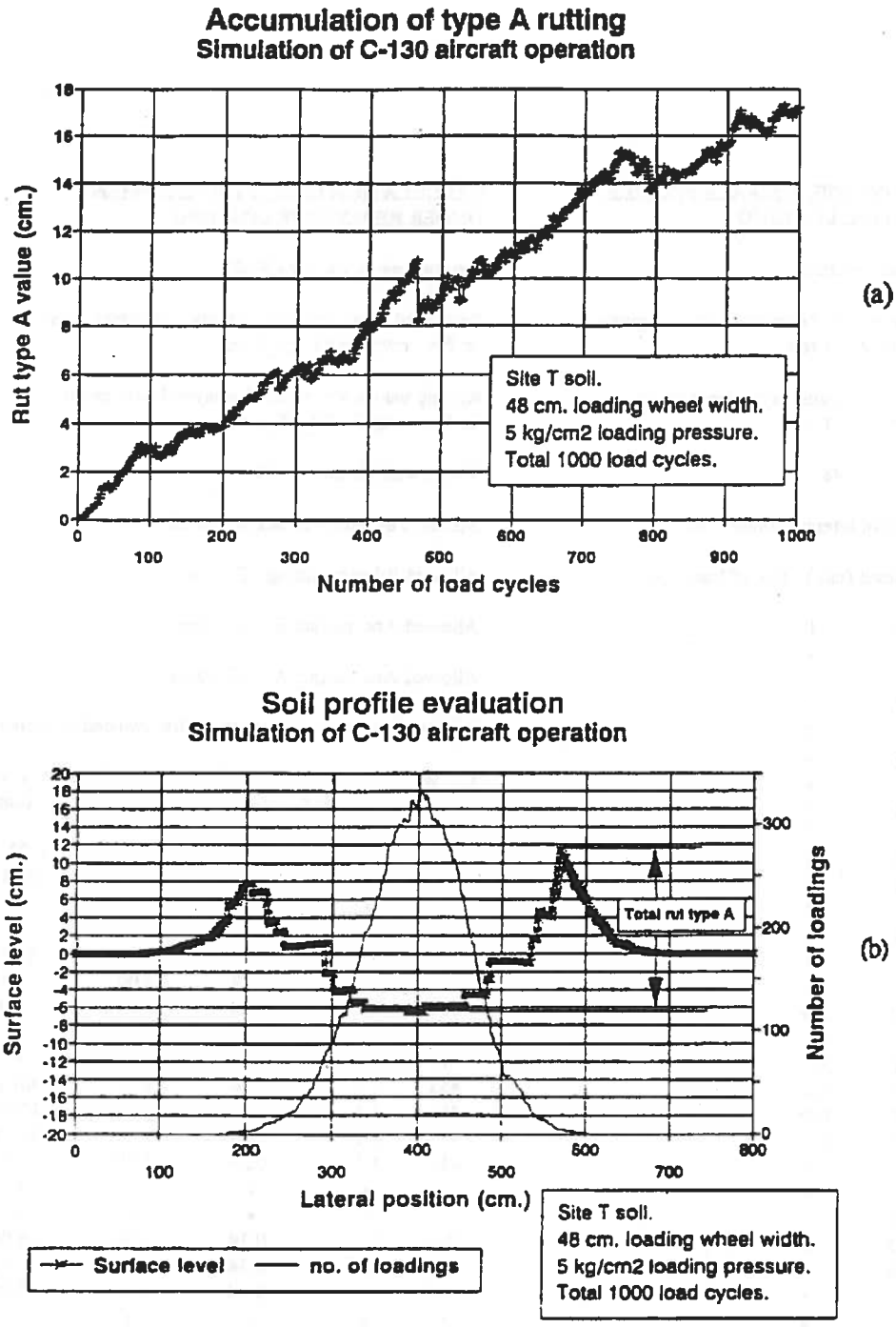


Fig. 6.25 Sub-system C - the accumulated rutting approach. Results of simulating C-130 aircraft operation on site T soil.
(a) Accumulation of total rut depth.
(b) Runway cross-sectional profile after 1000 load cycles.

ציור מס. 6.25 תת־מערכת C - גישת החריצה המצטברת. תוצאות סימולצית הפעלת מטוסי C־130 על קרקע מאתר T.
(a) התפתחות עומק החריצה הכולל.
(b) פרופיל רוחבי של המסלול לאחר 1000 מחזורי עמיסה.

B. The accumulated damage approach

The results of sub-system A and B1 were used as input for runway performance prediction, according to the accumulated damage approach. The prediction nomogram presented in Fig. 6.6 was used in the process (theoretically any accepted prediction nomogram may be used), for the evaluation of the incremental damage values. Fig. 6.26 presents the structure of the two input files used, and the user computer interaction before software operation. As an example and for reasons of comparison with the accumulated rutting approach, the site T soil properties and the same C-130 loading conditions were used. The results of sub-systems A and B1 for this problem are presented in Fig. 6.22a and Fig. 6.18a, respectively. Fig. 6.27 presents the output of the software system which details for each cycle the soil system condition, the incremental and the accumulated damage. For the above example, runway failure is predicted to happen following 375 load cycles. For comparative reasons, the number of cycles that would have been predicted whether the soil had a constant strength of the unremolded soil is more than 270,000, and only 1.5 cycles whether its strength was that of the remolded site T soil. It is interesting to note that although the accumulated rutting approach and the accumulated damage approach solve the problem of runway performance in an entirely different way and by using different sources of input, the results obtained for the above example are very similar.

## 6.5 Summary of the analytical system

The suggested mechanistic model for the behavior of remoldable soils under repetitive wheel loading, was the basis for the analytical system described and detailed in the present chapter. The main goals of the analytical system were to give numerical validation and quantification to the suggested model and provide directives as to possible practical uses of the model, in the performance prediction of unsurfaced runways. The numerical system was essentially built as a 2D system, and incorporated the mechanical model suppositions regarding soil constitutive and fatigue behavior. Most of the numerical system was written by the use of the FLAC system, a numerical finite-differences software system, while other parts were written in Turbo Pascal.

The analytical system was composed of three sub-systems, logically connected to each other:

- Sub-system A - Describes the development of a two-layer structure in the remoldable soil, caused by repetitive loading of the soil surface.

**Normalized remolded depth vs Accumulated number of cycles.**

| Cyc. no. | Remolded depth |
|---|---|
| 0 | 0 |
| 1 | 0 |
| 2 | 0 |
| 3 | 0 |
| • | • |
| • | • |
| 56 | 0.664375 |
| 57 | 0.664375 |
| 58 | 0.664375 |
| • | • |
| • | • |
| 96 | 0.805625 |
| 97 | 0.805625 |
| 98 | 0.805625 |
| • | • |
| • | • |
| 380 | 1.096458 |
| 381 | 1.096458 |
| 382 | 1.096458 |
| • | • |
| • | • |
| 496 | 1.096458 |
| 497 | 1.096458 |
| 498 | 1.096458 |
| 499 | 1.096458 |
| 500 | 1.096458 |

**Equivalent CBR vs Normalized remolded depth**

| Normalized remolded depth | Equivalent CBR % |
|---|---|
| 0 | 40 |
| 0.1653 | 36.01967 |
| 0.33735 | 34.70186 |
| 0.5165 | 23.70486 |
| 0.704 | 20.46412 |
| 0.8985 | 13.0763 |
| 1.101 | 6.121485 |
| 1.3125 | 5.747656 |
| 1.532 | 5.459889 |
| 1.761 | 5.041955 |
| 1.9995 | 5 |

**User - computer interaction preceding program operation**

Enter filename of Remolded layer depth Vs. Number of passes (including path)

c:\tp6\rafi\t_g5_1.rem

Enter filemane of Equiv depth Vs. remolded layer depth (including path)

c:\tp6\rafi\t_g5_1.str

Enter the following values regarding loading conditions:

| CONTACT PRESSURE psi | ESWL lb |
|---|---|
| 70 | 30000 |

Fig. 6.26 Sub-system C - the accumulated damage approach. Structure of input files and user-computer interaction.

ציור מס. 6.26 תת־מערכת C - גישת הנזק המצטבר. מבנה קבצי הקלט ואינטראקציה מחשב - משתמש.

**PREDICTION OF UNSURFACED RUNWAY PERFORMANCE BY ACCUMULATED DAMAGE APPROACH**

Remolded layer depth Vs. Number of passes, given in file - c:\tp6\rafi\t_g5_1.rem

Equiv. soil strength Vs. Remolded layer depth, given in file - c:\tp6\rafi\t_g5_1.str

Average contact pressure - 70.0 psi

ESWL - 30000.0 lb

| Cycle no. | Depth remolded / Load width | Equiv. Str. CBR % | Incremental damage | Accumulated damage |
|---|---|---|---|---|
| 1 | 0.0 | 40.00 | 3.694E-06 | 3.694E-06 |
| 2 | 0.0 | 40.00 | 3.694E-06 | 7.388E-06 |
| 3 | 0.0 | 40.00 | 3.694E-06 | 1.108E-05 |
| 4 | 0.0 | 40.00 | 3.694E-06 | 1.478E-05 |
| 5 | 0.0 | 40.00 | 3.694E-06 | 1.847E-05 |
| | | • | | |
| | | • | | |
| 244 | 0.8 | 16.60 | 6.204E-04 | 1.168E-01 |
| 245 | 0.8 | 16.60 | 6.204E-04 | 1.174E-01 |
| 246 | 0.8 | 16.60 | 6.204E-04 | 1.180E-01 |
| 247 | 0.8 | 16.60 | 6.204E-04 | 1.187E-01 |
| | | • | | |
| | | • | | |
| 370 | 0.9 | 11.32 | 5.778E-03 | 7.984E-01 |
| 371 | 0.9 | 11.32 | 5.778E-03 | 8.042E-01 |
| 372 | 0.9 | 11.32 | 5.778E-03 | 8.100E-01 |
| 373 | 0.9 | 11.32 | 5.778E-03 | 8.157E-01 |
| 374 | 0.9 | 11.32 | 5.778E-03 | 8.215E-01 |
| **375** | **1.1** | **6.28** | **1.796E-01** | **1.001E+00** |
| 376 | 1.1 | 6.28 | 1.796E-01 | 1.181E+00 |
| 377 | 1.1 | 6.28 | 1.796E-01 | 1.360E+00 |
| | | • | | |
| | | • | | |
| 998 | 1.1 | 6.28 | 1.796E-01 | 1.129E+02 |
| 999 | 1.1 | 6.28 | 1.796E-01 | 1.131E+02 |
| 1000 | 1.1 | 6.28 | 1.796E-01 | 1.133E+02 |

In a homogenous unremolded soil,failure would occur after - **270,724.4** cycles

In a homogenous remolded soil,failure would occur after - **1.5** cycles

Failure is expected in runway after - **375** cycles.

Fig. 6.27 Structure of the output file of sub-system C - accumulated damage approach.

ציור מס. 6.27 מבנה קובץ הפלט של תת-מערכת C - גישת הנזק המצטבר.

- Sub-system B - Finds the behavior of the two-layer soil structure as a function of the depth of the upper layer. The behavior is defined in terms of the equivalent CBR of the soil structure (sub-system B1), or in terms of rutting values caused by loading the two-layered soil (sub-system B2).

- Sub-system C - Combines the results of the two preceding sub-systems, in an attempt to account for the incremental deteriorative effect of wheel loading on the runway condition, and use it to predict the number of loadings up to runway functional failure.

A large number of cases were studied by operating sub-system A under various soil properties and loading conditions (part of which are given in table 6.2). The results obtained show, as expected by the mechanistic model, the gradual development of an upper remolded soil layer and the creation of a two layer soil structure. The depth of the remolded layer grows with the accumulation of loads applied onto the soil, and a stabilization of its value can be observed, in most cases, after a large number of load repetitions. The depth of the remolded layer at each stage of the runway life was found to be highly dependent upon the loading pressure, the fatigue parameters of the soil and the strength properties of the remolded and unremolded soil. Other factors which have less influence on the remolded layer depth are the loading wheel width (when the remolded depth is normalized) and, the elastic properties of the soil. Some limited verification of the numerical scheme response to loading was made by comparing results to known analytical solutions. Further verification of the mechanistic model and sub system A of the numerical system was performed through a series of moving wheel tests, as detailed in Chapter 7.

Sub-system B was dedicated to the study of the response of a two-layered soil structure to wheel loading. Two alternatives were investigated as possible descriptors of the soil structure response. The first measured (by the use of a numerical model) the soil penetration resistance at varying values of the upper layer depth. The numerical model simulated in many aspects the conventional CBR test. Some numerical verification of the model was done by stiffening the soil before activating the model, thereby enabling comparisons of the results with known bearing capacity solutions. The second alternative consisted of building a numerical model which measures ruts caused by a plate which loads the two-layer soil structure for different values of the upper layer depth. Both studied alternatives showed greater sensitivity to loading as the depth of the upper remolded layer grows. However, while the value of penetration resistance reached some degree of stabilization when the upper layer depth was more than 125% of the loading element width, the rutting values kept on growing for growing depth of the remolded layer (down to a depth of 250% of the loading element width and more).

Sub-system C integrated the results obtained in sub-systems A and B in an attempt to show possible ways to reach at an estimation of the unsurfaced runway performance. Two approaches meant to account for the progression of runway deterioration, were studied. The first, the accumulated rutting approach, consists of numerical estimation of ruts accumulation in the runway up to the point where some rutting criteria are violated. The second approach, the accumulated damage approach, makes use of existing prediction nomograms and Miner's law, in order to estimate and accumulate the incremental damage caused to the runway by the repetitive loading of the two-layer soil structure. Two separate software programs, implementing the principles of the two mentioned approaches, were written in Turbo-Pascal. Operation of both approaches for runway performance prediction was demonstrated by an example using the site T soil properties and typical loading data of the C-130 aircraft.

As mentioned in section 6.2.3, both the accumulated rutting and accumulated damage approaches have some advantages and disadvantages. The accumulated damage approach is simpler and the integration with conventional design methods has its own practical advantages. However it should be remembered that this approach relies on several problematic presuppositions, such as the validity of existing prediction nomograms and the ability to use Miner's law (which assumes linear damage accumulation) for the estimation of incremental runway damage.

The accumulated rutting approach, on the other hand, solves the problem by treating directly the accumulation of ruts which are the principal cause for the runway functional failure. One of the main advantages of the accumulated rutting approach is that it does not inherit the problems of the existing design methods. If rutting values can be found numerically with acceptable precision, then the presented analytical method can serve as a performance prediction tool independent of any existing method. However it should be remembered that its implementation requires relatively high precision in the numerical estimations of rutting. This task can only be achieved by more accurate modeling of the wheel-soil interface and the constitutive laws of the soil and requires an extensive validation and tuning process.

Practical implementation of the accumulated damage approach would be much easier. However, in the long run it seems that the accumulated rutting approach, reaching to the fundamental points of the problem, is the path that should be proceeded.

# CHAPTER 7: THE LABORATORY MOVING WHEEL TESTS

## 7.1 General considerations and the requirements of the present study

Moving wheel tests are meaningful in the context of the present research as they constitute the main tool for verifying the results of the numerical system, and may be used to obtain feedback for the fine-tuning of the system. Where remoldable soils are concerned, the moving wheel tests may be conducted under natural conditions, i.e., in-situ, or alternatively under laboratory conditions, on soil which has been prepared and cured to simulate natural conditions.

Actual aircraft landing results are, of course, preferable, as they reflect the actual in-situ situation. At the same time, the use of actual landing results has a number of drawbacks:

1. It is very expensive to effect aircraft landings for the purpose of research only. For this reason, use is usually made of results obtained from regularly conducted IAF aircraft landing exercises. In such cases, there is no control over the number of landings nor over the loading parameters which change from one landing to the next. The number of landings usually carried out during such exercises is small, and the results are therefore rather random.

2. The number of parameters which are involved in the wheel-soil interaction is very large. The values of the various parameters such as soil strength, soil longitudinal profile, etc., change both over time and location, and the scatter of these values is often very large.

In view of the above, it was decided that in order to enable an understanding of the studied subjects, it is better to concentrate on controlled laboratory tests. The experiments, in which it is possible to control plausibly the values of parameters relevant to the process, are to be preferred in the given conditions.

In laboratory tests of remoldable soils, the curing process of the soil is highly important. An appropriate curing procedure makes it possible to reconstruct soil samples with characteristics similar to the in-situ soil. The curing process gives rise to an additional strength element which enables the simulation of the natural soil in the laboratory. Where remoldable clayey soils are concerned, the curing process involves thixotropic processes which lead to the formation of a special structure between the clay particles and add to the soil strength.

In dry granular soils, which were the focus of the present study, it was necessary to formulate a meticulous curing procedure which entailed wetting the soil, compaction to the desired density, soaking with water (the reasons for which are explained below) and drying down to very low levels of moisture. Effecting this process on a large laboratory scale (such as in the special channels constructed in the Faculty of Agricultural Engineering) is an extremely complex project which requires considerable resources in both time and money. It can be estimated that due to the required drying phase, only the preparation and curing process of each experiment would have taken at least 4-5 months. More than that, the types of soils used and the large soil mass (2 / 5 m. cross-sectional dimensions), gave little assurance as to the ability to attain homogeneity in the strength values of the dried soil. In view of these difficulties, it was decided to perform the moving wheel tests in a system where the dimensions of the loading wheel are smaller than they are in reality.

The moving wheel experiments in the present study have imposed a number of requirements regarding the loading device and the soil samples. One of the important characteristics of the repetitive movement of aircraft over a runway, is the lateral wander of the traffic according to a given normal distribution. This issue becomes more meaningful when investigating the behavior of a soil system subjected to high plastic deformations. In order to simulate reality as closely as possible, it became necessary to construct a new loading device. The new pneumatically operated device makes it possible to change the lateral position of the loading wheel from one loading to the next. Other characteristics of the loading device are the ability to change the load on the wheel easily and to monitor the vertical and horizontal forces exerted on the loading wheel. The details of the loading device and its various characteristics, as well as its application, are given in section 7.2.

An additional issue which required special attention was that of determining the dimensions of the soil samples, and the samples preparation and curing procedures. One of the main difficulties involved in soil testing is the confinement effect caused by the walls and the floor of the sample mold. In order to minimize this phenomenon (which induces deviant experimental results), a sample with certain minimum dimensions as compared to the loading element dimensions is required. Increasing the sample dimensions has prompted other problems ensuing from the difficulties of uniformly curing large samples, handling soil samples weighing hundreds of kilograms, etc.

The compromise eventually decided on, included decreasing the dimensions of the loading wheel down to a diameter of about 8", thus allowing the tests to be carried out with a mold

weighing up to about 300 kg. The considerations which led to the selection of these mold dimensions and the samples preparation and curing procedures are detailed in section 7.3.

## 7.2 Pneumatic loading device - details and working methods

In order to perform the laboratory moving wheel tests, the existing moving wheel device located at the Technion Soil and Roads Laboratory (which was used in a number of past studies, see Ref. 58,59), was modified. This device is based on an electrically driven moving plate on which the test sample moves back and forth under a stationary loading wheel. The movement of the carrying plate allows a longitudinal range of movement of up to about 70 cm., at a rate of about 2 seconds per cycle. In its original design, the loading of the wheel on the soil was brought about by means of a 1:4 loading shaft at the end of which weights are hung according to the loading requirements.

Fig. 7.1 presents a general photograph of the new loading device which was designed and built for the purpose of conducting the moving wheel experiments in the present study. The device is mechanically activated by means of a pneumatic system which controls the loading, the descent of the wheel and its horizontal positioning along the width of the sample.

Fig. 7.2 presents a schematic drawing of the vertical movement and loading system. The loading wheel (A) with a diameter of up to 9", is held by a steel "fork" (B) capable of vertical movement. The direction of movement is secured by means of two polished steel rods (C) which move freely in a vertical direction inside special bushings (D). These bushings contain longitudinal bearings which prevent any horizontal wheel movement. The loading of the wheel is carried out by means of a pneumatic cylinder (E) which is fastened to the loading device basis in such a way that the cylinder's opening is facing downward. The loading device basis (on which the system of the moving wheel and the loading piston is placed) is suspended, by means of two pairs of horizontal bushings on top of two horizontal steel rods, 50 mm. in diameter. These rods are connected to the main steel frame anchored to the moving plate device. The horizontal steel rods permit moving the loading device along the width of the soil sample, in order to emulate the lateral wander. The lateral movement of the loading device is operated by means of an additional air cylinder (F, see Fig. 7.2) which is affixed to the loading device basis in such a way that the piston's end is held by the main steel frame.

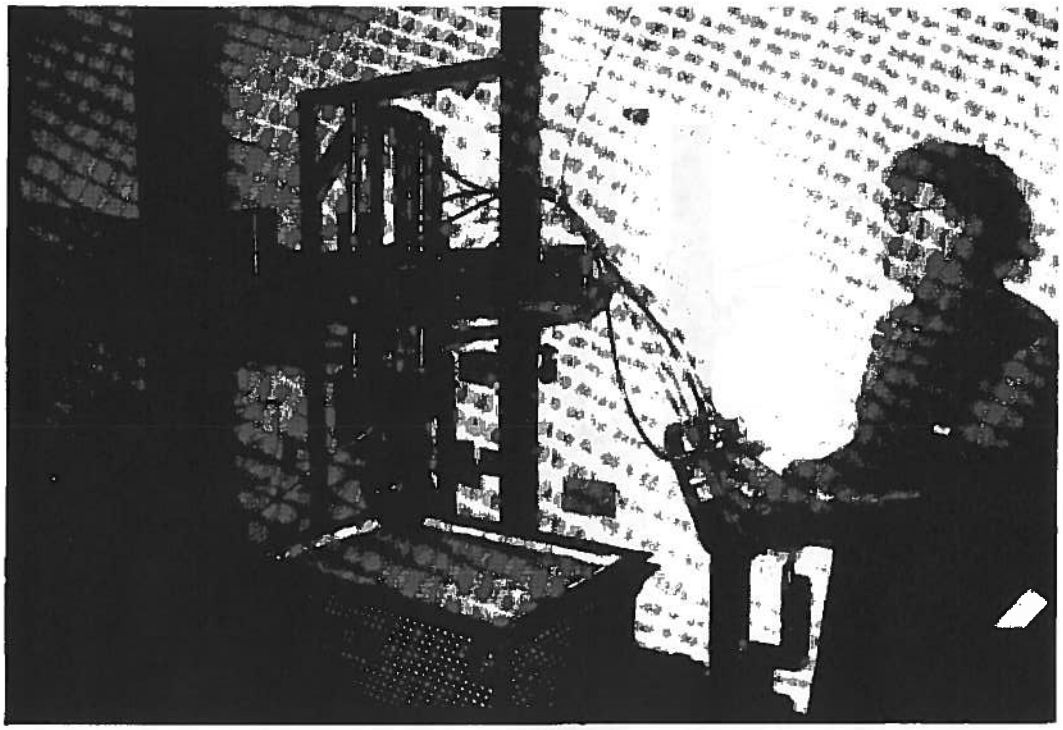

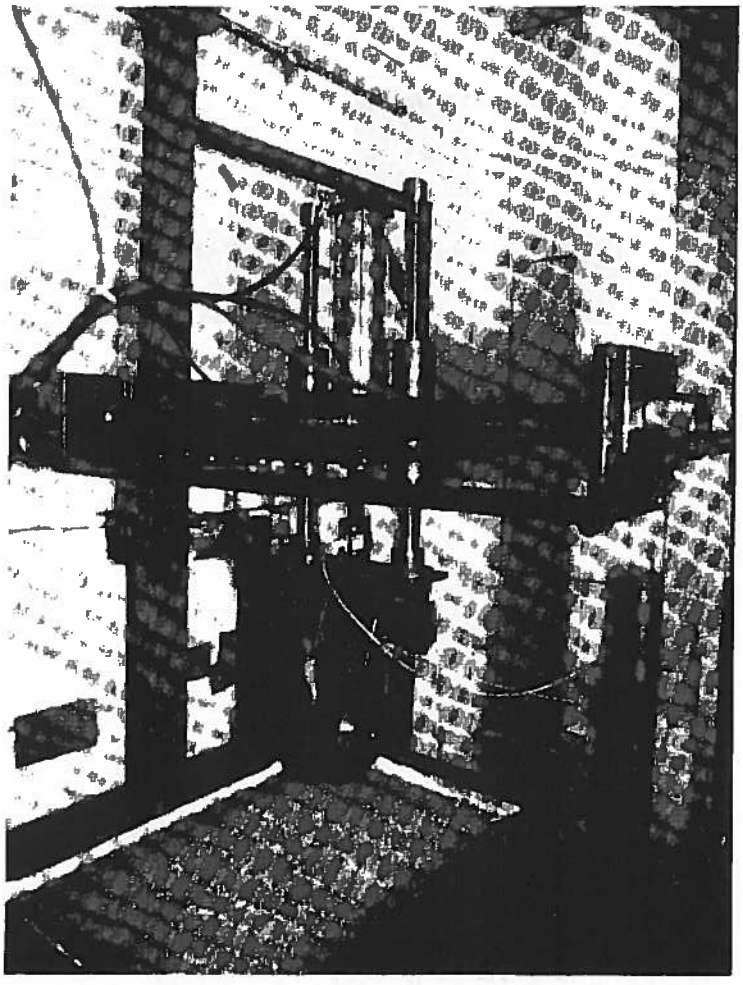

Fig. 7.1 General view of the moving wheel testing device.

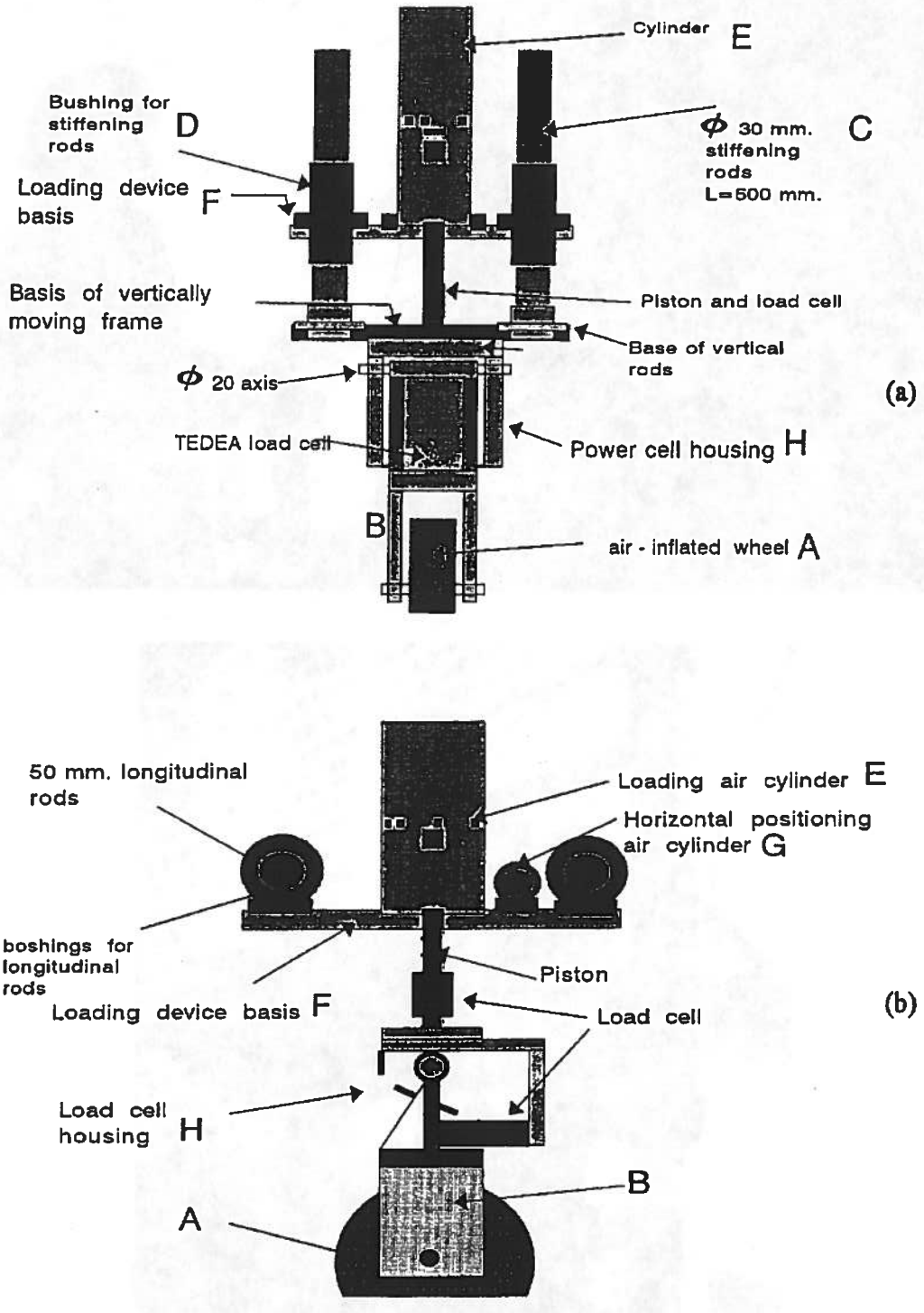


Fig. 7.2 A schematic drawing of the newly built loading wheel device
(a) Front view cut.
(b) Side cut.

ציור מס. 7.2 שרטוט סכימטי של מתקן עמיסת הגלגל
(a) חתך חזיתי
(b) חתך צד

The system functions by means of a main control panel which includes:

a. A switching system for activating and deactivating the moving plate.
b. A pneumatic operating handle for raising the wheel and lowering it onto the soil sample.
c. A pneumatic regulator which makes it possible to control the loading level of the wheel.
d. A pneumatic activation handle for moving the loading device horizontally. This handle may only be activated when the wheel is raised off the sample, in order to prevent any attempt to move the wheel horizontally during loading.

The control of the forces operating on the wheel is carried out by means of two power cells (manufactured by TEDEA) suitable for both pressure and tension. One power cell, suitable for a range of up to 300 kg., is installed (see Fig. 7.2) on the loading axis and measures the vertical force exerted on the wheel. The second power cell is installed within a special housing (G, see Fig. 7.2) and monitors the horizontal forces acting on the wheel at a ratio of 1:3. This latter power cell measures forces up to 500 kg. and thus makes it possible to measure horizontal forces of up to about 160 kg. The forces are monitored by means of an electronic strain indicator instrument. The system constructed in the present study is manually controlled, but has been so designed to allow future application of computerized control and monitoring.

The entire system is controlled from the control panel located at the front of the device. During regular operation. the moving plate is activated at the beginning of the experiment and moves continuously. The pressure regulator adjusts the loading level of the wheel which is monitored by the vertical power cell until the required level of loading is achieved. A pointing appliance (held to the loading device basis and moving with it) and a fixed metal ruler are used in order to move the loading device to its required lateral position. The operator is provided with a pre-fixed table of loadings which determines the number of loadings to be performed at each lateral location.

## 7.3 Preparation of the mold and the soil samples

The performance of moving wheel experiments on the soils which were the focus of the present study, required special procedures for the preparation of soil samples and their curing. Based on the accepted ratios quoted in the literature, of about 1:5 between the dimensions of the loading element and the dimensions of the sample; a 30-35 cm. deep and

45 cm. wide soil section was determined. These dimensions were determined for an 8" loading wheel with a loading width of about 4-5 cm. The width was established with consideration of the issue of the wheel's lateral wander and the desire to minimize the effects of the walls of the sample mold on the behavior of the system. The length of the sample was determined in the range of 70-80 cm, in order to utilize fully the range of movement of the driving system.

The dimensions of the mold were minimized as far as possible in order to limit the logistic problems involved in relocating the soil samples from the curing area to the testing room. With soil samples of large dimensions (the weight of the mold is about 50 kg and the weight of the soil itself is 200-250 kg), problems arise both in the preparation of the sample and in its curing. Limiting the samples' dimensions helps to obtain more uniform soil samples.

The mold for the soil samples was built of 5 mm. steel plate. The edges of the mold were specially shaped to add to its rigidity and prevent deformations during the experiments and when transferring the sample to the moving wheel device. The walls of the steel mold were perforated (Fig. 7.1) in order to facilitate the curing process and to ensure more uniform soil samples. The preparation and curing of the soil sample for the moving wheel testing included a number of steps:

A. Soil preparation.

The soil intended for use in the experiment was oven dried and partitioned into a number of fractions with the aid of mechanical sieving. The soil fractions were then blended again according to the gradation curve of the original soil. This was done to avoid distortion of the results caused by differences from one soil sample to another. In the moving wheel tests (contrary to the laboratory shear tests), all soil fractions were used except for aggregates whose size exceeded 1" (whose quantity in the site T material was extremely negligible). The particle size was limited in order to prevent local problems in the wheel-soil interaction.

The pre-determined moisture content (6% in the experiments conducted with soil taken from site T) was added to the soil and mixed in by means of an electric concrete mixer with a capacity of 25 kg. After wetting and mixing the soil, the material was transferred in closed buckets to the location where compaction was carried out.

B. The compaction process.

Most of the moving wheel tests were carried out with the same sieved soil as that used in the laboratory soil tests (Chapter 5). In one of the moving wheel tests, use was made with unsieved soil from site T. In this case it was required to determine the soil density which is equivalent to that of the sieved soil used in the laboratory tests. The required density of the soil sample was determined according to the following equation (see Ref. 60):

$$D = \frac{100}{(100 - P)/r * D_f + P/G_c} \qquad [7.1]$$

where:

D - is the soil's calculated dry density.

P - is the retained percent on #10 sieve.

$D_f$ - is the dry density of the material passing #10, which was used in the laboratory shear tests.

$G_c$ - is the bulk specific gravity of the aggregate retained on #10 sieve.

r - is an empirical correction coefficient according to the following table:

| P | r |
|---|---|
| 20 or less | 1.00 |
| 21 - 25 | 0.99 |
| 26 - 30 | 0.98 |
| 31 - 35 | 0.97 |
| 36 - 40 | 0.96 |
| 41 - 45 | 0.95 |
| 46 - 50 | 0.94 |
| 51 - 55 | 0.92 |
| 56 - 60 | 0.89 |
| 61 - 65 | 0.86 |
| 66 - 70 | 0.83 |

For example, for the soil taken from site T, whose characteristics were:

P = 51

r = 0.92

$D_f = 1650\ kg/m^3$

$G_c = 2.69$

the result is $D = 1950\ kg/m^3$.

This value of D is the dry density required in order to prepare soil samples for the moving wheel tests. This density is supposed to be equivalent to the density of the soil on which the laboratory shear tests were conducted, and which were carried out on the passing #10 fraction.

The sample compaction procedure was carried out as detailed in Ref. 61. The soil was compacted in 5 layers with an assumed undercompaction of 7% in the bottom layer. The logic of the assumption of undercompaction arises from the fact that the soil continues to condense during compaction of the upper layers. Accordingly, the height of the soil in the sample after compaction of the n layer is:

$$h_n = \frac{h_t}{n_t}\left[n + \frac{u_n}{100}\right] \qquad [7.2]$$

where:

$h_n$ - height of compacted material at the top of the n layer.

$U_n = U_1 - \left[\frac{U_1}{n_t - 1}(n-1)\right]$ - is the undercompaction level in layer n (in percent).

$U_1$ - is the undercompaction level in the first layer (7%).

$n$ - is the number of the layer under consideration.

$n_t$ - is the total number of compacted layers (5 in the case under consideration).

$h_t$ - is the total height of the sample (32 cm.).

The compaction of the soil was performed by tamping with a square 10x10 cm. compaction plate. The square shape was selected in order to enable the soil near to the edges and in the corners of the mold to be properly compacted. Before tamping the soil, the perforated sides and bottom of the mold were covered with a double layer of filter paper in order to facilitate soaking and subsequently drying the sample.

C. Curing the soil sample.

After the compaction was completed, the soil in the mold was soaked with water. The deep wetting of the sample was carried out in order to allow the accumulation of fines and capillary waters at the contact points between the coarser aggregates, in the course of the drying process applied later. If the wetting process is waived, the level of cohesion which develops in the soil during the drying process is far lower. The above process simulates natural processes which take place in the transition from the rainy season to summer, during which the soil dries and its level of cohesion increases. The wetting was carried out

by spreading water over the surface of the sample and by pouring water into two shallow troughs on both sides of the molds to allow for capillary suction from the bottom of the sample upwards. The water was added in a controlled way until the sample could no longer absorb water.

In the soil taken from site T, the soil's moisture content rose to about 9% after the wetting process was completed. The wetting process lasted about two days and the sample was then left in free air for an additional two-day period before the drying process was initiated. The drying of samples was implemented by means of 8 infra-red heating lamps of 250W each, which were positioned alongside the sample and above it (see Fig. 7.3). The perforated sides of the mold and the filter paper which separated the soil from the mold, made it possible to attain an efficient and more uniform drying of the sample.

The level of drying was controlled by weighing the entire sample by means of a derrick and power cell. The total drying period of samples continued for about 20-25 days, and the drying process was stopped at a moisture content of about 0.5%, when the difference in weight between two consecutive weightings could not be detected. After the drying process was completed, the sample was covered with polyethylene sheets and maintained in this condition until the time of the experiment.

## 7.4 Determination of the average contact pressure and contact width

One of the important parameters influencing the behavior of air inflated wheels on the soil is the contact pressure developing in the wheel-soil interface. Various factors such as the inflation pressure, dimensions and type of the tire, the total load, soil characteristics, etc., influence the value of the contact pressure. Although the distribution of pressures across the wheel-soil interface is not homogeneous and areas of stress concentration do develop, the value of the average contact pressure is usually used for design purposes.

Several research works, relating to the contact area geometry and contact pressure in the wheel-soil interface, have been published in the past (Ref. 61). In most cases tests were performed on non-yielding surfaces, so that the results could only approximate the situation pertaining on an yielding soil under a moving wheel. The general relationship established by different researchers between the inflation pressure and the average contact pressure is (Ref. 13):

$$p = c \bullet p_i + p_c \qquad [7.3]$$

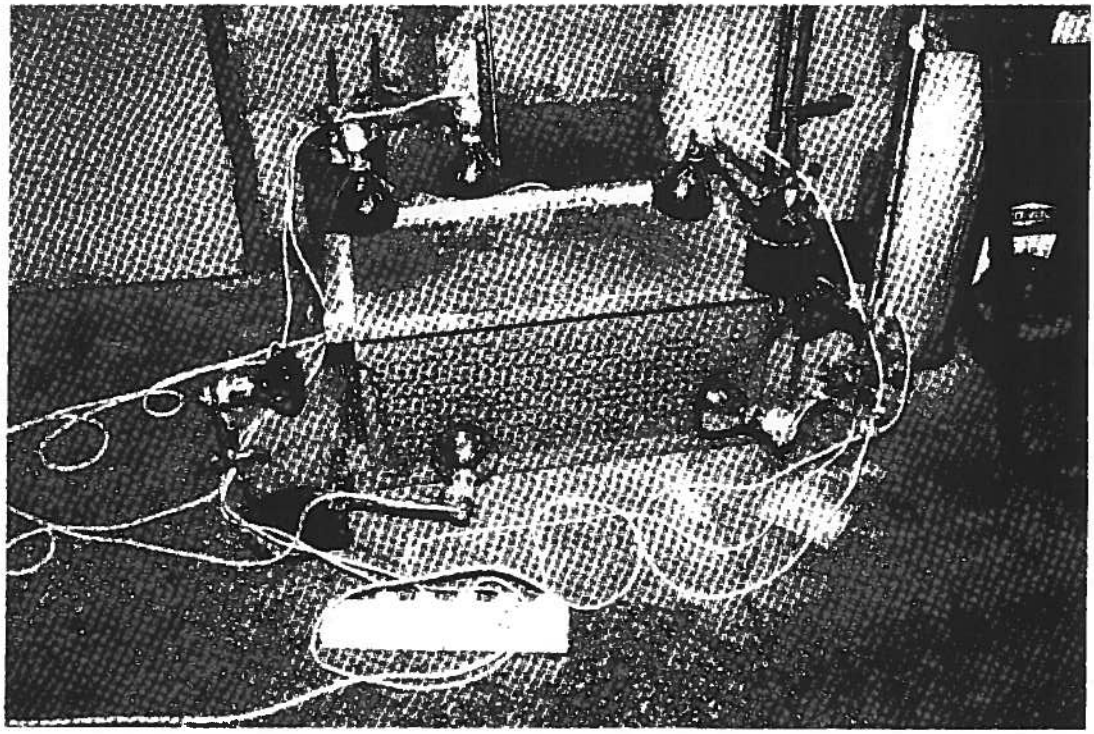

Fig. 7.3 A soil sample for the moving wheel testing, during the drying process.

ציור מס. 7.3 מדגם קרקע המיועד לנסויי גלגל נע, תוך תהליך יבוש.

where:

- $p$ - average contact pressure;
- $p_i$ - air inflation pressure;
- $c$ - a parameter representing the influence of the tire properties on stresses transformation to the loaded surface;
- $p_c$ - pressure resulting from tire carcass;

The value of $p_c$ depends on the tire type and $c$ approaches the value of 1.0 in most cases. The resulting values of the average contact pressure serve as input as well as off-the-road design systems.

According to the above, tests were conducted using the chosen wheel of the new device in order to determine the approximate dimensions of the contact area between the wheel and the soil and the average contact pressure. The tests were performed by spreading paint (with a brush) on the examined tire and then lowering it onto a hard non-yielding plate. The footprint of the tire on a sheet of paper (see for example Fig. 7.4), pre-placed on the plate, was used for the calculations of the desired relationships. The parameters which were changed during testing were the inflation pressure and the total wheel load.

Fig. 7.5a presents the relation between the load on the wheel and the average contact pressure. As can be seen, for the same inflation pressure, the average contact pressure increases with load, probably resulting from higher air pressures developing in the deformed tire. Fig. 7.5b describes the relation between wheel load to the width of the contact area. Fig. 7.5c gives the average contact pressure developing in the wheel-plate interface as a function of the inflation pressure. In all the observations the average contact pressure was found to be higher than the inflation pressure, probably resulting from the relatively low inflation pressures and the large deformations caused in the tire.

The contact pressure and contact width values obtained in the above tests were used as input data in the numerical system during the process of the model validation.

## 7.5 The experimental procedure.

The testing procedure using the new moving wheel device included:

1. Determining the vertical loading of the wheel, which can be changed by using the air pressure regulator on the control panel. Rough setting up is done with the aid of the

**Inflation pressure = 1.5 kg/cm²**

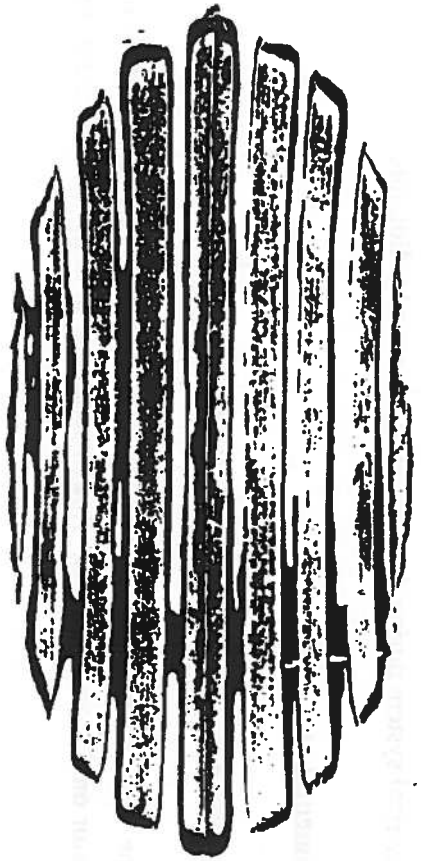

**Vertical load = 76.4 kg.**

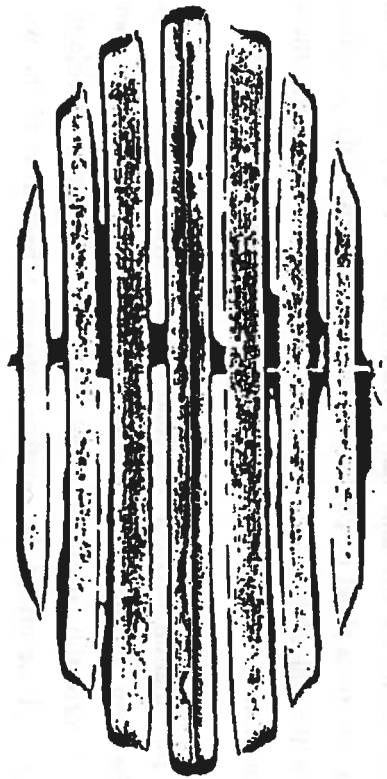

**Vertical load = 54.6 kg.**

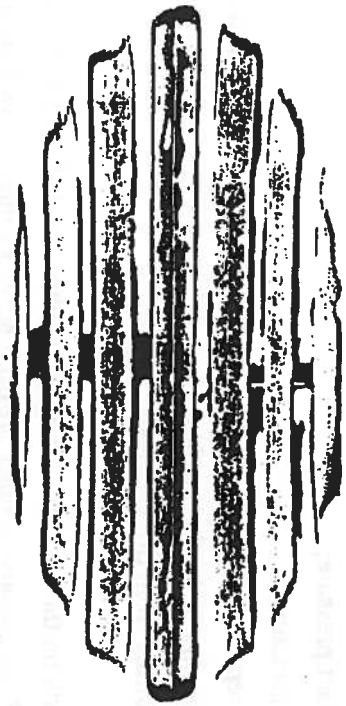

**Vertical load = 33.9 kg.**

Fig. 7.4 An example of the footprint of the 8" diameter wheel on a rigid surface.

ציור מס. 7.4 דוגמא לשטח המגע המתקבל בין גלגל "8 לבין משטח קשיח.

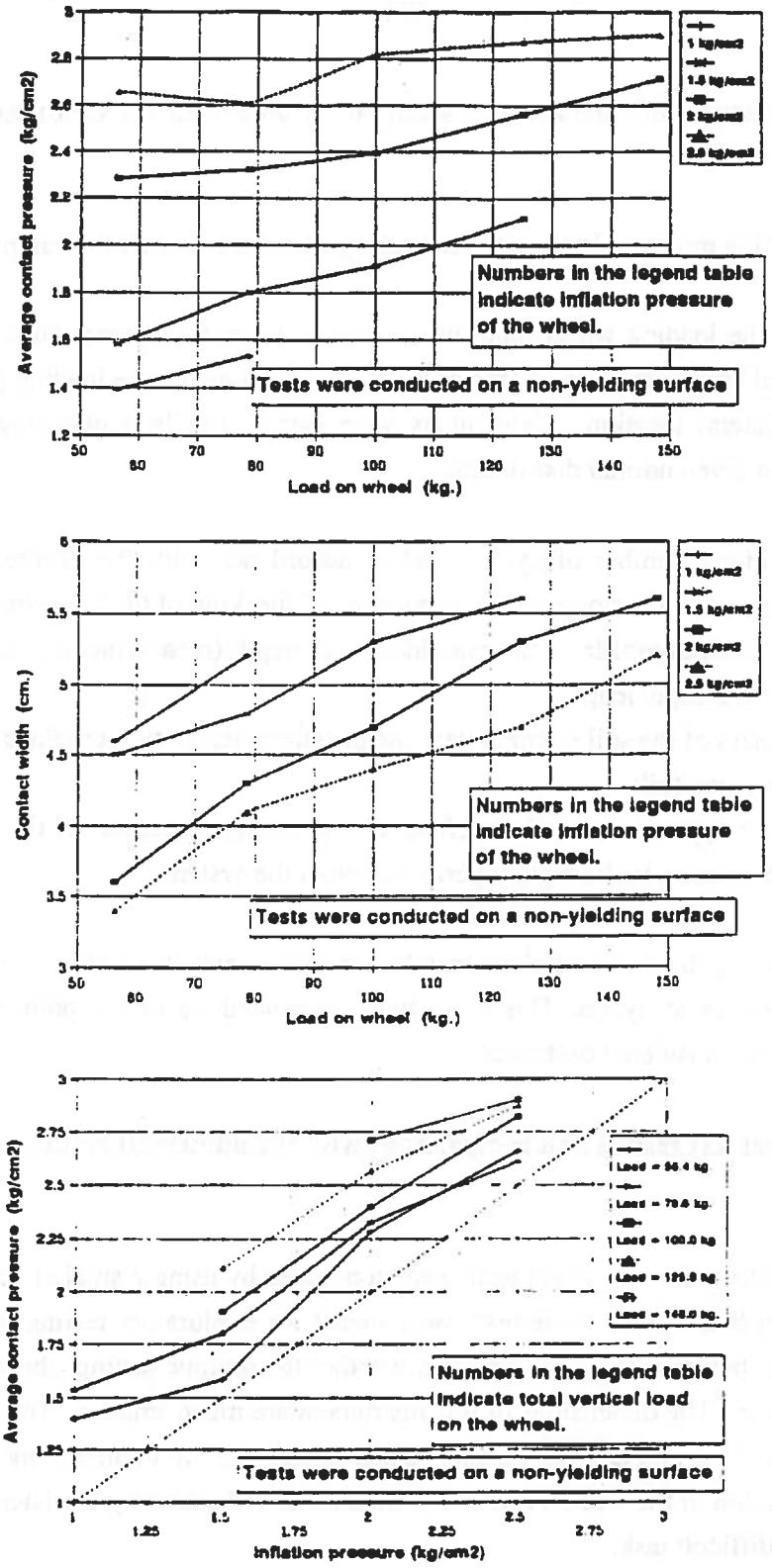


Fig. 7.5 8" Air-inflated wheel on rigid surface. Laboratory test results
(a) Average contact pressure vs total wheel load.
(b) Contact area width vs Total wheel load.
(c) Average contact pressure vs inflation pressure.

ציור מס. 7.5 הפעלת גלגל "8 על משטח קשיח. תוצאות נסויי מעבדה.
(a) לחץ מגע ממוצע כפונקציה של עומס גלגל כולל.
(b) רוחב שטח מגע כפונקציה של עומס גלגל כולל.

air pressure meter, while the accurate setting up is done with the aid of the vertical power cell readings;

2. Activation of the moving plate while the loading wheel is lifted off the sample;

3. Lowering of the loading wheel onto the moving soil sample in accordance with the predetermined lateral position. Some of the tests were done in one loading path in an unchanging lateral location, while others were carried out in a changing location according to a given normal distribution;

4. At a preset given number of cycles, and in accordance with the progress of soil remolding, the system is stopped for the purpose of checking of the following issues;
   a. A cross sectional profile of the remolded layer depth (measuring was done at the midst of the sample length);
   b. Measurement of the soil strength with the penetrometer, in the remolded layer and the unremolded soil;
   c. Testing the appearance of the surface to evaluate the measure of the remolded layer participation in the regular performance of the system.

5. After completing the series of checkings and measurements, the wheel is reactivated for another series of cycles. This procedure is repeated up to the point where the sample may be considered destroyed.

## 7.6 Moving wheel test results and comparisons with the numerical results

A. Initial tests

Preliminary laboratory moving wheel tests were conducted by using a smaller scale device than the one described above. These tests were meant for exploratory testing of different types of materials, before making the decision whether to continue testing these materials with the new device. The dimensions of this instrument are much smaller. The size of the soil sample is 36/18/10 cm, and the loading rubber wheel is 3" in diameter and about 2.0 cm wide. The motion of the wheel is basically channeled, and changing the lateral position of the wheel is a difficult task.

Fig. 7.6 illustrates the results of one of these tests. A sample of sandy soil containing 8% of mineral filler was prepared and cured (by soaking and drying) before testing on the moving wheel device. Pocket penetrometer tests revealed initial resistance to penetration of about 1.5 - 2.5 kg/cm$^2$. Activation of the moving wheel was performed with the exertion

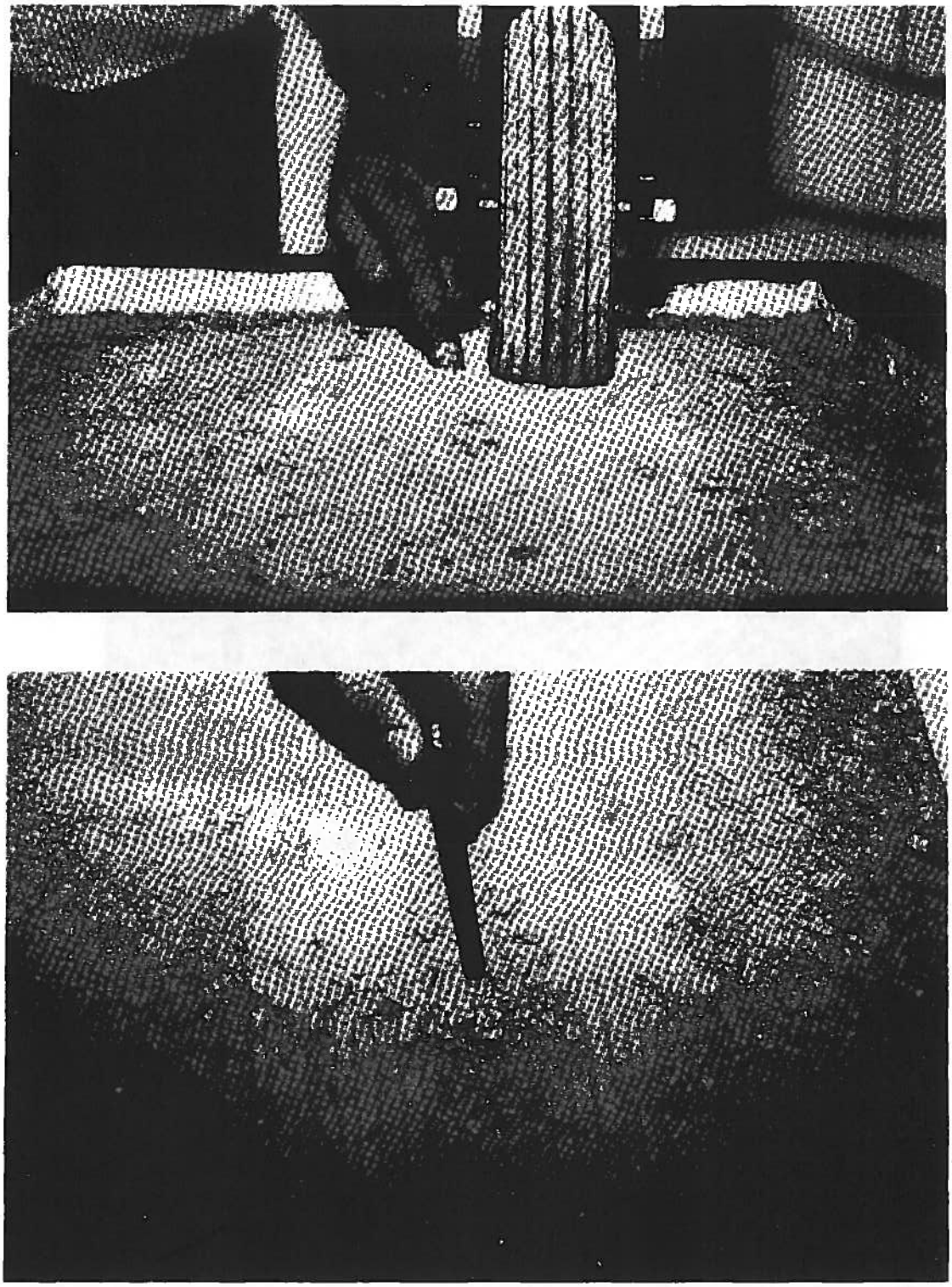

Fig. 7.7 Moving wheel test results. Surface of site T soil sample after 500 wheel passes.

ציור מס. 7.7 תוצאות נסוי בגלגל נע. פני מדגם קרקע מאתר T לאחר 500 מעברי גלגל.

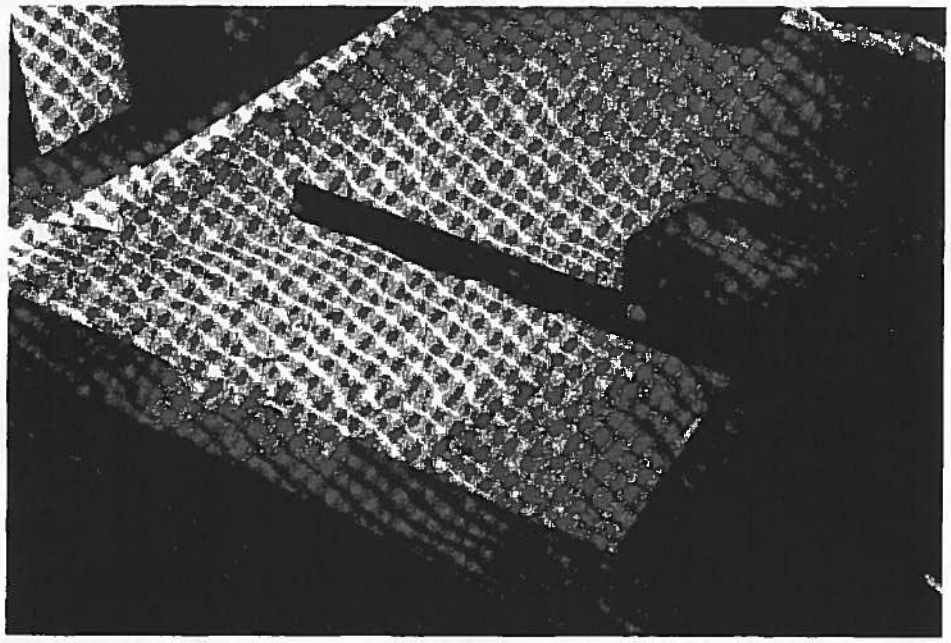

Fig. 7.8 Ruts created in the site T soil sample by 10 consecutive semi-rigid wheel passes on the same lateral location. Remolded layer depth at this stage was about 1.5-2 cm.

ציור מס. 7.8 חריצה שנוצרה במדגם קרקע מאתר T כתוצאה מ־ 10 מעברים עוקבים של גלגל־נע חצי קשיח, באותו מיקום רוחבי. עומק השכבה המופרת באותו שלב ־ 1.5־2.0 סמ.

To summarize, it can be concluded that testing with the site T material was problematic due to the following reasons:

- The inability to provide an air-inflated wheel which can be inflated to higher pressures (more than 2.5 kg/cm$_2$), to be used on the hard unremolded soil. The alternative use of a semi-rigid rubber wheel made it hard to estimate contact pressure and caused vibrations during operation of the testing device.

- The relatively coarse aggregates in the soil mix (up to 3/4", and according to the gradation curve of the site T soil), compared to the small dimensions of both the wheel (especially the semi-rigid one) and the anticipated depth of the remolded layer, hindered the ability to get good observable results. The presence of the coarse aggregates also made it difficult to detect the interface between the remolded and unremolded soil. More than that, it is very probable that the internal angle of friction of the unsieved soil used in the test was much higher than that of the site T soil as tested in the laboratory, due to the contribution of the coarse aggregates.

Two additional moving wheel tests were conducted in site S material, prepared and cured at a dry density of 1700 kg/m$^3$. The first soil sample was subjected to repetitive wheel loading of the 8" air-inflated wheel with 1.5 kg/cm$^2$ inflation pressure and 75 kg. vertical load (yielding about 1.75 kg/cm$^2$ contact pressure and 4.75 cm. load width, as can be seen in Fig. 7.5). Fig 7.9 describes the development of rut depth and remolded layer depth at the middle of the soil sample, as a function of the number of wheel passes (laterally distributed with 6.25 cm. standard deviation). The rut depth increases gradually to about 2 cm. after 300 passes, while the depth of the remolded layer reaches about 4 cm. from the original soil surface. The net depth of the remolded layer was found by deducting the average level of rut depth from the remolded layer depth,. Fig. 7.10 shows the development of the net remolded layer depth as obtained in the moving wheel test and compared to the results of the numerical model (sub-system A, case no. 21) with very similar soil and loading characteristics. At 300 passes the difference between the numeric results and the test results is about 45%. The fluctuations in the net depth of the remolded layer are mainly the result of fluctuations in the remolded soil surface level caused by consecutive wheel passes at different lateral positions.

Fig. 7.11 shows the development of rut and remolded layer depth as recorded during the second test carried out in a site S soil sample. The wheel loading characteristics in this test were the same as in the former test, and the test was conducted up to 200 wheel passes. Comparison with the numerical model (sub-system A results), see Fig. 7.12, gives good

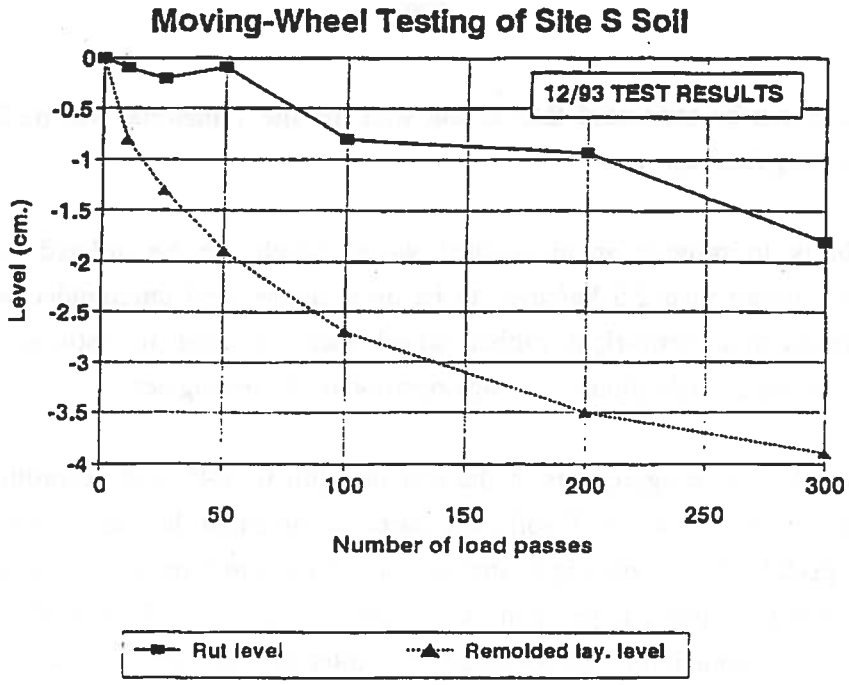


Fig. 7.9 Development of rut depth and remolded layer depth, at the middle of a site S soil sample (12/93 test), during a moving wheel test.

ציור מס. 7.9 התפתחות חריצה ועובי שכבה מופרת במרכז מדגם קרקע מאתר S (נסוי 12.93), תוך מהלך הנסוי.

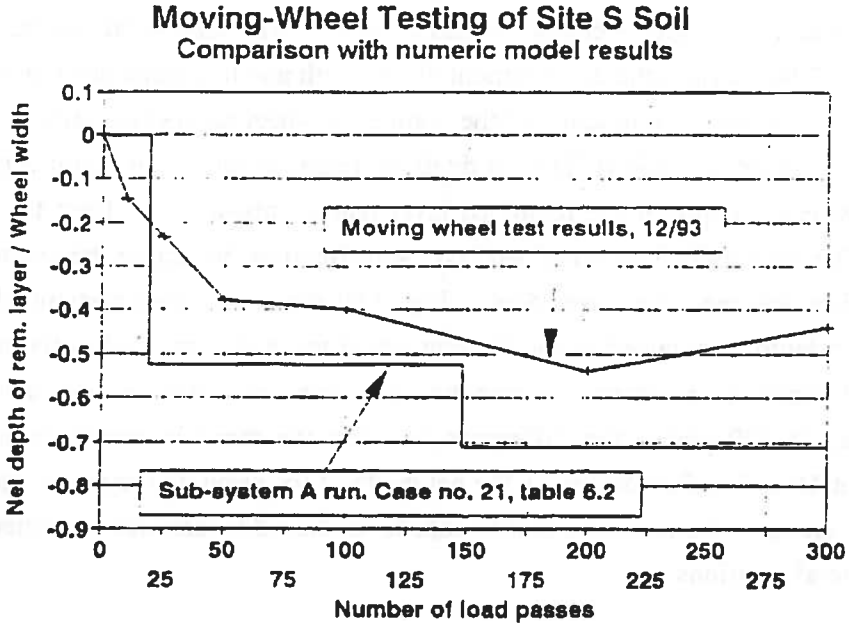


Fig. 7.10 Remolded layer depth values as obtained in a moving wheel test (12/93 test), compared to the results of the numerical system (case no. 21 table 6.2).

ציור מס. 7.10 ערכי עובי שכבה מופרת כפי שהתקבלו בנסוי גלגל נע (נסוי 12.93), בהשוואה לתוצאות המערכת הנומרית (מקרה מס' 21 טבלה 6.2).

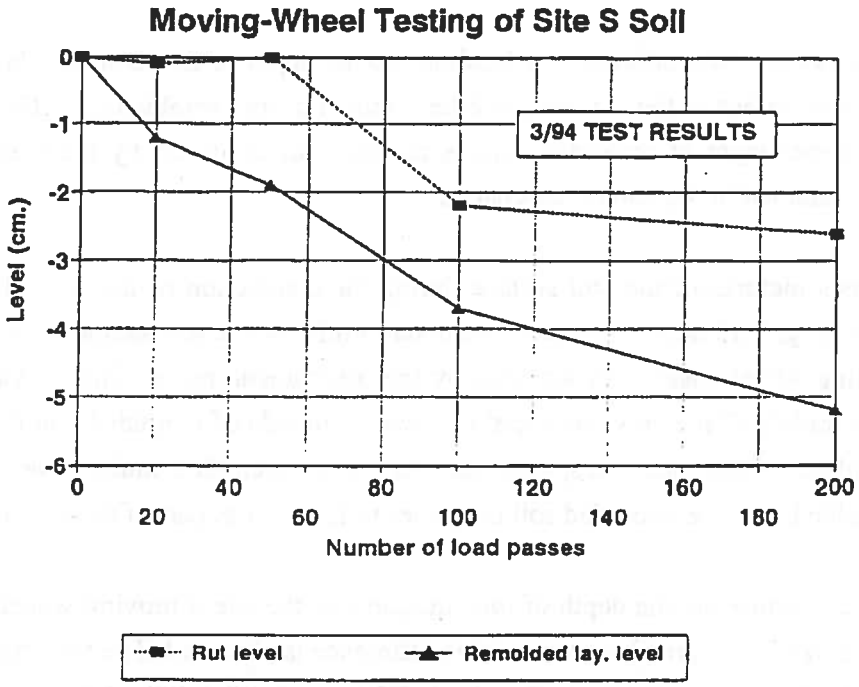


Fig. 7.11 Development of rut depth and remolded layer depth, at the middle of a site S soil sample (3/94 test), during a moving wheel test.

ציור מס. 7.11 התפתחות חריצה ועובי שכבה מופרת במרכז מדגם קרקע מאתר S (נסוי 3.94), תוך מהלך הנסוי.

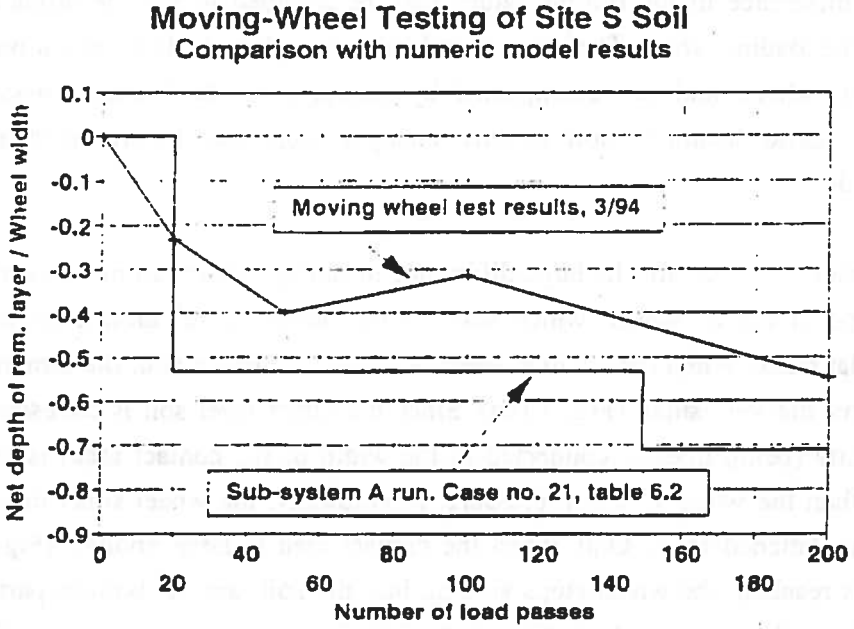


Fig. 7.12 Remolded layer depth values as obtained in a moving wheel test (3/94 test), compared to the results of the numerical system (case no. 21 table 6.2).

ציור מס. 7.12 ערכי עובי שכבה מופרת כפי שהתקבלו בנסוי גלגל נע (נסוי 3.94), בהשוואה לתוצאות המערכת הנומרית (מקרה מס' 21 טבלה 6.2).

accordance (less than 30% difference) regarding the net depth of the remolded layer. Fig. 7.13 presents the surface of the soil sample after removal of the remolded soil. The general shape of the upper layer of remolded soil, is the same as predicted by the mechanistic model and as obtained in the numerical system.

Fig. 7.14 shows pictures of the soil surface during the conduction of the second moving wheel test, and Fig. 7.15 depicts the cross sectional profile of the soil sample as a function of accumulating wheel passes. As foreseen by the mechanistic model, rutting values are highest at the middle of the cross sectional cut, while mounds of remolded soil ("negative ruts") accumulate on both sides. In spite of the fact that its strength is much lower than that of the unremolded soil, the remolded soil continues to function as part of the system.

However, when comparing the depth of ruts measured in the site S moving wheel tests, to those obtained in the numerical system, a large difference is observed. The accumulated rut values at the middle of the sample reach values of 2 to 3 cm. after 200 - 300 wheel passes, a phenomenon which is the direct result of excessive rutting caused by each wheel pass. Static loading of the wheel on the sample, with a remolded layer depth of 3 cm., yielded a rut of 1.1-1.2 cm. Running sub-system B2 of the analytical system with similar soil conditions yielded rut value of less than 1 mm.

Some of the difference in the rutting values may be ascribed to soil densification that occurs under the loading wheel. The upper remolded soil tends to be loosened at both sides of the loading wheel, and be recompacted by subsequent wheel loads passing at a neighbouring lateral location. Soil density changes were not incorporated into the numerical model.

The main reason however, for the large difference in rutting values, seems to be the cross sectional shape of the 8" wheel, which was (in the present case) almost circular with virtually no flat basis. When the loading wheel is lowered onto the soil, the dimensions of the contact area are very small (Fig. 7.16a). Since the upper layer soil is cohesionless, its bearing capacity (being linearly connected to the width of the contact area) is very low, much lower than the wheel inflation pressure. Accordingly, the wheel sinks into the soil without being flattened by it. Only when the contact area is large enough (Fig. 7.16b), equilibrium is reached, the wheel stops sinking into the soil, and its bottom part may be flattened by the soil resistance (depending on the inflation pressure and carcass stiffness).

Some sub-system B2 runs were operated in order to estimate rutting values for wheels having a similar cross section as that of the 8" wheel used during the moving wheel tests.

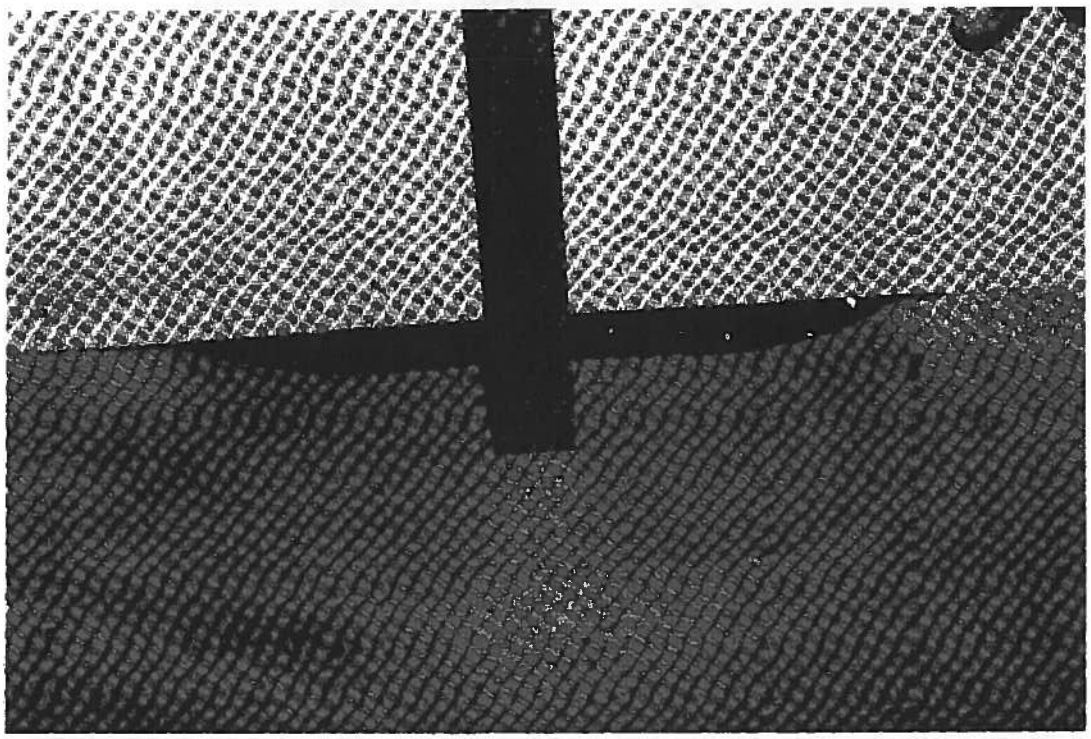

Fig. 7.13 The surface of a site S soil sample, after removal of the remolded layer soil.

ציור מס. 7.13 פני השטח של מדגם קרקע מאתר S , לאחר הסרת השכבה המופרת.

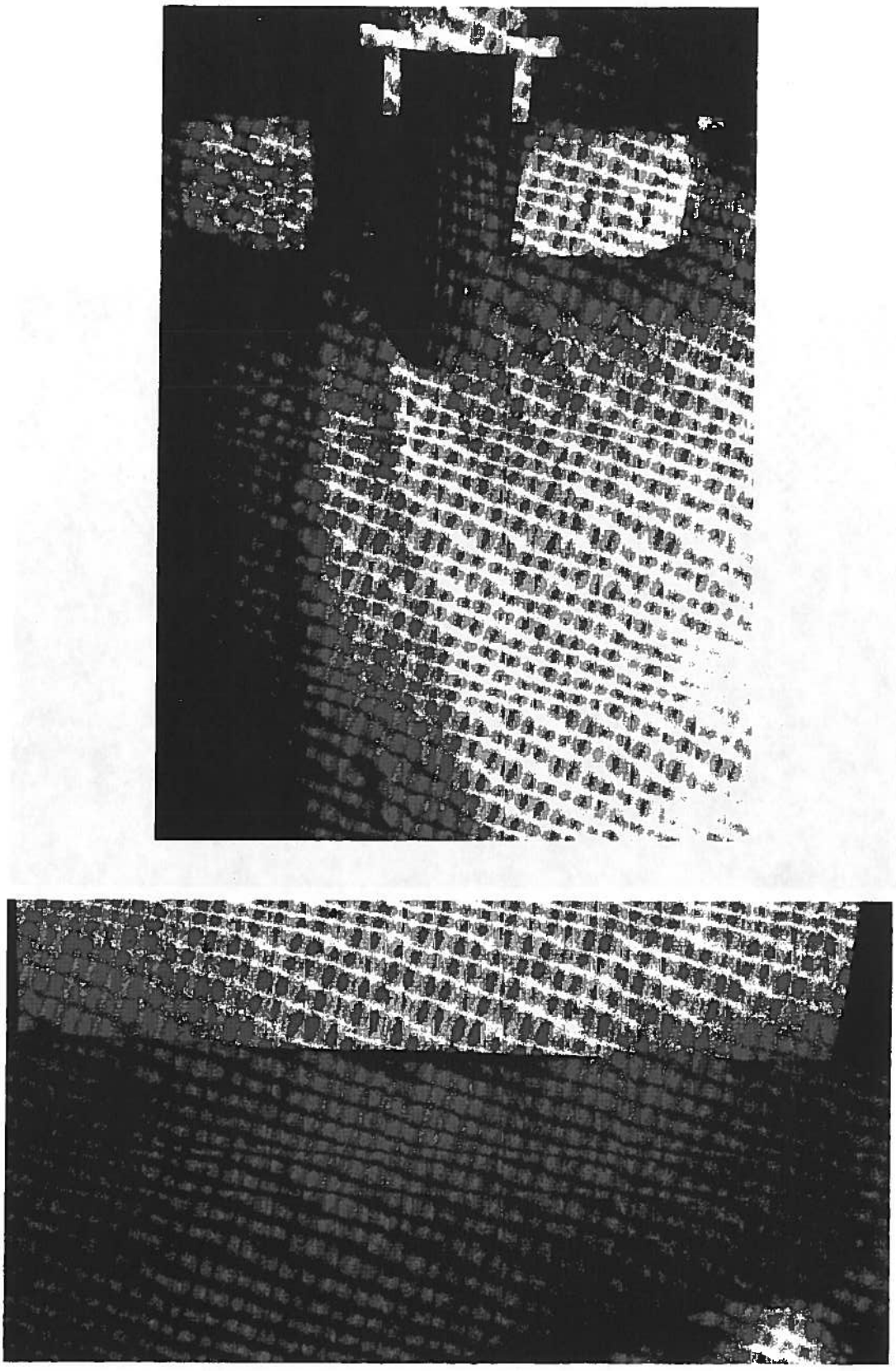

Fig. 7.14 Soil surface of site S soil during the conduction of a moving wheel test

ציור מס. 7.14 פני השטח במדגם קרקע מאתר S תוך מהלך נסוי בגלגל נע.

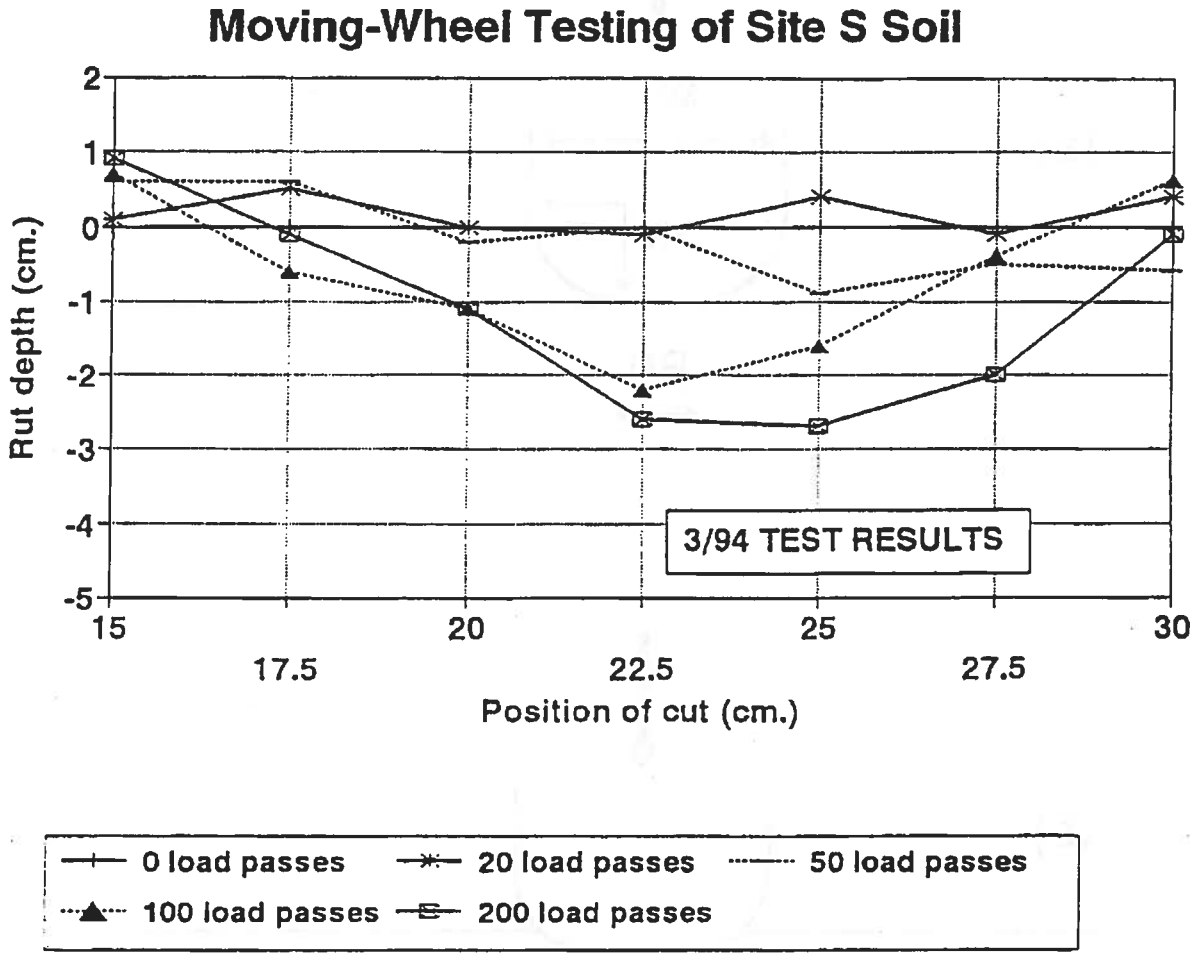


Fig. 7.15 Cross sectional profile of a site S soil sample as a function of accumulated number of wheel passes.

ציור מס. 7.15 התפתחות הפרופיל הרוחבי של מדגם קרקע מאתר S , כפונקציה של מספר מעברי גלגל.

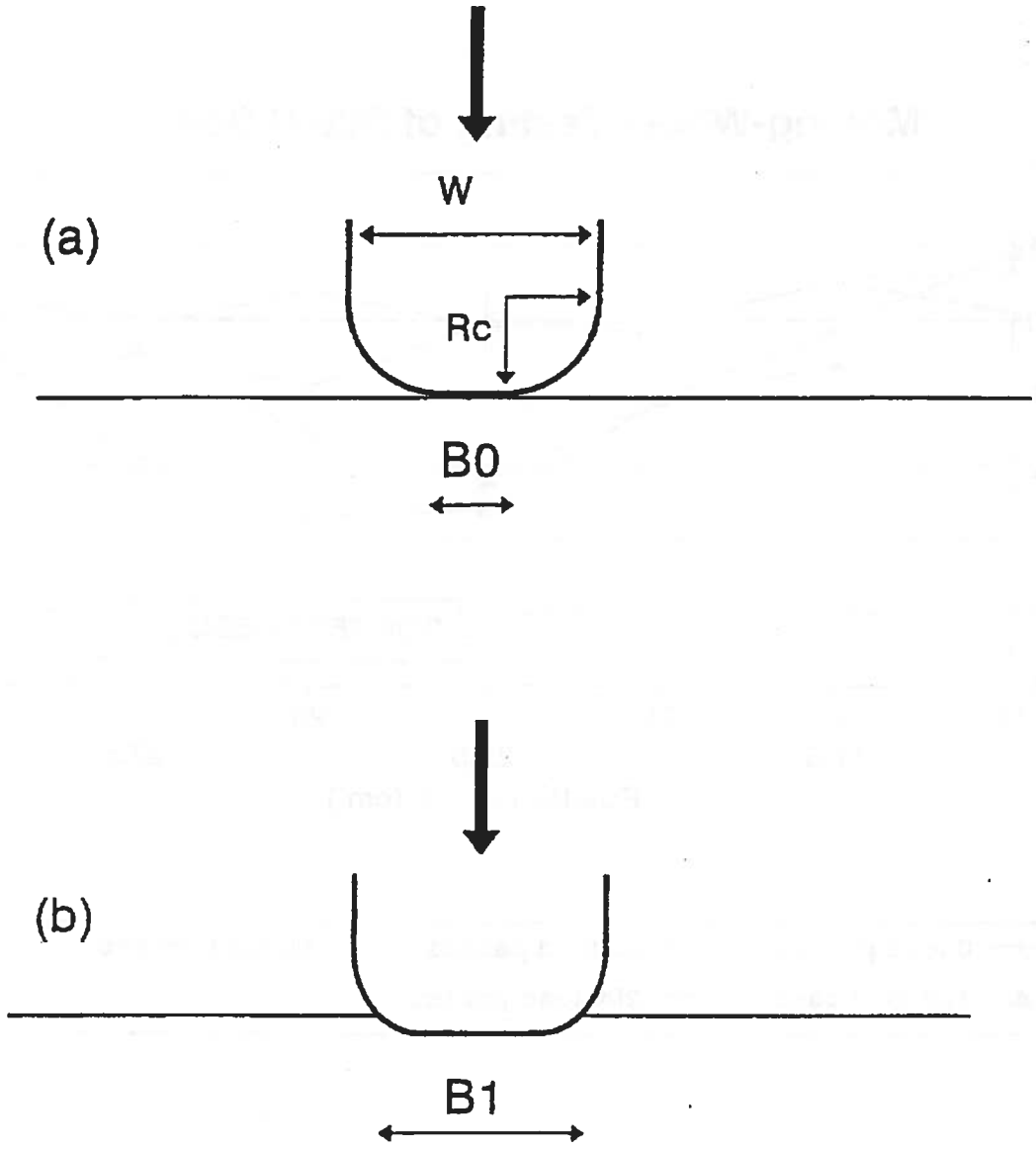


Fig. 7.16 Influence of wheel cross sectional shape on rutting values
(a) First contact between the wheel and the cohesionless soil
(b) Wheel shape after stabilization.

ציור מס. 7.16 השפעת החתך הרוחבי של גלגל על ערכי חריצה
(a) מגע ראשון בין הגלגל לקרקע חסרת הקוהזיה.
(b) צורת הגלגל לאחר התייצבות.

For example, for a circular plate having $R_c$=0.5*W/2 (see Fig. 7.16) the rutting value mounted to about 2 mm. (for W=7.8 cm.). When the angle of friction at the interface was assumed to be 20 deg. (instead of 50 deg. in a perfectly rough interface), the rutting value went up to more than 4 mm. For $R_c$=0.9*W/2, and a perfectly rough interface, rutting estimate made by sub system B2 went up to more than 10 mm. The above emphasizes the need for further investigation on the issue of rutting values, especially if the accumulated rutting approach is to be adopted for runway performance prediction.

## 7.7 Summary of the moving wheel tests

The main goal of the moving wheel testing program, was to provide basic validation to the mechanistic model and the analytical system that was based on it. In order to be able to simulate the laterally distributed aircraft operation on the runway, a new loading wheel device was designed and built. This device, is a pneumatically operated apparatus, where the lateral location of the wheel on the soil sample can be changed from one load cycle to the next. In addition, the new device provides means to easily change the total load on the wheel, as well as the ability to monitor the total vertical and horizontal forces acting on the wheel-soil interface. The type of soils used in the research required the adoption of meticulous procedures of sample preparation and curing, in order to simulate as closely as possible natural processes occurring in the field.

Two types of soils (the same soils that were studied in the laboratory phase), were tested in the new loading wheel device. Operating the analytical model using the soil properties allowed subsequent comparison with the results of the moving wheel tests. The tests provided qualitative validation of the mechanistic model and analytical system, in the following main subjects:

- The repetitive loading of a dry granular remoldable soil under laterally distributed loading wheel, causes the creation of a two-layer structure in the soil, where the upper layer soil is remolded.

- The depth of the upper remolded layer gradually grows with accumulating number of wheel loads. For higher values of load cycles, the rate of growth of the remolded layer depth decreases, toward stabilization of its depth.

- The remolded layer, though its strength may be much lower than that of the unremolded soil, goes on functioning as part of the soil structure under ongoing wheel

loads. The existence of this layer of soil has to be accounted for in the system analysis, and thus must not be overlooked.

- The cross-sectional profile of the soil surface, created during "runway" operation, is as predicted by the mechanistic model and the analytical system. Rutting values are highest in the middle of the cross sectional cut, while mounds of remolded soil gradually accumulate on both sides of the loaded strip. The estimation of the cross sectional profile of the runway is important for the calculation of the accumulated rutting which develops during runway operation.

Activation of sub-system A of the analytical model was performed with the same soil properties and loading conditions as used in the moving wheel tests. Comparisons made between the analytical and the tests results showed reasonable quantitative accordance. Rutting values however, as recorded during the tests, were found to be much higher than those predicted by the analytical system. The main reason for the high rutting values seems to be the cross section of the loading wheel that was used, which was almost circular with virtually no flat basis.

It should be remembered however, that the number of tests that were conducted was very limited. Quantitative verification and tuning of the analytical model, including all its sub-systems, requires an extensive moving wheel testing program. In future research, it is also recommended to consider the use of artificial cementing agents to simulate the natural cementation developing in soils. This will enable to avoid the cumbersome and lengthy preparation and curing procedures that were used, with better assurance as to the homogeneity of the properties within the soil samples.

# CHAPTER 8: SUMMARY, CONCLUSIONS AND RECOMMENDATIONS FOR FUTURE RESEARCH

## 8.1 Summary of the research objectives and methodologies

### 8.1.1 Research objectives

The existing methods for the prediction of unsurfaced runway performance are limited in accounting for the strength changes ensuing in soils which tend to be remolded under wheel loading. The principal aim of the research was to develop and present a mechanistic model that describes the behavior of remoldable soils under repetitive wheel loading. The study was confined to dry granular soils which exhibit some degree of natural cementation in their initial state. The main goal of the research was divided to the following objectives:

A. To investigate the behavior of dry granular soils which exhibit natural cementation;

B. To develop a mechanistic model and make use of different analytical tools in order to describe the process of soil remolding under repetitive wheel loading;

C. To provide qualitative experimental verification of the processes transpiring in the soil according to the mechanistic model;

D. To indicate means by which the suggested model can be implemented to improve the reliability of the performance prediction methods for unsurfaced runways.

### 8.1.2 Main findings of the literature survey

The most important points of the literature survey which were significant for the development of the mechanistic model and its implementation, are:

a. The behavior of remoldable soils under shear is usually predominantly elastic and quite rigid in the pre-peak zone, and the plastic strains are small. This behavior is very clear in dry granular soils which contain some degree of cementation, and in cohesive soils in which the additional strength is due to chemical bonding of the clay particles. After the soil reaches its peak strength (at low strain values) there is a rapid decrease in the soil strength toward the remolded strength of the soil. The above phenomenon is especially salient when the shearing process occurs under low confining pressures as in the case of unsurfaced runways;.

b. The stresses exerted on the soil by the moving wheel are high and frequently approach the peak strength of the soil. Existing empirical relations, describing the development of plastic strains with the number of loadings, claim to be valid only for low stress levels (up to about 40% of the peak strength). Therefore, it is questionable whether those relations can be utilized for the solution of the problem that is the concern of the present research;

c. Because of the relatively rigid structure of the unremolded soil, it seems that for the problem at hand, deformations and hence rutting of the soil, are mainly due to post peak deformations in the already remolded soil. Plastic strains in the unremolded soil are relatively negligible;

d. Remolding of a soil element may be caused by cyclic loading of the soil at levels that are lower than the peak strength of the unremolded soil. In these cases, special fatigue functions may be built which relate the stress level in the soil to the number of load applications until failure;

e. In unsaturated soils, density changes will usually transpire in the sheared soil. The soil density after shear is a function of the type of soil and the confinement pressure of the soil during the shear process:

f. In granular soils exhibiting cementation, it was found that the additional strength of the unremolded soil is mainly cohesive in nature. Destruction of the additional strength through the remolding of the soil led to the disappearance of the cohesive part of strength, while the frictional part, remained practically constant.

g. Observations carried out at a landing site where the soil was a potentially remoldable granular soil, indicated that the rutting process was carried out through the remolding of the upper part of the soil, and the loss of the cementational element of the soil. Beneath the loose upper layer, the soil retained its original strength;

h. The passage of a moving wheel over the soil creates a stress path of special character that includes changes in the direction of the principal stresses. In order to obtain a reliable prediction of soil behavior through laboratory tests, it is recommended to simulate this stress path as closely as possible;

i. Most of the references dealing with the prediction of aircraft performance over

unsurfaced runways do not consider the issue of soil strength change during operation. No model was found to describe the development of soil strength change, under the cyclic loading of a moving wheel;

j. The numerical analyses of the wheel-soil system reported in the literature are, in most cases, two-dimensional analyses. This approach is mainly a consequence of calculational constraints. The wheel-soil system is an extremely complex one and a 3-D description of the problem requires calculational resources that are usually unavailable.

8.1.3 Essentials of the proposed mechanistic model

The presented mechanistic model developed in the research, attempts to describe the behavior of soils subjected to remolding under repeated wheel loading. The model concentrates mainly on dry and brittle soil types, which change their strength properties during shear. The essence of the model is the gradual formation of a layered soil structure, where the upper layer comprises remolded soil whose strength is often significantly lower than that of the underlying unremolded soil.

The proposed model is based on the following principles:

1. The repeated wheel movement on the dry cohesive soil leads to remolding and a decrease in the strength of the original soil. The remolding process at any place in the soil is a consequence of either loading the soil element to the point of shear strength, or as a cause of fatigue processes in the soil;

2. The brittle character of the soils under consideration makes it possible to assume elastic-plastic constitutive behavior, where at the point of shear failure there is a very swift decrease in the soil's strength to its residual strength;

3. Due to the lateral wander of the repeated passes of aircraft wheels the system created can be viewed as a two-layer system, wherein the upper soil layer is remolded. The remolded soil is expected to continue functioning under the aircraft traffic;

4. The thickness of the remolded soil layer is a function of several factors, such as the soil strength characteristics before and after remolding, contact pressure and total load, loading wheel dimensions, etc.. The thickness of the remolded soil layer increases with the accumulated loading cycles, and usually stabilizes on a certain asymptotic value. The stabilization of the remolded layer thickness is the result of the

"isolation" effect and the protection provided by the upper layer (be it in the plastic state) as a consequence of the distribution of stresses with depth;

5. The structure obtained, particularly in the types of soil under consideration, is such that the upper soil layer may be close to or within a state of "plastic flow" during the loading of the wheel, whereas the lower layer is mainly in elastic state. Repeated passes of the wheel in various lanes within the range of the lateral wander of movement, cause the remolded soil to "flow" from side to side according to the point of loading. The surface of the soil along the width of the traffic lane is full of longitudinal ruts which change their location from one wheel loading to the next;

The results of the numerical system which was created on the basis of the mechanistic model describe the formation and functioning of the two-layer soil system under repetitive wheel loading. Another step which was taken in the present work was to recommend ways in which the results of the mechanistic model can be implemented in order to improve the ability of design methods to predict the performance of unsurfaced runways built in remoldable soils. Two main approaches are presented:

A. The accumulated rutting approach - attempts to estimate the process of rut accumulation during runway operation, up to the point where the rut depth is more than acceptable according to rutting criteria;

B. The accumulated damage approach - tries to assess the incremental damage caused to the runway by each additional pass of aircraft (over the runway whose strength is not constant), and accumulate it up to the runway failure. This approach is more simplistic and its implementation makes use of existing design nomograms.

### 8.1.4 Phases of the research

The research plan, built on the basis of the above described mechanistic model, comprised three main phases (see Fig. 8.1):

1. A series of laboratory tests aimed to investigate the behavior of soils, and to compare it to the presuppositions of the mechanistic model. Two types of dry granular soils

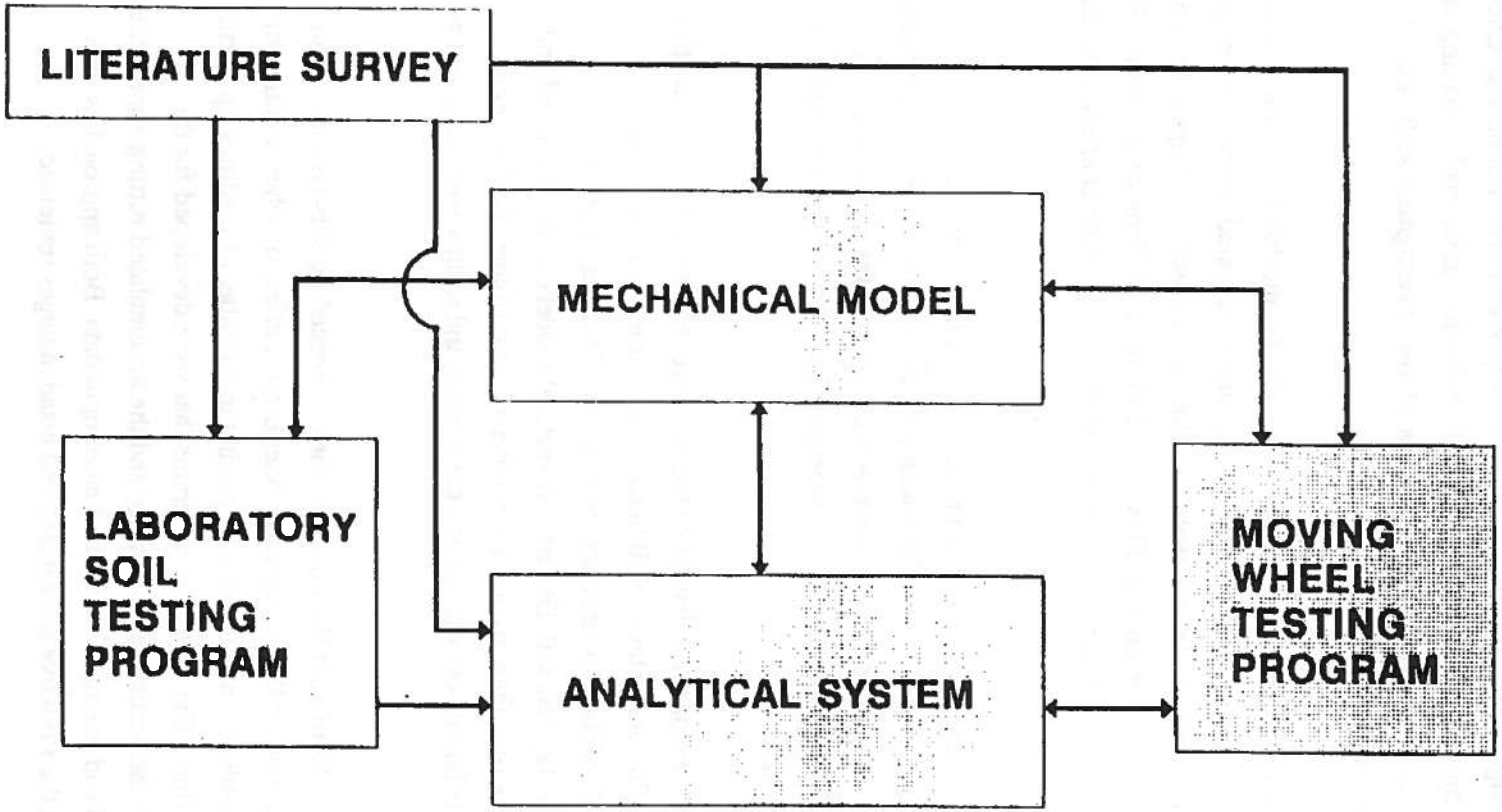


Fig. 8.1 The different research phases and their interconections

ציור מס' 8.1 חלקי המחקר העקריים והקשרים ביניהם

that contain some degree of cementation in their natural state were studied during the research. Various indicative and shear tests were conducted, in order to explore the properties and strength characteristics of the soils before and after remolding. Cyclic shear tests were conducted in order to study soil behavior under cyclic loading at a relatively high level of stresses. The properties of the investigated soils were later used for the operation of the analytical system.

2. The construction of a numerical system based on the mechanistic model, which describes the behavior of the remoldable soil, under repeated wheel movements within a specified range of lateral wander. The system was developed by using different numerical tools including FLAC, a 2-D finite difference software. The analytical system was composed of three sub-systems, logically connected to each other:

   - Sub-system A - Describes the development of a two-layer structure in the remoldable soil, caused by repetitive loading of the soil surface. Being the main part of the numerical model, sub system A was operated for a variety of soil properties and loading conditions, to investigate its behavior and sensitivity to various conditions.

   - Sub-system B - Finds the behavior of the two-layer soil structure as a function of the depth of the upper layer. Soil behavior is defined in terms of the equivalent CBR of the soil structure, or in terms of rutting values caused by loading the two-layered soil. Different numerical models were developed and operated for the two alternatives of soil behavior descriptors. Both models were run for different soil and loading conditions, and results were analyzed and discussed.

   - Sub-system C - Combines the results of the two preceding sub-systems, in an attempt to account for the incremental deteriorative effect of wheel loading on the runway condition, and to use it to predict the number of loadings up to runway functional failure. The computer programs that were developed for the application of the accumulated damage and the accumulated rutting approaches, are presented and exemplified for real case input data. Both approaches were analyzed and their relative advantages and disadvantages reviewed.

3. Conducting moving-wheel experiments for the purpose of qualitative validation and

verification of the mechanistic model and providing a means for feedback and tuning of the analytical system. In order to carry out these experiments, a new laboratory loading-wheel apparatus was built, which makes it possible to carry out wheel loading while changing the lateral location of the wheel along the width of the sample, thus emulating actual loading conditions as they occur in the field. Complex procedures for sample preparation and curing had to be adopted in order to allow the soil to attain cohesive strength during the drying process. Two types of soil ere used for the conduction of the moving wheel tests. Test results were analyzed versus the assumptions of the mechanistic model. Comparison was made between test results and the results of sub system A of the analytical system, as obtained for the same soil and loading conditions.

## 8.2 Research findings and conclusions

The operation of the analytical and laboratory testing systems within the framework of the research, may be summarized by the following main points:

A. Dry granular soils, which exhibit some degree of cementation in their natural state, tend to be remolded under the action of wheel loading. It was shown numerically, that the remolding action of elements in the soil transpires (not counting fatigue action) under loads which are much less than the bearing capacity of the unremolded soil. The nuclei of remolded elements cause a relatively fast remolding of neighboring elements. The results of the laboratory shear tests verified the assumption that the remolding action is characterized by the nullification of cohesive part of soil strength. At the same time, no significant change was noticed in the frictional part of strength, assuming no change takes place in the soil density;

B. The constitutive behavior of the naturally cemented soil before remolding, was verified during the laboratory tests, to be predominantly linear-elastic. Plastic strains in the pre-peak zone are negligible, and the soil elastic modulii are much higher than their value after remolding. Once a soil element reaches its strength envelope (according to Mohr-Coulomb failure criterion), there is a fast decrease in the soil strength toward the residual (remolded) strength. These points substantiate the validity of the assumed constitutive behavior of the unremolded soil, as presented in the mechanistic model .

C. Remolding may also be the result of fatigue in a soil element, induced by repetitive

loading of the element to high values of relative stress. This phenomenon was observed during the laboratory cyclic testing of the soils studied in the research. The number of loading cycles needed to cause sample failure, depend upon the stress level exerted on the sample and may be described by a semi-logarithmic fatigue function. Fatigue parameters were used as input for the operation of the numerical system, and the Miner law used for the accumulation of damage in each soil element.

D. The repetitive loading of a dry granular remoldable soil under laterally distributed loading wheel, causes the creation of a two-layer structure in the soil, where the upper layer soil is remolded. The depth of the upper remolded layer grows at a rate which depends on the properties of the soil (remolded and unremolded) and on loading characteristics. Most of the computer runs of the numerical system showed a stabilization of the upper layer depth after a certain amount of load cycles. This phenomenon predicted by the mechanistic model was also observed during the laboratory moving-wheel tests;

E. The remolded layer, though its strength may be much lower than that of the unremolded soil, goes on being part of the soil structure under ongoing wheel loads. Due to the lateral wander of consecutive wheel loads, the upper layer of remolded soil "flows" from side to side but continues to function in the system. The stabilization in the depth of the upper layer may be ascribed to the stress "isolation" supplied to the unremolded soil by the overlaying remolded layer. The above phenomenon was observed both in the numerical system and during the moving wheel tests. The existence of the upper layer of soil has to be taken into consideration during system analysis, and must not be overlooked.

F. The presupposition of the mechanistic model of the cross-sectional profile of the soil surface as created during runway operation, was verified by the moving wheel test results and by the analytical system. Rutting values are highest at the middle of the cross sectional cut, while mounds of remolded soil gradually accumulate on both sides of the loaded strip. The estimation of the cross sectional profile of the runway is important for the calculation of the accumulated rutting which develops during runway operation.

G. Two approaches for the accumulation of incremental deteriorative effect in the runway, were presented and elaborated. The accumulated damage approach which is integrated into existing design methods, is more simplistic and easy to implement. The accumulated rutting approach, on the other hand, solves the problem by treating

directly the accumulation of ruts, which are the principal cause for the runway functional failure. One of the main advantages of the accumulated rutting approach is that it does not inherit the problems of the existing design methods. In the long run it seems that the accumulated rutting approach is the path that should be proceeded. It should be remembered however, that its implementation requires relatively high precision in the numerical estimations of rutting. This task can only be achieved by more accurate modeling of the wheel-soil interface and the constitutive laws of the soil and requires an extensive validation and tuning process.

To summarize, the different research phases were built so as to achieve the main goal of this work, meaning the development of a new model for the description of remoldable soil behavior under repetitive wheel loading. The laboratory soil testing program verified some of the pressupositions regarding the soil constitutive behavior (objective A in section 8.1.1), and provided input for the operation of the analytical system. The analytical system that was developed, gave validation to the mechanistic model, in addition to the quantification of the assumed processes that happen in the soil (objective B). The moving wheel tests conducted in the laboratory, gave qualitative experimental verification of the mechanistic model, including some quantitative comparisions with the analytical system results (objective C). The last part of the analytical system indicated on two alternative ways by which the knowledge about the created soil structure may be utilized for better performance prediction of aircraft operation on remoldable soils (objective D in section 8.1.1).

## 8.3 Recommendations for future research

Based on the findings of the research and the conclusions drawn from the performance of the numerical and laboratory work, some recommendations for future research can be made::

A. Changing the numerical model to a 3D model. With the decrease in the cost of computing resources, it seems that a three dimensional modeling of the problem will be possible in relatively a short time. However, it must be remembered that such a numerical scheme will require resources which are at least 2 orders of magnitude greater than presently required. The above will permit simulation of the wheel-soil problem in a much more reliable way and include other issues such as the problem of wheel braking. According to Itasca, the manufacturers of FLAC, a 3D version of FLAC will be available at 1995.

B. Investigating dynamic aspects of the interaction between the wheel and the soil. This issue is very complex and includes the soil reaction to dynamic forces of moving aircraft, the dynamic properties of the aircraft landing gear, etc. The latest version of FLAC already includes a module for the solution of dynamic problems;

C. Conducting quantitative verification and tuning of the model by use of granular soils with artificially added cementation. The addition of Portland cement or gypsum in small quantities may provide a good simulation of naturally cemented soils, thus avoiding a problematic and lengthy process of preparation and curing of the soil samples;

D. Widening the scope of the model to include other types of remoldable soils. Some kinds of soils, mostly clayey, undergo a slower remolding action than that observed in the present work. In such cases, the change of soil properties with depth might be expected to be more gradual and continuous;

E. Continuing research work directed toward refinement and improvement of the suggested analytical system. Refinement of the numerical model mesh will enable better description of the wheel-soil interface and more accurate results. Following the accumulated rutting approach, further investigation and development is needed in defining the characteristics of the wheel-soil interaction, including wheel geometry, interface properties atc.

F. Carrying out an extensive moving-wheel testing program, preferably in larger scale simulative systems, intended for the quantitative verification and tuning of the presented model. This program should be conducted in more than one type of remoldable soil, and investigate the influence of different soil and wheel parameters on the behavior of the system. The experiments should be broadened to verification of the entire analytical system the investigation of the whole process, including rut creation and checking the number of wheel passes up to the violation of certain rutting criteria.

## Appendix A

# LISTINGS OF COMPUTER PROGRAMS

Contents:

## A1 - Listing of sub-system A program (written in Flac internal language)

The program finds the relationship between the number of loadings to the depth of the remolded layer.

```
;Filename - t504_3_3
; Initial internal angle of friction  - fric0=50 deg.
; Remolded internal angle of friction - fric1=40 deg.
; Initial cohesion - coh0=0.3 kg/cm2
; Cohesion in remolded state -  coh1=0.01 kg/cm2
; Width of wheel  - 5 cm.
; Contact pressure - 3 kg/cm2
; Fatigue parameters  C1=35 , C2=35
;
new
config extra=6
; ex_1,ex_2,ex_3 - last 3 sampling results of highest stressing ratio
; ex_4          - cummulative fatigue damage to element
; ex_5          - number of loads on surface point
; ex_6          - indicates highest(filtered) stressing ratio of
;                 elemment during each load process
set vga
set log on
;*****************
def dimens
 aai=50
 aaj=30
 len1=0.0125*aai    ; length of model
 dept1=-0.35        ; depth of model
 half_len=int(aai/2)
 half_len1=half_len+1
end
;***********************
set ste=3000 small clock = 100 fo 50
dimens
grid aai aaj
gen 0,dept1 0,0 len1,0 len1,dept1 rat 1 0.98
call c:\flac32\fish\mohr_fat.fis
model mohr_fat
;model mohr_fat acts similarly to the mohr model in addition to fatigue
; considerations introduced to the model
title
Normally Distributed Repetitive Loading of Remoldable Soil
;*********************************************
;function which finds depth of remolded layer
def low_coh
float low_coh
 low_coh=0.5*(y(half_len,jgp)+y(half_len1,jgp))
 loop qq(1,jzones)
  if m_coh(half_len,qq)<1000.0 then
   low_coh=0.5*(y(half_len,qq)+y(half_len1,qq))
   exit
  end_if
 end_loop
end
;*************************************************
def fatparam
```

```
float ac1 ac2
;ac1,ac2 - fatigue parameters (to be chequed by cyclic testing)
ac1=35.0
ac2=35.0
end
;*********************************************************
def fatigue0
; finds stress level at each element during the loading process
float dw1 dw2
loop ii(1,izones)
 loop jj(1,jzones)
  ;remold - indicates whether soil element is remolded. remold =1 - soil remolded
  if remold(ii,jj)=0.0 then
   ; max_str - max ratio of stressing (to max possible stressing) in zone
   dw1=max(ex_1(ii,jj),ex_2(ii,jj))
   dw2=max(ex_3(ii,jj),max_str(ii,jj))
   ; second highest str ratio in last four sampling is chosen
   dw2=min(dw1,dw2)
   ;ex_1,ex_2,ex_3 -last 3 sampling ratio of stressing
   ex_1(ii,jj)=ex_2(ii,jj)
   ex_2(ii,jj)=ex_3(ii,jj)
   ex_3(ii,jj)=max_str(ii,jj)
   ; stress condition after some filtering of numerical instabilities
   if dw2>ex_6(ii,jj) then
    ex_6(ii,jj)=dw2
   end_if
  end_if
 end_loop
end_loop
end

;*************************************************************
def fatigue1
float logn rd coh1 red_bulk red_shear
loop ii(1,izones)
 loop jj(1,jzones)
  :remold -indicates whether soil element is remolded. remold=1 -soil remolded
  if remold(ii,jj)#1.0 then
  :equation of fatigue
  logn=(ac1-ac2*ex_6(ii,jj))*2.3025
  :rd - relative damage to soil according to miner's law
  rd=1.0/exp(logn)
  ;ex_4 - cumulative damage to soil element
  ex_4(ii,jj)=ex_4(ii,jj)+rd
  :change soil properties if remolding occures
  if ex_4(ii,jj)>=1.0  then
   if ex_6(ii,jj)=1.0 then
; keeps track of elements remolded by fatigue
    ex_4(ii,jj)=ex_4(ii,jj)+10
   end_if
   remold(ii,jj)=1.0
   m_coh(ii,jj)=coh1
   m_k(ii,jj)=red_bulk*m_k(ii,jj)
   m_g(ii,jj)=red_shear*m_g(ii,jj)
  end_if
  ;nullifying ex_6 which contains max stressing of point during cycle
  ;nullify ex_1,ex_2,ex_3 - before next loading
  ex_6(ii,jj)=0.0
```

```
    ex_1(ii,jj)=0.0
    ex_2(ii,jj)=0.0
    ex_3(ii,jj)=0.0
    end_if
   end_loop
  end_loop
 end
 ;*****************************************
 ;initializes ex_n to zero
 def zer1
  loop dini(1,igp)
   ex_5(dini,jgp)=0.0
   if dini<igp then
    loop dinj(1,jzones)
     ex_1(dini,dinj)=0.0
     ex_2(dini,dinj)=0.0
     ex_3(dini,dinj)=0.0
     ex_4(dini,dinj)=0.0001
     ex_5(dini,dinj)=0.0
     ex_6(dini,dinj)=0.0
    end_loop
   end_if
  end_loop
  m_k(1,aaj)=red_bulk*m_k(1,aaj) ;change properties of corner elemnt for step
                      :  length reasons
  m_g(1,aaj)=red_shear*m_g(1,aaj)
 end
 ;*************************************
 def superstep
  loop ns(1,n_steps)
   left_stress=left_stress+stress_inc
   command
    apply syy=left_stress i=dd1,dd2 j =jjj
    step 10
   end_command
  end_loop
 end

 ;*****************************************

 ;main procedure.
 def rand2
  loop ff(1,500)
   fff=ff
   ;derivation of new wheel loading place
   rd1=grand
   dd0=half_len+int(rd1*5+sgn(rd1)*0.5)    ;center of normally dist. loading
   dd2=dd0+2
   dd1=dd0-2
   if abs(int(rd1*5+sgn(rd1)*0.5))>int(half_len-5) then
    exit
   end_if
   loop ddd(dd1,dd2)
    ;ex_5 - stores the number of load applications to the surface grid point
    ex_5(ddd,jjj)=ex_5(ddd,jjj)+1
   end_loop
   left_stress=0.0
   stress_inc=load1/n_steps  ;increases load gradualy
```

```
 superstep
 command
  set echo on
  set message on
  print fff
  set echo off
  set message off
 end_command
  loop while unbal>50
   command
    step 10
    fatigue0
   end_command
  end_loop
  ;fatigue1 is run after comletion of wheel loading and unloading.
  left_stress=load1
  stress_inc=-load1/n_steps  ;increases load gradualy
  superstep
  command
   solve
  end_command
  fatigue1
 fff1=fff/20
 if fff1*20=fff then
  command
  save c:\flac32\rafi\t50_3_3t.sav
  end_command
 end_if
end_loop
end
;*************************************************
def stam    :allows setting values to variables
float load1 coh0 coh1 fric0 fric1 red_bulk red_shear
int iii jjj
load1=0.0
iii=igp
jjj=jgp
coh0=0.0
coh1=0.0
fric0=0.0
fric1=0.0
red_bulk=0.0
red_shear=0.0
end
;*************************************************
opt stam fatparam fatigue1 zer1  fatigue0
stam
fix x i=1
pri iii
fix x i=iii
fix x y j=1
;********** MAIN AREA OF INPUT DATA
set coh0=30000.0 coh1=1000.0 fric0=50.0 fric1=40.0
set load1=-300000.0 n_steps=4  red_bulk=0.5 red_shear=0.5
prop den=1700  m_k=1.66e8 m_g=0.35e8  ;E=1e8 mu=0.4
;************************************
prop m_coh=coh0  m_dil=0  m_fric=fric0  m_ten=1e10 remold=0.0
init syy=0.0
```

```
init sxx=0.0
set gravity=9.81
solve                    ********************************
his n=1000 low_coh
his fff
his ydisp i half_len j jjj
his xdisp i half_len j jjj
zer1
fatparam
rand2
save c:\flac32\rafi\t50_3_3.sav
return
```

## A1 - Modified code of Flac's Mohr-Coulomb model, to account for fatigue.

(places of change are marked with ***)

```
;FISH version of standard Mohr-Coulomb model
set echo off
def mohr_fat
 constitutive_model
 f_prop  m_g m_k m_coh m_fric m_dil m_ind m_ten m_csnp
 f_prop  m_nphi m_npsi m_tenmn m_e1 m_e2 m_x1 m_sh2
 f_prop max_str remold ;max stressing ratio needed for fatigue calculations
                 ; remold=0 - soil is not remolded
 float $sphi $spsi $s11i $s22i $s12i $s33i $sdif $s0 $rad $s1 $s2 $s3
 float $si $sii $psdif $fs $alams $cs2 $si2 $dc2 $ds2 $ttol $dss
 float $apex $apsav
 float ax1 ay1 at1 ab1 ab2 r1 rf sr4 sr  ;variables needed for fatigue calcul
 float st_m1 st_m2  ;variables needed for fatigue calcul
 int   $icase $apex_flag $m_err

 Case_of  mode
; ------------------
; Initialisation section
; ----------------------
  Case 1
   $ttol = 1.00001
   $m_err = 0
   if m_fric > 89.0 then       ;checks value of param
    $m_err = 1
   end_if
   if abs(m_dil)  > 89.0 then
    $m_err = 2
   end_if
   if m_coh  < 0.0 then
    $m_err = 3
   end_if
   $sphi   = sin (m_fric * degrad)
   $spsi   = sin (m_dil * degrad)
   m_nphi  = (1.0 + $sphi) / (1.0 - $sphi)
   m_npsi  = (1.0 + $spsi) / (1.0 - $spsi)
   m_csnp  = 2.0 * m_coh * sqrt(m_nphi)
   m_e1    = m_k + 4.0 * m_g / 3.0
   m_e2    = m_k - 2.0 * m_g / 3.0
```

```
      m_x1   = m_e1 - m_e2*m_npsi + m_e1*m_npsi*m_nphi - m_e2*m_nphi
      m_sh2  = 2.0 * m_g
      if tenflg # 0 then
        if m_fric = 0.0 then
         m_tenmn = min(1.0e20,m_ten*$ttol)
        else
         m_tenmn = min(m_ten*$ttol,m_coh/tan(m_fric*degrad))
        end_if
      else
        m_tenmn = 1.0e20
      end_if
      if abs(m_x1) < 1e-6 * (abs(m_e1) + abs(m_e2)) then
       $m_err = 4
      end_if
      if $m_err # 0 then
       nerr  = 126
       error = 1
      end_if
    Case 2
; ------------
; Running section
; ------------
;change 2/94
;st_m1=0.0
;st_m2=0.0
;st_m3=0.0
      zvisc = 1.0
      $apex_flag = 0
      if m_ind # 0.0 then
       m_ind = 2.0
      end_if
;--- get new trial stresses from old. assuming elastic increments ---
      $s11i = zs11 + (zde22 + zde33) * m_e2 + zde11 * m_e1  ;sxx
      $s22i = zs22 + (zde11 + zde33) * m_e2 + zde22 * m_e1  ;syy
      $s12i = zs12 + zde12 * m_sh2                          ;sxy
      $s33i = zs33 + (zde11 + zde22) * m_e2 + zde33 * m_e1  ;szz
      $sdif = $s11i - $s22i                                 ;stress differ
      $s0   = 0.5 * ($s11i + $s22i)        ;location of mohr circle center
      $rad  = 0.5 * sqrt ($sdif*$sdif + 4.0 * $s12i*$s12i)  ;radius of mohr
;--- principal stresses ---   ;can still be changed according to sig 2 value
      $si   = $s0 - $rad    ;major principal stress (compression is negative)
      $sii  = $s0 + $rad    ;minor principal stress
      $psdif =  $si - $sii    ; twice radius value
;--- determine case ---
      section
       if $s33i > $sii then
;--- s33 is minor p.s. ---
        $icase = 3             ;indicates szz is minor principal stress
        $s1    = $si
        $s2    = $sii
        $s3    = $s33i
        exit section
       end_if
       if $s33i < $si then
;--- s33 is major p.s. ---
        $icase = 2             ;indicates szz is major principal stress
        $s1    = $s33i ;$s1 - major principal stress (compression is negative)
        $s2    = $si   ;$s2 - intermediate principal stress
```

```
      $s3   = $sii  ;$s3 - minor principal stress
      exit section
     end_if
;--- s33 is intermediate ---
     $icase = 1          ;indicates szz is intermediate principal stress
     $s1   = $si
     $s2   = $s33i
     $s3   = $sii
    end_section
;---------------------  now stresses are checked for plastic failure
    section
;--- general tension failure?
     if $s1 >= m_tenmn then       ;if sig1 is less than apex
      if m_tenmn > m_ten then
        $apex_flag = 1
      end_if
;------ set stresses to plastic apex ---
      zs11       = m_tenmn       ; puts all stresses equal to apex
      zs22       = m_tenmn
      zs12       = 0.0
      zs33       = m_tenmn
      if m_tenmn  = 0.0 then       ;if no cohesion
        m_ind   = 5.0
      else
        m_ind   = 1.0
      end_if
      zvisc = 0.0
      exit section
     end_if
;--- check for shear yield --- ;if no tension failure, check for shear failure
     $fs    = $s1 - $s3 * m_nphi + m_csnp   ;if f<0 than shear failure
     $alams = 0.0
     if $fs < 0.0 then
;--- yielding in shear ---
      $alams = $fs / m_x1
      $s1 = $s1 - $alams * (m_e1 - m_e2 * m_npsi)
      $s2 = $s2 - $alams * m_e2 * (1.0 - m_npsi)
      $s3 = $s3 - $alams * (m_e2 - m_e1 * m_npsi)
      m_ind = 1.0
     else
      if $s3 < m_tenmn then
;--- no failure at all ---
       zs11 = $s11i
       zs22 = $s22i
       zs33 = $s33i
       zs12 = $s12i
       exit section
      end_if
     end_if
;--- general tension failure?
     if $s1 >= m_tenmn then
      if m_tenmn > m_ten then
        $apex_flag = 1
      end_if
;------ set stresses to plastic apex ---
      zs11       = m_tenmn
      zs22       = m_tenmn
      zs12       = 0.0
```

```
        zs33      = m_tenmn
        if m_tenmn  = 0.0 then
          m_ind   = 5.0
        else
          m_ind   = 1.0
        end_if
        zvisc     = 0.0
        exit section
      end_if
;--- uniaxial tension ... intermediate p.s. ---
      if $s2 >= m_tenmn then
        if $fs < 0.0 then
          m_ind = 4.0
        else
          m_ind = 3.0
        end_if
        if m_tenmn > m_ten then
          $apex_flag = 1
        end_if
        $s2 = m_tenmn
        $s3 = m_tenmn
      else
;--- uniaxial tension ... minor p.s. ---
        if $s3 >= m_tenmn then
          if $fs < 0.0 then
            m_ind = 4.0
          else
            m_ind = 3.0
          end_if
          if m_tenmn > m_ten then
            $apex_flag = 1
          end_if
          $s3 = m_tenmn
          $s2 = min($s2,$s3)
        end_if
      end_if
;--- direction cosines ---
      if $psdif = 0.0 then
        $cs2  = 1.0
        $si2  = 0.0
      else
        $cs2  = $sdif     / $psdif
        $si2  = 2.0 * $s12i / $psdif
      end_if
;--- resolve back to global axes ---
      case_of  $icase
        case 1
          $dc2  = ($s1 - $s3) * $cs2
          $dss  =  $s1 + $s3
          zs11  = 0.5 * ($dss + $dc2)
          zs22  = 0.5 * ($dss - $dc2)
          zs12  = 0.5 * ($s1  - $s3) * $si2
          zs33  = $s2
        case 2
          $dc2  = ($s2 - $s3) * $cs2
          $dss  =  $s2 + $s3
          zs11  = 0.5 * ($dss + $dc2)
          zs22  = 0.5 * ($dss - $dc2)
```

```
        zs12  = 0.5 * ($s2  - $s3) * $si2
        zs33  = $s1
       case 3
        $dc2  = ($s1 - $s2) *$cs2
        $dss  =  $s1 + $s2
        zs11  = 0.5 * ($dss + $dc2)
        zs22  = 0.5 * ($dss - $dc2)
        zs12  = 0.5 * ($s1  - $s2) * $si2
        zs33  = $s3
      end_case
      zvisc = 0.0
    end_section

; ------ reset tensile strength --------
    if $apex_flag = 1 then
      $apex = $apex + 1.0
    end_if
    $apsav = 0.0
;********************************************** add fatigue consideration
  if remold=0.0 then                                                    ;****
  ax1=-zs11                                                             ;****
  ay1=-zs22                                                             ;****
  at1=zs12                                                              ;****
  ab1=(0.5*(ax1+ay1))                                                   ;****
  ab2=(0.5*(ax1-ay1))                                                   ;****
  ;r1 - radius of mohr circle                                          ;****
  r1=sqrt(at1*at1+ab2*ab2)                                             ;****
  ;rf - radius of theoretical mohr circle with the same average stress  ;****
  rf=(ab1+m_coh/tan(m_fric/180.0*3.14159))*$sphi                        ;****
; sr4 - ratio of stressing to max possible stressing                    ;****
  sr4=r1/rf                                                             ;****
;finds and sorts 2 highest stressed points in the element (out of 4)    ;****
if sr4>st_m1 then                                                       ;****
 st_m2=st_m1                                                            ;****
 st_m1=sr4                                                              ;****
else                                                                    ;****
 if sr4>st_m2 then                                                      ;****
  st_m2=sr4                                                             ;****
 end_if                                                                 ;****
end_if                                                                  ;****
;************************************************
    if zsub > 0.0 then
; stress ratio is set to second high stress ratio in the element and values are zeroed
; before next step
 sr=st_m2                                                               ;****
      max_str=sr                                                        ;****
      sr=0.0                                                            ;****
      st_m1=0.0                                                         ;****
      st_m2=0.0                                                         ;****
       $apsav = $apex / zsub
      if $apsav > 0.0 then
        if tenflg # 0 then
           m_ten = 0.0
        end_if
      end_if
; --- reset for next zone ------
      $apex = 0.0
    end_if
```

```
    Case 3
; ------------------
; Return maximum modulus
; ------------------
      cm_max = m_k + 4.0 * m_g / 3.0
      sm_max = m_g
    Case 4
; ------------------
; Add thermal stresses
; ------------------
      ztsa = ztea * m_k
      ztsb = zteb * m_k
      ztsc = ztec * m_k
      ztsd = zted * m_k
  End_case
end
opt mohr_fat
set echo on
```

## A2 - Listing of sub-system B1 program (written in Flac internal language)

The program finds the relationship between the bearing capacity of the soil and the depth of the remolded layer.

```
; program name lay_t3.dat
; soil stiffened, max_rut=15%
;unbalanced force kept proportional to forces in the system
; with T site material properties
; fric=47 coh0=0.85 den=1950
; this prog finds bearing capacity of a two layer soil  and creates
; a relationship between upper layer depth and soil bearing capacity
new
title
FRICTIONAL COHESIVE SOIL
g 40 40
mo mo
set vga large
gen 0 0 0 1 0.1 1 0.1 0 i 1 7 rat 1 0.98
gen s s 1 1 1 0 i 7 41 rat 1.03 0.98
ini syy=0 j 41
fix x i 1
fix x y j 1
fix x y i 41
;**********************
def servo  ;boundaries of unbal are important for proper operation
  while_stepping
    if unbal>2.5*l_unbal then
      loop i (1,7)
        yvel(i,41)=yvel(i,41)*0.975
      end_loop
    end_if
    if unbal<l_unbal then
      loop i (1,7)
        yvel(i,41)=max(yvel(i,41)*1.025,-1e-6)
      end_loop
    end_if
end
;**********************
def load
  while_stepping
    temp=0.0
    loop i (1,7)
      temp=temp+yforce(i,41)
    end_loop
  load = 2.0*temp/(x(7,41)+x(8,41))
;keeps track of max load
   if load<load_t then
    load=load_t
   end_if
end

;**** initialize grid before dippening upper layer
def ini_func
 loop ai(1,41)
  loop aj(1,41)
   y(ai,aj)=y(ai,aj)-ydisp(ai,aj)
```

```
   x(ai,aj)=x(ai,aj)-xdisp(ai,aj)
  end_loop
 end_loop
 command
 ini syy=0
 ini sxx=0
 ini sxy=0
 ini szz=0
 ini ydis=0
 ini xdis=0
 ini yvel=0
 ini xvel=0
 set gravity 9.81
 solve
 fix x y i 1 7 j 41
 ini yv -2e-7 i 1 7 j 41
 end_command
end
;*****************************
;A FUNCTION WHICH FINDS THE BEARING CAPACITY OF THE TWO LAYER STRUCTURE
def pl2
;initial value for load
 load1=-1e4
;initial value for maximum load
 load=0
 sds=999
 sds1=999
 loop ii1 (1,80)
  command
   print sds
   print load
   pri depth1
   step 1000
  end_command
  l1_unbal=0.005*(load*x(7,41)/7) ;unbalanced force used in servo
  l_unbal=max(l_unbal,l1_unbal)    ;is kept proportional to forces in system
  sds=abs((load-load1)/load1)
;if two consecutive measurements sds are less than 0.5%.bearing capacity
;                              is assumed
  if sds<0.005 then
   if sds1<0.005 then
    exit
   end_if
  end_if

;if rut is deeper than 0.15 B  bearing capacity is assumed
  if ydisp(1,41)<max_rut then
   exit
  end_if
  sds1=sds
  load1=load
 end_loop
end
;*********************************
;A FUNCTIN WHICH CHANGES REMOLDED LAYER DEPTH AN DACTIVATES PL2
def pl1
;changes layer depth
;
```

```
; max_rut is the max allowable sinkage and it equals to 15%
;  of the width of the rigid body forced into the soil.
 max_rut=-0.15*2*x(7,41)
 loop depa(0,10)
 l_unbal=1e2        ;keeps reasonable limits to unbalanced force
  dep=2*depa
  ini_func
  depp=41-dep
  depth1=y(1,41)-y(1,depp)
  if dep>0 then
   loop jj3(1,dep)
    dep1=41-jj3
    loop ii3(1,40)
     friction(ii3,dep1)=fric1
     cohesion(ii3,dep1)=coh1
     bulk_mod(ii3,dep1)=bulk0*red_bulk
     shear_mod(ii3,dep1)=shear0*red_she
    end_loop
   end_loop
  end_if
  pl2
  command
  ;saves current situation
  sav c:\flac32\rafi\layers\lay_t3.sav
   print load
   print sds
   pri depth1
  end_command
 end_loop
end
;*********************************
def prop0
 fric0=0
 coh0=0
end
;************** MAIN SECTION OF INPUT DATA
set fric1=47 coh1=1e3 fric0=47 coh0=0.85e5 dep=0 red_bulk=0.75 red_she=0.75
set bulk0=1.66e9 shear0=0.35e9  ;E=1e9 mu=0.4
prop s shear0 b bulk0 den=1950 coh=coh0 fric=fric0  ten 1e10
;*********************************
hist n=1000
hist depth1
hist load
his sds
hist yd i 2 j 41
hist yv i 2 j 41
pl1
save c:\flac32\rafi\layers\lay_t3.sav
return
```

## A3 - Listing of sub-system B2 program (written in Flac internal language)

A program which finds sinkage and rutting values of a circular "wheel", loading a two-layered soil system. Rutting is calculated as a function of the upper layer depth. Ruttings caused by second and third consecutive loadings on the same point are also recorded.

```
;program sink_sb6.dat
;finds behavior of 40 deg cohesionless soil layer
;calculates rut depth under wheel loading
;calculates also second and third loadings rut values
; coh0=0.3,fric0=50,small wheel dimensions and ver_pres=2

new
con axi extra=3
grid 65 30
m m i 1 50
set large for =1e1
set echo off
set message off
;axisymetric configuration.
;*****************************************
;loading properties
def load_prop
 mes1='After unloading'
 ver_pres=-2*1e5  ; average contact pressure in pascal
 rad_con=0.038   ; radius of circular contact area in m.
 hei_whe=1*rad_con ;height of "wheel" is the same as contact radius
 dep_bin=-10*rad_con ;depth of bin
 rad_bin=5*rad_con  ;radius of bin
 ;arc_cen=0.8*rad_con
 ;rad_arc=0.2*rad_con ;radius of arc on wheel corner
 n_steps=4 ; number of steps in loading and unloading process
end
;*************************************
;remolded and unremolded soil properties
def prop0
 fric0=50
 coh0=0.3e5
 fric1=40
 coh1=0
 fric_int=fric1          ; friction angle at wheel-soil interface
; elastic modulii
;  bg=E/[3*(1-2*mu)] - bulk modulus   E0=1000 kg/cm2 E1=750 kg/cm2  mu=0.3
;  sg=E/[2*(1+mu)]   - shear modulus
bg0=1000*1e5/3/(1-2*0.3)
sg0=1000*1e5/2/(1+0.3)
bg1=750*1e5/3/(1-2*0.3)
sg1=750*1e5/2/(1+0.3)
;  command
;   prop fric=phi cohesion=cc1
;   prop s=sg b=bg
;  end_command
end
;*************************************************
```

```
def load
 ;load is the sumation of forces on nodes under rigid body (NOT pressure)
 temp=0.0
 edge=65
 loop i (52,edge)
  area_i=3.14*(x(i+1,10)*x(i+1,10)-x(i,10)*x(i,10))
  temp=temp+syy(i,9)*area_i
 end_loop
 load=-temp*10 ;total load on "wheel" in kg.
end
;*************************************************
prop0
load_prop
load
gen 0,dep_bin 0,0 rad_con,0 rad_con,dep_bin i 1 15 j 1 31 rat 1 0.98
gen s s rad_bin,0 rad_bin,dep_bin i 15 51 j 1 31 rat 1.02 0.98
;above two lines  represent soil
m n i 51
m n i 52 65 j 10 30
m e i 52 65 j 1 9
gen 0,0 0,hei_whe rad_con,hei_whe rad_con,0 i 52,66 j 1 10
;gen arc arc_cen rad_arc arc_cen 0 90
;m n reg 65 1
;plot grid hold
;*************************************************************
;**** initialize grid before changing soil properties
def ini_func
 if large # 0 then
 ;if strains are set to "small" no change is made to Y and X
 loop ai(1,66)
  loop aj(1,31)
   y(ai,aj)=y(ai,aj)-ydisp(ai,aj)
   x(ai,aj)=x(ai,aj)-xdisp(ai,aj)
  end_loop
 end_loop
 end_if
 command
 ini syy=0
 ini sxx=0
 ini sxy=0
 ini szz=0
 ini ydis=0
 ini xdis=0
 ini yvel=0
 ini xvel=0
 set gravity 9.81
 step 10
 solve
 end_command
end
;*************************************************************
;*********************************************
prop d 2000 b bg0 s sg0 c coh0 f fric0 ten 1e10 i 1 50
prop d 100 b 2e8 s 1e8 i 52 65 j 1 9 ; wheel properties
prop d 100 b 2e9 s 1e9 i 52 65 j 10 ; more rigid upper face of "wheel"
;fix x i=52 65 j=10    no horizontal movement of upper face of "wheel"
fix x i=1
fix x i=51
```

```
fix x y i=1 51 j=1
fix x i=52
int 1 a fr 1 31 to 30 31     ;soil face
int 1 b fr 52 1 to 66 3     ;tyre face
int 1 kn 1e11 ks 1e11 c 0 f fric_int      ;properties of wheel soil interaction
ini sxx=0 syy=0
;set gra 9.81
;solve

;*****************************************
def superstep
 loop ns(1,n_steps)
  left_stress=left_stress+stress_inc
  command
   apply syy=left_stress i=52,66 j =10
   step 20
  end_command
 end_loop
end
;*****************************************
def pl3
;A function which loads the soil and monitors sinkage
 ;initial value for old ydisp
  ydisp0=-0.1
  sds=999
  sds1=999
  loop ii1 (1,80)
  command
   print sds
   print ydisp1
   pri depth1
   step 1000
  end_command
  ydisp1=ydisp(1,31)
  sds=abs((ydisp1-ydisp0)/ydisp0)
  ;if two consecutive measurements sds are less than 0.5%,bearing capacity
  ;                              is assumed
  if sds<0.005 then
   if sds1<0.005 then
    exit
   end_if
  end_if
  sds1=sds
  ydisp0=ydisp1
  end_loop
end
;*****************************************************
;A FUNCTIN WHICH CHANGES REMOLDED LAYER DEPTH AND ACTIVATES PL2
def pl1
;changes layer depth
 loop depa(0,15)
 dep=2*depa
 ini_func
 depp=31-dep
 depth1=y(1,31)-y(1,depp)
 if dep>0 then
  loop jj3(1,dep)
   dep1=31-jj3
```

```
   loop ii3(1,50)
    friction(ii3,dep1)=fric1
    cohesion(ii3,dep1)=coh1
    bulk_mod(ii3,dep1)=bg1
    shear_mod(ii3,dep1)=sg1
   end_loop
  end_loop
 end_if
 loop load_n(1,3)  ;activates load 3 times
 left_stress=0.0
 stress_inc=ver_pres/n_steps  ;increases load gradualy
 superstep
 pl3    ;activate loading and sinkage monitoring process
 command
  set echo on
  set mes on
  print depth1
  print ydisp i=1 j=31
  set echo off
  set mes off
 end_command
 ex_1(1,depp)=depth1
 ex_2(load_n,depp)=ydisp(1,31) ;contains sinkage
 left_stress=ver_pres
 stress_inc=-ver_pres/n_steps  ;increases load gradualy
 superstep
 command
  set echo on
  set mes on
  solve
  print depth1
  print mes1
  print ydisp i=1 j=31
  set mes off
  set echo off
 save c:\flac32\rafi\sink_sb6.sav
 end_command
 ex_3(load_n,depp)=ydisp(1,31) ;contains rut
end_loop
end_loop
end
;*************************************************
his n=1000
his yvel i 1 j 31
his ydisp i 1 j 31
pl1
save c:\flac32\rafi\sink_sb6.sav
return
;*************************************************
```

## A4 - Listing of sub-system C1 program (written in Turbo Pascal 6.0)

Computes number of wheel passes to failure according to the **accumulated rutting approach**

```
{sub_c1}
program shkiot1;
{the same as shkiot but for the moving wheel experiments}
const
lane_wid=800;   {total width of landing strip in cm.}
n_inc=15;   {no of increments in  function (remold dpth  VS  rut values)}
n_max=2000; {max number of load applic. Check Vs Load_no !!!!}
type
 arr=array [1..n_max,1..4] of real;
  {index - number of pass , 1 - depth of remolded layer}
  { 2 - Primary Rut  , 3 - Accumulated rut A , 4 - Accumulated rut B }
var
run1:arr;
shki,shki1:text;  {the file in which rutting results will be written }
s:array[0..lane_wid,1..3] of real;{array which includes rutting and loading data}
      {  1 - level of point   }
      {  2 - indicates recent loading of point  }
      {          0 - no recent loading,1 - loaded lastly,2 - loaded twice}
      {  3 -  accumulated number of loads on point  }
sk:array[0..100] of real;  { working array for rutting calculation                }
sink:array[1..3] of real;  { array which includes forseen ruttings caused by consecutive loading}
dep_rut:array [1..n_inc,1..4] of real;
{1 - depth of remolded layer,2 - first loading rut,3 -second.. 4 - third..}
 dep_n,rut_dep:text;
 { dep_n - contains depth of remolded layer VS no of passes (sub A)}
 {rut_dep - contains rut values VS depth of remolded layer (sub B)}
iset,j :integer;
gset,fac,r,v1,v2:real;
upheav1,sum1,avg1,comp:real;
ll,margin,x0,l1,l2,rr:integer;
l_width:real;
stn_dev,comp1:real;
load_no:integer; {total number of load applications  }
chk,ii,i,k:integer;
phi,dif:real;
k1:integer;
bb,bb1:real;
max1,max2,max3,max4,ave_low,ave_high:real;
ff1,ff2:integer;
allow_prim,allow_acc_a,allow_acc_b:real;
f_prim,f_acc_a,f_acc_b:integer;
file1,file2:string[25];
{************************************* }
procedure readf1;
 {reads relation between depth of remolded layer and no of passes}
 { and assigns values to array }
 var
 dep01,dep02:real;
 n01,n02,nn:integer;
 begin
  assign(dep_n,file1);
```

```
 reset(dep_n);
 read(dep_n,n01,dep01);
 if (n01<>0) then
 begin
  write('First record in input file is not correct,please make the necessary changes.');
  halt;
 end;
 while (not eof(dep_n)) and (n01<load_no)  do
 begin
  read(dep_n,n02,dep02);
  nn:=n02;
  if n02>load_no then
  nn:=load_no;
  for i:=n01+1 to nn do
  run1[i,1]:=dep01+(dep02-dep01)*(i-n01)/(n02-n01);
  n01:=n02;
  dep01:=dep02;
 end;
 if n02<load_no then
 for k:=n02+1 to load_no do
 run1[k,1]:=dep02;
 close(dep_n);
end;
{*************************************************************************}
{*************************************************************************}
procedure readf2;
 {reads relation between depth of remolded layer and rut values}
 { and assigns values to array }
var
dep,rut1,rut2,rut3:real;
begin
 assign(rut_dep,file2);
 reset(rut_dep);
 read(rut_dep,dep,rut1,rut2,rut3);
 if (dep<>0) then
 begin
  write('First record in input file is not correct,please make the necessary changes.');
  halt;
 end;
 k1:=1;
 while (not eof(rut_dep)) do
 begin
  dep_rut[k1,1]:=dep;
  dep_rut[k1,2]:=rut1;
  dep_rut[k1,3]:=rut2;
  dep_rut[k1,4]:=rut3;
  k1:=k1+1;
  read(rut_dep,dep,rut1,rut2,rut3);
 end;
 dep_rut[k1,1]:=dep;
 dep_rut[k1,2]:=rut1;
 dep_rut[k1,3]:=rut2;
 dep_rut[k1,4]:=rut3;
 k1:=k1+1;
 dep_rut[k1,1]:=9999;
 dep_rut[k1,2]:=rut1;
 dep_rut[k1,3]:=rut2;
 dep_rut[k1,4]:=rut3;
```

```
 close(rut_dep);
 end;
 {*********************************************************************}
{******************** Computes marginal rutting values for the remolded depth}
procedure marg_rut;
begin
 j:=0;
 repeat
 j:=j+1;
 until run1[ll,1]<dep_rut[j,1];
 if j=k1 then
 begin
  sink[1]:=dep_rut[k1,2];
  sink[2]:=dep_rut[k1,3];
  sink[3]:=dep_rut[k1,4];
 end
 else
 begin
  bb1:=(dep_rut[j,1]-dep_rut[j-1,1]);
  if bb1=0 then
  begin
   sink[1]:=dep_rut[j-1,2];
   sink[2]:=dep_rut[j-1,3];
   sink[3]:=dep_rut[j-1,4];
  end
  else
  begin
   bb:=(run1[ll,1]-dep_rut[j-1,1])/bb1;
   sink[1]:=dep_rut[j-1,2]+(dep_rut[j,2]-dep_rut[j-1,2])*bb;
   sink[2]:=dep_rut[j-1,3]+(dep_rut[j,3]-dep_rut[j-1,3])*bb;
   sink[3]:=dep_rut[j-1,4]+(dep_rut[j,4]-dep_rut[j-1,4])*bb;
  end;
 end;
end;
 {*****************************************************}
procedure prim_accu;
 {find primary and accumulated average rutting values}
begin
 max1:=0;
 max2:=0;
 max3:=0;
 max4:=0;
 for ii:=0 to lane_wid do
 begin
  if s[ii,1]<max1 then
  begin
   max4:=max3;
   max3:=max2;
   max2:=max1;
   max1:=s[ii,1];
  end
  else if s[ii,1]<max2 then
  begin
   max4:=max3;
   max3:=max2;
   max2:=s[ii,1];
  end
  else if s[ii,1]<max3 then
```

```
  begin
   max4:=max3;
   max3:=s[ii,1];
  end
  else if s[ii,1]<max4 then
  max4:=s[ii,1];
 end;
 ave_high:=(max1+max2+max3+max4)/4;
 {ave_high is the average level of the 4 highest points in the lane }
 ff1:=round(lane_wid/2);
 ff2:=round(l_width/2);
 ave_low:=(s[ff1,1]+s[ff1+ff2,1]+s[ff1+2*ff2,1]+s[ff1-ff2,1]+s[ff1-2*ff2,1])/5;
 {ave_low is the average level of mid-point of lane and 4 neighboring points}
 run1[ll,2]:=sink[1]; {present primary rut}
 run1[ll,3]:=ave_low; {present accumulated rut A}
 run1[ll,4]:=ave_low-ave_high; {present accumulated rut B}
 if sink[1]>allow_prim then
 begin
 writeln('Primary rut. crit. violated at cyc no. ',ll,'  Prim. rut.=',sink[1]:5:3,' cm.');
 if f_prim=0 then f_prim:=ll;
 end;
 if ave_low>allow_acc_a then
 begin
 writeln('Acc. rut. crit. A violated at cyc no. ',ll,'  Acc. rut. A=',ave_low:5:3,' cm.');
 if f_acc_a=0 then f_acc_a:=ll;
 end;
 if run1[ll,4]>allow_acc_b then
 begin
 writeln('Acc. rut. crit. B violated at cyc no. ',ll,'  Acc. rut. B=',run1[ll,4]:5:3,' cm.');
 if f_acc_b=0 then f_acc_b:=ll;
 end;
 end;
{************************************************  }
function norm:real;  {generates numbers of normal distribution;
begin
if iset=0 then
begin
 r:=2;
 repeat
  v1:=2*random-1;
  v2:=2*random-1;
  r:=sqr(v1)+sqr(v2);
 until r<1;
 fac:=sqrt(-2*ln(r)/r);
 gset:=v1*fac;
 iset:=1;
 norm:=v2*fac;
end
else
begin
 iset:=0;
 norm:=gset;
end;
end;
{************************************************}
procedure up1(jl1,jl2:integer);  { sets upheaval on wheel sides }
var
j:integer;
```

```
begin
j:=jl1;
repeat
 s[j,1]:=s[j,1]+upheav1;
 s[j,2]:=0;
 j:=j+1;
until j>jl2
end;
{*****************************************************************}
function tan(an:real):real;
begin
 tan:=sin(an)/cos(an);
end;

{*****************************************************************}
begin
fillchar(s,sizeof(s),#0);
{***********asks for input data*************}
 writeln;
 writeln('Enter filename of Remolded layer depth Vs. Number of passes (including path)');
 writeln;
 readln(file1);
 writeln;
 writeln('Enter filename of Ruts depth Vs. Remolded layer depth (including path)');
 writeln;
 readln(file2);
 writeln;
 writeln('Enter the following values regarding loading conditions:');
 writeln;
 writeln('Load width | Lateral wander | Phi | Primary rut | Total rut | Total rut ');
 writeln('          | std. deviation |     | criterion | criterion A | criterion B ');
 writeln('  cm.     |     cm.        | deg. |   cm.     |    cm.      |    cm.     ');
 writeln('          |                |      |           |             |            ');
 readln(l_width,stn_dev,phi,allow_prim,allow_acc_a,allow_acc_b);
 writeln;
 writeln('Enter total number of wheel passes');
 readln(load_no);

{*********************************************}
f_prim:=0;
f_acc_a:=0;
f_acc_b:=0;
{******************** AREA OF INPUT DATA **********************}
{ rutting calculations are made at 1 cm. intervals for a total width of 44 cm.}
{stn_dev:=7; }     {standard deviation of lateral wander of wheel }
{l_width:=4;}{width of loading wheel in cm. (should be an even integer number  }
        {and not above 100)  }
margin:=round(2.0*l_width);  { width of upheaval area }
comp:=0.0;    { part of rutting volume contributed by earth compaction }
{load_no:=600;} {total number of wheel passes  }
{phi:=45; }  {value of internal friction angle needed for smoothing stage}
{allowed rutting values}
{allow_prim:=0.2*l_width;}
{allow_acc_a:=3;}
{allow_acc_b:=5;}
{***************** END OF INPUT AREA **************************}
readf1;
readf2;
```

```
{*************************************************}
for ll:=1 to load_no do
 begin
 writeln(ll);
 marg_rut;  { calculate rutting at present loading}
 x0:=round(lane_wid/2+norm*stn_dev);
 { center of loading in a specific wheel pass }
 if x0<round(l_width) then x0:=round(l_width);
 if x0>round(lane_wid-l_width) then x0:=round(lane_wid-l_width);
 l1:=x0-round(l_width/2);      { limits of load }
 l2:=x0+round(l_width/2);      {limits of load  }
 sum1:=0;
 for j:=0 to round(l_width) do
 begin
  rr:=round(s[l1+j,2]+1);   { takes the current state of a point regarding }
                    { previous loadings   }
  sk[j]:=s[l1+j,1]+sink[rr];  { calculates rutting of a point (without taking }
                     { "neighbours" conditions into acount )   }
  sum1:=sum1+sk[j]      { calculate total rutting volume }
 end;
 avg1:=sum1/(round(l_width)+1);
                    {averaging rutting over all loaded points }
 for j:=0 to round(l_width) do
 begin
  sum1:=sum1-s[l1+j,1];{calculates total rutting caused by the current load }
  s[l1+j,1]:=avg1;       {set new rutting values under the wheel  }
  s[l1+j,3]:= s[l1+j,3]+1;       {change no. of accumulated loadings  }
  if s[l1+j,2]<2 then s[l1+j,2]:=s[l1+j,2]+1:
   {sets new values for sink usage}
 end;
 comp1:=comp/s[x0,3];  { y=a/x  taken as a rep. function of part of rutting }
                 {       caused by compaction. decreases as no of    }
                 {       coverages increases.                        }
 upheav1:=-(1-comp1)*sum1/2/margin;{ assuming constant heaving at all places}
                    {and taking into account soil compaction total  }
                    {rutting volume and width of upheaval area      }
 up1(l1-margin,l1-1); { calculating new rutting values for upheaving points}
 up1(l2+1,l2+margin);

 if int(ll/10)=ll/10 then

  repeat       {smoothes surface assuming no cohesion and PHI fric angle  }
  chk:=0;
  for ii:=0 to lane_wid-1 do
  begin
   dif:=s[ii,1]-s[ii+1,1];
   if abs(dif)>tan(phi/180*3.14) then
   begin
    chk:=1;
    s[ii,1]:=s[ii,1]-0.2*sink[3]*(dif/abs(dif));
    s[ii+1,1]:=s[ii+1,1]+0.2*sink[3]*(dif/abs(dif));
   end;
  end;
 until chk=0;
 prim_accu;
end;
{Output section ***************************************}
assign(shki,'sub_c1_a.out');
```

```
rewrite(shki);
writeln(shki,'CALCULATION OF SOIL SURFACE PROFILE UNDER REPETITIVE LOADING');
writeln(shki);
writeln(shki,'Program name - sub_c1.PAS ');
writeln(shki,' ');
writeln(shki,'Remolded layer depth Vs. Number of passes, given in file - ',file1);
writeln(shki,' ');
writeln(shki,'Rutting values Vs. Remolded layer depth, given in file - ',file2);
writeln(shki,' ');
writeln(shki,'Wheel width in cm. - ',l_width:3:0);
writeln(shki,' ');
writeln(shki,'Standard deviation of lateral wander - ',stn_dev:3:0);
writeln(shki,' ');
writeln(shki,'Point no.  Point level (cm.)  No. of loadings');
writeln(shki,' ');
for j:=1 to lane_wid do
begin
 writeln(shki,'  ',j,'        ',-s[j,1]:6:3,'       ',s[j,3]:6:0);
end;
close(shki);
assign(shki1,'sub_c1_b.out');
rewrite(shki1);
writeln(shki1,'CALCULATION OF SOIL SURFACE PROFILE UNDER REPETITIVE LOADING');
writeln(shki1);
writeln(shki1,'Program name - sub_c1.PAS ');
writeln(shki1);
writeln(shki1,'Remolded layer depth Vs. Number of passes, given in file - ',file1);
writeln(shki1,' ');
writeln(shki1,'Rutting values Vs. Remolded layer depth, given in file - ',file2);
writeln(shki1,' ');
writeln(shki1,'Wheel width in cm. - ',l_width:3:0);
writeln(shki1);
writeln(shki1,'Standard deviation of lateral wander - ',stn_dev:3:0);
writeln(shki1);
writeln(shki1,'Allowed Primary rutting - ',allow_prim:4:2,'cm.');
writeln(shki1);
writeln(shki1,'Allowed Acc. rutting A  - ',allow_acc_a:4:2,'cm.');
writeln(shki1);
writeln(shki1,'Allowed Acc. rutting b  - ',allow_acc_b:4:2,'cm.');
writeln(shki1);
if f_prim>0 then
writeln(shki1,'Primary rutting criterion first violated at cycle no. - ',f_prim);
if f_acc_a>0 then
writeln(shki1,'Accumulated rutting A criterion first violated at cycle no. - ',f_acc_a);
if f_acc_b>0 then
writeln(shki1,'Accumulated rutting B criterion first violated at cycle no. - ',f_acc_b);
writeln(shki1),
writeln(shki1,'Cy. no.  Rem. depth  Prim. rut. Acc. rut. A  Acc. rut. B');
writeln(shki1,'       / Load wid.  (cm.)     (cm.)     (cm.)       (cm.)  ');
for j:=1 to load_no do
begin
 writeln(shki1,' ',j:4,'      ',run1[j,1]:3:1,'       ',run1[j,2]:4:2,'      ',run1[j,3]:4:2,'       ',run1[j,4]:4:2);
end;
close(shki1);

{End of output section ***************************************}
end.
```

## A5 - Listing of sub-system C2 program (written in Turbo Pascal 6.0)

Computes number of wheel passes to failure according to the **accumulated damage approach**

```
program sub_c2;
const
 n_max=1000;     {max no of passes }
 n_inc=15;  {no of increments in  function (remold dpth  VS  rep strength)}
type
 arr=array [1..n_max,1..4] of real;
  {index - number of pass , 1 - depth of remolded layer,2 - rep. strength}
  { 3 - marginal damage to runway , 4 - accumulated damage to runway}
var
 dep_n,str_dep,sub_cc:text;
 { dep_n - contains depth of remolded VS no of passes (sub A)}
 {str_dep - contains strength VS depth of remolded layer (sub B)}
 {sub_cc - output of system}
 run1:arr;
 {run1 - array of results}
 pres,tot_p:real;
 {pres - contact pressure  ,tot_p - eswl       -needed for the use of the
                    equation of unsurfaced runway performance}
 i,j,j1,k,k1:integer;
 n_pas:integer;  { indicates pass no of functional failure  }
 rep_str:array [1..n_inc,1..2] of real;
 {1 - depth of remolded layer,2 - rep. strength}
  ln_np0,np0,ln_np1,np1:real; {indicates no of passes to failure in remolded
                      and unremolded soil }
{ ****************************************}
procedure readf1;
 {reads relation between depth of remolded layer and no of passes}
 { and assigns values to array }
 var
 dep01,dep02:real;

 n01,n02,nn:integer;

 begin
  assign(dep_n,'dep_n.dat');
  reset(dep_n);
  read(dep_n,n01,dep01);
  if (n01<>0) then
  begin
   write('First record in input file is not correct,please make the necessary changes.');
   halt;
  end;
  while (not eof(dep_n)) and (n01<n_max)  do
  begin
   read(dep_n,n02,dep02);
   nn:=n02;
   if n02>n_max then
   nn:=n_max;
   for i:=n01+1 to nn do
   run1[i,1]:=dep01+(dep02-dep01)*(i-n01)/(n02-n01);
   n01:=n02;
```

```
 dep01:=dep02;
 end;
 if n02<n_max then
 for k:=n02+1 to n_max do
 run1[k,1]:=dep02;
 close(dep_n);
end;
{*********************************************************************}
procedure readf2;
 {reads relation between depth of remolded layer and representative strength}
 { and assigns values to array }
var
dep,str:real;
begin
 assign(str_dep,'str_dep.dat');
 reset(str_dep);
 read(str_dep,dep,str);
 if (dep<>0) then
 begin
  write('First record in input file is not correct,please make the necessary changes.');
  halt;
 end;
 k1:=1;
 while (not eof(str_dep))  do
 begin
  rep_str[k1,1]:=dep;
  rep_str[k1,2]:=str;
  k1:=k1+1;
  read(str_dep,dep,str);
 end;
 rep_str[k1,1]:=dep;
 rep_str[k1,2]:=str;
 k1:=k1+1;
 rep_str[k1,1]:=9999;
 rep_str[k1,2]:=str;
 close(str_dep);
end;
{*********************************************************************}
procedure a1;
{calculates rep strength for each path }
{******************************************************* }
 procedure margin;
 { calculates marginal damage to runway according to miner's law
 and application of eq. 2.11 page 2-18 in phase 1 report 1989  }
 var
 ln_np,np:real;
 begin
 {  writeln;
  writeln('Enter the following values regarding loading conditions:');
  writeln;
  writeln('CONTACT PRESSURE |    ESWL    ');
  writeln('     psi       |     lb     ');
  writeln('               |            ');
  readln(pres,tot_p);                  }
  ln_np:=(ln(run1[i,2])+2.83227*ln(10)-0.48966*ln(pres)-0.580426*ln(tot_p))/0.1716;
  np:=exp(ln_np);
  run1[i,3]:=1/np;
  if i=1 then
```

```
 run1[i,4]:=run1[i,3]
 else
 run1[i,4]:=run1[i-1,4]+run1[i,3];
 if (run1[i,4]>1) and (n_pas=0) then n_pas:=i;
end;
{ ********************************************** }
var
bb,bb1:real;
begin
 n_pas:=0;
 for i:=1 to n_max do
 begin
  j:=0;
  repeat
  j:=j+1;
  until run1[i,1]<rep_str[j,1];
  if j=k1 then
  run1[i,2]:=rep_str[k1,2]
  else
  begin
   bb1:=(rep_str[j,1]-rep_str[j-1,1]);
   if bb1=0 then
   run1[i,2]:=rep_str[j-1,2]
   else
   begin
    bb:=(run1[i,1]-rep_str[j-1,1])/bb1;
    run1[i,2]:=rep_str[j-1,2]+(rep_str[j,2]-rep_str[j-1,2])*bb;
   end;
  end;
  margin;
  writeln(sub_cc,i,'  ',run1[i,1]:3:2,'   ',run1[i,2]:5:2,'  ',run1[i,3],'  ',run1[i,4]);
 end;
end;
{*************************************************}
{************************************************************ }
begin
assign(sub_cc,'sub_c.out');
tot_p:=30000;
pres:=70;
rewrite(sub_cc);
readf1;
readf2;
a1;
writeln;
ln_np1:=(ln(rep_str[k1,2])+2.83227*ln(10)-0.48966*ln(pres)-0.580426*ln(tot_p))/0.1716;
np1:=exp(ln_np1);
ln_np0:=(ln(rep_str[1,2])+2.83227*ln(10)-0.48966*ln(pres)-0.580426*ln(tot_p))/0.1716;
 np0:=exp(ln_np0);
writeln('In a homogenous unremolded soil,failure would occur after -',np0:9:1,'  passes' );
writeln('In a homogenous remolded soil,failure would occur after  -',np1:9:1,'  passes' );
writeln;
if n_pas=0 then
writeln('No failure is expected in runway after - ',n_max:6,' passes. ')
else
writeln('Failure is expected in runway after - ',n_pas:6,' passes. ')
end.
```

Appendix B

# THE BEARING CAPACITY OF SOIL WHICH POSSESS CHANGING STRENGTH PARAMETERS WITH DEPTH ,UNDER LOADING OF A PLATE GROUSER.

Contents:

## 1. INTRODUCTION

The remolding action caused in certain types of soils as a result of repetitive wheel loads, brings about the creation of soil structure where the soil strength changes with depth. Part of the analytical system presented in Chapter 6 of this work (sub-system B1), attempts to compare different soil structures by relating their resistance to penetration. This appendix presents and exemplifies a method which enables the calculation of the bearing capacity of different soil structures, having changing strength parameters with depth. The presented method may also be implemented for the calculation of bearing capacity values of soil structures under inclined loading.

The method of characteristics, on which this work was based, is one of the accepted methods for the estimation of the bearing capacity of soil under different conditions. The basic assumption is that the whole sheared mass of soil is in a state of failure, and no consideration is given to the elastic response of the soil. The basis for the solution are the soil equilibrium equations and its failure criteria. The obtained solution is a lower limit to the bearing capacity of the soil and is used in many cases as the calculational value for design purposes ( after using the appropriate safety factors ).

The conventional solutions usually assume that the strength parameters values are constant and do not change in the whole soil mass. Within the framework of this project, a solution was developed for determining a lower limit of the soil's bearing capacity under conditions of changing values of strength parameters with depth. The values of both the cohesion and the angle of friction are allowed to change. Similar partial solutions for cohesion or angles of friction changing with depth are presented in Refs. B-8 and B-10.

The importance of relating to changes in the values of soil strength is often encountered while tackling geomechanical engineering problems. Changes in the soil's water content, density and confining pressure in different depths lead to variations in the values of C and $\varphi$. Proper attention given to this issue may lead to more adequate planning under field conditions.

In most cases, the changes in values of the strength parameters of the soil are related to depth. In light of this, only these cases were treated, and the values C and $\phi$ are kept constant in the direction of X (the horizontal direction).

The presented work was carried out under the supervision of Prof. S. Friedman in the framework of studies in "Soil Plasticity in Geomechanics".

## 2. LIMIT EQUILIBRIUM IN THE SOIL WITH CHANGING VALUES OF C AND $\phi$.

A detailed description and analysis of Sokolovsky's basic equations, used for analyzing limit equilibrium in soil, is found in Ref. B-1. The basic assumptions in this process are that the values of the angle of internal friction and the soil cohesion remain constant. This development was done assuming plain strain conditions. The present work broadens the scope of the original equations to cases in which both strength parameters may change their values with depth.

The basic equations used for the solution are the Mohr-Coulomb failure criterion and the equations of equilibrium of forces in an element:

$$\frac{\partial \sigma_x}{\partial x} + \frac{\partial \tau_{xz}}{\partial z} = \gamma \cdot \sin(\alpha) \qquad \text{[B-1]}$$

$$\frac{\partial \sigma_z}{\partial z} + \frac{\partial \tau_{xz}}{\partial x} = \gamma \cdot \cos(\alpha) \qquad \text{[B-2]}$$

where $\alpha$ denotes the angle between the x axis and the horizontal.

Following the work presented in Ref. B-1, two work variables are introduced:

$$\sigma = C \cdot \mathrm{ctg}(\phi) + (\sigma_1 + \sigma_3)/2$$

and $\theta$ which indicates the angle between the direction of the major principal stress and the horizontal.

The stress variables are described through the work variables:

$$\begin{aligned} \sigma_x &= \sigma \cdot (1 + \sin(\phi) \cdot \cos(2\theta)) - C \cdot \cot(\phi) \\ \sigma_z &= \sigma \cdot (1 - \sin(\phi) \cdot \cos(2\theta)) - C \cdot \cot(\phi) \\ \tau_{xz} &= \sigma \cdot \sin(\phi) \cdot \sin(2\theta) \end{aligned} \qquad \text{[B-3]}$$

Equations [B-3] are substituted into equations [B-1] and [B-2], but contradictory to the original work of Sokolovsky, derivation of the strength parameters in the z direction is also performed. The resulting equations are:

$$\left(1+\sin(\phi)\bullet\cos(2\theta)\right)\bullet\frac{\partial\sigma}{\partial x}+\sin(\phi)\bullet\sin(2\theta)\bullet\frac{\partial\sigma}{\partial z}-2\bullet\sigma\bullet\left(\sin(2\theta)\frac{\partial\theta}{\partial x}-\cos(2\theta)\frac{\partial\theta}{\partial z}\right)+ \quad [B\text{-}4]$$

$$+\sigma\bullet\cos(\phi)\bullet\sin(2\theta)\bullet\frac{\partial\phi}{\partial z}=\gamma\bullet\sin(\alpha)$$

$$\sin(\phi)\bullet\sin(2\theta)\bullet\frac{\partial\sigma}{\partial x}+\left(1-\sin(\phi)\bullet\cos(2\theta)\right)\bullet\frac{\partial\sigma}{\partial z}+2\bullet\sigma\bullet\sin(\phi)\bullet\left(\cos(2\theta)\frac{\partial\theta}{\partial x}+\sin(2\theta)\frac{\partial\theta}{\partial z}\right)+ \quad [B\text{-}5]$$

$$+\left(\frac{C}{\sin^2(\phi)}-\sigma\bullet\cos(\phi)\bullet\cos(2\theta)\right)\bullet\frac{\partial\phi}{\partial z}-\cot(\phi)\bullet\frac{\partial C}{\partial z}=\gamma\bullet\cos(\alpha)$$

It can be seen that equations [B-4] and [B-5] are identical to the parallel equations presented in Ref. B-1, except for the expressions containing partial derivatives of C and $\phi$

The development is proceeded by multiplying equation [B-4] with $\sin(\theta\pm\mu)$ (where $\mu=45-\phi/2$) and equation [B-5] with $-\cos(\theta\pm\mu)$ and then summing the two equations. The resulting equation (after multiplying the above by the expression $\pm 1/\cos(\phi)$) is:

$$\left[\frac{\partial\sigma}{\partial x}\mp 2\bullet\sigma\bullet\tan(\phi)\bullet\frac{\partial\theta}{\partial x}-\gamma\bullet\frac{\sin(\alpha\mp\phi)}{\cos(\phi)}\right]\bullet\cos(\theta\mp\mu)+ \quad [B\text{-}6]$$

$$+\left[\frac{\partial\sigma}{\partial z}\mp 2\bullet\sigma\bullet\tan(\phi)\bullet\frac{\partial\theta}{\partial z}-\gamma\bullet\frac{\cos(\alpha\mp\phi)}{\cos(\phi)}\right]\bullet\sin(\theta\mp\mu)\pm$$

$$\pm\frac{\partial\phi}{\partial z}\bullet\left[\sigma\bullet\cos(\theta\mp\mu)-\frac{C\bullet\cos(\theta\mp\mu)}{\sin^2(\phi)\bullet\cos(\phi)}\right]\pm\frac{\partial C}{\partial z}\bullet\frac{\cos(\theta\pm\mu)}{\sin(\phi)}=0$$

As was done by Sokolovsky, the following new variables are introduced:

$$\chi=0.5\bullet\cot(\phi)\bullet\ln\left(\frac{\sigma}{C}\right)$$

$$\xi=\chi+\theta$$

$$\eta=\chi-\theta$$

Assuming the cohesion and angle of internal friction of the soil change linearly with depth, one gets:

$$\frac{\partial \phi}{\partial z} = c_{\phi}^{'}$$

$$\frac{\partial C}{\partial z} = c_{c}^{'}$$

After some elaboration (including the division of equation [B-6] by $2 \bullet \sigma \bullet \tan(\phi)$ and by $\cos(\theta \mp \mu)$, the following equation is obtained:

[B-7]

$$\frac{\partial \xi}{\partial x} + \tan(\theta + \mu) \bullet \frac{\partial \xi}{\partial z} = a = \frac{\gamma \bullet \cos(\theta + \alpha - \mu)}{2 \bullet \sigma \bullet \sin(\phi) \bullet \cos(\theta + \mu)} +$$

$$+ c_{\phi}^{'} \bullet \left[ \frac{1}{2 \bullet \tan(\phi)} - \frac{C \bullet \cos(\theta - \mu)}{2 \bullet \sin^{3}(\phi) \bullet \sigma \bullet \cos(\theta + \mu)} \right] + c_{c}^{'} \bullet \frac{\cos(\theta - \mu)}{2 \bullet \sigma \bullet \sin(\phi) \bullet \cos(\theta + \mu) \bullet \tan(\phi)}$$

[B-8]

$$\frac{\partial \eta}{\partial x} + \tan(\theta - \mu) \bullet \frac{\partial \eta}{\partial z} = b = -\frac{\gamma \bullet \cos(\theta + \alpha + \mu)}{2 \bullet \sigma \bullet \sin(\phi) \bullet \cos(\theta - \mu)} -$$

$$- c_{\phi}^{'} \bullet \left[ \frac{1}{2 \bullet \tan(\phi)} - \frac{C \bullet \cos(\theta + \mu)}{2 \bullet \sin^{3}(\phi) \bullet \sigma \bullet \cos(\theta - \mu)} \right] - c_{c}^{'} \bullet \frac{\cos(\theta + \mu)}{2 \bullet \sigma \bullet \sin(\phi) \bullet \cos(\theta - \mu) \bullet \tan(\phi)}$$

Equations [B-7] and [B-8] are identical to the equations presented in Ref. B-1 except for the parts containing $c_{\phi}^{'}$ and $c_{c}^{'}$. When the values of C and $\phi$ are constant, the basic Sokolovski's equations are obtained. For the case where $\alpha$=0 and $c_{\phi}^{'} = 0$ (only cohesion changes with depth), the single term that is different from Sokolovski's equations is $-\mathrm{ctg}(\phi) \bullet c_{c}^{'}$ (equation [B-5]). This term may be added to the value of $\gamma$ at the right hand side of the equation. For the above case ($\alpha$=0 and $c_{\phi}^{'} = 0$) the right hand sides of equations [B-7] and [B-8] become:

$$\frac{a}{b} = \pm\left(\gamma + c_{c}^{'} \bullet \cot(\phi)\right) \bullet \frac{\cos(\theta \mp \mu)}{2 \bullet \sigma \bullet \sin(\phi) \bullet \cos(\theta \pm \mu)} \qquad \text{[B-9]}$$

It can be seen that the influence of changes in the soil cohesion is similar to the influence of the soil density. A constant increase of cohesion with depth can be simulated by increasing the density of the given soil.

Solving the differential equations (as was done in Ref. B-1) yields the following two families of curves:

$$\frac{dz}{dx} = \tan(\theta - \mu) \qquad \frac{d\eta}{dx} = b \qquad \text{[B-10]}$$

$$\frac{dz}{dx} = \tan(\theta + \mu) \qquad \frac{d\xi}{dx} = a \qquad \text{[B-11]}$$

Using the chain rule to get the following differentials:

$$d\sigma = \frac{\partial\sigma}{\partial x} \bullet dx + \frac{\partial\sigma}{\partial z} \bullet dz = \frac{\partial\sigma}{\partial x} \bullet dx + \frac{\partial\sigma}{\partial z} \bullet \tan(\theta \pm \mu) \bullet dx$$

$$d\theta = \frac{\partial\theta}{\partial x} \bullet dx + \frac{\partial\theta}{\partial z} \bullet \tan(\theta \pm \mu) \bullet dx$$

Combining the above in equation [B-6] (considering the slopes of the characteristics) will give the change in the values of $\sigma$ and $\theta$ along the characteristic curves or slip lines. Dividing equation [B-6] with $\cos(\theta \mp \mu)$, multiplying with dx and rearranging will yield:

[B-12]

$$\left(\frac{\partial\sigma}{\partial x} \bullet dx + \frac{\partial\sigma}{\partial z} \bullet \tan(\theta \mp \mu) \bullet dx\right) \mp 2 \bullet \sigma \bullet \tan\phi \bullet \left(\frac{\partial\theta}{\partial x} \bullet dx + \frac{\partial\theta}{\partial x} \bullet \tan(\theta \mp \mu) \bullet dx\right) -$$

$$- \frac{\gamma}{\cos\phi} \bullet (\sin(\alpha \mp \phi) \bullet dx + \cos(\alpha \mp \phi) \bullet \tan(\theta \mp \mu) \bullet dx) \pm$$

$$\pm C_{\phi}' \bullet [\sigma - \frac{C}{\sin^2\phi \bullet \cos\phi}] \bullet dx \pm C_C' \bullet \frac{\cos(\theta \pm \mu)}{\sin\phi \bullet \cos(\theta \mp \mu)} \bullet dx = 0$$

As before, equation [B-12] is identical to the equations presented in Ref. B-1 except for the terms that contain $c_{\phi}'$ and $c_c'$.

Nullifying the value of $\alpha$ (the x axis is horizontal), and rewriting as finite differences equations, one gets along the $\eta$ characteristics:

[B-13]

$$(z_{i,j} - z_{i-1,j}) = (x_{i,j} - x_{i-1,j}) \bullet \tan(\bar{\theta}_j - \bar{\mu}_j)$$

$$(\sigma_{i,j} - \sigma_{i-1,j}) - 2 \bullet \bar{\sigma}_j \bullet (\theta_{i,j} - \theta_{i-1,j}) \bullet \tan(\bar{\phi}_j) = \gamma \bullet [(z_{i,j} - z_{i-1,j}) - \\ - \tan(\bar{\phi}_j) \bullet (x_{i,j} - x_{i-1,j})] - F_c \bullet (x_{i,j} - x_{i-1,j})$$

where:

$$F_c = c'_\phi \bullet \left( \bar{\sigma}_j - \frac{\bar{c}_j}{\sin^2(\bar{\phi}_j) \bullet \cos(\bar{\phi}_j)} \right) + c'_c \bullet \frac{\cos(\bar{\theta}_j + \bar{\mu}_j)}{\sin(\bar{\phi}_j) \bullet \cos(\bar{\theta}_j - \bar{\mu}_j)}$$

is the term which changes when the strength parameters are not constant.

And along the $\xi$ characteristics:

[B-14]

$$(z_{i,j} - z_{i,j-1}) = (x_{i,j} - x_{i,j-1}) \bullet \tan(\bar{\theta}_i - \bar{\mu}_i)$$

$$(\sigma_{i,j} - \sigma_{i,j-1}) - 2 \bullet \bar{\sigma}_i \bullet (\theta_{i,j} - \theta_{i,j-1}) \bullet \tan(\bar{\phi}_i) = \gamma \bullet [(z_{i,j} - z_{i,j-1}) - \\ - \tan(\bar{\phi}_i) \bullet (x_{i,j} - x_{i,j-1})] - F_d \bullet (x_{i,j} - x_{i,j-1})$$

where:

$$F_d = c'_\phi \bullet \left( \bar{\sigma}_i - \frac{\bar{c}_i}{\sin^2(\bar{\phi}_i) \bullet \cos(\bar{\phi}_i)} \right) + c'_c \bullet \frac{\cos(\bar{\theta}_i - \bar{\mu}_i)}{\sin(\bar{\phi}_i) \bullet \cos(\bar{\theta}_i - \bar{\mu}_i)}$$

The variable $\bar{v}$ denotes the variable value at an intermediate point. This value was iteratively computed during program execution. For example:

- first stage $\bar{v}_i = v_{i,j-1}$
- calculation of variables including $v_{i,j}$
- second stage $\bar{v}_i = 0.5 \bullet (v_{i,j-1} + v_{i,j})$

- recalculation of variables according to new value of $\bar{v}_i$ The variables $\theta,\sigma,\phi,\mu,c$ were calculated in the above fashion to get their values at the midpoint between two grid points on the network.

The resulting finite difference equations for the computation of $\theta,\sigma,x,z$ under conditions of changing strength parameters with depth are:

$$x_{i,j} = \frac{z_{i-1,j} - z_{i,j-1} + x_{i,j-1} \bullet \tan(\bar{\theta}_i + \bar{\mu}_i) - x_{i-1,j} \bullet \tan(\bar{\theta}_j - \bar{\mu}_j)}{\tan(\bar{\theta}_i + \bar{\mu}_i) - \tan(\bar{\theta}_j - \bar{\mu}_j)} \qquad [B\text{-}15]$$

$$z_{i,j} = z_{i-1,j} + \left(x_{i,j} - x_{i-1,j}\right) \bullet \tan(\bar{\theta}_j - \bar{\mu}_j)$$

$$\sigma_{i,j} = \frac{\gamma \bullet \left(c_1 \bullet \bar{\sigma}_i \bullet \tan(\bar{\phi}_i) + d_1 \bullet \bar{\sigma}_j \bullet \tan(\bar{\phi}_j)\right) + \sigma_{i,j-1} \bullet \bar{\sigma}_j \bullet \tan(\bar{\phi}_j)}{\bar{\sigma}_i \bullet \tan(\bar{\phi}_i) + \bar{\sigma}_j \bullet \tan(\bar{\phi}_j)}$$

$$+ \frac{\sigma_{i-1,j} \bullet \bar{\sigma}_i \bullet \tan(\bar{\phi}_i) + 2 \bullet \bar{\sigma}_i \bullet \bar{\sigma}_j \bullet \tan(\bar{\phi}_i) \bullet \tan(\bar{\phi}_j) \bullet (\theta_{i,j-1} - \theta_{i,j-1})}{\bar{\sigma}_i \bullet \tan(\bar{\phi}_i) + \bar{\sigma}_j \bullet \tan(\bar{\phi}_j)}$$

$$\theta_{i,j} = \frac{\gamma \bullet (d_1 - c_1) + (\sigma_{i,j-1} - \sigma_{i-1,j}) + 2 \bullet \left(\bar{\sigma}_i \bullet \tan(\bar{\phi}_i) \bullet \theta_{i,j-1} + \bar{\sigma}_j \bullet \tan(\bar{\phi}_j) \bullet \theta_{i-1,j}\right)}{2 \bullet \left(\bar{\sigma}_i \bullet \tan(\bar{\phi}_i) + \bar{\sigma}_j \bullet \tan(\bar{\phi}_j)\right)}$$

where:

$$c_1 = (z_{i,j} - z_{i-1,j}) - \left(x_{i,j} - x_{i-1,j}\right) \bullet \left(\tan(\bar{\phi}_j) + \frac{F_c}{\gamma}\right)$$

$$d_1 = (z_{i,j} - z_{i,j-1}) + \left(x_{i,j} - x_{i,j-1}\right) \bullet \left(\tan(\bar{\phi}_i) + \frac{F_d}{\gamma}\right)$$

Equations [B-15] are the basis for a computer software written in order to find a lower bound for the bearing capacity of a plate grouser. The main reason for choosing a plate grouser as the loading element was the ability to analyze the soil bearing capacity under inclined loading. The above is relevant both in geomechanical problems and in the analysis of ground movement of vehicles (tracked and wheeled).

## 3. COMMENTS ON THE COMPUTATIONAL SYSTEM

The computational software based on the finite difference equations [B-15], was written in Turbo Pascal. The graphical analysis of the results was implemented with the aid of Quattro Pro 4.

The following remarks relate to the calculational procedure and software system:

1. The element that loads the soil is a plate grouser that includes vertical and horizontal plates. The dimensions of both plates are changeable. It is assumed that the soil enclosed between the two plates and the diagonal is not active in the shearing process, but operates as part of the plate grouser;

2. During the first phase, the failure zones dimensions are determined assuming that the soil is weightless. The inclination of the slip line at point A (see Fig. B-1) is fixed as $\alpha$ (its value is changed from one iteration to the next). According to $\alpha$, the length of section AB (the diagonal of the plate grouser), and the angles BAC and ACB (which equals to $90-\phi$), the dimensions of the active zone are determined. Using the length of BC, the angle CBD ($45+\alpha-\phi/2$) and the formula of the logarithmic spiral , the radial zone dimensions are calculated next. Finally L, the length of the passive zone is determined by the use of section BD and the angles DBE and BED (equaling $45-\phi/2$). Since the boundary conditions on BE are known, the solution process starts from this line through the passive and radial zones up to the active zone whose vertex should coincide with point A. The boundary conditions on the line AB are the known ratio of x to z and the assumption that the inclination of all slip lines emanating from line AB is $\alpha$.

3. Each zone was divided into a network of characteristic lines on which the process proceeds. The passive zone was solved as a Cauchy problem and the radial zone as a Goursat problem. The active zone was solved as a mixed boundary-value problem where at the boundary line (the diagonal of the plate grouser), the values of $\theta$ (a function of $\alpha$ and $\varphi$) and the relationship between z and x are known.

4. The solution process (based on the initial assumption about the geometry of the plastic zones in a weightless soil), yields a grid where the apex of the active zone does not necessarily coincide with point A. The above process is iteratively repeated until the distance between the points is within predetermined tolerance. The obtained network contains the required solution for a certain $\alpha$ value.

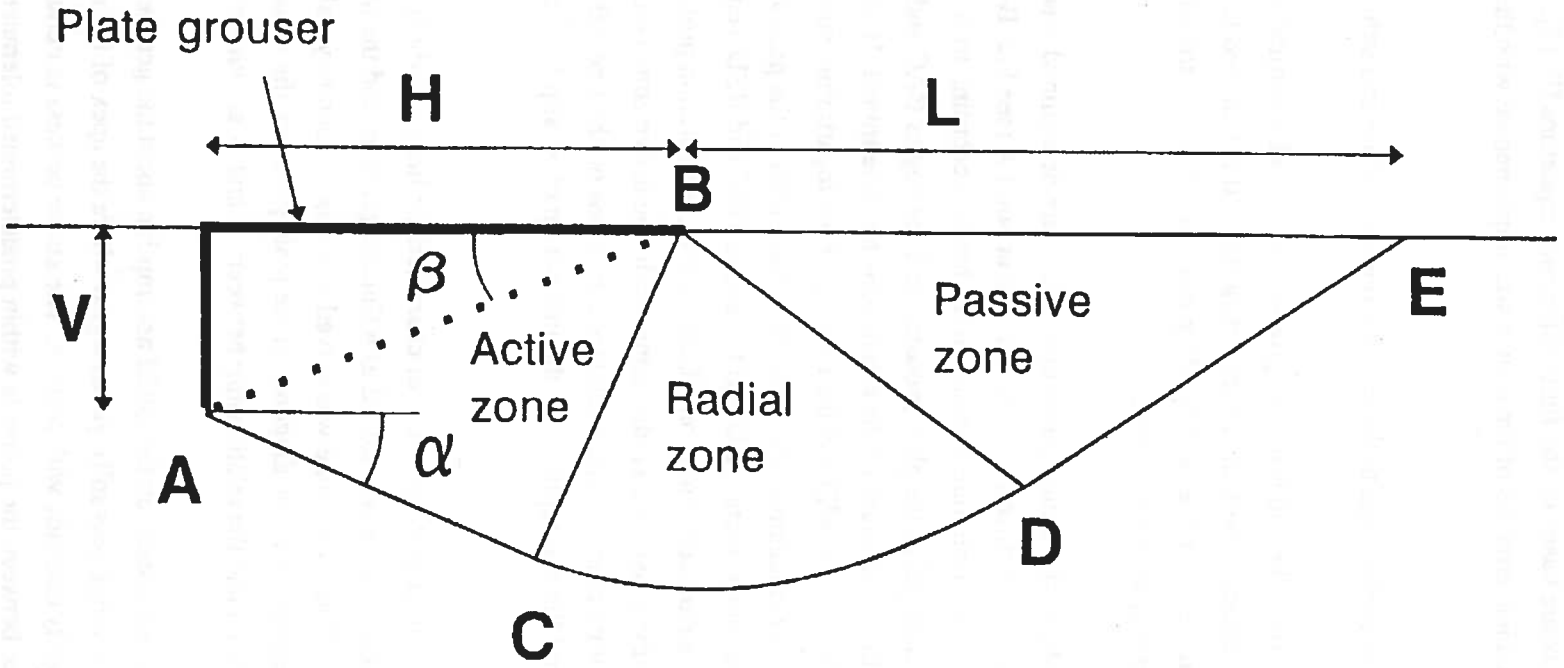


Fig. B-1 Schematic description of failure zones under a plate grouser.

ציור מס. B-1 תאור סכימתי של איזורי ההרס בקרקע תחת פלטת העמסה

5. When solution is reached for a given value of $\alpha$, the values of both $\sigma$ and $\theta$ are known at section AB. Summation of the forces at each grid point, in addition to the requirement of forces equilibrium on the plate grouser, yield the vertical and horizontal forces acted on the plate in a limit equilibrium state.

6. The program is operated for different values of $\alpha$ from zero at 5 deg. intervals until one of the following limits is met:

   1) $\alpha \leq 90 + \phi - \beta$
   2) $\alpha \leq 45 + \phi/2$

   The first condition defines the point at which the active zone disappears and line AB is turned to be a slip line. The second condition limits the direction of the slip line so that the value of $\theta$ will not exceed 90 deg. (assuming that the vertical plate is not pulled back).

7. The main code of computer programs was written in Turbo Pascal 6.0. The program (FDCINC.PAS) computes, for given data, the values of the force exerted on the plate grouser and the inclination of the force. all that as a function of $\alpha$. The data needed for the computing process are the soil strength parameters, strength parameters gradients and the dimensions of the plate grouser. In addition the program creates an output file containing the location of grid points in the network of characteristics for a given value of $\alpha$. Analysis and graphical presentation of the results were performed with Quattro Pro 4.0 on the output files obtained from the above program.

## 4. PRESENTATION OF RESULTS.

### 4.1. Constant C and $\phi$ values

The software was operated for constant strength parameters in order to allow comparison between the obtained results and known solutions for the bearing capacity of soil under vertical and inclined loading. Figs. B-2a and B-2b describe the results of the software operation under the following conditions:

A) $C = 0.5$ kg/cm$^2$
B) $\phi = 1°$ .very small value (zero cannot be handled due to numerical instabilization)
C) $\gamma = 1700$ kg/m$^3$
D) qpas = 0 , the plate is at ground level and no overburden on the ground.

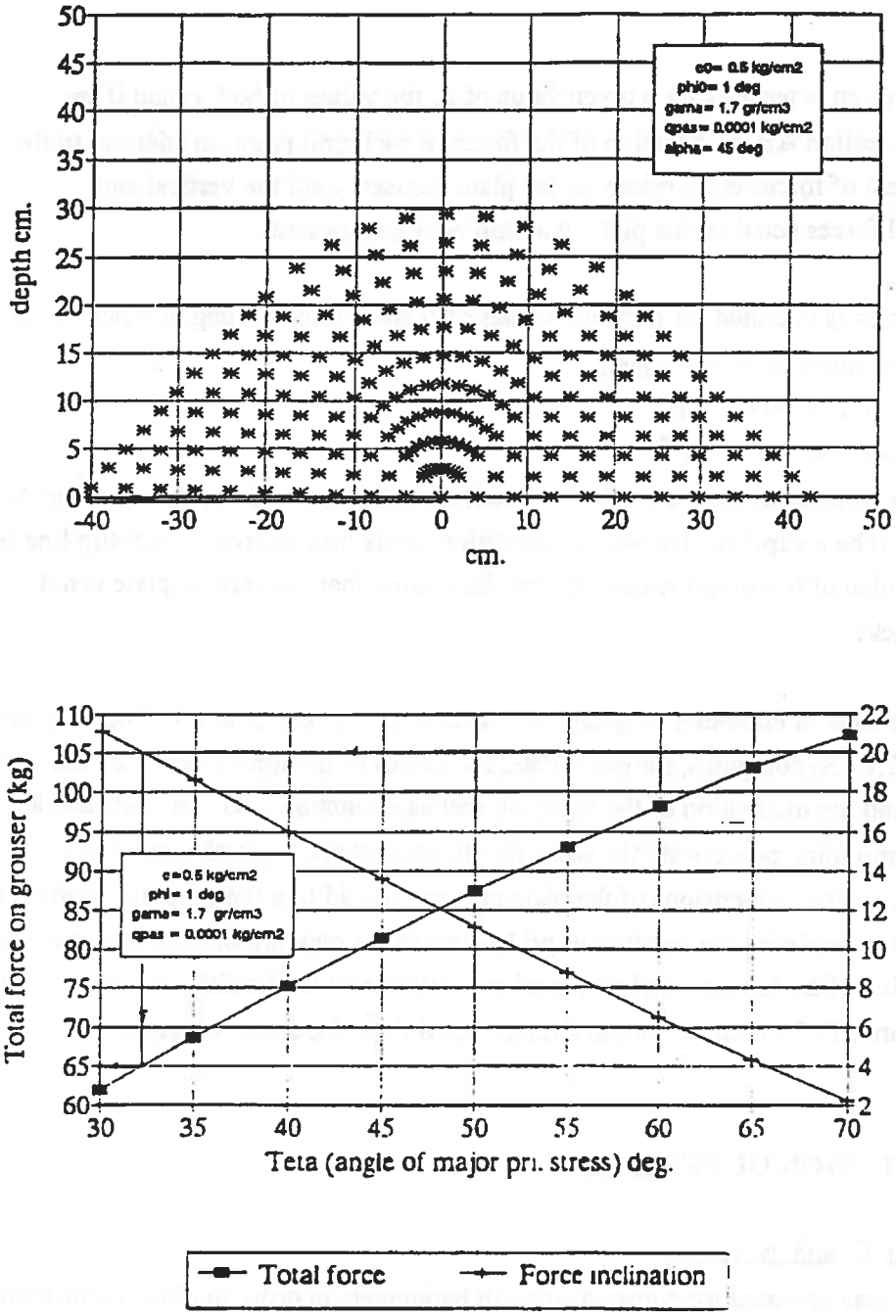


Fig. B-2 Behavior of a frictionless soil with constant strength parameters, under a plate grouser (1 cm. height and 40 cm. width) loading:
a. Slip line network for $\alpha$=45°.
b. Bearing capacity and force inclination.

ציור מס. B-2 התנהגות קרקע חסרת חיכוך עם פרמטרי חוזק קבועים, תחת פלטת העמסה (1 סמ. ג בה ר 40 סמ. רוחב):
a. רשת קווי החלקה עבור $\alpha = 45°$.
b. יכולת התסבולת ונטית הכח על פלטת העמיסה.

The general form of the slip lines and failure zones (Fig. B-2a) is in accordance with the known solutions in the literature. The vertical plate dimensions were minimized to 1 cm. (40 cm. length of the horizontal plate), so that the result should be very similar to that expected for a flat foundation in a purely cohesive soil. Fig. B-2b presents the relations between the maximal force which can be exerted on the plate and the inclination of that force. The maximal force in this case is about 108 kg. and the corresponding inclination angle is 2° (almost vertical). The pressure on the plate is (40 cm. plate width and considering the plain strain conditions):

$$q = \frac{108}{40 \cdot 1} = 2.7 \quad kg / cm2$$

For purely cohesive soil $N_C = 5.14$ according to Ref. B-4 and $N_C = 5.53$ according to Ref. B-3, and the resulting bearing capacity value is:

$$q = C \cdot N_C = 2.57 \div 2.765 \quad kg / cm2$$

As can be seen the results are practically the same.

Figs. B-3, B-4 and B-5 describe the results of the programs operated on a cohesionless soil with the following conditions:

A) $C = 0.001$ kg/cm$^2$. cohesion is given a very small value to prevent instabilization at the singular point.

B) $\phi = 40°$

C) $\gamma = 1700$ kg/m$^3$

D) qpas = 0 . the plate is at ground level and no overburden on the ground.

Figs. B-3 to B-5 present the results obtained for a plate grouser having a horizontal plate of 40 cm. length and vertical plate of 1 cm., 10 cm., and 20 cm. respectively.

The maximum load reached in the 1 cm. height plate grouser is (Fig. B-3b) 120 kg. which corresponds to **120/40/1=3.0 kg/cm$^2$**. The bearing capacity coefficients for the above soil are:

- according to Ref. B-3 - $N_C = 84$ $N_\gamma = 100$
- according to the more conservative Ref. B-4 - $N_C = 75$ $N_\gamma = 80$

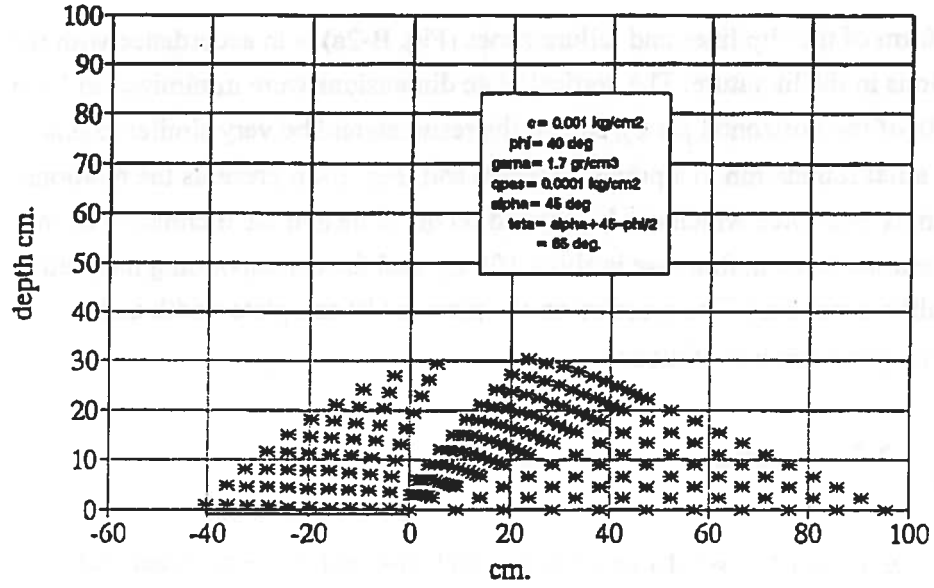


(a)

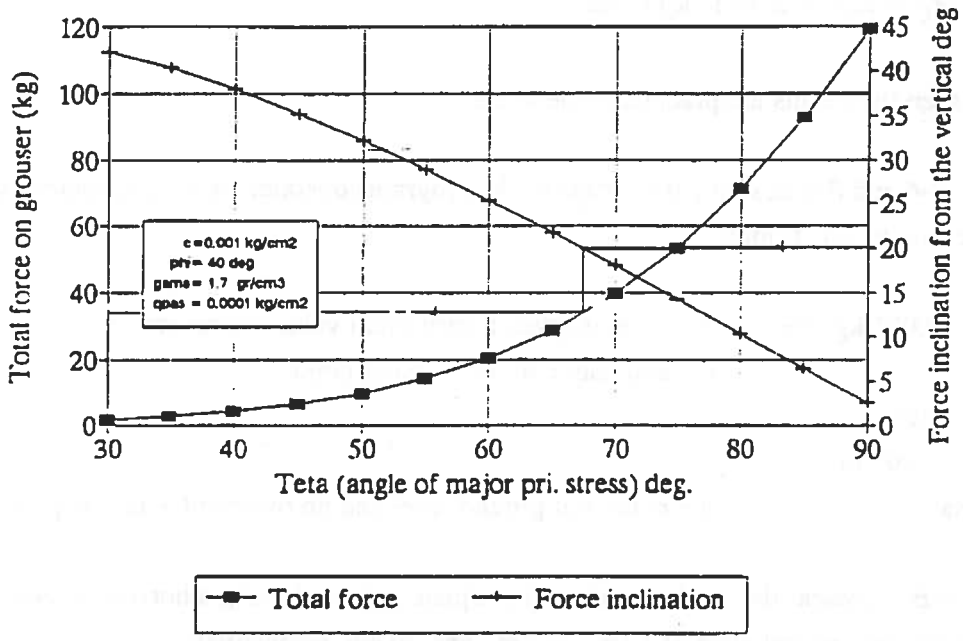


(b)

Fig. B-3 Behavior of a cohesionless soil with constant strength parameters, under a plate grouser (1 cm. height and 40 cm. width) loading:
a. Slip line network for $\alpha$=45°.
b. Bearing capacity and force inclination.

ציור מס. B-3 התנהגות קרקע חסרת קוהזיה עם פרמטרי חוזק קבועים, תחת פלטת העמסה (1 סמ. גובה ר 40 סמ. רוחב):
a. רשת קווי החלקה עבור $\alpha = 45°$.
b. יכולת התסבולת ונטית הכח על פלטת העמיסה.

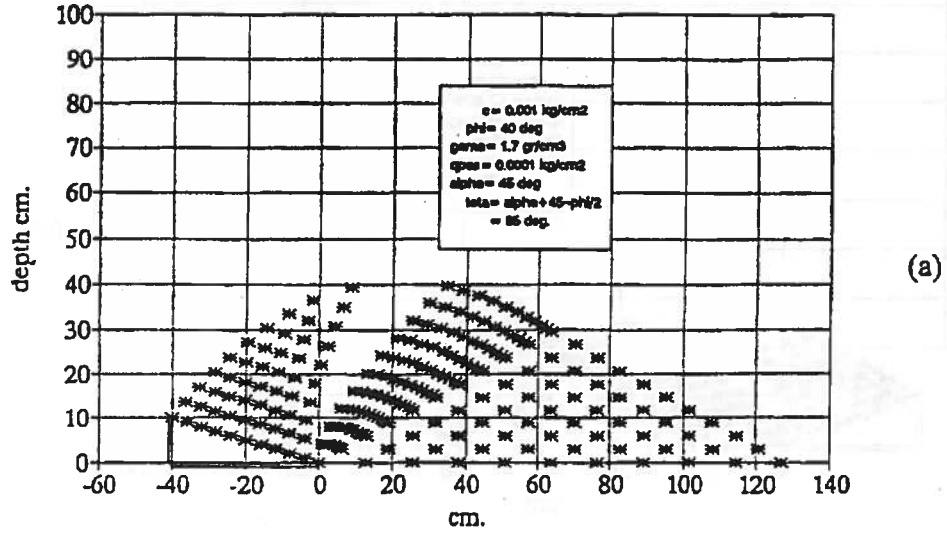


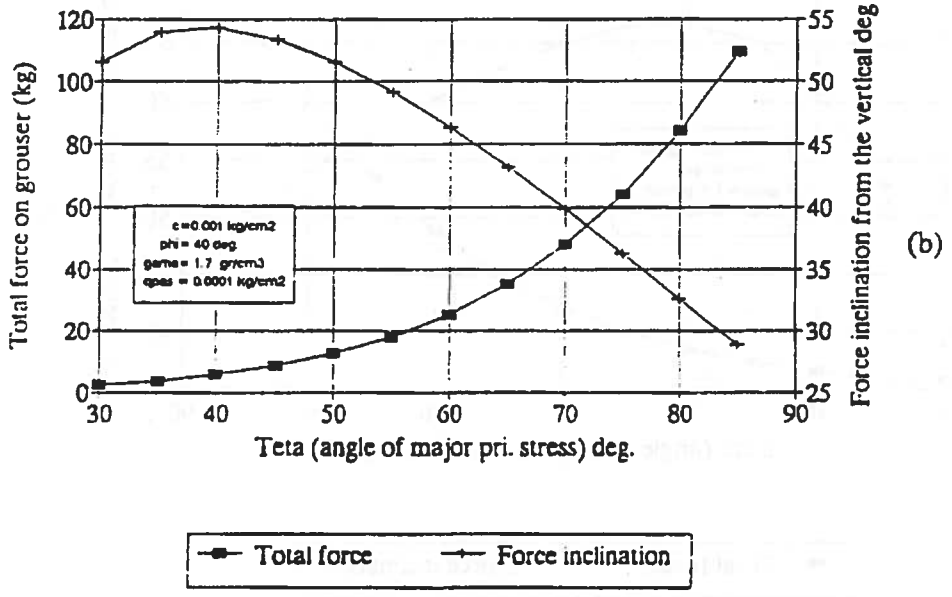


Fig. B-4 Behavior of a cohesionless soil with constant strength parameters, under a plate grouser (10 cm. height and 40 cm. width) loading:
a. Slip line network for $\alpha$=45°.
b. Bearing capacity and force inclination.

ציור מס. B-4 התנהגות קרקע חסרת קוהזיה עם פרמטרי חוזק קבועים, תחת פלטת העמסה (10 סמ. גובה ר 40 סמ. רוחב):
a. רשת קווי החלקה עבור $\alpha = 45°$.
b. יכולת התסבולת ונטית הכח על פלטת העמיסה.

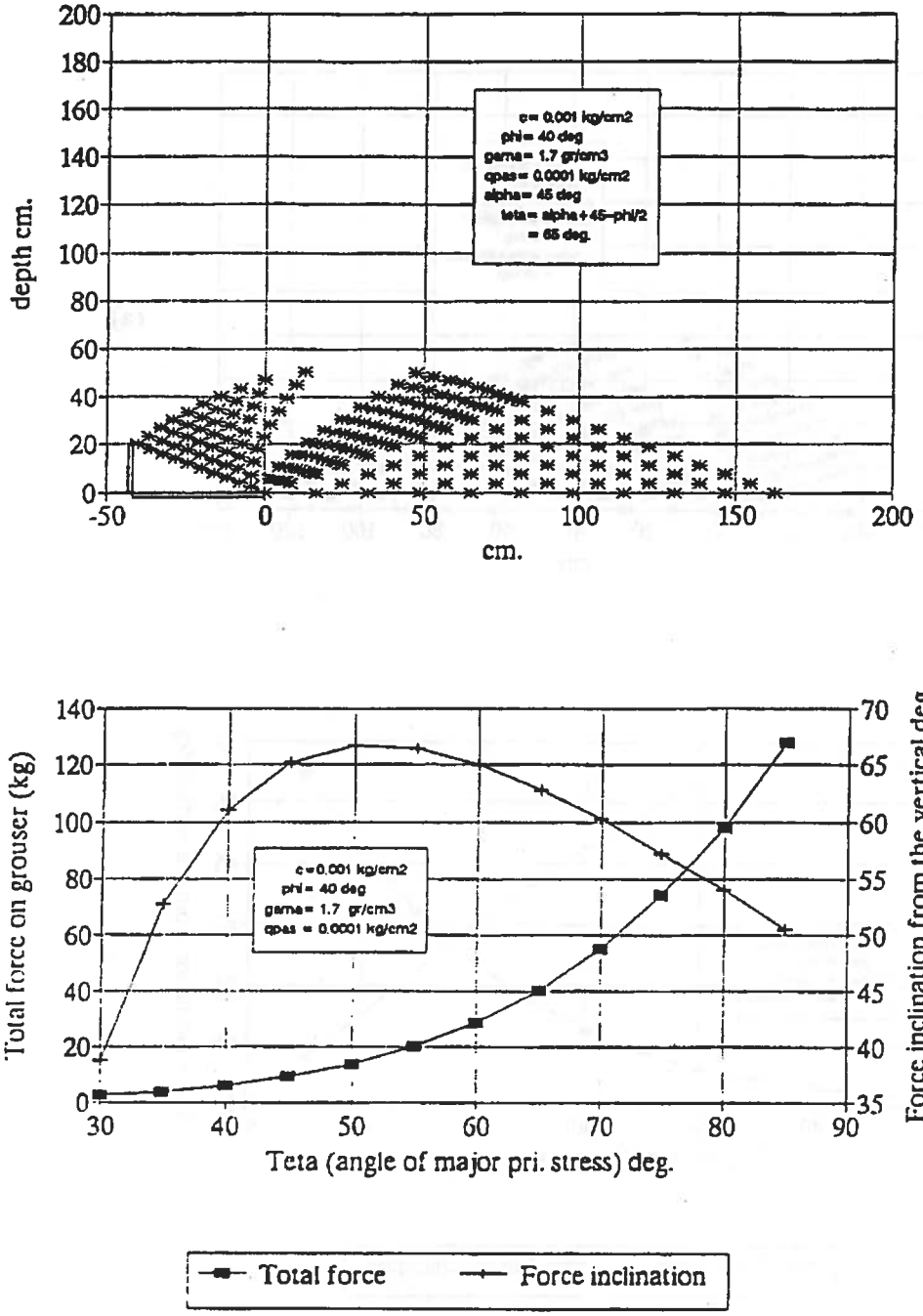


Fig. B-5 Behavior of a cohesionless soil with constant strength parameters, under a plate grouser (20 cm. height and 40 cm. width) loading:
a. Slip line network for $\alpha$=45°.
b. Bearing capacity and force inclination.

ציור מס. B-5 התנהגות קרקע חסרת קוהזיה עם פרמטרי חוזק קבועים, תחת פלטת העמסה (20 סמ. גובה ר 40 סמ. רוחב):
a. רשת קווי החלקה עבור $\alpha = 45°$.
b. יכולת התסבולת ונטית הכח על פלטת העמיסה.

And the calculated bearing capacity is:

$$q = C \bullet N_C + 0.5 \bullet \gamma \bullet B \bullet N_\gamma = 2.8 + 3.5 \ \ kg/cm2$$

As in the previous case the results are very close and satisfactory.

Comparisons were also made with published results of the bearing capacity under inclined loading. According to Ref. B-4, the following relation describes the changes in bearing capacity values with load inclination:

$$q = i_C \bullet C \bullet N_C + i_\gamma \bullet 0.5 \bullet \gamma \bullet B \bullet N_\gamma$$

where:

$$i_C = (1 - i/90)^2$$

$$i_\gamma = (1 - i/\phi)^2$$

i being the inclination in deg. and $\phi$ the internal angle of friction.

If we take as an example the results presented in Fig. B-2 for cohesive soil, at an inclination of 20° the maximal load is 65 kg. which corresponds to 65/108=0.60 of the maximum vertical load. The decrease in the bearing capacity value according to Ref. B-4 is:

$$i_C = (1 - 20/90)^2 = 0.6$$

For inclination angle of 10° the result of the presented computational system is 84% (of the maximum bearing capacity), compared to 79% as predicted by Ref. B-4.

The same comparisons were made for the frictional soil whose results are given in Fig. B-3. At an inclination angle of 40°, about 3% of the maximum load can still be carried, a result which is only slightly different to that expected in Ref. B-4 (bearing capacity decreasing to zero). The reason can be ascribed to the fact that the plate grouser's height is not zero but 1 cm., which "delays" nullification of the bearing capacity to an inclination angle of 43°. For an inclination angle of 20° the present computational system yields 28% of maximum load compared to 25% predicted by Ref. B-4.

Summarizing the above, it seems that operating the computational system on soils with constant strength parameters yields good results compared to those known in the literature. Comparing Figs. B-3 to B-5 shows that as expected, an increase in the dimension of the

vertical plate of the plate grouser, causes a parallel increase in both the maximum load and the maximum possible angle of inclination.

Use of the presented system may provide solutions for various geometric dimensions of the plate grouser. In foundation engineering, in cases where the horizontal load is high, it is sometimes recommended to increase the vertical dimension of the foundation in a similar way as can be done in the plate grouser. When vehicles wheels interaction with the soil is concerned, the presented system may be used to derive soil bearing capacity estimations under different loading conditions, including braking conditions where the horizontal component of the load is high.

4.2. Changing values of C and $\phi$

Figs. B-6 and B-7 describe the results of the system operation under the following conditions:

A) $C = 0.001$ kg/cm$^2$
B) $\phi = 35°$, at surface level
C) $\gamma = 1700$ kg/m$^3$
D) qpas = 0

Fig. B-6 presents the results for the case where $\phi$ grows with depth at a rate of 0.1 deg/cm. These phenomena are observed in conditions where soil density increases with depth. Fig. B-7 shows the results for the case of decreasing $\phi$ value at a rate of 0.1 deg/cm. The above is often expected due to the increase in the confinement pressure with depth. Both examples were run for a flat plate grouser with dimensions of 1/40 cm. Fig. B-8 and B-9 contain the results for cases similar to the above but with a plate grouser having dimensions of 20/40 cm.

Fig. B-10 gives the results for a purely cohesive soil where cohesion is 0.1 kg/cm$^2$ at ground surface and growing at a rate of 0.05 kg/cm$^2$/cm. with depth. The results were compared to the case of an increased $\gamma$ value of the soil (see section 2 and equation [B-9]) and the results were identical.

A plastic solution for frictionless soil whose cohesion grows linearly with depth was presented in Ref. B-8. Comparisons made between the results given in Ref. B-8 and the more general system presented herein, gave identical results. Ref. B-9 compares and

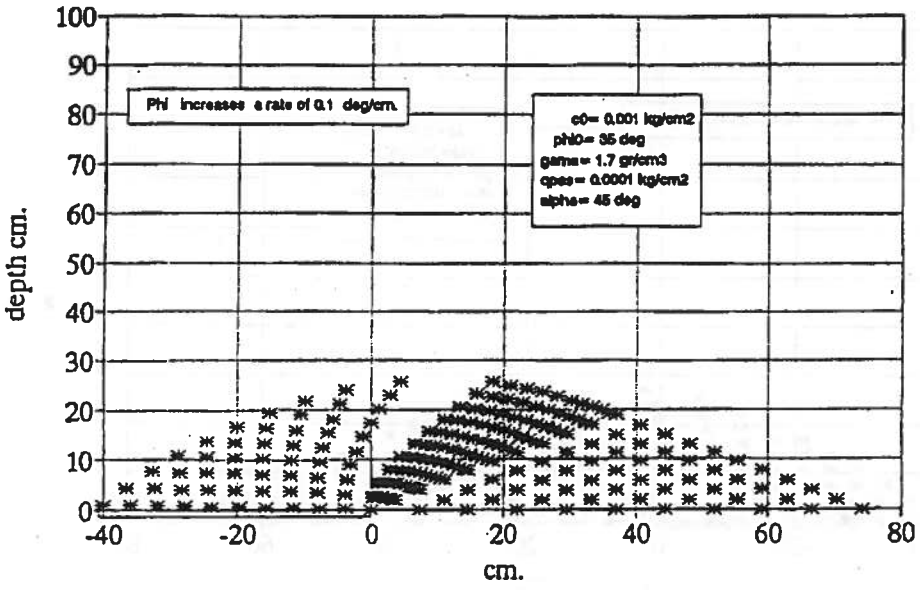


a.

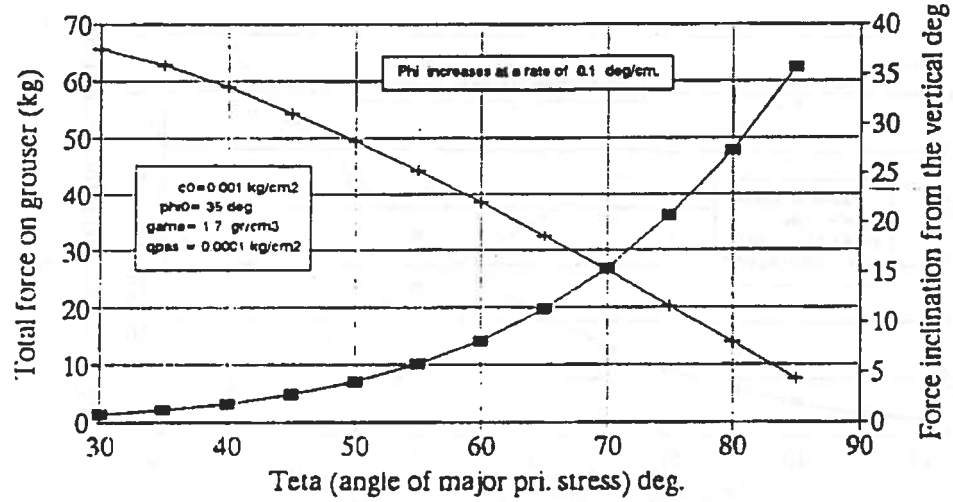


b.

Fig. B-6 Behavior of a cohesionless soil with an increasing $\phi$ value with depth, under a plate grouser (1 cm. height and 40 cm. width) loading:
a. Slip line network for $\alpha=45°$.
b. Bearing capacity and force inclination.

ציור מס. B-6 התנהגות קרקע חסרת קוהזיה כשערך $\phi$ עולה עם העומק, תחת פלטת העמסה (1 סמ. גובה ר' 40 סמ. רוחב):
a. רשת קווי החלקה עבור $\alpha = 45°$.
b. יכולת התסבולת ונטית הכח על פלטת העמיסה.

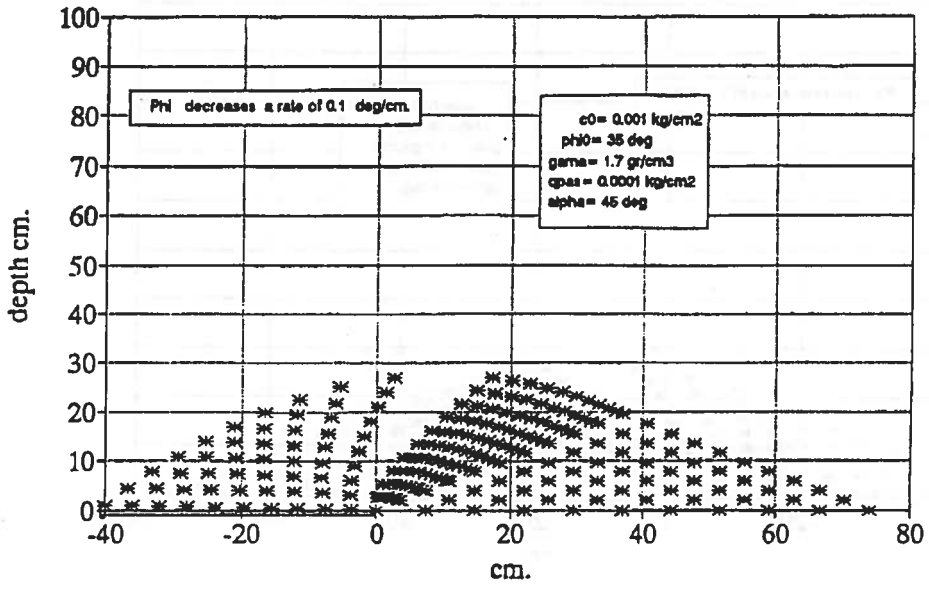


a.

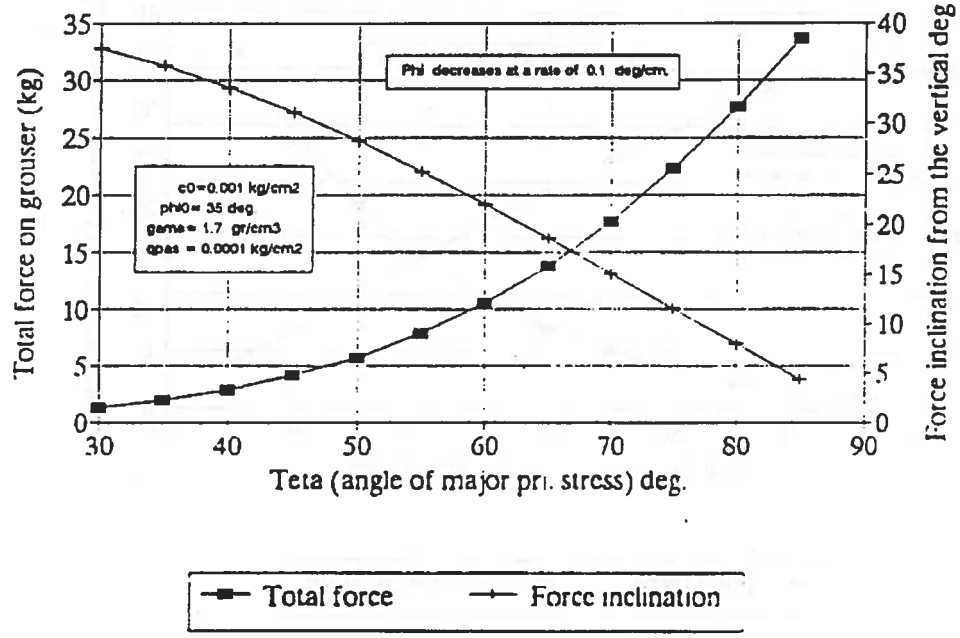


b.

Fig. B-7 Behavior of a cohesionless soil with a decreasing $\phi$ value with depth, under a plate grouser (1 cm. height and 40 cm. width) loading:
a. Slip line network for $\alpha$=45°.
b. Bearing capacity and force inclination.

ציור מס. B-7 התנהגות קרקע חסרת קוהזיה כשערך $\phi$ יורד עם העומק, תחת פלטת העמסה (1 סמ. גובה ר 40 סמ. רוחב):
a. רשת קווי החלקה עבור $\alpha = 45°$.
b. יכולת התסבולת ונטית הכח על פלטת העמיסה.

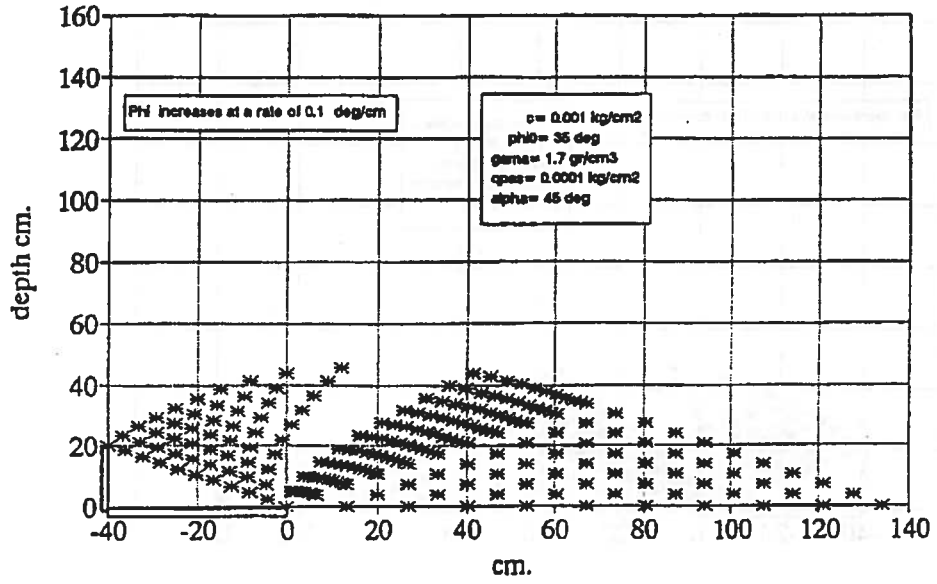


a.

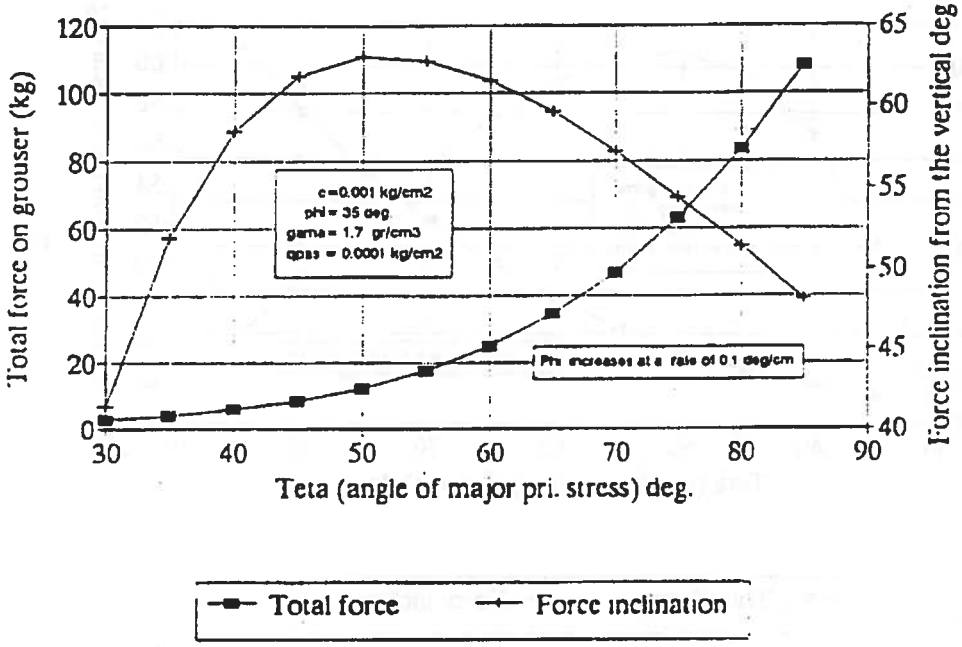


b.

Fig. B-8 Behavior of a cohesionless soil with an increasing $\phi$ value with depth, under a plate grouser (20 cm. height and 40 cm. width) loading:
a. Slip line network for $\alpha$=45°.
b. Bearing capacity and force inclination.

ציור מס. B-8 התנהגות קרקע חסרת קוהזיה כשערך $\phi$ עולה עם העומק, תחת פלטת העמסה (20 סמ. גובה ר 40 סמ. רוחב):
a. רשת קווי החלקה עבור $\alpha = 45°$.
b. יכולת התסבולת ונטית הכח על פלטת העמיסה.

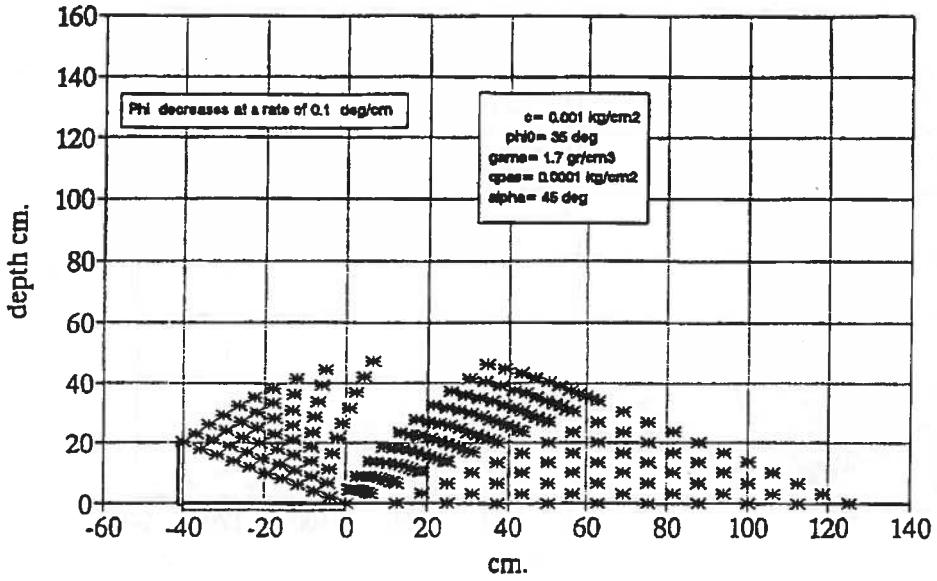


a.

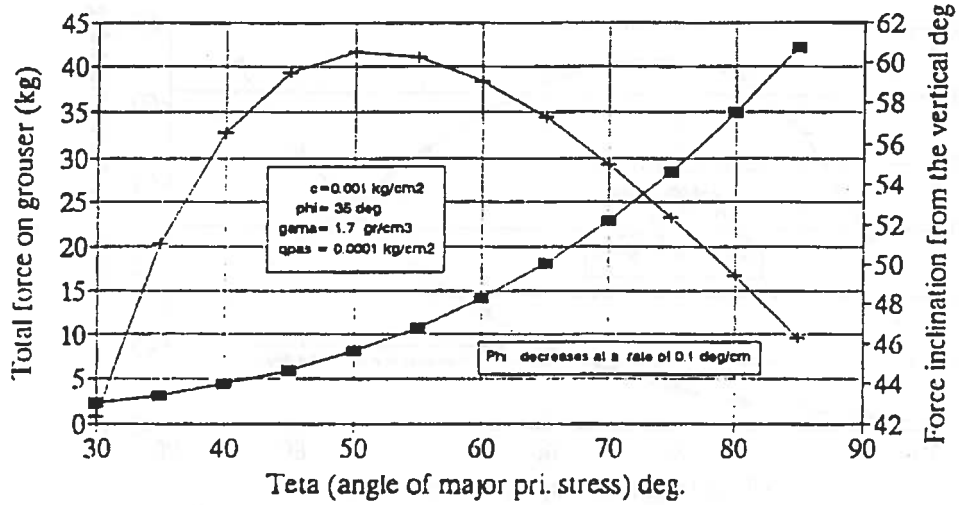


b.

Fig. B-9 Behavior of a cohesionless soil with a decreasing $\phi$ value with depth, under a plate grouser (20 cm. height and 40 cm. width) loading:
a. Slip line network for $\alpha$=45°.
b. Bearing capacity and force inclination.

ציור מס. B-9 התנהגות קרקע חסרת קוהזיה כשערך $\phi$ יורד עם העומק, תחת פלטת העמסה (20 סמ. גובה ר 40 סמ. רוחב):
a. רשת קווי החלקה עבור $\alpha = 45°$.
b. יכולת התסבולת ונטית הכח על פלטת העמיסה.

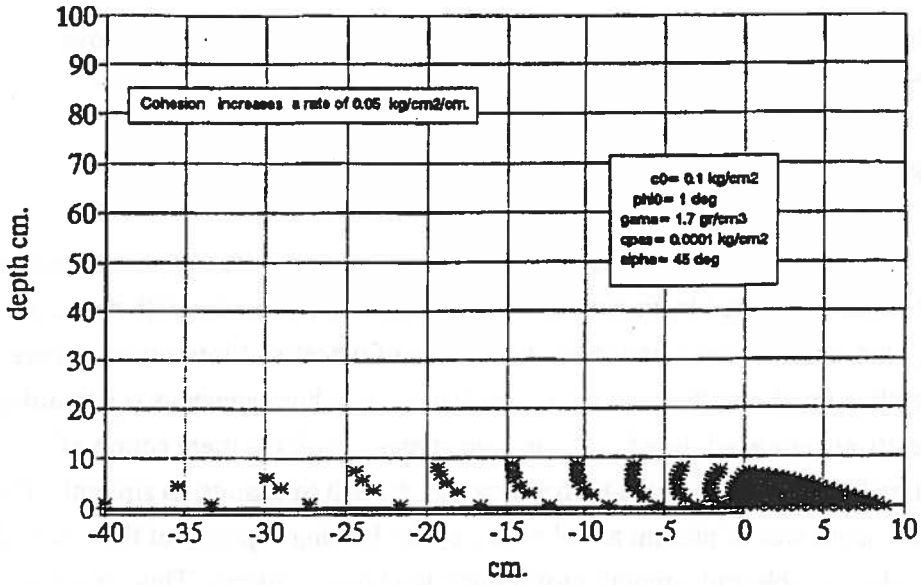


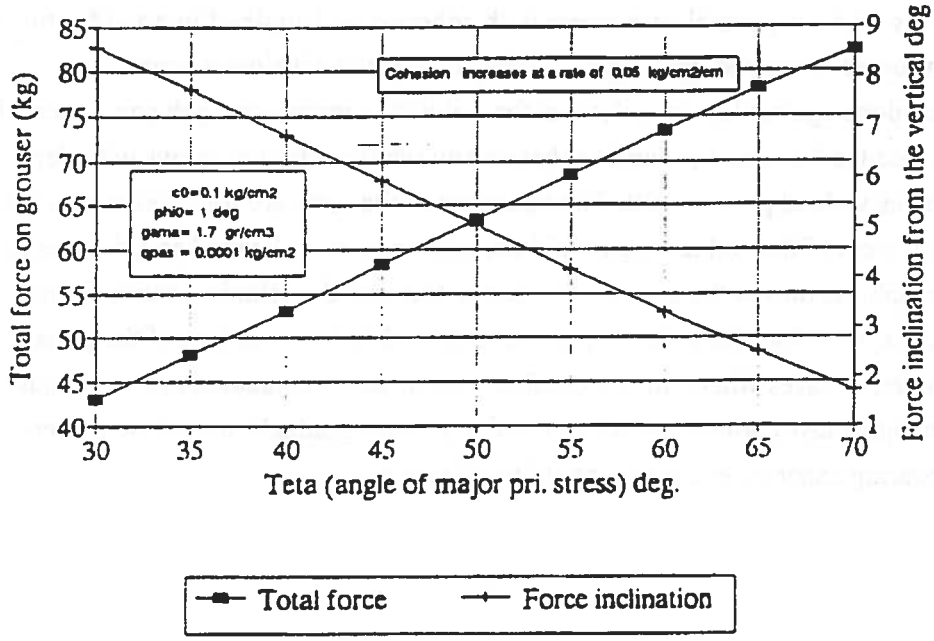


Fig. B-10 Behavior of a frictionless soil with an increasing C value with depth. under a plate grouser (1 cm. height and 40 cm. width) loading:
a. Slip line network for $\alpha$=45°.
b. Bearing capacity and force inclination.

ציור מס. B-10 התנהגות קרקע חסרת חיכוך כשערך C עולה עם העומק, תחת פלטת העמסה (20 סמ. גובה ר 40 סמ. רוחב):
a. רשת קווי החלקה עבור $\alpha = 45°$.
b. יכולת התסבולת ונטית הכח על פלטת העמיסה.

concludes with preference of the method given in Ref. B-8 over two earlier methods dealing with the same problem.

## 5. SUMMARY

Changes with depth in the value of the soil strength parameters are often observed in the field. These changes are caused by variations in the confinement pressure with depth, in the soil density and water content, and more. In the area of wheel-soil interaction, where the relevant depth is much smaller than in Geomechanics, non homogeneous soil profiles are also frequently encountered. In addition, in some types of soil the mere action of repetitive loading by vehicles or aircraft wheels causes the soil to change its strength. The main goal of this work was to present a tool where by the bearing capacity of the soil could be evaluated under variable soil strength profiles and loading conditions. This tool may help in assessing soil behavior in the above mentioned cases.

The work deals with the general case where both cohesion and angle of internal friction of the soil are allowed to change with depth. Verification of the developed computer programs was done against known solutions for soil with constant strength parameters, for cases of inclined loading and for purely cohesive soil whose cohesion grows with depth. All comparisons yielded good results. The operation of the software for cases where the strength parameters of the soil undergo rapid changes, such as in layered soil, frequently resulted in instabilization of the system. The above fact was the principal cause for not integrating the system into the solution process proposed in the main part of the present thesis. However, in cases where the remoldable soils model is expanded to other kinds of soils (for example clayey soils in which remolding is more gradual), use of the present system for bearing capacity evaluation could be effective.

## 6. REFERENCES TO APPENDIX B


B-1 Harr, M.E. "Foundations of Theoretical Soil Mechanics." McGraw-Hill, 1966.

B-2 Karafiath, L.L. & Nowatyki, E.A. "Soil Mechanics for Off-Road Vehicle Engineering." Trans. Tech., 1978.

B-3 "Foundation and Earth Structure." Design Manual 7.2, NAVFAC DM- 1986.

B-4 Canadian Foundation Engineering Manual, 1985.

B-5 Meyerhof, G.G. "Some Recent Research on the Bearing Capacity of Foundations." Canadian Geotechnical Journal, Vol. 1, 1963.

B-6 Wu, T.H. "Soil Mechanics." Allyn & Bacon, 1976.

B-7 Sokolovski, V.V. "States of Soil Media." (translated by Jones & Schofield). Butterworth, 1960.

B-8 Davis, E.H. & Booker, J.R. "The Effect of Increasing Strength with Depth on the Bearing Capacity of Clays." Geotechnique, Vol. 23, No. 4, 1973.

B-9 Nakase, A. "Bearing Capacity of Rectangular Footings on Clays of Strength Increasing Linearly with Depth." Soils and Foundations, Vol. 21, No. 4, 1981.

B-10 James, R.G. & Tennekoon, B.L. "Experimental & Theoretical Determination of the Bearing Capacity of a Model Strip Footing on Sand." 4th Southeast Asian Conference on Soil Engineering, Kuala Lumpur, Malaysia, April 7th-10th, 1975.

## 7. LISTING OF COMPUTER SOURCE CODE.

### program fdcinc.pas (written in Turbo Pascal 6.0)

```
program fdcinc(input,output);          { alpha - assigned angle of failure plane     }
const                                  {       at point A,down from horizon }
bb=10;                                  { alpha1 - angle of radial zone at O  }
type                                   { rad1,rad2 - lengths of radial zone  }
 arr=array[0..bb,0..bb,1..4] of real;  { diag - diagonal of graouser }
var                                    { l - length of passive zone }
 pa,ra,ac:arr;                          { beta - angle of grouser  }
 wfile,w1file:text;                      { angle - computed angle of failure plane at point A}
 i,j,k,ff:integer;
 b,c,d,phi,mu,tp,gama,l,qpas,cc:real;
 v,h,alpha,alpha1,beta:real;
 rad1,rad2,diag:real;  {geometric parameters}
 sec,totnorm,totshear,pp,pv,ph:real;
 inc1,bb2,bb1:real;
 totp,pp2,pp1,inc2:real;
 phi0,c0,cphi,ccc:real;
 ff1:integer;      {value of alpha in deg. at which the network is recorded}
{*************************************** }
function tan(an:real):real;
begin
 tan:=sin(an)/cos(an);
end;
{*****************************************}
{********************** CHANGING PHI and C **********************}
{updates c and phi values depending on depth }
procedure fic(z1:real;var phi1,mu1,c1:real);
begin
 phi1:=phi0+cphi*z1;  {updated phi value}
 mu1:=3.14/4-phi1/2;
 c1:=c0+ccc*z1;      {updated c value  }
end;
{*****************************************************************}
procedure value(m,n:integer;var a:arr);
var
l1,l2,c1,d1,st,tetai,tetaj,sigi,sigj,x,z,sig,teta,ll:real;
phii,phij,mui,muj,ci,cj,fc,fd,zmani1,zmani2:real;
label
 iteration;
begin
 ll:=0;
 tetai:=a[m,n-1,4];
 tetaj:=a[m-1,n,4];
 sigi:=a[m,n-1,3];
 sigj:=a[m-1,n,3];
 fic(a[m,n-1,2],phii,mui,ci);
 fic(a[m-1,n,2],phij,muj,cj);
 iteration:
 l1:=tan(tetai+mui);
 l2:=tan(tetaj-muj);
 x:=(a[m-1,n,2]-a[m,n-1,2]+a[m,n-1,1]*l1-a[m-1,n,1]*l2)/(l1-l2);
 z:=a[m-1,n,2]+(x-a[m-1,n,1])*l2;
 fc:=cphi*(sigj-cj/(sqr(sin(phij))*cos(phij)))+ccc*cos(tetaj+muj)/(sin(phij)*cos(tetaj-muj));
 fd:=cphi*(sigi-ci/(sqr(sin(phii))*cos(phii)))+ccc*cos(tetai-mui)/(sin(phii)*cos(tetai+mui));
 c1:=(z-a[m-1,n,2])-(tan(phij)+fc/gama)*(x-a[m-1,n,1]);
```

```
 d1:=(z-a[m,n-1,2])+(tan(phii)+fd/gama)*(x-a[m,n-1,1]);
 zmani1:=gama*(c1*sigi*tan(phii)+d1*sigj*tan(phij));
 zmani2:=2*sigi*sigj*tan(phii)*tan(phij)*(a[m,n-1,4]-a[m-1,n,4]);
 sig:=(zmani1+zmani2+a[m,n-1,3]*sigj*tan(phij)+a[m-1,n,3]*sigi*tan(phii))/(sigi*tan(phii)+sigj*tan(phij));
 st:=2*(tan(phii)*sigi+tan(phij)*sigj);
 teta:=(a[m,n-1,3]-a[m-1,n,3]+2*(tan(phii)*sigi*a[m,n-1,4]+tan(phij)*sigj*a[m-1,n,4])+gama*(d1-c1))/st;
 ll:=ll+1;
 if (ll=1) then
 begin
  tetai:=0.5*(a[m,n-1,4]+teta);
  tetaj:=0.5*(a[m-1,n,4]+teta);
  sigi:=0.5*(a[m,n-1,3]+sig);
  sigj:=0.5*(a[m-1,n,3]+sig);
  fic(0.5*(a[m,n-1,2]+z),phii,mui,ci);
  fic(0.5*(a[m-1,n,2]+z),phij,muj,cj);
  goto iteration
 end;
 a[m,n,1]:=x;
 a[m,n,2]:=z;
 a[m,n,3]:=sig;
 a[m,n,4]:=teta;
end;
{*********************************************************
 FD1 ************ FD1  ***********PASSIVE*****************}
procedure passive;
var
 i,j,k:integer;
 b,d:real;
{***********************************************}
procedure init; {initiate passive array -pa }
var
 i,j,k:integer;
begin
 FillChar(pa, SizeOf(pa),#0);
 for j:=0 to bb do
 begin
  i:=bb-j;
  pa[i,j,1]:=1*j/bb; { x value on passive zone boundary}
  pa[i,j,2]:=0;     { z value on passive zone boundary}
  fic(pa[i,j,2],phi,mu,c);
  pa[i,j,3]:=(qpas+c/tan(phi))/(1-sin(phi)); { sigma value on passive zone boundary}
  pa[i,j,4]:=0;  { teta value on passive zone boundary}
 end;
end;
{***********************************************}
{main passive program}
begin
 init;
 for k:=1 to bb do
 begin
  j:=k;
  i:=bb;
  repeat
  value(i,j,pa);
  i:=i-1;
  j:=j+1;
  until j>bb;
 end;
end;
```

```
{*****************************************************************
******** FD2 *************** FD2 ********************}
{************ FD2 ************ RADIAL  *********************}
procedure radial;
var
 i,j,k:integer;
 b,d:real;
{*************************************** }
procedure init2; {initiate radial array -ra }
var
 i,j,k:integer;
begin
 FillChar(ra, SizeOf(ra),#0);
 for j:=0 to bb do
 for k:=1 to 4 do
  ra[0,j,k]:=pa[bb,j,k];
 cc:=ra[0,0,3]*exp(-2*ra[0,0,4]*tan(phi0));
 for i:=1 to bb do
 begin
  ra[i,0,1]:=0;
  ra[i,0,2]:=0;
  ra[i,0,4]:=ra[0,0,4]+(alpha1)*i/bb;
  ra[i,0,3]:=cc*exp(2*ra[i,0,4]*tan(phi0));
end;
end;
{***********************************************}
{main radial program}
begin
 init2;
 for i:=1 to bb do
 for j:=1 to bb do
 value(i,j,ra);
end;
{*****************************************************************
************ FD3 ********* FD3 ********************** }
{ ***************** FD3    ******** ACTIVE *********************}
procedure active;
var
 i,j,k:integer;
 {*********************************************}
procedure valuemix(m,n:integer;var a:arr); {gives values to the diagonal of the mixed boundary problem }
var
fc,c1,tetaj,sigj,x,z,sig,teta,zmani:real;
phij,muj,cj:real;
{********************}
procedure itersig;
begin
 fc:=cphi*(sigj-cj/(sqr(sin(phij))*cos(phij)))+ccc*cos(tetaj+muj)/(sin(phij)*cos(tetaj-muj));
 c1:=(z-a[m-1,n,2])-(tan(phij)+fc/gama)*(x-a[m-1,n,1]);
 sig:=gama*c1+2*sigj*(a[m,n,4]-a[m-1,n,4])*tan(phij)+a[m-1,n,3];
end;
{********************}
procedure iterz(zzz:real);
begin
 fic(zzz,phij,muj,cj);
 teta:=alpha+muj;
 tetaj:=0.5*(a[m-1,n,4]+teta);
 zmani:=1+(h/v)*tan(tetaj-muj);
 z:=(a[m-1,n,2]-a[m-1,n,1]*tan(tetaj-muj))/zmani;
```

```
 end;
 {*********************}
 begin
  iterz(a[m-1,n,2]);
  iterz(0.5*(a[m-1,n,2]+z));
  x:=-(h/v)*z;
  fic(z,phi,mu,c);
  fic(0.5*(a[m-1,n,2]+z),phij,muj,cj);
  a[m,n,4]:=alpha+mu;
  sigj:=a[m-1,n,3];
  itersig;
  sigj:=0.5*(sig+a[m-1,n,3]);
  itersig;
  a[m,n,1]:=x;
  a[m,n,2]:=z;
  a[m,n,3]:=sig;
 end;
 {*****************************************************************}
 procedure init3; {initiate active array -ac }
 var
 i,j,k:integer;
 begin
  FillChar(ac, SizeOf(ac),#0);
  for j:=0 to bb do
  for k:=1 to 4 do
   ac[0,j,k]:=ra[bb,j,k];
 end;
 {***********************************************}
 {main active program}
 begin
  init3;
  for j:=1 to bb do
  for i:=1 to j do
  begin
   if i=j then
   valuemix(i,j,ac)
   else value(i,j,ac);
  end;
 end;

 {*****************************************************************
 ************ FD3 end ***************** FD3 end
 ****************}{*****************************************************
 ************** FD4 ***************** FD4 ************}
 procedure geo (alph:real);
 {calculates preliminary dimensions of shear zones }
 begin
  beta:=arctan(v/h);
  diag:=sqrt(sqr(h)+sqr(v));
  fic(v,phi,mu,c);
  alpha1:=3.14/4+alph-0.5*phi;
  rad1:=diag*sin(beta+alph)/sin(3.14/2-phi);
  rad2:=rad1*exp(alpha1*tan(phi));
  l:=2*rad2*cos(3.14/4-phi/2);
 end;

 {*************************************************************
 ***************** FD4 end ************** FD4 end ************}
 {************************* TOTAL P ************************}
```

```
{calculates total forces on grouser }
procedure totalp;
begin
 totnorm:=0;
 totshear:=0;
 for i:=0 to bb do
 begin
  if ((i=0) or (i=bb)) then pp:=0.5 else pp:=1;
  fic(ac[i,i,2],phi,mu,c);
  totnorm:=totnorm+pp*sec*(ac[i,i,3]*(1-sin(phi)*cos(2*abs(beta)-2*abs(ac[i,i,4])))-c/tan(phi));
  {accumulates normal forces on grouser's diagonal }
  totshear:=totshear+pp*sec*(ac[i,i,3]*sin(phi)*sin(2*abs(ac[i,i,4])- 2*abs(beta)));

 end;
 pv:=-totshear*sin(beta)+totnorm*cos(beta);   {tot vertical force on grouser}
 ph:=+totshear*cos(beta)+totnorm*sin(beta);    {tot horizontal force on grouser}
 totp:=sqrt(sqr(pv)+sqr(ph));
end;
{***********     MAIN PROGRAM ********************************}
begin
 c0:=1.0;      { soil cohesion at surface}        {unit are kg,cm}
 ccc:=0.0;        { cohesion change per unit depth}
 phi0:=1*3.14/180;  { soil internal friction angle}
 cphi:=0*3.14/180;   { phi change per unit depth }
 gama:=1.7/1000;     { specific weight of soil}
 qpas:=0.01;     { vertical load on free surface  }
 v:=0.5;          { grouser height }
 h:=100;          { grouser length }
 ff1:=45;         {value at which network details are written to file }
 assign(w1file,'fd\fdcinc1.dat');
 rewrite(w1file);
 writeln(w1file,'Strength parameters of soil');
 writeln(w1file,'Surface cohesion (kg/cm2)= ',c0:3:2,' In depth coh. change (kg/cm3)=  ',ccc:3:2);
 writeln(w1file,'Sur. angle of friction (deg.)= ',phi0:4:1,'  In depth fric. change (deg/cm)=  ',cphi:3:2);
 writeln(w1file);
 writeln(w1file,'Grouser and loading data');
 writeln(w1file,'Grouser width (cm.)= ',h:6:1,' Grouser height (cm.) =  ',v:3:1);
 writeln(w1file,'Soil density (kg/cm3)=  ',gama:4:2,' Surface load (kg/cm2)=  ',qpas:4:3);
 writeln(w1file);
 writeln(w1file,'Alpha    Vertical force  Horizontal force  Total force  Force inclination ');
 writeln(w1file,' deg.       kg/cm.          kg/cm.          kg/cm          deg.       ');
 for ff:=1 to 2 do   {iterates over a range of alpha values}
 begin
 alpha:=5*ff*3.14/180;
 {alpha - angle between horizon and charac. line at lower point of grouser}
 geo(alpha);       {calculates preliminary shear zones geometry }
 fic(v,phi,mu,c);  {calculates strength parameters at depth v }
 if (alpha<=45*3.14/180+phi/2) and (alpha+beta<=90*3.14 180+phi) then
 {alpha can take a limited range of values }
 begin
 sec:=diag/bb;
 inc1:=0.2*l;
 bb1:=100*v;
 repeat
  passive;   {calculate passive zone}
  radial;    {calculate radial zone }
  active;    {calculate active zone }
  bb2:=ac[bb,bb,2]-v;  { bb2 - diversion of calculated depth of point A from }
                 {  its real value  }
```

```
 if abs(bb2)>v/1000 then  { if  solution is not adequate }
 begin
  if  (bb2*bb1<0)  then
  inc1:=0.3*inc1;
  bb1:=bb2;
  l:=l-(bb2/abs(bb2))*inc1;     {change passive zone length }
  end;
until abs(bb2)<=v/1000;     { and repeat solution process }
  totalp;          {calculates total forces on grouser }
  writeln('alpha = ',alpha*180/3.14:5:2, 'totp  = ',totp:7:2,' P INC.=',ArcTan(ph/pv)*180/3.14:5:2);
  if 5*ff=ff1 then   { writes detailed network data for alpha=ff1 }
  begin
   assign(wfile,'fd\fdcinc.dat');
   rewrite(wfile);
   for i:=0 to bb do
   for j:=0 to bb do
   writeln(wfile,' ',i:2,' ',j:2,' pa ',pa[i,j,1]:5:2,'  ',pa[i,j,2]:5:2,'  ',pa[i,j,3]:5:2,'  ',pa[i,j,4]:5:2);
   for i:=0 to bb do
   for j:=0 to bb do
   writeln(wfile,' ',i:2,' ',j:2,' ra ',ra[i,j,1]:5:2,'  ',ra[i,j,2]:5:2,'  ',ra[i,j,3]:5:2,'  ',ra[i,j,4]:5:2);
   for i:=0 to bb do
   for j:=0 to bb do
   writeln(wfile,' ',i:2,' ',j:2,' ac ',ac[i,j,1]:5:2,'  ',ac[i,j,2]:5:2,'  ',ac[i,j,3]:5:2,'  ',ac[i,j,4]:5:2);
   close(wfile);
  end;
  write(w1file,' ',alpha*180/3.14:5:2,'      ',pv:6:2,'        ',ph:6:2);
 writeln(w1file,'        ',totp:7:2,'          ',ArcTan(ph/pv)*180/3.14:5:2);
end;
end;
close(w1file);
end.
```

# LIST OF REFERENCES


1. Kezdi, A., "Handbook of Soil Mechanics; Vol. I: Soil Physics." Elsevier Scientific Publishing Company, New York, 1974.

2. Mitchell, J.K., "Fundamentals of Soil Behavior." University of California, Berkeley. John Wiley & Sons, Inc., New York, 1976.

3. Skempton, A.W., "Residual Strength of Clays in Landslides, Folded Strata and the Laboratory." Geotechnique 35, No. 1, pp. 3-18, 1985.

4. Lupini, J.F., Skinner, A.E., and Vaughan, P.R., "The Drained Residual Strength of Cohesive Soils." Geotechnique 31, No. 2, pp. 181-213, 1981.

5. Yong, R.N., and Warkentin B.P., "Soil Properties and Behavior." Elsevier Scientific Publishing Company, New York, 1975.

6. Clough, G.W., et al., "Cemented Sands Under Static Loading." Journal of Geotechnical Engineering Division, ASCE Vol. 107, 1981.

7. Ismael, N.F., "Strength and Bearing Capacity of Artificially Cemented Sands." Geotechnical Engineering, Vol. 21, 1990.

8. Ismael, N.F., Mollah M.A., and Ak-Khalidi O., "Geotechnical Properties of Cemented Soils in Kuwait." Australian Road Research 16(2), pp. 94-104, 1986.

9. Saxena, S.K., Reddy, K.R., and Avramidis, A.S., "Static Behavior of Artificially Cemented Sand." Indian Geotechnical, Vol. 18(2), 1988.

10. Boey, C.F., and Carter, J.P., "Manufacture and Mechanical Testing of an Artificially Cemented Carbonate Soil." Geotechnical Engineering, Vol. 20, 1989.

11. Frydman, S., "Calcareous Sands of the Israeli Coastal Plain." Geotechnical Properties, Behavior and Performance of Calcareous Soils. ASTM STP 777, K.R., pp. 226-251, 1982.

12. Wong, J.Y., "Terramechanics and Off-Road Vehicles." Elsevier Scientific Publishing Company, New York, 1989.

13. Karafiath, L.L., and Nowatzki, E.A., "Soil Mechanics for Off-Road Vehicle Engineering." Trans Tech Publications, 1978.

14. Trafficability Research Team (IDF Corps of Engineers), "Forecasting of Trafficability after Traffic for Sands Possessing Structures." Proceedings, 1st International Conference on the Mechanics of Soil-Vehicle Systems, 1961.

15. Ahlvin, R.G., "Evaluation of Contingency Surfaces for Low Volume Aircraft Traffic - Phase I." U.S. Army Engineers, WES, December, 1987.

16. Ishai, I., Livneh, M. and Yaron, R., "Carrying Capacity of Unsurfaced Runways for Low Volume Aircraft Traffic, Phase IV: Aircraft Landing Exercises on Unsurfaced Runways." Draft Copy, AFESC, March 1991.

17. Khedr, S.A., "Residual Characteristics of Untreated Granular Base Course and Subgrade Soils." Ohio State University, Ph.D. Thesis, 1979.

18. Lentz, R.W., and Baladi, G.Y., "Simplified Procedure to Characterize Permanent Strain in Sand Subjected to Cyclic Loading." Int. Symp. on Soils Under Cyclic and Transient Loading. Swansea, 7-11 January, 1980.

19. Uzan, J., "Permanent Deformation in Pavement Design and Evaluation." Int. Sym. on the Bearing Capacity of Roads and Airfields, Trondheim, Norway, 1982.

20. Barksdale, R.D., "Laboratory Evaluation of Rutting in Base Course Materials." Proceedings, 3rd International Conference on the Structural Design of Asphalt Pavements, Vol. 1, England, 1972.

21. Koba, H., and Stypulkowski, B., "The Mechanical Properties of Cement Stabilized Soils in the Conditions of Load Repetitions." International Symposium on Soils Under Cyclic and Transient Loading, Swansea, 1980.

22. De Beer, M.,"Compression Failure of Lightly Cementitious Materials". Flexible Pavement Programme,Division of Roads and Transport Technology, DPVT-36,Pretoria,1989.

23. Ishihara, K., "Soil Response in Cyclic Loading Induced by Earthquakes, Traffic and Waves," Proceedings, 7th Asian Regional Conference on SMFE, pp. 42-66, Israel, 1983.

24. Freitag, D.R. "A Dimensional Analysis of the Performance of Pneumatic Tires on Soft Soils." Technical Report No. 3-688, 1965.

25. Turnage, G.W. "Tire Selection and Performance Prediction for Off-Road Wheeled-Vehicle Operations." Proceedings, 4th International Conference, ISTVS, Vol. 1, 1972.

26. Turnage, G.W. "A Synopsis of Tire Design and Operational Considerations Aimed at Increasing In-Soil Tire Drawbar Performance." Proceedings, 6th International Conference, ISTVS, pp. 757-81O, 1978.

27. Yong, R.N., Fattah, E.A., and Skiadas, N., "Vehicle Traction Mechanics". Elsevier Science Publishers, 1984.

28. Wong, J.Y.,"Some Recent Developments in Vehicle-Terrain Interaction Studies". Journal of Terramechanics, Vol. 28, No. 4, 1991.

29. Womack, L.M. "Tests with a C-13OE Aircraft on Unsurfaced Soils." U.S. Army Waterway Experiment Station. Corps of Engineers. 1965.

30. Israel Air Force (IAF). "Carrying Capacity of Unsurfaced Runways - Literature Survey for Practical Purposes". Prepared by L.C.I. - Transportation Engineers Consultants for the IAF - Department of Construction, Design and Development Branch, Runways Section, July 1981. (In Hebrew).

31. Livneh, M., and Ishai, I., "Carrying Capacity of Unsurfaced Runways for Low Volume Aircraft Traffic, Phase III: Application of the Dynamic Cone Penetrometer". Draft Copy, AFESC, April 1990.

32. Livneh, M., and Ishai, I., "Carrying Capacity of Unsurfaced Runways for Low Volume Aircraft Traffic, Phase I: Review of Current Technology." Draft Copy, AFESC, August 1989.

33. Turnage, G.W. and Brown, E.H., "Prediction of Aircraft Ground Performance by Evaluation of Ground Vehicle Rut Depth." U.S. Army Engineer Waterway Experiment Station, AD-775-744, 1974.

34. Directorate of Training and Doctrine U.S. Army Engineer School, "Planning and Design of Roads, Airfields, and Heliports in the Theater of Operations." Fm 5-330 Coordinating Draft, 1988.

35. Melzer, K.J., "Possibilities of Evaluating the Traction of Tires for Off-Road Transportation Vehicles." Journal of Terramechanics, Vol. 21, No. 4, pp. 309-333, 1984.

36. Ladd, D.M., "Soil Strength Criteria for Operation of Fighter Aircraft on Unsurfaced Airfields." U.S. Army Engineer WES, Misc. Paper S-70-24, 1970.

37. Mandel, J., and Salencon J.,"Force portante d'un sol sur une assise rigide (etude theorique)." Geotechnique 22, No.1, 1972.

38. Siraj-Eldine K., and Bottero, A.,"Etude experimentale de la capacite portante d'une couche de sol pulverulent d'epaisseur limitee." Can. Geotechnical Journal, Vol. 24, 1987.

39. Meyerhof, G.G., and Hanna ,A.M.,"Ultimate Bearing Capacity of Foundations on layered Soils Under Inclined Loads". Can. Geotechnical Journal, Vol. 15, 1978.

40. Meyerhof, G.G.,"Ultimate Bearing Capacity of Footings on Sand Layer Overlying Clay". Can. Geotechnical Journal, Vol. 11,1974.

41. Vesic,A.S.,"Analysis of Ultimate Loads of Shallow Foundations." Journal of Soil Mechanics and Foundations Division,ASCE,Vol.99,No.SM1,1973.

42. Turnbull, W.J., Maxwell, A.A., & Burns, C.D. "Strength Requirements in Unsurfaced Soils for Aircraft Operations." Proc., 5th ICSMF, Paris, 1961.

43. Material Testing TM 5-530/NAVFAC MO-330/AFM 89-3, U.S.A., Feb. 1971.

44. "Planning and Design of Roads, Airbases and Heliports in the Theater of Operations." Dept. of the Army Technical Manual, TM 5-330, AFM 86-3, Vol. II, Dept. of the Army and the Air Force, September 1968.

45. Phillips, N.S., Kraft, D.C., Saliba, J.E., & Cook, R.F. "Planning and Design for Operations of Aircraft on Soil Surfaces: A User-Oriented Guide." University of Dayton, AFESC ESL-TR-86-3, July 1987.

46. Livneh, M. & Ishai, I. "Evaluation of Flexible Pavements and Subsoils Using the South African Dynamic Cone Penetrometer," (in Hebrew). Transportation Research Institute, Soil and Road Testing Laboratory, Pub. No. 85-3O1, September 1985.

47. Saliba, J. "An Elastic-Viscoplastic Finite Element Model for Representing Layered Soils: Vol. 1, Description." Final Report, Engineering and Services Laboratory, Air Force Engineering & Services Center, Tyndall Air Force Base, FLA., U.S., January 1983-September 1984.

48. Koba, H. and Stypulkowski, B. "The Mechanical Properties of Cement Stabilized Soils in the Conditions of Load Repetitions". International Symposium on Soils under Cyclic and Transient Loading, Swansea 1980.

49. Bela I. Sandor, "Fundamentals of Cyclic Stress and Strain". The University of Wisconsin Press, 1972.

50. Talesnic, M.L., "The Cyclic and Monotonic Shear Behavior of a Marine Clay." Technion, Ph.D. Thesis, Israel, 1990.

51. Saada, A.S., "Hollow Cylinder Torsional Devices: Their Advantages and Limitations." Advanced Triaxial Testing of Soil and Rock, ASTM STP-977, (ed.:) Donaghe, Chaney and Silver, 1988.

52. Khedr, S.A., "Residual Characteristics of Untreated Granular Base Course and Subgrade Soils." Ohio State University, Ph.D., 1979.

53. Poulous, H.G. and Davis, E.H., "Elastic Solutions or Soil and Rock Mechanics". John Wiley & Sons, Inc., N.Y., 1974.

54. Livneh, M., Ishai, I., and Livneh, N., "Carrying Capacity of Unsurfaced Runways for Low Volume Aircraft Traffic, Supplement to Phase III: Automated DCP Device Vs. Manual DCP Device." Draft Copy, AFESC, August 1989.

55. Ishai, I., Livneh, M., and Yaron, R., "Remolding of Soils under Aircraft Loading - Literature Survey and Research Plan", Phase II: Draft Copy. AFESC, September 1992.

56. ITASCA Consulting Group Inc., "FLAC - Fast Lagrangian Analysis of Continua, Ver 3.2, Vol I: User's Manual". Minneapolis, Minnesota, U.S.A., 1992.

57. Scott,R.F.,"Principles of Soil Mechanics". Addison-Wesley Inc.,1963

58. Uzan, J., "An Evaluation Scheme for Conventional Requirements of Design and Construction Quality for Asphalt Concrete". Proceedings, Association of Asphalt Paving Technologists Technical Sessions, Vol. 51, Kansas City, Missouri, 1982.

59. Ishai, I., Cohen, E., Shklarsky, E., Livneh, M., "Study of Asphalt Parameters for Pavement Design". Transportation Research Institute Report No. 78-4, 1978 (in Hebrew).

60. Standard Specifications for Transportation Materials and Methods of Sampling and Testing: AASHTO Standard Method of Test for Correction for Coarse Particles in the Soil. Compaction Test T 224-86, 1990.

61. Ladd, R.S., "Preparing Test Specimens Using Undercompaction". Geotechnical Journal,

62. Baladi, G.Y. & Rohani, B. "Development of a Soil-Wheel Interaction Model." Proceedings, 8th International Conference, ISTVS, Cambridge, U.K., 1984.

63. Lambe, T. W., and Whitman, R.V., "Soil Behavior." Massachusetts Institute of Technology. John Wiley & Sons, Inc., New York, 1969.